Methods in Molecular Biology 1656

Springer Protocols

Karen Mossman *Editor*

Innate Antiviral Immunity

Methods and Protocols

Humana Press

METHODS IN MOLECULAR BIOLOGY

Series Editor
John M. Walker
School of Life and Medical Sciences
University of Hertfordshire
Hatfield, Hertfordshire, AL10 9AB, UK

For further volumes:
http://www.springer.com/series/7651

Innate Antiviral Immunity

Methods and Protocols

Edited by

Karen Mossman

Biochemistry and Biomedical Sciences, McMaster University, Hamilton, ON, Canada

Humana Press

Editor
Karen Mossman
Biochemistry and Biomedical
Sciences
McMaster University
Hamilton, ON, Canada

ISSN 1064-3745 ISSN 1940-6029 (electronic)
Methods in Molecular Biology
ISBN 978-1-4939-7236-4 ISBN 978-1-4939-7237-1 (eBook)
DOI 10.1007/978-1-4939-7237-1

Library of Congress Control Number: 2017947873

Printed on acid-free paper

This Humana Press imprint is published by Springer Nature
The registered company is Springer Science+Business Media LLC
The registered company address is: 233 Spring Street, New York, NY 10013, U.S.A.

Preface

This book on *Innate Antiviral Immunity* explores methods to study the complex and evolving interplay between a virus and its host that range from model systems to the detection of chemical molecules. The collection starts with the application of humanized mice and zebrafish as model organisms to study virus-host interactions and induction of innate immune responses. Subsequent chapters outline diverse methods to detect small interfering RNAs, microRNAs, and virus-derived dsRNA from a variety of cells, tissues, and organisms. Several chapters are dedicated to interrogating the cytosolic RNA and DNA sensing pathways, including using RNA PAMPs as molecular tools, purification of cGAMP from virus particles and infected cells, and mechanisms to visualize the subcellular localization and activation of the adaptor proteins MAVS and STING. Cutting-edge methods, including high-throughput and genome-wide CRISPR/Cas9 screens, chromosome conformation capture, and whole-exome sequencing, are described to identify novel mediators, pathways, and variants underlying host susceptibility. Given the importance of studying these pathways and players under physiologic conditions, methods describing the isolation of primary mouse sensory neurons and group 2 innate lymphoid cells are also provided. Finally, this collection comes full circle back to the whole organism level and concludes with epidemiological methods to investigate virus-host interactions and the induction of innate immunity. Thus, this collection in *Methods in Molecular Biology* spans a diverse array of approaches to study and elucidate the intricacies of innate antiviral immunity.

Hamilton, ON, Canada ***Karen Mossman***

Contents

Contributors

Ali A. Ashkar • *Department of Pathology and Molecular Medicine, McMaster Immunology Research Centre, Hamilton, ON, Canada; MG DeGroote Institute for Infectious Disease Research, McMaster Immunology Research Centre, Hamilton, ON, Canada*

Dia C. Beachboard • *Department of Molecular Genetics and Microbiology, Duke University Medical Center, Durham, NC, USA*

Anne Bridgeman • *Medical Research Council Human Immunology Unit, Radcliffe Department of Medicine, Medical Research Council Weatherall Institute of Molecular Medicine, University of Oxford, John Radcliffe Hospital, Oxford, UK*

Jorge R. Cabrera • *Department of Microbiology and Immunology, Geisel School of Medicine, Dartmouth University, Lebanon, NH, USA*

Victor R. DeFilippis • *Vaccine and Gene Therapy Institute, Oregon Health and Science University, Beaverton, OR, USA*

Stephanie J. DeWitte-Orr • *Departments of Health Sciences and Biology, Wilfrid Laurier University, Waterloo, ON, Canada*

Claudia U. Duerr • *Department of Microbiology and Immunology, McGill University Research Centre on Complex Traits (MRCCT), McGill University, Montreal, QC, Canada*

Jörg H. Fritz • *Department of Microbiology and Immunology, McGill University Research Centre on Complex Traits (MRCCT), McGill University, Montreal, QC, Canada; Department of Physiology, McGill University Research Centre on Complex Traits (MRCCT), McGill University, Montreal, QC, Canada*

Michael Gale Jr. • *Department of Immunology, Center for Innate Immunity and Immune Disease, University of Washington School of Medicine, Seattle, WA, USA*

Bryan J. Gall • *Vaccine and Gene Therapy Institute, Oregon Health and Science University, Beaverton, OR, USA*

Elizabeth C. Giles • *Department of Pathology and Molecular Medicine, McMaster Immunology Research Centre, Hamilton, ON, Canada; MG DeGroote Institute for Infectious Disease Research, McMaster Immunology Research Centre, Hamilton, ON, Canada*

Stacy M. Horner • *Department of Molecular Genetics and Microbiology, Duke University Medical Center, Durham, NC, USA; Department of Medicine, Duke University Medical Center, Durham, NC, USA*

Renee C. Ireton • *Department of Immunology, Center for Innate Immunity and Immune Disease, University of Washington School of Medicine, Seattle, WA, USA*

Volkhard Kaever • *Research Core Unit Metabolomics, Hannover Medical School, Hannover, Germany*

Ulrich Kalinke • *Institute for Experimental Infection Research, TWINCORE, Centre for Experimental and Clinical Infection Research, Hannover Medical School, Hannover, Germany*

Sarah Katzenell • *Department of Microbiology and Immunology, Geisel School of Medicine, Dartmouth University, Lebanon, NH, USA*

Tae Hoon Kim • *Department of Biological Science and Center for Systems Biology, The University of Texas at Dallas, Richardson, TX, USA*

Yoon Jung Kim • *Department of Biological Science and Center for Systems Biology, The University of Texas at Dallas, Richardson, TX, USA*
David A. Leib • *Department of Microbiology and Immunology, Geisel School of Medicine, Dartmouth University, Lebanon, NH, USA*
Gabriel A. Leiva-Torres • *Department of Human Genetics, McGill University, Montreal, QC, Canada; McGill University Research Center on Complex Traits, Montreal, QC, Canada; Department of Medicine, McGill University, Montreal, QC, Canada*
Mark Loeb • *Department of Medicine, McMaster University, Hamilton, ON, Canada; Department of Pathology and Molecular Medicine, McMaster University, Hamilton, ON, Canada; Department of Health Research Methods, Evidence, and Impact, McMaster University, Hamilton, ON, Canada*
Tianyun Long • *Department of Biological Sciences, Louisiana State University, Baton Rouge, LA, USA*
Rui Lu • *Department of Biological Sciences, Louisiana State University, Baton Rouge, LA, USA*
Jonathan Maelfait • *Medical Research Council Human Immunology Unit, Radcliffe Department of Medicine, Medical Research Council Weatherall Institute of Molecular Medicine, University of Oxford, John Radcliffe Hospital, Oxford, UK; Laboratory of Immunoregulation and Mucosal Immunology, VIB Center for Inflammation Research, Ghent, Belgium; Department of Internal Medicine, Ghent University, Ghent, Belgium*
Alice Mayer • *Medical Research Council Human Immunology Unit, Radcliffe Department of Medicine, Medical Research Council Weatherall Institute of Molecular Medicine, University of Oxford, John Radcliffe Hospital, Oxford, UK*
Chandra S. Mukhopadhyay • *School of Animal Biotechnology, Guru Angad Dev Veterinary and Animal Sciences University (GADVASU), Ludhiana, Punjab, India*
Nestor Nebesio • *Department of Human Genetics, McGill University, Montreal, QC, Canada; McGill University Research Center on Complex Traits, Montreal, QC, Canada; Department of Medicine, McGill University, Montreal, QC, Canada*
Pin Nie • *State Key Laboratory of Freshwater Ecology and Biotechnology, Institute of Hydrobiology, Chinese Academy of Sciences, Wuhan, Hubei Province, China*
Brian J. North • *Department of Microbiology and Immunology, Geisel School of Medicine, Dartmouth University, Lebanon, NH, USA*
Jennifer Paijo • *Institute for Experimental Infection Research, TWINCORE, Centre for Experimental and Clinical Infection Research, Hannover Medical School, Hannover, Germany*
Vladislav Pokatayev • *Department of Microbiology, University of Texas Southwestern Medical Center, Dallas, TX, USA*
Sarah J. Poynter • *Department of Biology, Wilfrid Laurier University, Waterloo, ON, Canada*
Jan Rehwinkel • *Medical Research Council Human Immunology Unit, Radcliffe Department of Medicine, Medical Research Council Weatherall Institute of Molecular Medicine, University of Oxford, Oxford, UK*
Jasdeep Singh • *Department of Experimental Medicine and Biotechnology, PGIMER, Chandigarh, Punjab, India*
Fatemeh Vahedi • *Department of Pathology and Molecular Medicine, McMaster Immunology Research Centre, Hamilton, ON, Canada; MG DeGroote Institute for Infectious Disease Research, McMaster Immunology Research Centre, Hamilton, ON, Canada*

Christine Vazquez • *Department of Molecular Genetics and Microbiology, Duke University Medical Center, Durham, NC, USA*

Ramneek Verma • *School of Animal Biotechnology, Guru Angad Dev Veterinary and Animal Sciences University (GADVASU), Ludhiana, Punjab, India*

Silvia M. Vidal • *Department of Human Genetics, McGill University, Montreal, QC, Canada; McGill University Research Center on Complex Traits, Montreal, QC, Canada; Department of Medicine, McGill University, Montreal, QC, Canada*

Biao Wang • *Department of Pathology and Molecular Medicine, McMaster University, Hamilton, ON, Canada*

Wensheng Wei • *Biodynamic Optical Imaging Center (BIOPIC), Beijing Advanced Innovation Center for Genomics, Peking-Tsinghua Center for Life Sciences, State Key Laboratory of Protein and Plant Gene Research, School of Life Sciences, Peking University, Beijing, China*

Courtney Wilkins • *Department of Immunology, Center for Innate Immunity and Immune Disease, University of Washington School of Medicine, Seattle, WA, USA*

Nan Yan • *Department of Immunology and Department of Microbiology, University of Texas Southwestern Medical Center, Dallas, TX, USA*

Yuexin Zhou • *Biodynamic Optical Imaging Center (BIOPIC), Beijing Advanced Innovation Center for Genomics, Peking-Tsinghua Center for Life Sciences, State Key Laboratory of Protein and Plant Gene Research, School of Life Sciences, Peking University, Beijing, China*

Shiyou Zhu • *Biodynamic Optical Imaging Center (BIOPIC), Beijing Advanced Innovation Center for Genomics, Peking-Tsinghua National Institute of Biological Sciences, State Key Laboratory of Protein and Plant Gene Research, School of Life Sciences, Peking University, Beijing, China*

Peng Fei Zou • *College of Fisheries, Jimei University, Xiamen, Fujian Province, China*

Chapter 1

The Application of Humanized Mouse Models for the Study of Human Exclusive Viruses

Fatemeh Vahedi, Elizabeth C. Giles, and Ali A. Ashkar

Abstract

The symbiosis between humans and viruses has allowed human tropic pathogens to evolve intricate means of modulating the human immune response to ensure its survival among the human population. In doing so, these viruses have developed profound mechanisms that mesh closely with our human biology. The establishment of this intimate relationship has created a species-specific barrier to infection, restricting the virus-associated pathologies to humans. This specificity diminishes the utility of traditional animal models. Humanized mice offer a model unique to all other means of study, providing an in vivo platform for the careful examination of human tropic viruses and their interaction with human cells and tissues. These types of animal models have provided a reliable medium for the study of human-virus interactions, a relationship that could otherwise not be investigated without questionable relevance to humans.

Key words Animal models, Disease Models, Human, Humanized mice, Immune system, Viruses

1 Introduction

1.1 Why Do We Need the Humanized Mouse Model for the Study of Human Tropic Viruses?

As viruses progress through the process of infection, environmental pressures from within the host demand the virus develop adaptive strategies to ensure its survival. The most fit viral particles are selected, which then produce incredible amounts of viral descendants proficient in manipulating the susceptible host for continued viral replication, survival, and transmission [1]. The immune responses to a pathogen contain distinct mechanisms unique to the infected host species, creating successful viral progeny highly skilled in manipulating the host through which selection occurred. These species differences create a profoundly specific interaction between the pathogen and its co-evolved host [1, 2]. The scientific journey to fully comprehend the relationship developed between human and virus has been incredibly strenuous. Following the formal recognition of the ethical concerns behind the use of

Fatemeh Vahedi and Elizabeth C. Giles contributed equally to this work.

Karen Mossman (ed.), *Innate Antiviral Immunity: Methods and Protocols*, Methods in Molecular Biology, vol. 1656, DOI 10.1007/978-1-4939-7237-1_1, © Springer Science+Business Media LLC 2017

human subjects [3], the severe restrictions placed on human experimentation necessitate alternative models to study human disease [4].

In vitro models serve as fundamental tools to study the viral life cycle. Cell culture systems provide a carefully controlled platform for the examination of how the virus enters its tropic cell lines, replicates, assembles, and secretes budding viral progeny [5]. However, in vitro systems are highly isolated conditions unable to recreate the dynamic features present within an in vivo environment [6]. The absence of these features sources discrepancy between results derived from the use of an in vitro system and results obtained from in vivo investigation. Furthermore, features highly influential on viral infection are commonly altered within cell lines. Oftentimes genes and cell cycle profiles are expressed in a way unorthodox to the cells present within a living organism [7]. Alternatively, in vivo models resolve this problem presented in in vitro cultures. The quintessential model for the investigation of human and virus interactions would permit invasive examination into an infected host with an internal environment capable of manifesting disease outcome as if it were a human [8, 9]. However, the co-evolutionary history established between virus and human has created a relationship of intimacy between pathogen and host that cannot be truly replicated in traditional in vitro or in vivo models [9]. The value of this model is placed in its ability to provide a means for investigating the biological activity that occurs within a host throughout the process of viral infection [8, 9].

Nonhuman primates have become an incredibly valued tool for enriching our understanding of the mechanisms underlying the pathogenic process of viral infection and revealing the potential clinical efficacy of antiviral therapeutics [10, 11]. Their value is a result of their close phylogenetic relation to humans [10, 11], providing a model capable of closely resembling human biology [11]. However, this close phylogenetic relationship is what brings ethical concerns, in which the complexity of debate with regards to their use continues to grow [12, 13]. The difficulty in using non-human primates stems from their tight regulation [13, 14], demanding requirements for proper care [14], and high cost which limits cohort size [2, 9]. Even with their close phylogenetic relationship, the representation of disease pathogenesis remains inaccurate. Several diseases impact humans in a more severe manner than they do in nonhuman primates, discrepancies likely attributed to the inter-species immune system differences [2, 15]. Considering these growing limitations, it is ill advised to remain dependent on nonhuman primate experimentation [13].

The mouse model offers an abundant resource of genetic diversity and permits the creation of unique strains of transgenic mice since they can tolerate extensive genetic manipulation [9, 16]. Additionally, mice are capable of achieving pure strains, allowing

for the generation of reproducible results during experimentation [9]. These factors have established the mouse as the dominating animal in research [16]. However, even such a fundamental model is not suited to recreate the pathogenic process of every virus, especially those with highly species specific cellular tropism [16]. Human tropic pathogens have developed specific molecules and factors that have been established to interact with and manipulate the specific components of its co-evolved human host [1]. Traditional animal models, no matter the species, if they are other than human, will not show the interaction of human cells with the virus [9, 13]. Additionally, within the environment of these surrogate models, the replication and progression of disease is often unable to occur as a result of the species barrier. Humanized mice remove this barrier to infection and disease progression, thus offering a unique means of investigating viral pathogenesis [13, 17].

1.2 Humanized Mice: A Practical Solution for the In Vivo Study of Human-Specific Viral Infection

Several types of humanized mouse models exist, each displaying unique features of the pathogenic process of human infection. To "humanize" a mouse, human cells or tissues are engrafted into a recipient mouse with an injury in the murine equivalent organ you wish to examine. In attempts to remove the occurrence of xenograft rejection, mice with an immunodeficient background are used. Depending on the cellular and tissue tropism of the virus, various human organs would be implanted accordingly [9, 18]. Cells engrafted into the recipient mice retain their functional capacity, occupy their respective murine niches, and offer the virus its susceptible and permissive cells for viral infection and spread [9, 13]. In an ideally constructed humanized mouse model, the viral pathogen goes about infection as it would if it were in its human host, and the mouse responds as if it were a human [8, 9, 13].

A highly involved component in human viral infection is the human immune system. Thus, the study of the immune system and its interaction with the virus is an important component in understanding viral pathogenesis. Appropriately, the types of humanized mice frequently used for the study of viral infection are often reconstituted with human immune cells. Although the term "humanized mice" extends beyond the implantation of human immune cells, this is a primary method of humanization in the study of infectious disease. In fact, the study of major human pathogens such as Dengue (DENV), Ebola (EBOV), Epstein-Barr (EBV), human cytomegalovirus (HCMV), Human T-cell Leukemia Type-1 (HTLV-1), Human Immunodeficiency virus (HIV), and Hepatitis C (HCV) often involves the use of this type of humanized mouse model.

For simplicity's sake, human immune system (HIS) mice can be categorized into two types: mice created by the transplantation human hematopoietic stem cells (HSCs) or peripheral blood mononuclear cells (PBMCs) into a recipient immunodeficient

mouse [8, 19]. In using HSCs, human T and B cell progenitors are able to go through the maturation process in the environment of the mouse recipient. As a result, negative and positive selection of the human immune cells occurs within the mouse, giving the immune cells an opportunity to develop a tolerance toward the murine host [19]. The PBMC model does not provide this process however, the transplantation of functionally mature leukocytes allows for human immune cell function to be examined more immediately [19]. Reservoir sources of HSCs often used in mouse humanization include umbilical cord blood, mobilized peripheral blood [19, 20], bone marrow, and fetal liver [19, 21]. Studies have also utilized thymus, lymph node, and skin [22]. Each source allows for the subsequent reconstitution of human immune cell components [19]. These sources have been used in combination, such as the bone marrow, liver, thymus (BLT) model [23], and the SCID-hu thymus and liver (SCID-hu Thy/Liv) mouse, in which SCID (severe combined immunodeficient) mice are engrafted with human thymus and liver tissue [24], or used individually. Comparatively, PBMCs can be obtained in a simple process from either whole blood samples or spleens [19]. An incredible aspect of "humanizing" immunodeficient mice is how with different sources of human immune cells, the reconstitution of human immune cell populations, and subsequently, the display of infection, can be presented in very different ways depending on the source [13].

1.3 The Gradual Transformation of the Humanized Mouse Model

The evolution of the humanized mouse has coincided with the advancements in the immunodeficient mouse models. The development of a more sophisticated immunodeficient strain of recipient mice has allowed for enhanced engraftment and reconstitution of human components within their respective murine biological niches [8, 9, 13]. Attempts to construct a human hematolymphoid system within a mouse model began with athymic (nude) mice [25]. The significant depletion of T cell maturation and T cell activity gave them promise [9, 26, 27]. Unfortunately, despite extensive efforts, results were continually unsatisfactory and the successful engraftment of normal human tissues appeared impossible [25]. It was the remaining components of the murine immune system, functional B cells and natural killer (NK) cells that created significant obstacles to achieving adequate humanization. The presence of these cells leads to the gradual rejection of transplanted human cells and tissues [9].

In 1983 [28], the discovery of the severe combined immunodeficient (SCID) mouse greatly enhanced the humanization process [8]. A spontaneous mutation within the Prkdc (protein kinase, DNA activated, catalytic polypeptide) gene of C.B-17 mice was found to produce mice with serious depletions in the functional capacity of the murine B and T lymphocytes. The reconstitution of the human immune system is enhanced within SCID mice in

comparison to athymic mice; however, they do not come without limitations. SCID mice undergo a phenomenon termed "leakiness" in which murine T and B cells are spontaneously generated throughout the natural aging process of the mouse. This sporadic production of functional murine T and B cells interferes with the engrafted human cells, eventually causing rejection of the human graft. An additional factor at play is the presence of high functioning NK cells and other innate immune cell types of mouse origin, recognizing the human cells as foreign, thus disrupting successful engraftment [8, 29].

In 1992, in efforts to remove the problem of "leakiness" and enhance the ability of recipient mice to accept human tissues and cells, Mombaerts et al. [30] and Shinkai et al. [31] created mice with targeted mutations in the V(D)J recombination-activating gene 1 and 2 (Rag 1/2) loci, respectively [8]. The presence of these mutations removes the natural process of T and B lymphocyte maturation [8, 30, 31]. These mutant mice retain high levels of NK cell activity, restricting their engraftment potential [8, 31]. In 1995, Shultz et al. were able to mitigate the problem of the persisting murine innate immune response. Through a process of backcrossing the SCID mutation onto the non-obese diabetic (NOD/Lt) mouse background, Shultz et al. created the NOD/SCID mouse, containing several functional deficiencies in the murine innate and adaptive immune response [8, 9, 31, 32]. Accordingly, these mice have allowed for improved reconstitution of human hematopoietic stem cells. However, this improved model remains to have several faults, complicating its use for accepting human cells and tissues, and studying virally induced pathologies [8, 32]. NOD/SCID mice contain residual NK cell and innate immune cell function and possess a fairly limited life span. The presence of these interfering factors enables the problem of impaired engraftment to persist in the NOD/SCID mouse model [32]. In the mid-2000s, the introduction of a targeted mutation in the interleukin (IL)-2 receptor gamma chain loci (IL-2rg) caused mice to develop severe impairments in the maturation process and functional capacity of B and T cells, and eradicated NK cell development [8, 9, 13, 33]. These immunodeficient mutations have been combined to recreate numerous types of immunodeficient mice, often enhancing the immune depletions and thus the engraftment success within the mice [8, 9].

To recreate a functional human immune system within a mouse, the process requires more than just the immune cells itself. For the development, survival, and function of human hematolymphoid cells, there are a number of hormones, growth factors, and cytokines essential to ensure optimal health and function of human cells [25]. The presence of residual immune system components

within the immune deficient mice can encourage the production of cytokines capable of inducing differentiation of engrafted human cells. However, the presence can have a negative effect, resulting in graft rejection. Additionally, the mouse equivalents of necessary immune factors are often inadequate replacements as a result of species specificity [13, 25, 33]. To overcome these obstacles and enhance engraftment, investigators have provided these human factors through exogenous administration to the human hemato-lymphoid cell-engrafted mice or through the transgenic expression of these essential components [9, 13, 25, 33]. Another limiting factor of traditional mice strains is the presence of murine major histocompatibility complex (MHC). MHC hinders the ability of human T cells to communicate with human antigen presenting cells within the murine host [33]. For appropriate thymic selection and antigen-specific restriction by human T cells, expression of human leukocyte antigen (HLA) molecules is required to be present on the murine host thymic epithelium. To address this problem and enhance the accuracy of the humanized mouse model for human virus research, numerous transgenic mice expressing HLA molecules have been created [9, 13, 25, 33].

With each modification, researchers get closer to creating a more accurate representation of human infection and disease within the mouse model, permitting the study of several human pathogens that have been previously restricted as a result of poor animal models. Different types of models, depending on how they are generated, have a unique means of expressing viral infection, and thus can offer insight into different aspects of viral pathogenesis. There is no humanized mouse model that is optimal for addressing the incredibly large amount of questions to be considered for the study of human tropic pathogens. However, humanized mouse models have made addressing some of these questions possible for the first time, ever [9, 13, 25, 33].

2 Materials

2.1 Common Materials

1. Phosphate-buffered saline (PBS), sterile.
2. Wash media: 2% FBS in PBS.
3. Sterile alcohol swab or 70% ethanol spray.
4. Autoclaved, filtered, ventilated device for housing mice (*see* **Note 1**).
5. Laminar flow BSL class II hood.
6. Bench top centrifuge.
7. Ice bucket.

2.2 Generating the Humanized NRG Mouse Model

2.2.1 CD34+ Cell-Enrichment of Fresh Human Cord Blood (See **Note 2**)

1. Umbilical cord blood (*see* **Note 3**).
2. Ficoll paque or Lymphoprep, stored at room temperature.
3. Fetal bovine serum (FBS).
4. HetaSep erythrocyte aggregation agent (*see* **Note 4**).
5. RosetteSep™ human hematopoietic progenitor cell enrichment cocktail.
6. Trypan blue.
7. Hemocytometer.
8. Dimethyl sulfoxide (DMSO).
9. A selection kit for CD34+ cell-enrichment of fresh cord blood (*see* **Note 5**).
10. Freezing solution: 10% DMSO in FBS.

2.2.2 CD34+ Cell-Enrichment of Human Fetal Liver

1. Collagenase IV.
2. Dulbecco's Modified Eagle's medium (DMEM).
3. Collagenase solution: 1 mg/mL collagenase IV in DMEM.
4. 0.2 μm filter.
5. Cell scraper.
6. 100 μm nylon mesh.
7. RosetteSep™ human hematopoietic progenitor cell enrichment cocktail.
8. Petri dish.

2.2.3 Immunosuppression of NRG Mice Through Irradiation or 5-Fu (See **Notes 6** and **7**)

1. Gamma irradiator (e.g., Gammacell 3000) (*see* **Note 8**).
2. Mouse irradiation container.
3. NRG mice (*see* **Note 9**).
4. Fluorouracil 5-Fu.

2.2.4 Injection of Human Hematolymphoid Cells (See **Note 10**)

1. 0.3 mL U 100, 29 G needle (for pups).
2. 1 mL insulin syringe, 30 G needle (for adults).
3. Warming lamp.
4. Mouse restrainer.
5. Ethanol, 70%.
6. Sterile gauze.

2.2.5 Evaluating the Degree of Human Immune Cell Reconstitution

1. hCD45 antibody conjugated.
2. mCD45 antibody conjugated.
3. Human FcR blocking antibody (FC block) (*see* **Note 11**).
4. Solution for fixing and lysing red blood cells from whole blood samples (e.g., Fix/Lyse solution, eBioscience) (*see* **Note 12**).

2.3 Creation of the Double Humanized FRG Mouse: The Human Liver and Immune System Chimera

2.3.1 Hepatocyte and Lymphoid Progenitor Cell Isolation from Human Fetal Liver

1. DMEM.
2. Cell scraper.
3. Collagenase IV.
4. 100 μm nylon mesh.
5. Trypan blue.
6. FBS.
7. DMSO.
8. Petri dish.

2.3.2 Depletion of hCD3+ Cells Using the PE Selection Kit

1. EasySep™ Magnet, Immunomagnetic column-free magnet.
2. 5 mL polystyrene round tubes (12 × 75 mm).
3. Human FcR blocking antibody.

2.3.3 Immunosuppression of FRG Mice by Irradiation or 5-Fu

1. Gamma irradiator (e.g., Gammacell 3000).
2. Mouse irradiation container.
3. Fluorouracil (5-Fu).
4. FRG mice (*see* **Note 13**).

2.3.4 Intrasplenic Injection of Human Liver Cells and Human Hematopoietic Cells [19]

1. Sterile petrolatum ophthalmic ointment.
2. 0.01 mg/mL buprenorphine.
3. Ketamine/xylazine cocktail.
4. Electric clippers.
5. Betadine.
6. Sterile surgical instruments: scissors, forceps, needle holder (*see* **Note 14**).
7. 1 mL syringes with 27-G × ½-in. needle.
8. Sterile cotton swabs.
9. 3-0 coated vicryl suture.
10. Wound clips.
11. Sterile gauze.
12. Warming pad or warming lamp.
13. Anesthetic equipment according to institutional guidelines.

3 Methods

3.1 Generating the Humanized NRG Mouse Model

3.1.1 CD34+ Cell-Enrichment of Fresh Human Cord Blood (Fig. 1)

1. Using a 10 mL pipette, transfer the fresh cord blood, which has been collected in blood collection tubes containing anticoagulants, to a 50 mL Falcon tube. If the sample is less than 40 mL, transfer all contents to one 50 mL tube. If there is over 40 mL of cord blood, divide equally among several tubes so that each tube contains less than 40 mL. Preserve and freeze 500 μL of

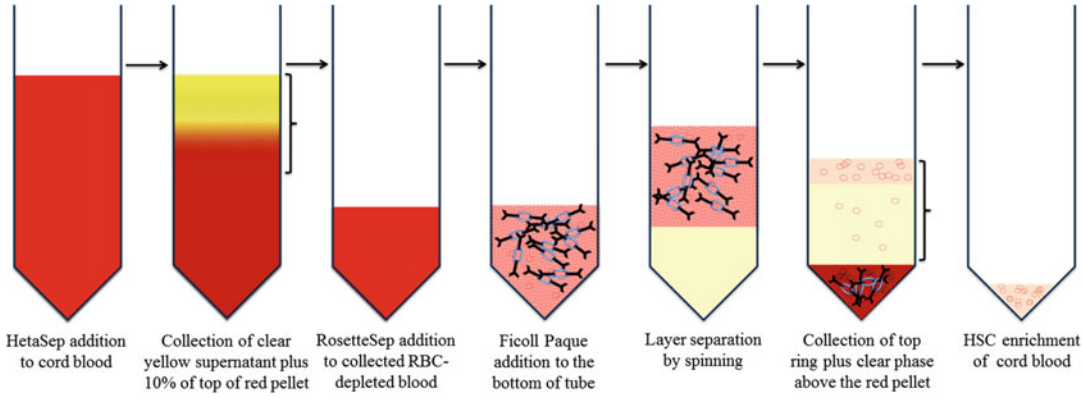

Fig. 1 Schematic representation of the hCD34+ cell-enrichment process of fresh human cord blood

blood in a microtube for future analysis. For example, HLA typing may be required (*see* **Note 15**).

2. To deplete the sample of red blood cells (RBCs), add 2 mL of HetaSep per 10 mL of blood and mix by inverting the tubes.
3. Centrifuge at 132 × *g* for 5 min at 4 °C, with the break off.
4. Slowly, with a 25 mL pipette, transfer the supernatant and the top 10% of the formed pellet to a new 50 mL tube. Add wash media to top up each tube to 40 mL. Invert tubes to mix.
5. Pellet the cells by spinning at 529 × *g* for 7 min 4 °C, with the break on.
6. Slowly remove the supernatant with a 25 mL pipette and avoid disturbing the pellet. If you start with more than one 50 mL tube, combine all pellets to one of the tubes and then wash the tube with a small volume of wash buffer. If the total pellet is less than 15% of the original volume, top the total volume of the tube up to 10–15% of the original blood volume with wash buffer media.
7. To isolate progenitor cells from cord blood and whole blood by negative selection, add 75 μL of the RosetteSep™ per 10 mL of initial blood volume. Mix by swirling gently by hand and incubate for 10 min at room temperature (RT).
8. Top up the blood with wash buffer to 20 mL and mix gently by hand.
9. Slowly add 10 mL of Ficoll Paque to the bottom of the tube using a sterile Pasteur pipette.
10. Centrifuge at 680 × *g* for 20 min, 18 °C. The brake should be off. It is important that the centrifuge is well balanced (*see* **Note 16**).

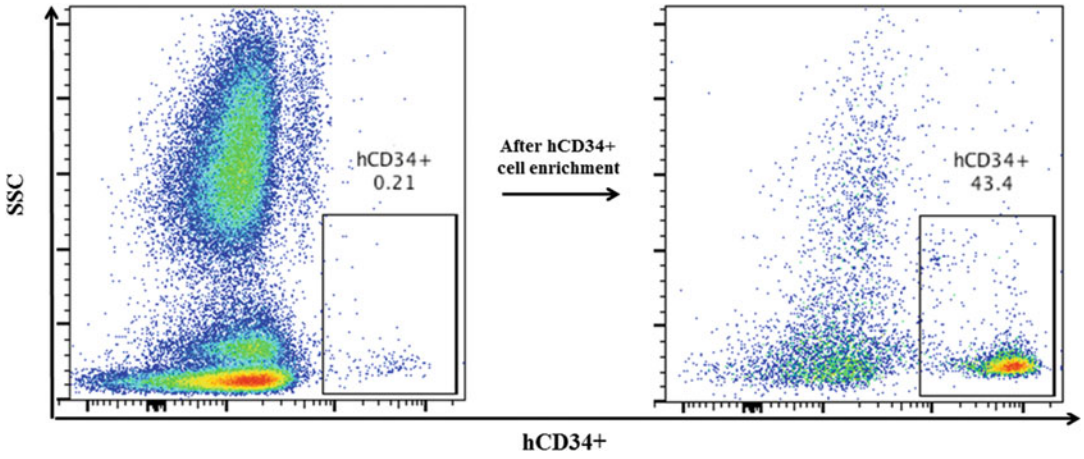

Fig. 2 Flow cytometric analysis of hCD34+ cells present in cord blood before and after the enrichment process. Enrichment results in a significant increase in the percentage of hCD34+ cells extracted from human cord blood (here from 0.21% to 43.4%)

11. Transfer the layer between red phase and white ring to a 15 mL falcon tube. Top up the transferred liquid to 14 mL with wash buffer and centrifuge at 529 × *g* for 7 min 4 °C, brake on.
12. Remove the supernatant by pipetting off.
13. Stain the cells with Trypan blue and count the live cells.
14. (Optional) Stain the cells with hCD34 and hCD3 conjugated antibodies and analyze with flow cytometry (Fig. 2).
15. The isolated cells can be used immediately or frozen down in freezing solution for further use (*see* **Note 17**).

3.1.2 CD34+ Cell-Enrichment of Human Fetal Liver

1. Place the fetal liver (between 18–22 weeks gestational age) in a petri dish filled with 20 mL of DMEM.
2. Cut the liver into small pieces using a cell scraper to make a cell suspension (*see* **Note 18**).
3. Transfer the cell suspension to a 50 mL Falcon tube. Wash down excess tissue by adding more DMEM to the petri dish. Bring the tissue suspension to a total volume of 40 mL per Falcon tube with DMEM.
4. Spin at 529 × *g* for 7 min to pellet the cells, and then remove the supernatant.
5. Add 10 mL of sterile freshly prepared collagenase solution (*see* **Note 19**).
6. Incubate the cells at 37 °C for 30 min with shaking at 200 rpm.
7. Filter the tissue suspension through a 100 μm mesh cell strainer. Grind non-filtered tissue particles with the end of a

10 mL syringe plunger against the mesh to ensure that there are no remaining clumps.

8. Transfer filtered medium into a fresh 50 mL Falcon tube. Spin at 529 × *g* for 7 min to pellet the cells. Following centrifugation, remove the supernatant.
9. To achieve CD34+ cell enrichment and remove unwanted cells, add 200 μL of RosetteSep™ per 1 mg of the initial weight of the liver sample. Mix by swirling gently by hand and then incubate for 10 min at RT.
10. Top up the mixture with wash buffer to 20 mL and mix gently by hand.
11. Slowly add 10 mL of Ficoll Paque to the bottom of the tube using a sterile Pasteur pipette.
12. Centrifuge at 680 × *g* for 20 min, 18 °C with the brake off. At this step, it is important that the centrifuge is well balanced (*see* **Note 20**).
13. Transfer the layer between red phase and white ring to a 15 mL falcon tube.
14. Top up to 14 mL with wash buffer and centrifuge at 529 × *g* for 7 min 4 °C, brake on.
15. Remove the supernatant by pipetting off.
16. Stain the cells with Trypan blue and count the live cells.
17. The isolated cells can be used immediately or frozen down for further use.
18. Resuspend the cells with freezing media and aliquot 1 mL of the cell-media suspension into separate cryovials, and then freeze.

3.1.3 Immunosuppression of NRG Mice Through Irradiation or 5-FU

1. *Adult mice*: (*see* **Note 20**) Irradiation should be delivered in one dose (550 cGY). Only one or two mice can be restrained in the specific container for irradiation at a time. Immediately following irradiation, mice are injected with the isolated cells. Following this process mice are returned to their cage.
2. *Newborn pups*: Newborn pups are irradiated within 72 h of birth with two doses of 9 cGy, separated by 3 h. Immediately after the second dose of irradiation, hematopoietic stem cells are injected intrahepatically. The pups should be placed back in their cage with the parents and wean at 21 days of age (*see* **Note 21**).
3. *Adult mice*: Three days before cell injection, treat the adult mice with 5-FU at 150 mg/kg. 5-FU is administered via i.p. injection at a concentration of 10 mg/mL.

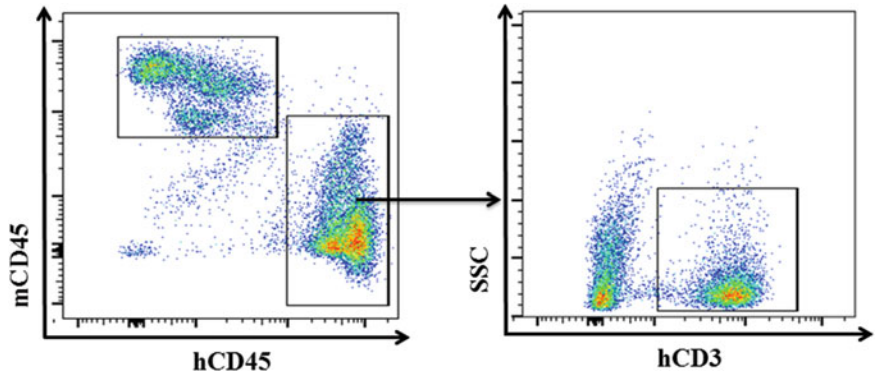

Fig. 3 Flow cytometric analysis of hCD45+ cell population in the blood of humanized mice. Shown are representative flow cytometric profiles from a humanized mouse 12 weeks after hCD34+ cell engraftment. Blood was stained with mCD45, hCD45, and hCD3 antibodies

3.1.4 Injection of Human Hematolymphoid Cells

1. *Intrahepatic (Pups)*: Resuspend 1×10^6 to 2×10^6 of thawed or freshly isolated HSCs in 30–40 μL of PBS (*see* **Note 22**).
2. Immediately following irradiation, inject pups intrahepatically with a 29 G needle. Return pups to their parents and wean at 21 days of age.
3. *IV (Adult)*: Put mice under a heat lamp to cause vasodilation. Ensure that the temperature does not exceed 32 °C (90 °F). Use a restrainer to immobilize mice. Swab the tail with an alcohol gauze.
4. Inject irradiated mice with 1×10^6 to 2×10^6 of thawed or freshly isolated HSCs resuspended in 200–300 μL of PBS into their lateral tail vein using a 1 mL insulin syringe, 30 G needle.
5. At 12 weeks post injection, retrieve 100 μL (2–3 drops) of blood from each mouse through facial bleeding. Stain blood samples with hCD45 and mCD45 antibodies and analyze the percentage of human CD45+ population (*see* **Note 23**) (Fig. 3).

3.2 Creating the Double Humanized FRG Mouse: The Human Liver and Immune System Chimera

3.2.1 Hepatocyte and Lymphoid Progenitor Cell Isolation from Human Fetal Liver

1. Place the fetal liver (between 18–22 weeks gestational age) in a petri dish filled with 20 mL of DMEM.
2. Cut the liver into small pieces using a cell scraper to make a cell suspension.
3. Transfer the cell suspension to a 50 mL Falcon tube. Wash down excess tissue by adding more DMEM to the petri dish and transfer to Falcon tube. Bring the tissue suspension to a total volume of 40 mL per Falcon tube with DMEM.
4. Spin at $529 \times g$ for 7 min to pellet the cells, and then remove the supernatant.

5. Add 10 mL of sterile freshly prepared collagenase solution to the cells and incubate at 37 °C for 30 min with shaking at 200 rpm.
6. Filter the tissue suspension through a 100 μm mesh cell strainer. Grind non-filtered tissue particles with the end of a 10 mL syringe plunger against the mesh to ensure that there are no remaining clumps.
7. Transfer filtered medium into a fresh 50 mL Falcon tube. Spin at 529 × *g* for 7 min to pellet the cells, and then remove the supernatant by pipetting off.
8. Stain the cells with Trypan blue and count the live cells.
9. The isolated cells can be analyzed by flow cytometry, used immediately, or frozen down for future use.
10. Resuspend the cells with freezing medium and aliquot 1 mL of the cell-media suspension among the appropriate number of cryovials.
11. If CD3+ cells are present following this isolation process and you wish to remove these cells, positive selection of hCD3+ cells is suggested (*see* **Note 24**).

*3.2.2 Depletion of hCD3+ Cells Using the PE Selection Kit (See **Note 25**)*

1. Resuspend the cells in DMEM to obtain a cell concentration of 2×10^8/mL and transfer up to 2.5 mL to a 5 mL polystyrene round Falcon tube (12 × 75 mm). If you exceed 2.5 mL, simply distribute the cell-media suspension among more tubes.
2. Add 100 μL/mL of human FcR blocking antibody to the cell suspension and mix.
3. Add the PE-conjugated antibody at a final concentration of 3 μg/mL to the cell suspension. Mix well and incubate at RT for 15 min.
4. Add EasySep PE selection cocktail at 100 μL/mL, mix well and incubate at RT for 10 min.
5. Add DMEM to the cell suspension to bring the final volume up to 2.5 mL. Mix the cells by gently pipetting up and down two to three times. Place the tube into the magnet and let it sit for 5 min.
6. Pour off the supernatant fraction into a 15 mL tube by inverting the attached magnet and tube.
7. Add 2.5 mL of DMEM to the tube and leave for 5 min. Repeat collecting the supernatant and add it to the tube containing the supernatant from the previous wash.
8. Spin at 529 × *g* for 7 min to pellet the cells and remove the supernatant by pipetting off (Fig. 4).

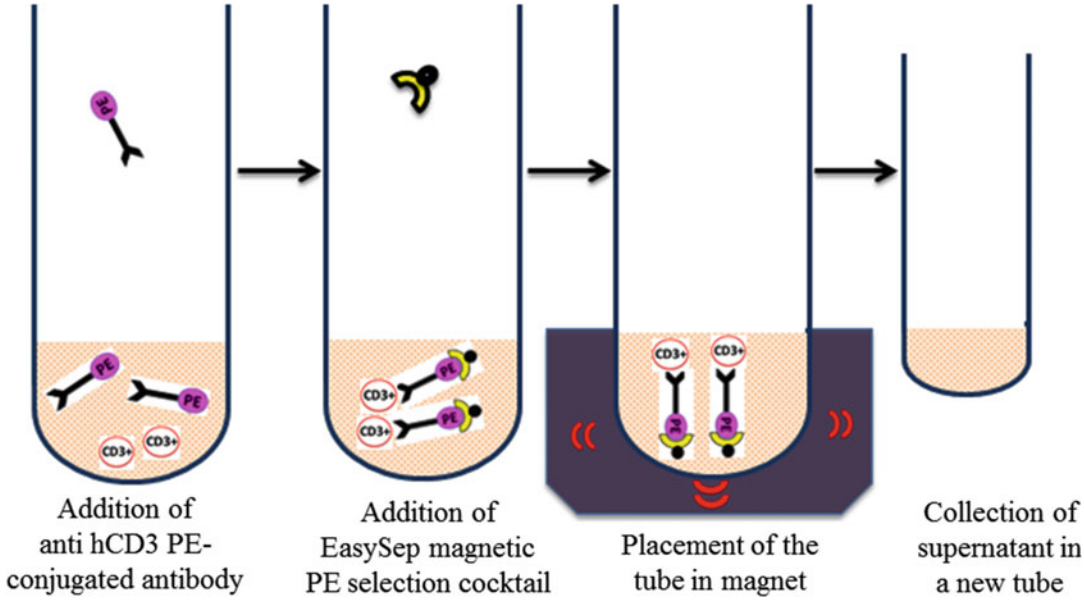

Fig. 4 Schematic overview of the hCD3+ cell depletion procedure using the PE selection kit

3.2.3 Immunosuppression of FRG Mice by Irradiation or 5-Fu

1. Irradiation should be delivered in one dose of 100 cGY before injection (*see* **Note 26**). After this irradiation process, and the subsequent injection of human cells, mice can be taken back to their cage.
2. For immunosuppression by 5-Fu, treat the adult mice with 5-FU at 150 mg/kg 3 days prior to cell injection. The 5-FU is administered through i.p. injection at a concentration of 10 mg/mL solution.

*3.2.4 Intrasplenic Injection of Human Liver Cells and Human Hematopoietic Cells [19] (See **Note 27**)*

1. Anesthetize mice by intraperitoneal injection of a cocktail of 100 mg/kg ketamine and 20 mg/kg xylazine. Administer Buprenorphine at 0.05 mg/kg via subcutaneous injection. During anesthesia, smear sterile petrolatum ophthalmic ointment onto the eyes of the mice to prevent the development of eye dryness as mice are unconscious and unable to prevent this from occurring.
2. Place the anesthetized recipient in a right lateral recumbence position, so that the left lateral side is exposed.
3. Using an electric razor, shave the hair over the left lateral side.
4. Wipe the area with 70% ethanol and sterile gauze; scrub area twice with Betadine.
5. Make a 1-in. vertical incision through the skin, above the spleen to expose the peritoneal musculature. Make a second incision of the peritoneal musculature under the opening of the

skin and gently exteriorize the spleen through the two incisions using forceps.

6. Use forceps to stabilize the spleen, inject human cells in a volume of 50 μL directly into the spleen.
7. To minimize the potential of cell backflow after the needle is withdrawn, place a cotton swab at the injection site with the needle still inserted into the spleen. Hold the swab at the injection site while removing the needle and remain holding the cotton swab at the site for an additional 5 s following the removal of the needle.
8. Carefully replace the spleen inside the peritoneal wall and suture the peritoneal cavity using 3-0 coated vicryl in an interrupted stitch pattern. Close outer incision with three small wound clips.
9. Wrap the mouse loosely in sterile gauze and place on a warming pad or under a warming lamp until the mouse is fully recovered from the anesthesia. Once ambulatory, return the mice to their cage. Monitor mice for signs of distress and treat humanely in accordance with institutional animal care protocols. Wound clips should be removed after 7–10 days.

Withdraw NTBC gradually over the next 5 days (*see* **Note 13**). Two weeks after stopping NTBC, the mice should be put back on NTBC for 5 days and then permanently taken off the treatment.

After 4 weeks, take blood from the surviving mice and measure human serum Albumin levels as an indicator of engrafted human liver cell function. After 12 weeks, analyze blood for the extent of hCD45+ cell reconstitution. The hCD45-reconstituted mice that produce human albumin can be used as humanized mice model for the study of hepatitis infection (Figs. 5 and 6) [19].

3.3 Discussion

3.3.1 The Contribution of Humanized Mouse Models to the Progression of Human-Specific Virus Research

The described processes of humanization and the types of immunodeficient mice used create a more complete and sophisticated humanized mouse model in comparison to the initial humanized mice developed. Even so, the more rudimentary humanized mouse models have played, and continue to play, an important role in our understanding of viral pathogenesis and the testing of therapeutic strategies. The new models have continued to enhance their benefits and contributions to the field of biomedical research [9, 19]. Unlike traditional animal models, human chimeric mice harbor diverse reservoirs of functional human immune cells, tissues, and/or organs [13], offering a platform for examining the human and virus interactions [9, 13]. The understanding of viral disease is becoming more clear as humanized mice are producing encouraging, clinically relevant data [9]. Humanized mice are allowing for the investigation of major human tropic viruses that have been previously deemed to create a pathogenic outcome exclusively

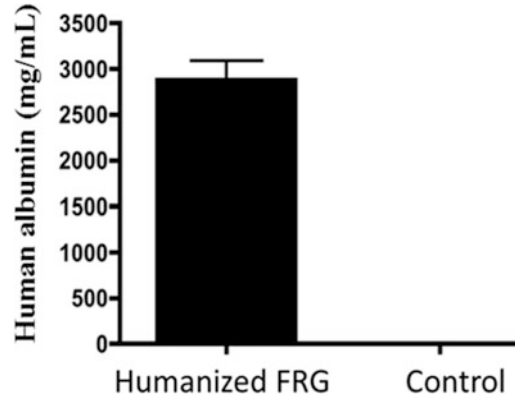

Fig. 5 Human albumin levels in the serum of engrafted FRG mice with human liver cells. The level of human albumin was measured by ELISA. Engraftment and clonal expansion of human hepatocytes within the mouse liver resulted in stable human albumin secretion into the blood. Human albumin production was not detected in FRG mice (control) without human liver cells. Error bars indicate SEM. Unpublished data from Ashkar lab

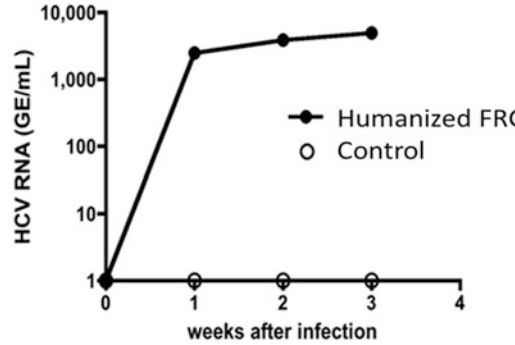

Fig. 6 Successful infection and proliferation of HCV in engrafted FRG mice with human liver cells. The level of HCV RNA in blood of double humanized mice was measured by Real Time PCR. HCV RNA was not detected in FRG mice (control) without human liver cells. Unpublished data from Ashkar lab

seen in humans. Human chimeric mice have proven to be capable of embodying the display of several human-specific viruses including, but certainly not limited to, DENV, EBOV, EBV, HCMV, HTLV-1, HIV, and HCV. As a result, humanized mice models are helping to reveal potential therapeutic targets and viral characteristics, thus providing insight into novel means of treatment and transmission prevention [8, 9, 33].

3.3.2 Dengue Virus (DENV)

In humans, it was previously believed that infection of Dengue virus (DENV) resulted in a self-limited disease, rarely with associated lethal consequences. In 1956, this perception changed when a deadly

variant of dengue emerged, causing fatal hemorrhagic fever in Southeast Asian children [34]. Since the 1950s, there has been considerable expansion in the geographic distribution of dengue throughout the world [34, 35] and an exponential increase in disease incidence [35], classifying dengue virus is the leading arthropod-borne virus to infect humans [34, 36]. It is now understood that DENV infection can result in a diverse spectrum of clinical manifestations, from a silent infection, often going unnoticed, to Dengue Fever (DF), Dengue Hemorrhagic Fever (DHF), and Dengue Shock Syndrome (DSS) [37]. The clinical syndromes are generally distinguished based on the severity of vascular leak and how severely the patient expresses signs of hemorrhaging. Clinical presentations can include fulminant hemorrhagic disease accompanied by the development of organ failure and encephalopathy; however, this is quite rare [37]. It is postulated that the immune mechanisms of antibody enhancement and T cell immunopathology have a critical role in the development of these severe diseases [35]. However, how a bite from an infected mosquito turns into these DENV-associated pathologies remains poorly understood [38].

3.3.3 The Humanized Mouse Model as a Faithful Tool for the Study of DENV Infection

In 1995, the potential use of the hu-PBL-SCID mouse was evaluated by Wu et al. [39–41]; however success was limited. Upon DENV inoculation, no signs of viral replication were observed, levels of viremia were very low, and no DENV-associated pathologies were observed. The low reconstitution of human monocytes and dendritic cells (DCs) within this model was suggested to account for this outcome. Fortunately, the succeeding humanized mouse models have been much more successful [39, 41] . In fact, a diverse range of humanized mice have been shown to be suitable for the investigation of DENV pathogenesis and disease. To achieve a more accurate representation of DENV infection within human chimeric mice, models reaching high levels of immune cell reconstitution of monocytes, and especially immature dendritic cells (DCs) with phenotypic profiles representative of human Langerhans cells present in the human skin, have been used [41]. NOD/SCID mice engrafted with CD34+ HSCs have demonstrated the ability to support reconstitution and development of functional DCs in relatively high amounts, displaying phenotypes characteristic to what define a complete DC repertoire in humans. Within NOD/SCID mice, DCs have a systemic distribution, described to be harbored within multiple organs, including the skin, lung, liver pancreas, spleen, bone marrow, and blood [41–43]. This enhanced support of the human DC population has led to its promise as an animal model for DENV. Upon subcutaneous inoculation, to mimic mosquito transmission, the virus is able to replicate, produce viremia and invade the spleen, skin, and liver. DENV is able to

induce the development of features indicative of human DF; mice present signs of fever, thrombocytopenia, and erythema [38, 41].

The humanized Balb/c Rag2−/− IL2rg−/− or double knockout (DKO-hu) mouse has also been shown to permit DENV infection, develop viremia, fever and uniquely, produce human anti-dengue neutralizing antibodies, of both IgM and IgG subtypes, in response to infection. This observation was the first documentation of a humanized mouse model to elicit dengue-specific primary immune responses during infection. This ability gives this model the potential for examining DENV-associated immunopathologies and novel vaccine strategies [44].

Another potential model for the study of DENV has proven to be the humanized NOD.Cg-Prkdc^{scid}Il2rg^{tm1Wjl}/SzJ (NSG) mouse. Following the subcutaneous, or "mosquito-like" inoculation of DENV, these mice are capable of embodying the human-like characteristics of DF showing viremia, fever, erythema, and thrombocytopenia [45]. The use of the HLA-A2 transgenic NSG mice has created a model in which DENV-specific HLA-A2 restricted T cell activity and antibody responses can be elicited following DENV inoculation [46]. To improve upon the established hu-NSG model, Jaiswal et al. implanted additional fetal thymus and liver tissues into the previously humanized NSG mice, developing the BLT-NSG mouse. In response to DENV, at frequencies similar to what is observed in humans, mice elicited HLA-A2 restricted T cell responses specific for multiple non-structural proteins. In comparison to the hu-NSG mice, the BLT-NSG mouse generated elevated antibody responses, persisting for several weeks during acute infection. The human B cells of these mice were also shown to be capable of maintaining their ability to secrete DENV-specific neutralizing antibodies long-term [47]. Jaiswal et al. then went on to conduct a detailed analysis of the human B cell compartment developed within the BLT-NSG mice and the impact of DENV infection on these mice. Similar to the functional characteristics described in the human antibodies isolated from patients, human antibodies isolated from mice during acute infection and from immunized BLT-NSG mice have been observed to be highly cross-reactive, have poor neutralizing ability, and are specific for intact virions [48].

The utility of the BLT-NOD/SCID mice and their applicability to preclinical testing has been described by Frias-Staheli et al. [49]. Sustained viremia and infection of leukocytes in lymphoid and non-lymphoid organs was observed post DENV inoculation. DENV infection stimulated the increase in serum cytokine levels and stimulated DENV-neutralizing IgM antibody production. Additionally, mice responded positively to antiviral drug treatment, thus highlighting the potential utility of this mouse model in testing novel therapeutics [49]. The previously described humanized mouse models are able suitable for the study of DENV; however, the only one model has been extensively used, the hu-NSG mouse.

3.3.4 Advancing Our Understanding of DENV Infection and Novel Antiviral Treatments Through the Humanized Mouse Model

The hu-NSG mouse has been used to examine the in vivo variances of DENV strains, examining a Southeast Asian (SE), American, Indian, and West African genotypes. In comparison to the impact the other virus genotypes had on the mice, the SE Asian virus consistently demonstrated a substantial enhancement of disease severity and viremia in both magnitude and duration. Results from these mice displayed patterns in accordance with the patterns of virulence and transmission observed among the geographical regions harboring these DENV genotypes. This model is capable of further examining the epidemiology of the virus [45]. The hu-NSG mouse has also been used in examining the amplifying role of mosquito inoculation and saliva. The mosquito bite as a means of transmission has been understood to play an integral role in the stimulation of cytokine secretion and the generation of DENV-specific antibodies. *Aedes aegypti*, the natural mosquito vector of DENV, was used to inoculate hu-NSG mice. Following mosquito inoculation, mice displayed heightened signs of pathogenesis and enhanced stimulation of the immune response to DENV [50]. Higher levels and sustained presentations of viremia, erythema, and thrombocytopenia were observed. Mice mounted an innate immune response, producing interferon (IFN)-gamma (γ) and soluble interleukin (IL)-2 receptor alpha. An adaptive immune response of anti-DENV antibodies was also produced. The reaction to an uninfected mosquito bite in hu-NSG mice stimulated the production of immunomodulatory factors including tumor necrosis factor alpha (TNF), IL-4, IL-10, and thrombocytopenia development [50]. This study offered the first investigation into the impact DENV infection on human immunity in the natural context of mosquito transmission [50].

The use of this humanized NSG mouse has also been described in examining the in vivo effect of the most virulent dengue serotype 2 strain. The administration of DENV resulted in infection of several tissues harboring human cells. In addition to the monocyte and macrophage-infected cells, T and B leukocytes were targeted within the spleen and bone marrow. As a result of this cellular targeting of the virus, production of the cytokines IFN-γ, TNF-α, IL-2, soluble IL-2 receptor, IL-10, IL-6, and chemokines MCP-1, IL-8 and VEGF occurred in a relatively similar profile observed in patients of either DHF or DF [51].

Humanized NSG mice have also been used to examine potential therapeutic approaches to DENV infection. A potential therapeutic option for dengue involves the delivery of small interfering RNAs (siRNA) to DCs and macrophages, the major in vivo targets of the virus and also the source of proinflammatory cytokines. A unique means of siRNA delivery, using a chimeric peptide consisting of the DC-targeting peptide fused to a nona-D-arginines (9dR), was used to target siRNA selectively to DCs. This DC3-9dR-

mediated delivery of the siRNAs was shown to suppress viral replication and restrain harmful virus-induced host immune responses to DENV within hu-NSG mice [52]. Hu-NSG mice have been used to examine the causal mechanisms to the common feature of DENV, thrombocytopenia. Significant depletion of megakaryocytes in the bone marrow of infected mice provided evidence, suggesting that depletion of human platelets may be a result of specific inhibition of the production of human megakaryocytes and their progenitor cells within the bone marrow [53].

3.3.5 Ebola Virus (EBOV)

Following the discovery of Ebola virus (EBOV) in 1976, the virus has resurfaced several times, producing disturbing epidemics, as case fatality rates reach an unsettling 90% [54]. The frequency of EBOV recurrence and consistently high rates of death has created a frightening pattern that has only recently generated a serious initiative for the development of vaccines and therapeutics. This recent drive stemmed from the 2013–2015 EBOV crisis, the largest epidemic since its discovery [55]. The hysteria and devastation that accompanied the display of EBOV's epidemic potential highlighted the unfortunate reality of how unprepared the health care system is in containing EBOV [56].

3.3.6 The Untapped Potential of Humanized Mice for the Study of EBOV

Only recently has there been consideration of humanized mice to study EBOV pathogenesis. To date, two models have been proposed for EBOV research; immunodeficient mice engrafted with human hematopoietic stem cells (HSCs) and the bone marrow, liver, thymus (BLT) model, each offering unique opportunities for the study of EBOV pathogenesis.

The first description of how humanized mouse models can be utilized for EBOV infection begins with the work done by Lüdtke et al. [57], where it was demonstrated that mice transplanted with human HSCs have the capacity to reproduce fundamental features representative of EBOV disease (EVD). The Lüdtke group utilized the immunodeficient NOD.Cg-Prkdc^{scid} Il2rg^{tm1Wjl} Tg (HLA-A2.1) 1Enge/SzJ (NSG-HLA-A2.1) mouse strain and engrafted CD34+ positive cells, derived from human umbilical cord blood of HLA-A2+ donors into the mice. Following the transplantation, peripheral blood, spleen, and bone marrow samples were found to contain human HSCs in the lymphoid and peripheral tissues. These tissues were occupied with fully differentiated human lymphocytes including T, B, NK, and NKT cells, as well as myeloid cells, including monocytes, granulocytes, and dendritic cells [57]. The presence of these cells is incredibly valuable in studying EBOV pathogenesis. How EBOV interacts with its initial target cells, dendritic cells, and macrophages, during the early stages of infection and how EBOV modulates the activation of these cells is highly influential on pathogenesis. Viral interactions with these cell types

dictate the quality and the development of the subsequent adaptive immune response, and ultimately, the outcome of infection. Examining the interaction of EBOV with endothelial cells and hepatocytes and how this interaction is involved in pathogenesis does not appear to necessitate further human organ transplantation as the murine equivalent cells have shown to be susceptible and permissive to infection [58].

A significant advantage to this model is that it permits the use of the wild-type EBOV isolates, which then causes disease. The use of wild-type EBOV has been unsuccessful prior to the use of humanized mice [57]. The Lüdtke group has provided the first small animal model with a human hematopoietic system that recapitulates main features of EVD pathogenesis, including viremia, cell and organ damage, and high lethality rates. Surprisingly, liver steatosis and hemorrhaging were also observed, which are features of EBOV disease in humans that remain to be well understood [59] and tend to not be recreated in the alternative mouse, and even nonhuman primate models [60]. Thus, this model can provide rare glimpses into EBOV pathogenesis [59, 60]. The utility of the BLT model for EBOV pathogenesis was recently examined by Bird et al. [61], showing that BLT mice are able to support EBOV infection and display characteristic disease symptoms, and eventually lead to a lethal disease roughly 2-weeks post inoculation. These mice were infected with wild-type EBOV isolates derived from human cases from the 1976 and 2014 outbreaks. The humanization of highly immunodeficient NOD.Cg-Prkdc^{scid}Il2rg^{tm1Wjl}/SzJ (NSG) mice with human bone marrow, liver, and thymus to create hu-BLT mice resulted in the enhancement of EBOV replication and virulence within the mice models. Infected mice were capable of supporting high levels of EBOV replication, developed histological changes within the liver, and alterations to their cytokine and chemokine profiles, each associated with fatal outcomes in patients [60, 61]. TNF-α, RANTES, IL-1a, IL-1RA, IL-6, IL-8, and IL-15 were all elevated in the hu-BLT mice, all of which are also associated with fatal human outcomes. This display of disease symptoms was consistently observed across each of the hu-BLT mice [61]. Engraftment of the human cellular immune system appeared to be an essential component for virulence within mice, as non-engrafted mice were unable to support productive EBOV replication or progress to a lethal disease [61].

To our knowledge, these humanized mouse models have yet to be utilized in the investigation of EBOV disease pathogenesis. The BLT and HSC models provide a valuable opportunity for the study of EBOV pathogenesis that has not been previously considered. Their utility should be taken advantage of and be used to evaluate EBOV pathogenesis in an in vivo human immune system model. These publications have highlighted models that provide opportunities that may lead to further insights into the immune mechanisms underlying human EBOV-associated disease [57, 61].

3.3.7 Epstein-Barr Virus (EBV)

Epstein-Barr virus (EBV) is a human herpesvirus [62], thought to have evolved with its human host species [63, 64] creating a predominantly harmless coexistence between EBV and the immunocompetent host [65]. The long history between EBV and humans has allowed EBV to acquire highly efficient mechanisms to modulate the human immune system and become an incredibly successful pathogen [64]. Through the simple exchange of infected saliva [66], EBV has been able to persist in over 95% of the adult population [64]. In immunodeficient hosts of EBV, the EBV-specific cytotoxic T cell response is absent, disturbing the equilibrium between virus and host defense. This removes the presence of a harmless cohabitation, giving an opportunity for EBV-induced B cell outgrowth and the development of EBV-associated diseases [65]. Once in contact with a human host, viral particles enter susceptible and permissive epithelial cells of the nasopharynx [64, 65, 67] where EBV then has access to naive B cells present in the submucosal tonsillar lymphoid tissues [65, 66]. These are the cells in which EBV establishes latency [65]. The majority of primary infections occur during the time of infancy and childhood, often resulting in an asymptomatic infection [68]. In adolescents and young adults primary EBV infection can be expressed as a lymphoproliferative disorder termed infectious mononucleosis [62, 63, 66, 68, 69]. In rare cases, primary EBV infection has the potential to develop into fatal infectious mononucleosis [68]. This human virus is associated with an incredibly large list of diseases, including lymphoproliferative diseases (LPD), malignancies, and autoimmune diseases [62, 63, 70]. EBV was the first human tumor virus described [66, 69, 71, 72], isolated over 50 years ago, yet the mechanisms of pathogenicity remain unclear, and there is no available therapeutic treatment or prophylactic vaccine [66, 71].

3.3.8 Hu-PBL-SCID Mouse: A Model for the EBV-Infected Immunocompromised Host

The hu-PBL-SCID model has been shown to represent an internal environment and elicit a response to EBV infection that is highly indicative of the immunocompromised host. Initial studies of the hu-PBL-SCID mouse for EBV provided the first available small animal model for EBV pathogenesis [62]. In 1988, Moiser et al. observed EBV-positive human B-cell lymphoma development following the injection of human peripheral blood leukocytes (PBLs) from EBV-seropositive donors [73]. Tumors were initially thought to resemble Burkett's lymphoma [65, 74]; however, further investigation by Okano et al. in 1990 [73, 75] and Rowe et al. in 1991 [65] found that the tumors that developed more closely resemble large cell lymphomas, of which are commonly seen in the immunocompromised patient [65, 75, 76]. In accordance with the presumed process of tumorigenesis within immunocompromised hosts, it has been speculated that the hu-PBL-SCID mice elicit weak immune responses to EBV, enabling B cell outgrowth [73, 76]. The B cells

of tumors developed within mice expressed productive cycle EBV antigens. Replicating forms of EBV DNA have been shown in biopsied tumors from EBV-infected immunodeficient patients; however, early and late proteins themselves have not been detected. This finding in the hu-PBL-SCID mice is the first documented evidence of EBV productive cycle antigen expression in human B cells in vivo, suggesting a role of EBV replication in B cell lymphomas [65].

In the original studies conducted by Mosier et al. in 1988, it was reported that the development of tumors from EBV-seropositive donors was not universal [73, 77]. A study by Picchio et al. further examined this heterogeneity among EBV-seropositive donor tumor induction [64, 78]. It was found that donors classified as "high-incidence" induced tumor development within all engrafted mice, and consistently displayed signs of EBV replication. Those donors with low or moderate incidence of tumor formation within engrafted mice showed varying levels of EBV replication among tumors. These results suggest that EBV replication is a nonessential component for tumorigenesis; however, it may have enhancing abilities [78]. This display of donor sensitivity may allow the hu-PBL-SCID mouse to serve as a tool for screening high-risk individuals, and predict the potential for EBV-associated lymphoma development [64, 78].

The hu-PBL-SCID mice have also demonstrated the importance of the CD4+ T cells in the development of EBV-associated lymphomas. These mice have shown that without the presence of CD4 or CD8 cells within EBV+ PBMC inoculum, there is a significant impediment on tumor formation. The CD4-depleted inoculum was shown to have a greater negative impact on tumor formation. This suggests that the presence of CD4+ T cells may assist in B cell expansion and tumor development [79]. This same concept has been shown through the administration of anti-CD4 ligand antibodies, delaying the appearance of tumors [79, 80]. Within hu-PBL-SCID mice, there is also a significant increase in IL-10 production, which is thought to be T-cell derived, encouraging malignant outgrowth by inducing cell immortalization and proliferation. This further suggests a role of T cells in EBV-associated tumorigenesis [81].

The SCID-hu model has mostly provided a means for the study of tumorigenesis in infected cells. The in vivo study of EBV infection had not been properly addressed [82], simply because the model is unable to do so; this model does not possess human immune effector populations, cannot support horizontal EBV transmission, and does not display the different stages involved in human B cell differentiation [83].

3.3.9 The Hu-NOD-SCID Mouse: A Model for Disease, the T Cell Response, and the Immunocompetent Patient

NOD/SCID mice engrafted with human peripheral blood mononuclear cells (PBMCs) (hu-PBL-NOD-SCID) have been shown to support EBV replication and latency within human B cells. EBV-associated lymphomas were not developed in this model. The hu-PBL-NOD-SCID mice were however able to elicit a CD8+ T cell response following EBV inoculation, most likely resulting in their resistance to EBV-associated lymphomas [84]. This model has thus highlighted the importance of the CD8+ immune response in maintaining a relatively harmless infection of EBV in its host. Wager et al. [84] have also shown that the resistance of these mice is removed following the depletion of CD8+ T cells, as mice quickly develop EBV-LPD [84]. This is an interesting contrast to the impact CD8+ T cells had on the development of lymphomas in the hu-PBL-SCID mice [77, 79, 80]. In a separate study humanizing NOD/SCID mice with CD34+ cells (hu-HSC-NOD-SCID), a similar role of T cells was observed [82]. Although the display of EBV infection in hu-HSC-NOD-SCID mice and the previously described hu-PBL-NOD-SCID mice [84] was very different, the role of T cells in dampening the occurrence of tumors remained. Within hu-NOD-HSC-SCID mice, the presence of engrafted T cells is very low, and the B cell population is dominating. However, within this humanized mouse model, unlike the hu-PBL-NOD-SCID model, EBV infection resulted in tumor development in multiple organs [82]. As previously mentioned, the removal of CD4+ or CD8+ T cells has shown to reduce the incidence of tumor development in hu-PBL-SCID mice infected with EBV [79, 80, 82]. However, the results in this current study suggest that tumor development is not dependent on T cell-B cell interactions or soluble factor(s) derived from human T cells. However, there may be a possibility of human T cells below the detection of flow cytometry, and this population of human T cells may be enough to stimulate tumor development [82].

3.3.10 The Hu-NOG Mouse Model: Offering a Complete Display of the EBV-Associated Diseases

Yajima et al. have revealed that EBV-associated pathologies in hu-NSG mice are developed in a viral dose-dependent manner [85]. Mice receiving low viral loads developed transient viral replication and developed asymptomatic infection. Mice receiving high doses developed LPD [85]. This dose dependency suggests that the horizontal transmission of the virus is an important factor in EBV-associated lymphoma formation [83]. Yajima et al. later showed that the CD8+ T cell response induced within the hu-NOG mice was able to suppress EBV-induced transformation of B cells, showing that the involvement of the CD8+ T cell response is what results in the effective containment of viral infection [86]. Humanized NOG mice with full T cell development were shown to have significantly longer life spans after EBV infection compared to those with minimal T cell development. Removal of CD3+ or CD8 + T cells from EBV-infected humanized mice was shown to reduce

the lifespan of mice infected with EBV [86]. The results imply an important protective role for the reconstituted human T cells present within hu-NOG mice during EBV infection, an observation possibly translatable to human infection [79].

Additionally, the NOD/Shi-sicd/IL-2rg^{null} (NOG) mouse has also shown to display symptoms of EBV pathogenesis unique to all other humanized mouse models, allowing for the investigation of EBV-associated pathologies beyond lymphomas. These mice have been shown to display symptoms representative of what is seen in patients with EBV-associated Rheumatoid arthritis (RA). The ability of these mice to display these symptoms has provided the first documented description of direct evidence for the relationship of EBV and RA [87]. This unique display of EBV-associated pathologies extends to Hemophagocytic Lymphohistiocytosis (HLH), a rare life-threatening disease induced by EBV infection [87, 88]. Humanized NOG mice were shown to display symptoms indicative of HLH [89]. Interestingly, the NOG mice capable of displaying HLH and B cell lymphomas were humanized in the same manner. Differences in the sex and age of the mice may have contributed to these findings. This observation is quite fascinating, showing how malleable humanized mice are; by making small changes in the protocol, they can become a platform for entirely different pathologies [89].

The hu-NOG model has been used to examine potential vaccine strategies, such as examining the potential protective effect of targeting the EBV nuclear antigen 1 (EBNA1) to the human multilectin DEC-205 receptor. Vaccination of hu-NOG mice with the aDEC-205-EBNA1 antibodies revealed that this targeting primes EBNA1-specific T cells and stimulates antibody production [87]. This data suggests that DEC-205 targeting may be a potential vaccination approach against symptomatic primary EBV infection and EBV-associated malignancies [87].

3.3.11 The Hu-NSG Mouse Model: A Reliable Recreation of EBV Infection and Pathogenesis

Lee et al. [90] have revealed the influential role of the immune cell composition of the hu-NSG mouse on the outcome of EBV infection and the progression to Hodgkin (HL) or non-Hodgkin's lymphoma (NHL). Mice with human T cell dominant immune profiles were observed to develop additional pathologies, including diffuse large B-cell lymphoma (DLBCL) and HLH in comparison to mice with a more dominant B cells population. HLH development was exclusively seen in mice with an activated T-cell environment, while those mice with an environment of suppressed T-cell activity often progressed to NHL. In those mice with a suppressed T-cell milieu, immature B cells were the principal immune cell at the time of EBV inoculation [90].

Humanized NSG mice have been used to investigate the role of the lytic cycle of EBV in EBV pathogenesis and tumorigenesis.

NSG mice, humanized with CD34+ cells and thymic/liver tissues, were inoculated with either a replication-defective EBV mutant, or a lytically active control strain. The frequency of tumor progression appeared to be impaired in mice infected with the replication-defective mutant in comparison to the enhanced tumor development observed in mice infected with lytically active EBV. The results suggest that the development of B cell lymphomas may be highly influenced by lytic EBV infection in the context of an active host immune response. The work by Ma et al. was the first documented examination into the influence of the EBV lytic cycle on lymphoma progression within the context of a self-educated immune system [83].

Humanized NSG mice have been utilized in highlighting the importance of the NK cell response to EBV infection and the dynamics of this viral-specific immune control. These mice have revealed that during primary EBV infection, if unrestrained by NK cells, EBV can replicate at high viral titers, driving lymphocytosis and promoting EBV-associated lymphoma development. In the huNSG mouse model, features of symptomatic primary EBV infection are enhanced in mice depleted of human NK cells. The protective effect of NK cells in response to EBV appears to be absent when combating latent infection [91]. This model holds great value in the investigation of primary EBV infection and the development of therapeutics and vaccines, shifting the focus toward a novel approach and harnessing the capabilities of the NK cell response. The observation that insufficient NK cell activity can increase the incidence of EBV-associated cancers can be used as a diagnostic tool for identifying uninfected individuals at risk for developing infectious mononucleosis. Prophylactic approaches can then be developed for this population [91].

Humanized NSG mice have shown the surprising in vivo influence of the EBV latency-associated gene product, EBNA3B [92]. In vitro, EBNA3B-knockout EBV mutants have been shown to transform B cells with efficiencies identical to the wild-type virus. EBNA3B knockout mutants within humanized NSG mice, however, have shown heightened tumorigenic capacities, demonstrating a potential role for EBNA3B in tumor suppression [63, 92]. In hu-NSG mice, the loss of EBNA3B resulted in profound deviations in the character, immune evasion, and aggressiveness of the EBV-associated cancers. Displaying features reminiscent of DLBCL patients, cancers contained no infiltrating T cells and presented as monomorphic DLBCL-like tumor masses, invading and destroying the integrity of the spleen of the mice [92]. This discovery of the EBNA3B function in human lymphomas emphasizes the predictive power of humanized mice as they more accurately represent a human environment to examine viral pathogenesis [92].

Humanized NSG mice have been used to examine the in vivo role of EBV BHRF1 miRNAs in attempts to determine their utility as a viral target in the treatment of latency III EBV-associated malignancies. Results indicate that BHRF1 miRNAs accelerate the development of acute systemic EBV infection; however, they are not required, nor do they enhance the formation of latency III EBV-associated malignancies [93].

Furthermore, these mice have been able to demonstrate the utility of the adoptive transfer of EBV-specific CD8+ T cell clones, showing their ability to transiently modulate EBV infection. CD8+ T cells against the lytic EBV antigen, BMLF1, were shown to eliminate lytically replicating EBV-transformed B cells, and regulate the viremia of the infected huNSG mice. These findings suggest a protective role for lytic EBV antigen-specific CD8+ T cells against EBV infection and virus-associated tumors in extra-lymphoid organs. This may be very useful in the development of vaccines [94].

3.3.12 An Additional Humanized Mouse Model for the Study of EBV Pathogenesis

Balb/c Rag2−/− IL2rg−/− (DKO) mice engrafted with human CD34+ stem cells have been shown to support EBV infection and mount CD8+ T cell immune responses specific for EBV [95]. However, it has yet to be used in testing EBV pathogenesis or antivirals.

3.3.13 Human Cytomegalovirus (HCMV)

Human cytomegalovirus (HCMV) is one of the human tropic pathogens that commonly exists within its natural host giving little indication of infection. As a result of its silent existence, HCMV has established infection inside the majority of the human population [96–98]. HCMV remains latent within the myeloid cells of the bone marrow and undergoes intermittent cycles of reactivation [97]. The promiscuity of HCMVs cellular tropism enables a more effortless systemic spread within and between hosts. HCMV tropism extends from epithelial cells of gland and mucosal tissue to smooth muscle cells, fibroblasts, macrophages, dendritic cells, hepatocytes, and vascular endothelial cells [97]. The relatively harmless infection established within immunocompetent hosts becomes life-threatening in those with immune deficiencies [97]. HCMV is recognized as the leading infectious cause of birth defects and life-threatening lung-associated diseases in premature infants and immunocompromised children [99]. Furthermore, chronic HCMV infection may lead to excess mortality within the general population. The extensive cellular tropism of HCMV is a likely contributing factor to its ability to causes a diverse range of pathologies [99]. There have been several HCMV antiviral drugs approved; however, the associated toxicity and the possibility of drug resistance decrease their value. It is thus imperative to develop alternative therapeutics for those living with HCMV and a vaccine strategy to prevent transmission, especially to those with high risk of developing fatal illness as a result of infection [100].

3.3.14 How the Simplest of Humanized Mice Have Expanded Our Understanding of HCMV

The use of the SCID-hu Thy/Liv mouse in 1993 was not only the first documented use of humanized mice for HCMV, but also the first animal model allowing for the study of HCMV tissue tropism, latency, pathogenesis, and therapeutics. Mocarski et al. revealed the ability of the SCID-hu Thy/Liv mice to support the replication of HCMV and make the in vivo study of this virus a possibility [101]. Additional experimentation of SCID mice implanted with human lung, colon, and skin was also shown to support viral growth. In each implant type, the detection of HCMV was restricted to the implanted human tissues [101]. This model has helped to investigate the tissue and cell tropism of HCMV in an in vivo context, displaying results contrary to in vitro findings. The cellular tropism displayed in vitro suggests a proclivity for viral replication within human myeloid and lymphoid cells; however, HCMV infection in the SCID-hu Thy/Liv mouse has not shown widespread viral replication within these cell types [101]. The replication and latent infection of myeloid cells is an important feature that should be observed within a humanized mouse model [102], although lymphoid cells have not been described as a primary target of HCMV [103]. The results obtained from the SCID-hu Thy/Liv mice more accurately demonstrate the importance of epithelial cells in the process of HCMV infection [101]. This initial utilization of the SCID-hu Thy/Liv mice emphasized the unique experimental conditions that these humanized mice offer that cells grown in culture are incapable of providing [101].

From this initial use, several aspects of HCMV have been examined through the use of the SCID-hu Thy/Liv model and SCID-hu variations. The SCID-hu Thy/Liv model has been used to examine variances of virulence among different HCMV strains and the role accumulating mutations can have on infectivity as a result of propagating HCMV in cell cultures. To do so, Brown et al. in 1995 evaluated the low-passage strain, Toledo, and compared its activity to the highly passaged strains, AD169 and Towne [104]. The Toledo strain achieved higher levels of efficient replication within the humanized mice in comparison to the high-passage strains. This experiment shows how features critical to in vivo infection can be lost through in vitro culturing [104]. An extension to the study by Brown et al. examined the 15-kB segment, which is a significant differentiating factor between the low and high-passage HCMV strains. This segment is found to be present among all virulent HCMV strains; however, it is often found deleted in attenuated strains. This pattern proposes a critical role for these genes for the in vivo replication of HCMV [98, 105]. With the use of the SCID-hu Thy/Liv mice, Wang et al. were able to provide the first confirmation of this critical role these 15-kB genes have on HCMV replication [105]. The role of additional genes for HCMV replication has been examined in SCID-hu Thy/Liv mice, including the UL27 gene [100], which was determined to be nonessential [98,

100]. Regardless of the technical restraints on this system [105], this work [100, 101, 104, 105] has shown how respectable the SCID-hu model can be for investigating the functions of HCMV genes and their role in the virulence [105]. Of course, these are not the only critical aspects to HCMV infection. In humans, HCMV causes a systemic infection capable of invading every organ of the body. Unfortunately, the SCID-hu mouse model is unable to provide a means of examining the complete spectrum of tissue tropism, nor can this model help in our understanding of latency or reactivation. Additionally, the SCID-hu model does not elicit an acquired immune response to HCMV, removing their potential for studying post-vaccine challenges [105]. However, in attempts to expand the SCID-hu model's ability to examine various aspects of HCMV infection, several modifications have been made. Implantations of various human tissues within the SCID mouse have allowed for the recapitulation and study of additional HCMV-associated pathologies.

SCID mice, humanized with human fetal liver tissue, have offered the first demonstration of HCMV-induced fetal pathogenesis [40]. Maidji et al. have shown that this unique model system is capable of recreating the process of fetal and neonatal lung development, highly permissive for HCMV infection. One of the major targets for HCMV is the fetal lung, yet, this form of HCMV-induced pathogenesis had not been explored prior to the use of this humanized mouse model [99]. The utility of alternative SCID-hu models also extends to examining the series of injuries during congenital HCMV infection that lead to disease. Tabata et al. made used of a humanized SCID mouse to model placentation by engrafting human placental villi into SCID mice [106]. It was shown that the ability to invade and remodel resident arteries was significantly hindered in HCMV-infected cytotrophoblasts [98, 106]. Transgenic liver injury SCID/ALB-UPA (severe combined immunodeficient/urokinase type plasminogen activator under the control of an albumin promoter) mice, humanized with adult hepatocytes, have provided a means for exploring HCMV pathogenesis within the liver [107]. Infection of these mice resulted in the distinctive "Owl's eyes" formation to occur within infected human hepatocytes. In the same study, the potential of NK cell adoptive therapy for relieving HCMV liver infection was examined. Remarkably, the adoptive transfer of human liver NK cells prior to viral inoculation reduced HCMV viral loads, signifying a role for human liver NK cells in inhibiting HCMV replication [98, 107]. Retinal transplant models have also allowed for the investigation of viral replication dynamics and viral genetics [38]. This mouse was used to examine the replicative ability of the AD169, Towne, and Toledo strains of HCMV [108]. Similar to Brown et al. [104], observations in HCMV replication kinetics were analogous; neither

AD169 nor the Towne strains of HCMV were capable of replicating in the implanted human retinal tissue, while the replication of the Toledo strain was very proficient within the human cells [108].

As a means of investigating potential antiviral therapies, humanized SCID mice engrafted with human thymus and liver, or human retinal tissues have been a reliable platform for examination [98, 108–110]. Each model possesses susceptible human cells in different regions of the mouse anatomy. This differential placement of cells capable of supporting HCMV infection may result in each model representing separate drug bioavailability characteristics due to the potential impact of the blood-eye barrier in the retinal SCID-hu model. For this reason, it has been proposed that the evaluation of antiviral activity of potential therapeutics should involve both the SCID-hu Thy/Liv model and the retinal implant SCID-hu model [98, 108].

To test novel antiviral drug candidates, additional variations of the SCID-hu mouse model have also been quite useful. These models attempt to offer a means of human cell implantation that removes the technical challenge and eliminates the human fetal tissue requirement present in other SCID-hu mice [110–112]. For example, a model developed by Weber et al. involved the transplantation of hollow fibers encompassing HCMV-infected human cells into immunodeficient NOD-SCID mice. This variation of the humanized mouse model has been used to investigate the anti-HCMV ability of the novel non-nucleosidic compound 3-hydroxy-2,2-dimethyl-*N*-[4(([5-(dimethylamino)-1-naphthyl]sulfonyl)amino)-phenyl] pronanamide (BAY 38-4766). The BAY 38-4766 drug candidate was determined to parallel the antiviral activity levels of ganciclovir [98, 112]. Bravo et al. have explored the usefulness of engrafting Gelfoam gelatin sponges harboring HCMV-infected human foreskin fibroblasts into SCID mice, and the potential value of this model in evaluating new anti-HCMV compounds [98, 110]. The Gelfoam sponges technique used in a mouse model of HCMV was first described by Chong et al. HCMV was reported to replicate to high viral titers within SCID mice and responded positively to antiviral therapy [110]. Bravo et al. extended these results, further illustrating how HCMV replication occurs within this model and its use as a drug-testing platform. Vascularity was described to have a persuasive role in the antiviral activity of drugs, with increased vascularity leading to enhanced antiviral ability [110]. By a similar means of investigation, Lischka et al. examined the novel anti-viral properties of AIC246 [40, 52], which were shown to exhibit a potent in vivo efficacy within this mouse xenograft model [111].

3.3.15 The More Sophisticated Humanized Mice and the Investigation of HCMV Latency and Reactivation

The humanized mouse models built on more refined immunodeficient backgrounds have been well suited for the study of HCMV latency and reactivation [98]. The humanized NSG mouse has been described as the first documented humanized mouse model to provide a suitable platform for the in vivo investigation into the mechanisms behind HCMV latency and reactivation [102]. Prior to 2010, the SCID-hu Thy/Liv model was the dominating humanized mouse for the study of HCMV [102]. However, the functional pitfalls of this model restricted investigation to HCMV replication and antivirals. It is no doubt that this model has been useful; however, latency and reactivation are critical aspects of HCMV that must also be examined to develop highly effective prophylactic and therapeutic drugs [102]. The hu-NSG mouse has been able to confirm the importance of the granulocyte-colony stimulating factor (G-CSF) in stimulating the reactivation of HCMV from within latently infected myeloid cells and the subsequent dissemination of HCMV to other tissues of the host [98, 102]. This observation may give insight into the observed increase of HCMV-related disease development within patients receiving G-CSF-mobilized blood products [102]. In a complementary study, Hakki et al. [113] utilized the humanization process of the NSG mouse to simulate the transmission of HCMV by means of transplanted G-CSF mobilized peripheral blood stem cells from a seropositive donor to a seronegative patient. It was determined that these cells represent a source of infectious virus, capable of transmission and dissemination of HCMV [98, 113]. This hu-NSG model offers a platform to explore the influence of factors present within the allograft that have been found to be associated with transmission [113]. Furthermore, hu-NSG mice have provided insight into the characteristic functions of HCMV gene products involved in the establishment and maintenance of latency and their purpose in reactivation [98]. Umashankar et al. have examined the role of the UL133–UL138 locus in viral persistence and spread. Following stem cell mobilization, viral mutants lacking the UL133–UL138 locus developed infection with increased viral replication and dissemination to the wild-type virus within infected hu-NSG mice. It was determined that this locus is an important modulator of latency and reactivation within the viral life cycle of HCMV [98, 114].

3.3.16 Hepatitis C Virus (HCV)

First identified in 1975 as "non-A, non-B viral hepatitis," hepatitis C virus (HCV) [115] like all viruses mentioned in this paper has established itself as a major human-specific pathogen creating global health concerns [9]. Initially, HCV was infecting the world's blood supply; however, despite the tools created to control its spread through means of transfusion [115], over 30 years later, there are at least 175 million individuals currently infected [9, 116]. A minority of infected individuals (10–20%) are capable of

spontaneously clearing HCV, and for the remaining large majority of individuals, infection becomes chronic [9]. Chronic HCV infection often results in hepatitis, liver fibrosis, cirrhosis and the development of hepatocellular carcinoma (HCC) [9, 116]. The human immune system holds an incredibly valuable role in both the potential clearance of infection, and if not achieved, has contribution in the progression of disease. Given these circumstances, detailed studies of the immune response are critical to fully understand the factors permitting viral clearance and disease progression to create successful preventative and therapeutic approaches [9].

3.3.17 The Human Liver Chimeric Model

The human liver chimeric mouse has provided the unique ability to investigate HCV in its native human liver milieu [117]. A model like this is an exceptional preclinical tool for examining drug metabolism and pharmacokinetics, and understanding the pathogenic mechanisms of hepatotropic pathogens, like HCV [118]. To create this mouse model, human hepatocytes are engrafted into an immunodeficient mouse strain suffering from liver injury. The proliferative stimulus provided by the liver injury offers the human cells an aggressive growth advantage over the inadequately functioning hepatocytes of the mouse recipient [117]. The human hepatocytes harbored in the mouse liver retain their normal function [119] and human-like metabolic and toxicologic profiles [117, 119]. This process of reconstitution results in mice with a human chimeric liver that renders them highly susceptible for human hepatotropic pathogens, hence enabling the study of HCV biology and the evaluation of different antiviral strategies [120]. These models are capable of supporting the replication of clinical isolates, a unique observation in comparison to the in vitro models that are incapable of supporting clinical HCV isolates [120]. Susceptibility to HCV infection in human liver chimeric mice has been described in several mouse strains with varying types of liver injury. These mice include the Alb-uPA [119, 121], FAH−/− [122], MUP-uPA [123], and TK-NOG [124] strains.

3.3.18 The Human Liver Chimeric Alb-uPA Transgenic Mouse, the First Fully Permissive Murine Model for HCV Research

In 1990, Heckel et al. created the Alb-uPA transgenic mouse model, expressing the urokinase-type plasminogen activator, under the control of the mouse albumin enhancer/promoter [119, 125] creating a functional liver deficit in the mice, providing the supportive niche for liver regeneration [119, 126]. When backcrossed onto a genetically immunodeficient mouse strain, most commonly SCID, this transgenic mouse has the ability to allow for liver repopulation by human hepatocytes [119, 121]. This model has been described as the first murine model fully permissive to HCV and capable of supporting long-term infection [120]. From the several studies conducted with these mice, the value of the SCID/Alb-uPA in the study of drug metabolism and hepatitis research is markedly evident [127].

Several aspects of HCV virology, transmission, and disease have been examined in this model. It has been previously understood that HCV itself does not kill liver cells, but the indirect stimulation of the immune system in attempts to kill HCV-infected liver cells is what causes this apoptosis. However, SCID/Alb-Upa mice lack a functional adaptive immune system, yet infected liver cells were still observed to be dead. Thus, these liver chimeras have revealed new insight into means of HCV liver damage in chronic HCV carriers [128]. The SCID/Alb-uPA mouse has also been used in examining the viral evasion strategies in recurrent infection following liver transplantation [129]. This study confirmed the presence of rapid evolution of the quasispecies and evasion of host immunity following the liver transplant, emphasizing the incredible adaptive ability of HCV to a changing environment [129]. In a separate study, the development of HCV variants following transmission was examined. It was shown that HCV envelope variants acquired post transmission developed phenotype enhancing its ability for cell entry in comparison to the variant in the initial inoculum. All post-transmission E1E2 glycoprotein gene sequences had lost a potential N-linked glycosylation site in E2, a feature that appeared to be integral for the improved entry phenotype [130]. These liver chimeric mice have also highlighted a correlation between the microRNA, miR-27, expression levels, and lipid accumulation in HCV infection. This relationship revealed a novel factor in the mechanism for hepatic steatosis development [131]. This model has been used to study the importance of the conserved RNA stem-loop structures predicted in the HCV core encoding region in HCV replication [132]. This strain of liver chimeric mice has also enabled the in vivo examination of the environmental and thermostability of the known HCV genotypes for understanding HCV cross-contamination within the environment [132]. Mice have been used to examine the potential utility of reporter viruses for high-throughput fluorescence- and luminescence-based studies of HCV-receptor interactions and serum-neutralizing antibodies [133] and investigate the in vivo behaviors of in vitro culture adapted HCV genomes [134, 135].

3.3.19 The SCID/Alb-uPA Liver Chimeric Mouse for Examining HCV Therapies

In HCV patients of both acute and chronic infection, the presence of neutralizing antibodies in their plasma implies a role in infection yet to be determined [119]. The chimeric liver mouse model has revealed an in vivo protective role of neutralizing antibodies in the transmission of HCV [119, 136]. In a separate study, monoclonal antibodies against the HCV E2 protein isolated from a patient with chronic HCV infection were shown to achieve effective passive immunization of SCID/Alb-uPA mice. Treatment provided a transient protective effect against an HCV isolate from a heterologous patient with the same HCV genotype [119, 137]. The results from

these studies on the liver chimeric mouse have been promising for the development of vaccines and prophylactic therapies using monoclonal antibodies. However, the transient protection demands for the search of a stronger antibody with long-term protective effects [119]. Opposed to the development of an HCV-specific antibody, studies have tested the utility of antibodies against the cellular receptors involved in the HCV infection, interfering with this viral-host interaction [119]. Antibodies against the CD81 cellular receptor offered complete protection from HCV in the liver chimeric mice [119, 138].

The utility of the SCID/Alb-uPA chimeric mouse in examining treatment options is validated by their human paralleled responsiveness to the IFN-α, BILN-2061, and HCV371 antiviral regimens [139]. Following the discontinued BILN-2016 clinical trial, studies on this drug using chimeric mice displayed disturbing pathological effects of cardiotoxicity, confirming the potential adversities as indicated by the Reiser et al. study on rhesus monkeys [140]. The observed similarities further validate the use of SCID/Alb-uPA mice in examining the preclinical efficacy and safety of antiviral compounds [141]. To test the therapeutic potential of DEBIO-025, a molecule derived from cyclosporine A (CsA) that lacks its immunosuppressive effects, DEBIO-025-treated mice were challenged with HCV; however, administration as a monotherapy was unsuccessful [119, 142] . The combinatorial effect with pegylated-IFNα-2a (Peg-IFN) decreased HCV RNA levels over 100-fold. The use of CsA in combination with Peg-IFN caused death in all mice within a four-day span. This study revealed the potential of more tolerable DEBIO-025 in vivo as an anti-HCV when in combination with Peg-IFN [142]. Another potential means of HCV therapy involved the inhibition of serine palmitoyltransferase (SPT), suppressing HCV replication [143]. The SPT inhibitor, myriocin, was shown to suppress HCV replication within the liver chimeric mice with enhanced effects when combined with Peg-IFN. Following this treatment, high levels of HCV re-established within the mice [119, 143]. Additionally, the toxicity of myriocin renders it unsustainable as an anti-HCV drug in humans. However, results indicate targeting SPT should be further examined as an anti-viral and inhibitors similar to myriocin should be explored in the development of anti-HCV drug [143]. A novel gene therapy approach by Hsu et al. aimed to induce the apoptosis of HCV, targeting the NS3/NS4A serine protease of the virus. The precursors of caspase-3 and BID were engineered to contain a specific cleavage site recognized by the NS3/NS4A protease. It was demonstrated that non-replication adenovirus expressing modified BID can cause HCV-dependent apoptosis in the infected liver chimeric mice and reduce serum viral titers by 100- to 1000-fold. In mice with low viral titers at the time of the therapeutic trails, HCV was found to be cleared [119, 144].

3.3.20 The Potential for the Liver Chimeric FRG Mouse in the Study of HCV Pathogenesis and Therapeutic Strategies

Another mouse strain harboring massive liver injury is the strain-deficient tyrosine catabolic enzyme fumatylacetoacetate (FAH−/−) [127, 145, 146]. The creation of the triple mutant, FAH−/− / Rag2−/−/Il2rg−/− (FRG) mouse, permits the expansion of human hepatocytes [127, 146]. A unique feature of this model is that the liver injury can be modulated through the administration or removal of the protective drug 2-(2-nitro-4-trifluoromethylbenzoyl)-1,3-cyclohexanedione (NTBC) [127, 146]. When liver chimerism is high, this model can support HCV infection [122]. Additionally, when tested with HCV antivirals, where the expected response is known, all chimeric mice responded as anticipated and tolerated the therapies well. These tests included the combined therapy of Peg-IFN and the nucleoside analog ribavirin, and DEBIO-025. Furthermore, when inoculated with a clinical isolate of HCV genotype 3a, the foreseen sensitivity to Peg-IFN treatment was observed within mice [122].

Two additional models MUP-uPA [123] and TK-NOG [124] have been shown to successfully support human liver reconstitution and HCV infection. Despite their potential, their use in HCV research has not been extensive.

3.3.21 Creating the Ideal Human Liver and Immune System Mouse: A Complete Model for HCV Research

The human liver chimeric mouse has established the foundation for creating the most ideal animal model for the study of HCV, and until recently has been the most advanced small animal model available [147]. Despite the merit of this model, it does not possess a human immune response [116]. In the absence of this essential component, comprehending the full story behind the HCV-host interaction and examining potential immunotherapies and vaccines becomes a questionable task. The development of an immunocompetent model has been an ongoing task. One means of achieving this model has been to create a chimeric mouse containing a human liver and an immune system [147].

In 2011, Washburn et al. took the first step in creating the double humanized mouse [147]. To facilitate the engraftment of syngeneic human hepatocytes and HSCs, a unique ACF8-hu HIS/Hep model was created [116, 147]. In Balb/c Rag2−/−γc-null mice, to encourage human hepatocyte engraftment, the FK506 binding protein (FKBP) and caspase 8 were expressed under the control of the albumin promoter (AFC8), which induces liver cell death. Following the engraftment of both HSCs and hepatocyte progenitors, the resulting double humanized mouse was able to support HCV infection of primary isolates. In response to HCV, mice generated a T-cell-specific immune response and developed liver pathologies including hepatitis and fibrosis [116, 147]. These observations had not been described previously in the chimeric liver models. Despite the promise of this model, it should be noted that HCV was detected at low levels only within the liver of the animal

and failed to be present within the serum. This frail response may result from inadequate liver reconstitution (10–30%), while over 50% repopulation is usually required for a robust persistent HCV infection. Furthermore, the lack of antibody response as a result of fully functional B cell reconstitution eliminates the potential for examining this role in pathogenesis and may impede on the development of effective preventative vaccines [147].

The pursuit for the superior strain of mouse for dual reconstitution and available tissue sources continues [148]. In 2013, Gutti et al. examined the potential dual reconstitution in uPA-NOG mice, comparing adult and fetal hepatocyte reconstitution and the impact of mismatched donors. The source of the hepatocytes and HSCs must be syngeneic for immune system reconstruction in experimental animals. The fetal liver provides both cell types; however, the expansion and survival of these cells has not been entirely successful in the adult mouse liver. Obtaining two types of cells from the same adult donor is very difficult, limited to only a few centers with human tissue biorepositories. Thus, MHC mismatched hepatocytes and HSCs transplanted into these mice were used in addition to testing reconstitution with fetal hepatocytes. Stable dual reconstitution was achieved with mature hepatocytes, and not fetal hepatocytes, with MHC mismatched HSCs [148]. In a separate study, a different mouse strain, BALB/c Rag2−/−IL-2R*γ*c−/− NOD.*sirpa* uPA$^{tg/tg}$ (BRGS-uPA), was successfully humanized with mismatched fetal HSCs and adult hepatocytes. High levels of liver chimerism and a robust engraftment of human myeloid and lymphoid cell subsets were observed to be maintained for the duration of 5 months [149]. Billerbeck et al. [18] described a syngeneic model in FNRG, fah−/− NOD rag1−/−il2rg^{null} successfully reconstituting fetal-derived HSCs and hepatocytes and developing a profound immune population, with T cells, B cells, monocytes, and NK cells. The key ingredient to their success of fetal hepatocyte engraftment was human Oncostatin M. Mice were described to support HCV infection and develop viremia [18].

These models have yet to be used for studying HCV, and of course further improvement should be made to create the best model. However, given their unique ability to permit HCV infection, mount an immune response to infection, and develop liver pathologies, the predictive power of the double humanized mouse model has the potential to offer new fundamental insight to HCV pathogenesis and vaccine development.

3.3.22 Human Immunodeficiency Virus (HIV)

In the 1980s, the human retrovirus, Human T cell leukemia virus type III (HTLV-III), was discovered to be the etiological agent of Acquired Immunodeficiency Syndrome (AIDS) [150, 151]. The virus, later given the name, Human Immunodeficiency virus type 1 (HIV-1) [150], has since established itself as a global health burden

and the leading cause of death and disease, especially in sub-Saharan Africa [152]. The development of antiretroviral therapy (ART) has led to the decline of HIV-related mortality and morbidity [153] and has decreased the occurrence of HIV-1 transmission [154]. However, the efficacy of ART is variable [153], and the establishment of drug-resistant strains is a concerning reality for infected individuals [155]. A safe and effective vaccine would be the most cost-effective means to control the HIV-1 pandemic. However, despite the enormous amounts of effort being put into this investigation, such an ideal vaccine does not exist for clinical implementation [152, 153]. The difficulty in creating a suitable animal model and the disparity for finding useful therapeutics and vaccines has previously pushed discoveries directly from the bench to the clinic, an incredibly risky, and potentially dangerous practice [22]. Initially, a vaccine was expected to be produced within the span of merely 2 years since the discovery of its causal associated with AIDS. A vaccine trial was implemented in 1986; however, it was unsuccessful and caused uproar for being run without the knowledge of the international committee, involving children, and used unapproved materials for its creation [153]. Since this first trial, several attempts have been made; however, the results have yet to be successful. In fact, there has been serious consideration to discontinue HIV-1 vaccine development [153]. Additionally, despite years of extensive study, basic observations about HIV-1 disease, such as the pathogenesis of CD4+ T cell depletion, remain unexplained [156].

3.3.23 The SCID-Hu Mouse, the Beginning Developments of a System for Studies in HIV

An incredibly large amount of research using humanized mice has been conducted. The first two humanized models of HIV infection were the SCID-hu thy/liv and SCID-hu PBL mouse models [157]. In 1988, both the SCID-hu Thy/Liv and the SCID-hu-PBL models were developed with the intent of providing a model for the study of HIV [80]. Within each of these models, HIV-1 infection of the hu-PBL-SCID and the SCID-hu Thy/Liv mouse leads to the characteristic depletion of human CD4+ T cells [80]. Within each of the SCID-hu models, a milieu supporting the growth and development of natural target cells of HIV-1 is established. This access to fundamental components of the HIV-1 host-virus interaction has resulted in their extensive use to address the questions of HIV-1 infection, viral replication, mechanisms of pathogenesis, and potential pharmacological and biological interventions [80, 157–162].

The SCID-hu-PBL mouse model has contributed to our understanding of HIV-1 infection, from viral cytopathic effects to potential vaccine approaches [163]. The hu-PBL-SCID mouse possesses an interesting feature, where it is able to receive the PBL graft from donors who have recently been immunized. This transplantation permits the adoptive transfer of an ongoing

immune response into the SCID mouse. This approach has been used to evaluate the resistance of the hu-SCID-PBL mouse to HIV-1 infection receiving inoculum derived from donors undergoing a HIV-1 vaccine trial [80, 159]. T cells appeared to have a good positive correlation with HIV-1 resistance, while the antibody response was subpar in comparison [80, 159]. The hu-PBL-SCID mouse has been used in additional studies to examine the protective effect of neutralizing antibodies [160, 161] and CTLs [162] to gain insight into potential means of immunization [80]. Attempts at evaluating vaginal HIV-1 transmission and prevention have been made using the SCID-hu-PBL model [162]. However, these mice lack HIV-1 target cells in their vaginal mucosa, adding degrees of uncertainty regarding the applicability of these studies to humans [163]. The presence of the human thymic organoid within the SCID-hu Thy/Liv model made it very suitable for the application of understanding events that influence its involvement in HIV infection. Rightfully so, the use of the SCID-hu Thy/Liv mouse has been heavily focused on the thymic environment and understanding the mechanisms behind thymic depletion following HIV infection [158, 164]. Additionally, this model has been shown to have great predictive potential and has been used in the preclinical evaluation of antiretroviral therapies [163, 165]. The SCID-hu Thy/Liv mouse model has played an integral part in explaining the characteristics of latency development early in HIV infection [166], revealing fundamental observations of HIV latently infected T cells. This model has been used to demonstrate the process of viral latency in vivo [167]. This understanding of HIV quiescence has led to efforts in antiviral strategies to remove infected cells out of their latent state for their potential targeting, eliminating the latent HIV reservoir [168, 169]. In a study Brooks et al. demonstrated potential impact the "shock and kill" approach can have on eliminating the latent HIV virus, and eradicating the population within the infected mice [168]. This understanding has shaped our therapeutic approaches and provided incredibly valuable information for potential post-exposure therapies.

Regardless of their apparent value in some aspects of HIV infection, these models are limited in their use for HIV study. Unfortunately, these models are unable to provide a means for examining the anti-HIV human immune responses, pathogenesis or mucosal HIV transmission [157].

3.3.24 Novel Humanized Mouse Models for Expanding the Scope of the In Vivo Examination of HIV

The gradually increasing sophistication of the humanized mouse models has allowed for unique opportunities in examining aspects in HIV infection. The most commonly used immunodeficient mouse strains to study HIV infection have been the NOD/SCID, DKO, and NSG mouse, with either the use of CD34+ cell transplantation or BLT [157]. Humanized mice have been shown to be

susceptible to a broad variety of HIV-1 isolates [157, 170]. The use of these models and their display of HIV pathogenesis have previously been extensively reviewed [152, 157, 170]. These new models have provided the unique means of examining mucosal aspects of HIV infection and the innate, adaptive, and humoral responses to HIV.

3.3.25 Human Hematolymphoid Chimeric Mice and the Study of HIV

DKO, NSG, and NOG mice humanized with HSCs results in similar manifestations of HIV infection. Systemic dissemination occurs and there is CD4+ T cell depletion, CD8+ T cell infiltration, regardless of the route of viral inoculation [157]. In hu-NSG and hu-NOG mice, reconstitution of human immune cells within the intestines and female reproductive tracts has yet to be described [157]. However, mucosal engraftment with human cells has been seen in the gut, rectal, and vaginal mucosa of the hu-DKO mice [171, 172]. The capacity for mucosal reconstitution is present in hu-DKO mice; however, uncertainty remains in the extent to which human immune cells can be reliably reconstituted in these mucosal sites of HIV-1 transmission [157]. In response to HIV-1 infection, these mice have been shown to develop HIV-specific human immune responses. However, the hu-NOG/NSG/DKO mice do not consistently induce humoral immune responses [157].

With the use of hu-HSC mice, Choudhary et al. have shown that even with the use of ART, hu-DKO mice remain to harbor latent HIV particles within cell and tissue reservoirs, similar to the long-lived HIV reservoirs present in HIV-infected humans [173]. This study has highlighted the utility of the hu-DKO model as a platform for the preliminary assessments of novel eradication approaches and combinatorial antiviral strategies for HIV infection [166, 173]. Profound resistance to HIV-1 infection in European populations is found as a result of a genetic mutation in the CCR5 gene, of the major co-receptor CCR5 used by HIV. Hu-NSG mice have been used to examine the potential therapeutic capabilities of targeted gene disruption. Interestingly, mice with the developed zinc finger nuclease-treated HSCs had significantly lower HIV-1 levels and preserved human cells throughout their tissues [174]. In a more recent study, Halper-Stromberg et al. have shown the impact of the combinatory administration of broadly neutralizing antibodies and viral inducers on the prevention HIV-1 viral rebound from the reservoirs of humanized mice [175]. Kumer et al. have used the hu-HSC model to test a novel technique targeting siRNAs specifically to a combination of host and viral proteins. This siRNA therapy efficiently suppressed viremia in HIV-1-infected mice [176, 177].

In using hu-HSC mice, it should be noted that many organ pathologies induced as a result of HIV-1 infection are unable to be faithfully recreated. The in vivo reconstitution of human tissues is

restricted to the progeny of the CD34+ cells initially transplanted into the mice. An exception to this is the BLT model. This model permits the study of human thymic pathologies in the context of human epithelium. BLT mice consistently reconstitute cells in their gastrointestinal and vaginal mucosa in a robust and sustained manner [157].

3.3.26 The BLT Humanized Mouse and HIV Research

Currently, the most advanced humanized mouse model available for HIV research is the BLT model [163]. The BLT model is capable of achieving systemic human immune cell reconstitution with multiple hematopoietic lineages, developing human cells within the peripheral blood, human thymic organ, bone marrow, spleen, lymph nodes, liver, lungs, small and large intestines and the female reproductive tract [157, 178, 179]. The human reconstitution has been described as incredibly specific within the BLT model. As an example of this ability, the human CD8+ CD4+ T lymphocytes development within the intestine of the mouse exhibits a human gut-specific surface phenotype [157, 178]. Given the importance of the human gut and female reproductive tract in transmission and disease pathogenesis, the reliable and extensive humanization observed within the mucosa of the intestine [178] and female reproductive tract [179], and the ability for HIV replication, is incredibly useful in HIV research [157].

Unique to the BLT mouse, a primary immune response against HIV-1 is elicited, yet mice retain their susceptible and permissive environment for HIV infection. In this way, the BLT model represents the most realistic and complete mouse model for HIV studies [166]. In a recent study, the BLT mouse has been used to help achieve a clearer understanding of the in vivo role of the viral Nef protein. The expression of Nef was demonstrated to be an essential component for HIV-1 to induce systemic T-cell activation and cause a significant reduction in CD4+ T cell from blood and tissues. These observations strongly support the developed understanding that Nef is the main driver of pathogenicity. Additionally, this BLT model presented the first substantial host-specific suppression of HIV-1 replication in a small animal model [180]. In examining potential therapeutics for HIV-1, Denton et al. tested the use of targeted cytotoxic killing persistent viral RNA cells, in BLT mice undergoing ART. Treatment profoundly depleted the systemic presence of productively infected cells [166, 181]. The BLT mouse model has been used in testing the efficacy of a RNA interference mediated treatment, directed to the HIV CCR5 co-receptor. This will result in the development of downregulated CCR5 CD4+ T lymphocytes. This anti-HIV agent was shown to provide HIV-1 resistance in the memory T cells of the BLT mouse [166, 182].

3.3.27 Human T-Cell Leukemia Virus-1 (HTLV-1)

In 1980, the first human retrovirus, Human T-cell leukemia virus type 1 (HTLV-1), was discovered [183, 184]. In accordance with its name, this retrovirus displays preferential tropism toward human T lymphocytes, specifically CD4+ lymphocytes [185]. This is a stark contrast to the wide versatility in its cellular tropism observed within cell culture systems, infecting a spectrum of cell types from different species [186]. Typically, primary infection is asymptomatic, and disease manifests within the host following a long period of latency [184]. This quiet infection allows for spread of the virus to go unnoticed through sexual encounters, breast feeding, and blood transfusions [184]. This virus has been identified as the etiological agent of adult T-cell lymphoma/leukemia (ATL) [183, 184], an aggressive malignancy of mature CD4 T cells [187]. The pathogenic ability of HTLV-1 extends to the development of neurological diseases such as primarily HTLV-1 associated myelopathy/tropical spastic paralysis (HAM/TSP) [183, 184]. ATL is a disease more commonly presented within adult hosts who have been harboring latent HTLV-1 since their primary infection during childhood. On the other hand, the manifestations of neurological diseases from HTLV-1 are more often accompanying those who have become infected later in life [183]. In addition to these diseases, HTLV-1 also encourages the development of uveitis, rheumatic syndromes, and predisposes its infected host to helminthic and bacterial infections [184]. No prospective vaccines exist, creating an unfortunate reality of those living in endemic regions [184].

3.3.28 The Display of HTLV-1 Infection Within Humanized Mice

Several studies have shown the potential value the humanized mice hold in investigating aspects of HTLV-1 pathogenesis and disease. These humanized mice models have been shown to represent environments of both asymptomatic and disease patients. Early efforts for the study of HTVL-1 involved the use of the hu-SCID-PBL model, where CB-17-*scid* mice were inoculated with PBMCs from HTLV-1-infected donors [188–190]. For their time, these experiments gave promise as an in vivo model; however, engraftment inefficiencies and poor detection of viral integration limited their success [190].

The hu-PBL-NSG model allowed for the first evaluation of primary in vivo HTLV-1 infection within human lymphocytes [191]. Unlike the hu-PBL-SCID model, mice were infected following the engraftment of human cells. This model holds merit in its ability to allow for vigorous proliferation of human lymphocytes, enabling HTLV-1 to rapidly spread via cell-to-cell contact, the characteristic means of HTLV-1 "infectivity" among cells [191]. Although no signs of HTLV-1-associated disease developed, these mice showed redeeming qualities in their ability to positively respond to pre-existing antiretroviral drugs, creating a possibility for its use as a platform for testing novel treatments or vaccines [191]. In a separate study, NOG mice were humanized with

autologous adult human donor PBMCs from asymptomatic HTLV-1 carriers [192]. The situation created within the mice was similar to that of HTLV-1 carriers: HTLV-1 expression can be detected in PBMCs, yet, the virus particles themselves are not detectable [192]. Thus, this model may provide insight into the human environment of an asymptomatic carrier and be useful in developing preventative treatments or therapies to those already infected, however, have not progressed to disease [192]. The utility of the humanized NSG model comes with its ability of developing abnormalities frequently observed within ATL including, hepatosplenomegaly, lymphadenopathy, and lymphoma/thymoma several months after infection [193, 194]. Tezuka et al. have reported NOG-SCID mice to develop ATL-like disease when CD133+ HSCs infected with HTLV-1 are introduced via intra-bone marrow transplantation [195, 196]. The described disease within these hu-NOG-SCID mice is representative of characteristic of the late-stage ATL cells in human patients [196].

The induction of an immune response as a result of HTLV-1 infection has not been previously described. However, this factor is highly important to examine. Humoral immunity and the cytotoxic activity of cytotoxic T lymphocytes (CTL) are an essential component to containing HTLV-1 proliferation and the selection of HTLV-1-infected T-cell clones [187]. An interesting model called the "IBMI-huNOG mouse" was able to induce HTLV-1-specific adaptive immune responses. This humanized mouse model is generated through the intra-bone marrow injection of human CD133 + stem cells into NOG mice. Several pathological characteristics of ATL were mimicked within these mice. In addition to this, like HTLV-1-infected carriers, these mice were observed to mount HLA-restricted CTLs against the Tax protein. IgG production against HTLV-1 structural protein was observed. Interestingly, leukemia was almost exclusively developed in HTLV-1-infected IBMI-huNOG. This is in contrast to how HTLV-1 infection presents itself in other humanized mouse models, as lymphoma or thymoma [187]. Within HTLV-1-infected mice, dual expression of Tax and HBZ was observed, reminiscent to what is commonly found within humans in the early phases of infection. These IBMI-huNOG mice might provide a respected means of examining the natural history of HTLV-1 infection [197].

3.3.29 How Humanized Mice Have Been Used to Understand the HTLV-1 Virus

The models developed to examine HTLV-1 have allowed for the exploration of several aspects of the HTLV-1 virology, pathogenesis, and potential utility of novel therapeutics and vaccines.

The SCID-hu Thy/Liv mouse has been used to examine the in vivo cellular tropism of HTLV-1 and the potential role of this tropism in pathogenesis [198]. Inoculation of SCID-hu Thy/Liv mice with either HTLV-1-infected T cells or enriched populations

of CD34+ cells resulted in productive viral infection of thymocytes and dysregulation of thymopoeisis in the fraction of SCID-hu mice with high levels of HTLV-1 replication. Increased IL-2 receptor (CD25) expression was also found to be present in these mice with higher levels of HTLV-1, features characteristic of HTLV-1-transformed T cells and ATL leukemic T cells. These findings suggest the human thymus to be an HTVL-1 reservoir and that increased viral replication within this lymphoid tissue and abnormalities of thymopoeisis may be the transforming events leading up to ATL development. The authors proposed that the increased viral replication may encourage specific T-cell selection for clones with increased advantageous proliferative abilities. In combination with other genetic changes, these processes may encourage ATL development [198].

Tezuka et al. have used the hu-NOG-SCID mouse in attempts to clarify the significance of the HTLV-1 tax gene expression in leukemogenesis [196]. The expression of the IL-2 receptor (CD25) [198] was observed to be activated with the induction of tax. From this, tax function was indicated to be responsible for the CD25 expression. However, when CD4+ T cells from HTLV-1-infected splenocytes were divided into CD25+ and CD25− cells, the majority of tax expression was mainly in CD25− CD4+ T cells. These results indicate that Tax function may not be involved in CD25 expression in vivo [196].

Villaudy et al. used the hu-DKO model to examine the effects of HTLV-1 infection on human T-cell development. Profound alterations to the thymus of hu-DKO mice were observed following HTLV-1 infection with large disturbances in thymopoeisis. With increasing proviral loads, the severity of the altered T-cell subset distributions within the thymus increased accordingly [193, 194]. The observed disturbances offer evidence that during HTLV-1 infection, the thymus forces infected thymocytes through the process of maturation and T-cell development, favoring the activation and the proliferation of these cells. This action provides a substrate population for further altered gene expression that would allow the emergence of a malignant clone [194].

A novel PBMC-NOG model was used to examine a potential means of transmission prevention of HTLV-1. In their model, NOG mice were simultaneously implanted with HTLV-1 negative PBMCs and HTLV-1 producing T cells. Using this model, it was observed that monoclonal antibodies (mAbs) specific to HTLV-1 as well as human IgG isolated from HAM/TSP patients (HAM-IgG) were capable of preventing HTLV-1-infection [199]. Through this study, Saito et al. have indicated that it is the neutralizing antibody function, not the specificity of the antigen that is the vital component for restricting the in vivo HTLV-1 spread. With the use of the PBMC-NOD model, they have shown the

importance of passive immunization for the containment of HTLV-1 transmission [199].

The hu-NOG mouse model has been used to help establish a candidate anti-HTLV-1 therapeutic agent [200]. This anti-viral was created in attempts to remove the foreseeable progression of ATL development in high-risk asymptomatic carriers. To develop this therapy, Hiyoshi et al. tested whether truncated *Pseudomonas* exotoxin (PE38) fused to a CCR4 ligand, CCL17/thymus and activation-regulated chemokine (TARC), designated TARC–PE38, and could selectively eliminate HTLV-1-infected cells expressing CCR4. Through the administration of TARC-PE38, HTLV-1 infection and proliferation within human CD4+CD25+ or CD4 +CD25+CCR4+ cells within humanized mice was significantly impeded and the proviral loads of HTLV-1 found in PBMCs was significantly reduced. The presence of TARC-PE38 also diminished the size of solid tumors within mice. TARC-PE38 was determined to regulate HTLV-1 infection, eliminating infected cells through a CCR4- and furin-dependent manner. These results show the admirable potential of TARC–PE38 as a therapeutic agent [200].

In infected carriers of HTLV-1, cytotoxic T-lymphocytes (CLTs) against HTLV-1 Tax have been demonstrated to play a vital role in controlling HTLV-1-infected cells. Fujisawa et al. utilized this idea to examine the efficacy of Tax peptide vaccination in the hu-NOG mouse model. Control mice died from leukemia, while Tax-immunization was shown to impede the outgrowth of human lymphocytes following HTLV-1 infection. Additionally, two of five mice survived with a limited number of infected T cells residing within them. Furthermore, it was shown that the intranasal inoculation of Tax peptides has a comparable effect on the onset of leukemia in the hu-NOG systems to the subcutaneous administration. These results suggest that the Tax peptide vaccination can elicit protective immunity against HTLV-1 infection and/or ATL developments [200].

3.4 Concluding Remarks

The humanized mouse model has allowed the holes in our knowledge of human tropic pathogens to slowly become filled in. Humanized mice have proven to be capable of displaying signs of human viral infection unattainable in any other animal model. These mice have shown to embody a large spectrum of human viral-associated pathologies, recreate the human immune response to infection, and serve as a platform for vaccine and therapeutic testing. Although further modifications to the mice models should be done to enhance the human-like qualities of these chimeric mice, even as an imperfect model, it has provided invaluable results and clinical relevance for the study of human-specific viruses [9, 13].

4 Notes

1. Special irradiation containers or devices that are easy to sterilize should be used.
2. To obtain HSCs from human umbilical cord blood, anti-human CD34 monoclonal antibodies targeting the specific HSC cell surface antigen, CD34, are used in an immunopositive selection process. HSCs are enriched through a process of negative selection where unwanted cells are labeled with antibodies against known markers for mature hematopoietic cells (CD2, CD3, CD14, CD16, CD19, CD24, CD56, CD66b, and glycophorin A) and are removed from the human cord blood sample. Remaining cells are mostly CD34+.
3. Ethical approval by the institution, informed consent from donors, and adherence to the specified guidelines for using human derived samples are required.
4. The HetaSep™ is a solution of hetastarch, an erythrocyte aggregation agent used to quickly separate nucleated cells from red blood cells (RBC) in whole blood. Aggregated erythrocytes settle much faster than dispersed cells. This creates an obvious gradient and easy removal of unwanted RBCs.
5. Progenitor cells from cord blood are isolated by negative selection using the RosetteSep™Human cord blood progenitor cell enrichment cocktail. Unwanted cells are targeted for removal with Tetrameric Antibody Complexes recognizing CD2, CD3, CD14, CD16, CD19, CD24, CD56, CD61, CD66b, and glycophorin A on red blood cells (RBCs).
6. Within the immunodeficient mouse strains, even in some of the best immunodeficient types created, small amounts of immune cells remain lingering within the mice. The presence of these cells can lead to graft versus host disease (GVHD) or graft rejection. To remove this potential pitfall, mice undergo whole body irradiation. Sensitivity of mice to irradiation is dependent on strain and age of the mice (newborn pups or adult). NRG mice can tolerate higher dose of irradiation than NSG and NOG mice, while adult mice are more tolerant than newborn pups. For mice highly sensitive to irradiation, an alternative method of myeloblation is the use of chemotherapeutic agents. This method is preferably used in adult mice or when constraints are placed on the use of an irradiator.
7. The irradiation must be exclusively performed by trained personnel and in accordance with the safety guidelines.
8. ^{137}Cs gamma irradiator or any radiation device can be used.
9. These NRG mice are NOD-congenic mice harboring the *Rag1*^{null} mutation (Rag1KO or *Rag1*^{tm1Mom}) on chromosome

2 and the *IL2rγ*^{null} mutation (IL2RγcKO or *Il2rg*^{tm1Wjl}) on the X chromosome. These NRG mutant mice are also called NOD-*Rag1*^{null} *IL2rγ*^{null} double mutant mice or NOD.Rag1KO. IL2RγcKO mice (donated to The Jackson Laboratory by Dr. Leonard D. Shultz).

10. Different routes of immune cell injections into newborn pups and adults have been reported. Intraheptic (IH), intraperitoneal (IP), and intravenous (IV) injections via intracardiac or facial vein route are four means of injection that have been reported for the engraftment of human cells into newborns. IP injection is the most optimal route of engraftment, offering high efficiency and ease of injection as the skin of newborn pups is semitransparent and their peritoneal cavity is relatively large. For adult engraftment, IV injection via the tail vein and intrafemoral or intratibial routes are used. Within adult mice, the IV route is most common due to its relative ease of injection and the removal of the bone marrow homing requirements otherwise demanded when using the different routes of immune cell engraftment.
11. FC block is a purified recombinant Fc protein that blocks nonspecific binding of Fc receptor expressing cells, such as myeloid and B cells. The optimal concentration of the Fc block is dependent on the cell type and number. Human Fc block should be titered for optimal results.
12. Fix/Lyse Solution enables lysis of red blood cells after staining peripheral blood cells with fluorochrome conjugated antibodies. This solution has been specially formulated to lyse nonnucleated erythrocytes while maintaining a fixed and labeled leukocyte population. Therefore, whole blood samples can be stained for the appropriate markers, RBC lysed and fixed, washed, and then analyzed by flow cytometry.
13. The FRG mice are immunodeficient knockout in the tyrosine catabolic enzyme fumarylacetoacetate hydrolase (Fah), lacking the genes for Rag-2 and the common gamma chain of the interleukin receptor (Fah−/−/Rag2−/−/Il2rg−/−). These animals breed normally while on 2-(2-nitro-4-trifluoromethylbenzoyl)-1,3-cyclohexanedione (NTBC) treatment. NTBC, also known as nitisinone, is an inhibitor of 4-hydroxyphenylpyruvate dioxgenase (HPPD), and is used to prevent the liver and kidney toxicity associated with tyrosinemia type 1, a metabolic disorder in the tyrosine catabolism caused by fumarylacetoacetate hydrolase (FAH) deficiency.
14. Disposable instruments or autoclaved surgical instruments should be used.
15. HLA typing is required to be matched for human immune system reconstitution in A2 + HLA NSG mice.

16. Imbalance of the tubes while undergoing centrifugation interferes with the separation process.
17. Using Mr. Frosty provides the optimal cooling rate (1 °C/min) for cell preservation. Leave the cryovials overnight in Mr. Frosty. Transfer to liquid nitrogen the next day. Alternative cooling systems can be used.
18. As the hepatic cells are sensitive to physical damage, the cutting should be done gently.
19. Dissolve Collagenase IV with 10 mL of DMEM and filter the suspension using a 0.2 μm filter.
20. The best age for adult mice is at least 6–10 weeks.
21. As the mice are sensitive to odors, rub your gloves with bedding from the mouse cage prior to handling to mask any foreign odors. Additionally, place a small amount of bedding into the mouse irradiation container before mice undergo irradiation. These techniques help to ensure that the mothers accept their pups after handling.
22. The cell number may vary depending on the experiment.
23. CD45 is the main marker for leukocytes. Other cell markers can be used to evaluate cell differentiation and cell populations.
24. The presence of hCD3+ cells in the cell suspension to be injected increases the rate of Graft versus host disease (GVHD) and encourages unsuccessful engraftment of human cells.
25. In using a PE Positive Selection Kit, the hCD3+ cells are labeled with anti hCD3 PE-conjugated antibody and are targeted with Tetrameric Antibody Complexes recognizing PE and dextran-coated magnetic particles. Labeled cells are separated using an EasySep™ magnet without the use of columns.
26. Mice with an NSG background are more sensitive to irradiation and using high doses of irradiation can be lethal.
27. Intrasplenic engraftment is time consuming and requires the individuals performing this procedure to be highly proficient in their surgical ability.

References

1. Worobey M, Bjork A, Wertheim JO (2007) Point, counterpoint: the evolution of pathogenic viruses and their human hosts. Annu Rev Ecol Evol Syst 38(1):515–540. doi:10.1146/annurev.ecolsys.38.091206.095722
2. Haley PJ (2003) Species differences in the structure and function of the immune system. Toxicology 188(1):49–71
3. Yan EG, Munir KM (2004) Regulatory and ethical principles in research involving children and individuals with developmental disabilities. Ethics Behav 14(1):31–49. doi:10.1207/s15327019eb1401_3
4. Partridge TA (2013) The mdx mouse model as a surrogate for Duchenne muscular dystrophy. FEBS J 280(17):4177–4186. doi:10.1111/febs.12267

5. Wilson GK, Stamataki Z (2012) In vitro systems for the study of hepatitis C virus infection. Int J Hepatol 2012:292591. doi:10.1155/2012/292591
6. Marsden MD, Zack JA (2015) Studies of retroviral infection in humanized mice. Virology 479–480:297–309. doi:10.1016/j.virol.2015.01.017
7. Vandamme TF (2015) Rodent models for human diseases. Eur J Pharmacol 759:84–89. doi:10.1016/j.ejphar.2015.03.046
8. Shultz LD, Ishikawa F, Greiner DL (2007) Humanized mice in translational biomedical research. Nat Rev Immunol 7(2):118–130
9. Akkina R (2013) New generation humanized mice for virus research: comparative aspects and future prospects. Virology 435 (1):14–28. doi:10.1016/j.virol.2012.10.007
10. Sibal LR, Samson KJ (2001) Nonhuman primates: a critical role in current disease research. ILAR J 42(2):74–84. doi:10.1093/ilar.42.2.74
11. Messaoudi I, Estep R, Robinson B et al (2011) Nonhuman primate models of human immunology. Antioxid Redox Signal 14(2):261–273. doi:10.1089/ars.2010.3241
12. Lankau EW, Turner PV, Mullan RJ et al (2014) Use of nonhuman primates in research in North America. J Am Assoc Lab Anim Sci 53(3):278–282
13. Shultz LD, Brehm MA, Garcia-Martinez JV et al (2012) Humanized mice for immune system investigation: progress, promise and challenges. Nat Rev Immunol 12(11):786–798
14. Bontrop RE (2001) Non-human primates: essential partners in biomedical research. Immunol Rev 183:5–9
15. Barreiro LB, Marioni JC, Blekhman R et al (2010) Functional comparison of innate immune signaling pathways in primates. PLoS Genet 6(12):e1001249. doi:10.1371/journal.pgen.1001249
16. Justice MJ, Siracusa LD, Stewart AF (2011) Technical approaches for mouse models of human disease. Dis Model Mech 4 (3):305–310. doi:10.1242/dmm.000901
17. Davis PH, Stanley SL (2003) Breaking the species barrier: use of SCID mouse–human chimeras for the study of human infectious diseases. Cell Microbiol 5(12):849–860. doi:10.1046/j.1462-5822.2003.00321.x
18. Billerbeck E, Mommersteeg MC, Shlomai A et al (2016) Humanized mice efficiently engrafted with fetal hepatoblasts and syngeneic immune cells develop human monocytes and NK cells. J Hepatol 65(2):334–343. doi:10.1016/j.jhep.2016.04.022
19. Pearson T, Greiner DL, Shultz LD (2008) Creation of "humanized" mice to study human immunity. Curr Protoc Immunol. Chapter 15:Unit 15.21. doi:10.1002/0471142735.im1521s81
20. Leung W, Ramirez M, Civin CI (1999) Quantity and quality of engrafting cells in cord blood and autologous mobilized peripheral blood. Biol Blood Marrow Transplant 5 (2):69–76
21. Holyoake TL, Nicolini FE, Eaves CJ (1999) Functional differences between transplantable human hematopoietic stem cells from fetal liver, cord blood, and adult marrow. Exp Hematol 27(9):1418–1427. doi:10.1016/S0301-472X(99)00078-8
22. McCune J, Kaneshima H, Krowka J et al (1991) The SCID-hu mouse: a small animal model for HIV infection and pathogenesis. Annu Rev Immunol 9:399–429. doi:10.1146/annurev.iy.09.040191.002151
23. Denton PW, Olesen R, Choudhary SK et al (2012) Generation of HIV latency in humanized BLT mice. J Virol 86(1):630–634. doi:10.1128/JVI.06120-11
24. McCune JM (1996) Development and applications of the SCID-hu mouse model. Semin Immunol 8(4):187–196. doi:10.1006/smim.1996.0024
25. Nomura T, Watanabe T, Habu S (2008) Humanized mice. Preface. Curr Top Microbiol Immunol 324:v–vi
26. Hioki K, Kuramochi T, Endoh S et al (2001) Lack of B cell leakiness in BALB/cA-nu, scid double mutant mice. Exp Anim 50(1):67–72
27. Gershwin ME, Merchant B, Gelfand MC et al (1975) The natural history and immunopathology of outbred athymic (nude) mice. Clin Immunol Immunopathol 4(3):324–340
28. Bosma GC, Custer RP, Bosma MJ (1983) A severe combined immunodeficiency mutation in the mouse. Nature 301(5900):527–530
29. Bosma MJ, Carroll AM (1991) The SCID mouse mutant: definition, characterization, and potential uses. Ann Rev Immunol 9 (1):323–350. doi:10.1146/annurev.iy.09.040191.001543
30. Mombaerts P, Iacomini J, Johnson RS et al (1992) RAG-1-deficient mice have no mature B and T lymphocytes. Cell 68(5):869–877. doi:10.1016/0092-8674(92)90030-G
31. Shinkai Y, Rathbun G, Lam KP et al (1992) RAG-2-deficient mice lack mature lymphocytes owing to inability to initiate V(D)J rearrangement. Cell 68(5):855–867
32. Shultz LD, Schweitzer PA, Christianson SW et al (1995) Multiple defects in innate and

adaptive immunologic function in NOD/LtSz-scid mice. J Immunol 154(1):180–191
33. Brehm MA, Shultz LD, Luban J et al (2013) Overcoming current limitations in humanized mouse research. J Infect Dis 208(Suppl 2): S125–S130. doi:10.1093/infdis/jit319
34. Halstead SB (2015) Pathogenesis of dengue: dawn of a new era. F1000Res 4. doi:10.12688/f1000research.7024.1
35. Screaton G, Mongkolsapaya J, Yacoub S et al (2015) New insights into the immunopathology and control of dengue virus infection. Nat Rev Immunol 15(12):745–759. doi:10.1038/nri3916
36. Zompi S, Harris E (2012) Animal models of dengue virus infection. Virus 4(1):62–82. doi:10.3390/v4010062
37. Whitehead SS, Blaney JE, Durbin AP et al (2007) Prospects for a dengue virus vaccine. Nat Rev Microbiol 5(7):518–528. doi:10.1038/nrmicro1690
38. Bente DA, Melkus MW, Garcia JV et al (2005) Dengue fever in humanized NOD/SCID mice. J Virol 79(21):13797–13799. doi:10.1128/JVI.79.21.13797-13799.2005
39. Yauch LE, Shresta S (2008) Mouse models of dengue virus infection and disease. Antivir Res 80(2):87–93. doi:10.1016/j.antiviral.2008.06.010
40. Wu SJ, Hayes CG, Dubois DR et al (1995) Evaluation of the severe combined immunodeficient (SCID) mouse as an animal model for dengue viral infection. Am J Trop Med Hyg 52(5):468–476
41. Bente DA, Rico-Hesse R (2006) Models of dengue virus infection. Drug Discov Today Dis Models 3(1):97–103. doi:10.1016/j.ddmod.2006.03.014
42. Palucka AK, Gatlin J, Blanck JP et al (2003) Human dendritic cell subsets in NOD/SCID mice engrafted with CD34+ hematopoietic progenitors. Blood 102(9):3302–3310. doi:10.1182/blood-2003-02-0384
43. Cravens PD, Melkus MW, Padgett-Thomas A et al (2005) Development and activation of human dendritic cells in vivo in a xenograft model of human hematopoiesis. Stem Cells 23(2):264–278. doi:10.1634/stemcells.2004-0116
44. Kuruvilla JG, Troyer RM, Devi S et al (2007) Dengue virus infection and immune response in humanized RAG2(−/−)gamma(c)(−/−) (RAG-hu) mice. Virology 369(1):143–152. doi:10.1016/j.virol.2007.06.005
45. Mota J, Rico-Hesse R (2009) Humanized mice show clinical signs of dengue fever according to infecting virus genotype. J Virol 83(17):8638–8645. doi:10.1128/jvi.00581-09
46. Jaiswal S, Pearson T, Friberg H et al (2009) Dengue virus infection and virus-specific HLA-A2 restricted immune responses in humanized NOD-scid IL2rgammanull mice. PLoS One 4(10):e7251. doi:10.1371/journal.pone.0007251
47. Jaiswal S, Pazoles P, Woda M et al (2012) Enhanced humoral and HLA-A2-restricted dengue virus-specific T-cell responses in humanized BLT NSG mice. Immunology 136(3):334–343. doi:10.1111/j.1365-2567.2012.03585.x
48. Jaiswal S, Smith K, Ramirez A et al (2015) Dengue virus infection induces broadly cross-reactive human IgM antibodies that recognize intact virions in humanized BLT-NSG mice. Exp Biol Med (Maywood) 240(1):67–78. doi:10.1177/1535370214546273
49. Frias-Staheli N, Dorner M, Marukian S et al (2014) Utility of humanized BLT mice for analysis of dengue virus infection and antiviral drug testing. J Virol 88(4):2205–2218. doi:10.1128/JVI.03085-13
50. Cox J, Mota J, Sukupolvi-Petty S et al (2012) Mosquito bite delivery of dengue virus enhances immunogenicity and pathogenesis in humanized mice. J Virol 86 (14):7637–7649. doi:10.1128/jvi.00534-12
51. Mota J, Rico-Hesse R (2011) Dengue virus tropism in humanized mice recapitulates human dengue fever. PLoS One 6(6): e20762. doi:10.1371/journal.pone.0020762
52. Subramanya S, Kim SS, Abraham S et al (2010) Targeted delivery of small interfering RNA to human dendritic cells to suppress dengue virus infection and associated proinflammatory cytokine production. J Virol 84 (5):2490–2501. doi:10.1128/JVI.02105-08
53. Sridharan A, Chen Q, Tang KF et al (2013) Inhibition of megakaryocyte development in the bone marrow underlies dengue virus-induced thrombocytopenia in humanized mice. J Virol 87(21):11648–11658. doi:10.1128/JVI.01156-13
54. Johnson KM, Lange JV, Webb PA et al (1977) Isolation and partial characterisation of a new virus causing acute haemorrhagic fever in Zaire. Lancet 1(8011):569–571
55. Martinez MJ, Salim AM, Hurtado JC et al (2015) Ebola virus infection: overview and update on prevention and treatment. Infect Dis Ther 4(4):365–390. doi:10.1007/s40121-015-0079-5
56. Lever RA, Whitty CJ (2016) Ebola virus disease: emergence, outbreak and future

directions. Br Med Bull 117(1):95–106. doi:10.1093/bmb/ldw005

57. Ludtke A, Oestereich L, Ruibal P et al (2015) Ebola virus disease in mice with transplanted human hematopoietic stem cells. J Virol 89 (8):4700–4704. doi:10.1128/JVI.03546-14
58. Bray M (2001) The role of the type I interferon response in the resistance of mice to filovirus infection. J Gen Virol 82(Pt 6):1365–1373. doi:10.1099/0022-1317-82-6-1365
59. Ebihara H, Takada A, Kobasa D et al (2006) Molecular determinants of Ebola virus virulence in mice. PLoS Pathog 2(7):e73. doi:10.1371/journal.ppat.0020073
60. Prescott J, Feldmann H (2016) Humanized mice—a neoteric animal disease model for Ebola virus? J Infect Dis 213(5):691–693. doi:10.1093/infdis/jiv539
61. Bird BH, Spengler JR, Chakrabarti AK et al (2016) Humanized mouse model of Ebola virus disease mimics the immune responses in human disease. J Infect Dis 213 (5):703–711. doi:10.1093/infdis/jiv538
62. Fujiwara S, Matsuda G, Imadome K (2013) Humanized mouse models of epstein-barr virus infection and associated diseases. Pathogens 2(1):153–176. doi:10.3390/pathogens2010153
63. Fujiwara S, Imadome K, Takei M (2015) Modeling EBV infection and pathogenesis in new-generation humanized mice. Exp Mol Med 47:e135. doi:10.1038/emm.2014.88
64. Munz C (2015) EBV infection of mice with reconstituted human immune system components. Curr Top Microbiol Immunol 391:407–423. doi:10.1007/978-3-319-22834-1_14
65. Rowe M, Young LS, Crocker J et al (1991) Epstein-Barr virus (EBV)-associated lymphoproliferative disease in the SCID mouse model: implications for the pathogenesis of EBV-positive lymphomas in man. J Exp Med 173(1):147–158
66. Gujer C, Chatterjee B, Landtwing V et al (2015) Animal models of Epstein Barr virus infection. Curr Opin Virol 13:6–10. doi:10.1016/j.coviro.2015.03.014
67. Ok CY, Li L, Young KH (2015) EBV-driven B-cell lymphoproliferative disorders: from biology, classification and differential diagnosis to clinical management. Exp Mol Med 47: e132. doi:10.1038/emm.2014.82
68. Takashima K, Ohashi M, Kitamura Y et al (2008) A new animal model for primary and persistent Epstein-Barr virus infection: human EBV-infected rabbit characteristics determined using sequential imaging and pathological analysis. J Med Virol 80 (3):455–466. doi:10.1002/jmv.21102
69. Kutok JL, Wang F (2006) Spectrum of Epstein-Barr virus-associated diseases. Annu Rev Pathol 1:375–404. doi:10.1146/annurev.pathol.1.110304.100209
70. Ahmed EH, Baiocchi RA (2016) Murine models of Epstein-Barr virus-associated lymphomagenesis. ILAR J 57(1):55–62. doi:10.1093/ilar/ilv074
71. Chatterjee B, Leung CS, Munz C (2014) Animal models of Epstein Barr virus infection. J Immunol Methods 410:80–87. doi:10.1016/j.jim.2014.04.009
72. Lieberman PM (2014) Epstein-Barr Virus Turns 50. Science (New York, NY) 343 (6177):1323–1325. doi:10.1126/science.1252786
73. Mosier DE, Gulizia RJ, Baird SM et al (1988) Transfer of a functional human immune system to mice with severe combined immunodeficiency. Nature 335(6187):256–259. doi:10.1038/335256a0
74. Mosier D, Gulizia R, Baird S et al (1989) B cell lymphomas in SCID mice engrafted with human peripheral blood leukocytes. Blood 74 (Suppl 1):52a
75. Okano M, Taguchi Y, Nakamine H et al (1990) Characterization of Epstein-Barr virus-induced lymphoproliferation derived from human peripheral blood mononuclear cells transferred to severe combined immunodeficient mice. Am J Pathol 137(3):517–522
76. McCune JM (1991) SCID mice as immune system models. Curr Opin Immunol 3 (2):224–228. doi:10.1016/0952-7915(91)90055-6
77. Johannessen I, Crawford DH (1999) In vivo models for Epstein-Barr virus (EBV)-associated B cell lymphoproliferative disease (BLPD). Rev Med Virol 9(4):263–277
78. Picchio GR, Kobayashi R, Kirven M et al (1992) Heterogeneity among Epstein-Barr virus-seropositive donors in the generation of Immunoblastic B-cell lymphomas in SCID mice receiving human peripheral blood leukocyte grafts. Cancer Res 52(9):2468–2477
79. Veronese ML, Veronesi A, D'Andrea E et al (1992) Lymphoproliferative disease in human peripheral blood mononuclear cell-injected SCID mice: I. T lymphocyte requirement for B cell tumor generation. J Exp Med 176 (6):1763–1767
80. Mosier DE (1996) Viral pathogenesis in hu-PBL-SCID mice. Semin Immunol 8 (4):255–262. doi:10.1006/smim.1996.0032

81. Baiocchi RA, Ross ME, Tan JC et al (1995) Lymphomagenesis in the SCID-hu mouse involves abundant production of human interleukin-10. Blood 85(4):1063–1074
82. Islas-Ohlmayer M, Padgett-Thomas A, Domiati-Saad R et al (2004) Experimental infection of NOD/SCID mice reconstituted with human CD34+ cells with Epstein-Barr virus. J Virol 78(24):13891–13900. doi:10.1128/JVI.78.24.13891-13900.2004
83. Ma SD, Hegde S, Young KH et al (2011) A new model of Epstein-Barr virus infection reveals an important role for early lytic viral protein expression in the development of lymphomas. J Virol 85(1):165–177. doi:10.1128/JVI.01512-10
84. Wagar EJ, Cromwell MA, Shultz LD et al (2000) Regulation of human cell engraftment and development of EBV-related lymphoproliferative disorders in Hu-PBL-scid mice. J Immunol 165(1):518–527
85. Yajima M, Imadome K, Nakagawa A et al (2008) A new humanized mouse model of Epstein-Barr virus infection that reproduces persistent infection, lymphoproliferative disorder, and cell-mediated and humoral immune responses. J Infect Dis 198 (5):673–682. doi:10.1086/590502
86. Yajima M, Imadome K, Nakagawa A et al (2009) T cell-mediated control of Epstein-Barr virus infection in humanized mice. J Infect Dis 200(10):1611–1615. doi:10.1086/644644
87. Kuwana Y, Takei M, Yajima M et al (2011) Epstein-Barr virus induces erosive arthritis in humanized mice. PLoS One 6(10):e26630. doi:10.1371/journal.pone.0026630
88. Goudarzipour K, Kajiyazdi M, Mahdaviyani A (2013) Epstein-barr virus-induced hemophagocytic lymphohistiocytosis. Int J Hematol Oncol Stem Cell Res 7(1):42–45
89. Sato K, Misawa N, Nie C et al (2011) A novel animal model of Epstein-Barr virus-associated hemophagocytic lymphohistiocytosis in humanized mice. Blood 117(21):5663–5673. doi:10.1182/blood-2010-09-305979
90. Lee EK, Joo EH, Song KA et al (2015) Effects of lymphocyte profile on development of EBV-induced lymphoma subtypes in humanized mice. Proc Natl Acad Sci U S A 112 (42):13081–13086. doi:10.1073/pnas.1407075112
91. Chijioke O, Muller A, Feederle R et al (2013) Human natural killer cells prevent infectious mononucleosis features by targeting lytic Epstein-Barr virus infection. Cell Rep 5 (6):1489–1498. doi:10.1016/j.celrep.2013.11.041
92. White RE, Ramer PC, Naresh KN et al (2012) EBNA3B-deficient EBV promotes B cell lymphomagenesis in humanized mice and is found in human tumors. J Clin Invest 122 (4):1487–1502. doi:10.1172/JCI58092
93. Wahl A, Linnstaedt SD, Esoda C et al (2013) A cluster of virus-encoded microRNAs accelerates acute systemic Epstein-Barr virus infection but does not significantly enhance virus-induced oncogenesis in vivo. J Virol 87 (10):5437–5446. doi:10.1128/JVI.00281-13
94. Antsiferova O, Muller A, Ramer PC et al (2014) Adoptive transfer of EBV specific CD8+ T cell clones can transiently control EBV infection in humanized mice. PLoS Pathog 10(8):e1004333. doi:10.1371/journal.ppat.1004333
95. Traggiai E, Chicha L, Mazzucchelli L et al (2004) Development of a human adaptive immune system in cord blood cell-transplanted mice. Science 304 (5667):104–107. doi:10.1126/science.1093933
96. Griffiths P, Baraniak I, Reeves M (2015) The pathogenesis of human cytomegalovirus. J Pathol 235(2):288–297. doi:10.1002/path.4437
97. Jean Beltran PM, Cristea IM (2014) The life cycle and pathogenesis of human cytomegalovirus infection: lessons from proteomics. Expert Rev Proteomics 11(6):697–711. doi:10.1586/14789450.2014.971116
98. Crawford LB, Streblow DN, Hakki M et al (2015) Humanized mouse models of human cytomegalovirus infection. Curr Opin Virol 13:86–92. doi:10.1016/j.coviro.2015.06.006
99. Maidji E, Kosikova G, Joshi P et al (2012) Impaired surfactant production by alveolar epithelial cells in a SCID-hu lung mouse model of congenital human cytomegalovirus infection. J Virol 86(23):12795–12805. doi:10.1128/JVI.01054-12
100. Prichard MN, Quenelle DC, Bidanset DJ et al (2006) Human cytomegalovirus UL27 is not required for viral replication in human tissue implanted in SCID mice. Virol J 3:18. doi:10.1186/1743-422X-3-18
101. Mocarski ES, Bonyhadi M, Salimi S et al (1993) Human cytomegalovirus in a SCID-hu mouse: thymic epithelial cells are prominent targets of viral replication. Proc Natl Acad Sci U S A 90(1):104–108

102. Smith MS, Goldman DC, Bailey AS et al (2010) Granulocyte-colony stimulating factor reactivates human cytomegalovirus in a latently infected humanized mouse model. Cell Host Microbe 8(3):284–291. doi:10.1016/j.chom.2010.08.001
103. Revello MG, Gerna G (2010) Human cytomegalovirus tropism for endothelial/epithelial cells: scientific background and clinical implications. Rev Med Virol 20(3):136–155. doi:10.1002/rmv.645
104. Brown JM, Kaneshima H, Mocarski ES (1995) Dramatic interstrain differences in the replication of human cytomegalovirus in SCID-hu mice. J Infect Dis 171 (6):1599–1603
105. Wang W, Taylor SL, Leisenfelder SA et al (2005) Human cytomegalovirus genes in the 15-kilobase region are required for viral replication in implanted human tissues in SCID mice. J Virol 79(4):2115–2123. doi:10.1128/JVI.79.4.2115-2123.2005
106. Tabata T, Petitt M, Fang-Hoover J et al (2012) Cytomegalovirus impairs cytotrophoblast-induced lymphangiogenesis and vascular remodeling in an in vivo human placentation model. Am J Pathol 181 (5):1540–1559. doi:10.1016/j.ajpath.2012.08.003
107. Kawahara T, Lisboa LF, Cader S et al (2013) Human cytomegalovirus infection in humanized liver chimeric mice. Hepatol Res 43 (6):679–684. doi:10.1111/j.1872-034X.2012.01116.x
108. Kern ER, Rybak RJ, Hartline CB et al (2001) Predictive efficacy of SCID-hu mouse models for treatment of human cytomegalovirus infections. Antivir Chem Chemother 12 (Suppl 1):149–156
109. Kern ER, Hartline CB, Rybak RJ et al (2004) Activities of benzimidazole D- and L-ribonucleosides in animal models of cytomegalovirus infections. Antimicrob Agents Chemother 48 (5):1749–1755
110. Bravo FJ, Cardin RD, Bernstein DI (2007) A model of human cytomegalovirus infection in severe combined immunodeficient mice. Antivir Res 76(2):104–110. doi:10.1016/j.antiviral.2007.06.008
111. Lischka P, Hewlett G, Wunberg T et al (2010) In vitro and in vivo activities of the novel anticytomegalovirus compound AIC246. Antimicrob Agents Chemother 54(3):1290–1297. doi:10.1128/AAC.01596-09
112. Weber O, Bender W, Eckenberg P et al (2001) Inhibition of murine cytomegalovirus and human cytomegalovirus by a novel nonnucleosidic compound in vivo. Antivir Res 49 (3):179–189
113. Hakki M, Goldman DC, Streblow DN et al (2014) HCMV infection of humanized mice after transplantation of G-CSF-mobilized peripheral blood stem cells from HCMV-seropositive donors. Biol Blood Marrow Transplant 20(1):132–135. doi:10.1016/j.bbmt.2013.10.019
114. Umashankar M, Petrucelli A, Cicchini L et al (2011) A novel human cytomegalovirus locus modulates cell type-specific outcomes of infection. PLoS Pathog 7(12):e1002444. doi:10.1371/journal.ppat.1002444
115. Houghton M (2009) Discovery of the hepatitis C virus. Liver Int 29(Suppl 1):82–88. doi:10.1111/j.1478-3231.2008.01925.x
116. Washburn ML, Bility MT, Zhang L et al (2011) A humanized mouse model to study hepatitis C virus infection, immune response, and liver disease. Gastroenterology 140 (4):1334–1344. doi:10.1053/j.gastro.2011.01.001
117. von Schaewen M, Ploss A (2014) Murine models of hepatitis C: what can we look forward to? Antivir Res 104:15–22. doi:10.1016/j.antiviral.2014.01.007
118. Marra E, Turrini P, Tripodi M et al (2012) Intrablastocyst injection with human CD34+/CD133+ cells increase survival of immunocompetent fumarylacetoacetate hydrolase knockout mice. Lab Anim 46(4):280–286. doi:10.1258/la.2012.012038
119. Meuleman P, Leroux-Roels G (2008) The human liver-uPA-SCID mouse: a model for the evaluation of antiviral compounds against HBV and HCV. Antivir Res 80(3):231–238. doi:10.1016/j.antiviral.2008.07.006
120. Mesalam AA, Vercauteren K, Meuleman P (2016) Mouse systems to model hepatitis C virus treatment and associated resistance. Virus 8(6):176. doi:10.3390/v8060176
121. Dandri M, Burda MR, Torok E et al (2001) Repopulation of mouse liver with human hepatocytes and in vivo infection with hepatitis B virus. Hepatology 33(4):981–988. doi:10.1053/jhep.2001.23314
122. Bissig KD, Wieland SF, Tran P et al (2010) Human liver chimeric mice provide a model for hepatitis B and C virus infection and treatment. J Clin Invest 120(3):924–930. doi:10.1172/JCI40094
123. Tesfaye A, Stift J, Maric D et al (2013) Chimeric mouse model for the infection of hepatitis B and C viruses. PLoS One 8(10):e77298. doi:10.1371/journal.pone.0077298

124. Kosaka K, Hiraga N, Imamura M et al (2013) A novel TK-NOG based humanized mouse model for the study of HBV and HCV infections. Biochem Biophys Res Commun 441 (1):230–235. doi:10.1016/j.bbrc.2013.10.040
125. Heckel JL, Sandgren EP, Degen JL et al (1990) Neonatal bleeding in transgenic mice expressing urokinase-type plasminogen activator. Cell 62(3):447–456
126. Rhim JA, Sandgren EP, Degen JL et al (1994) Replacement of diseased mouse liver by hepatic cell transplantation. Science 263 (5150):1149–1152
127. Azuma H, Paulk N, Ranade A et al (2007) Robust expansion of human hepatocytes in fah−/−/Rag2−/−/Il2rg−/− mice. Nat Biotechnol 25(8):903–910. doi:10.1038/nbt1326
128. Joyce MA, Walters KA, Lamb SE et al (2009) HCV induces oxidative and ER stress, and sensitizes infected cells to apoptosis in SCID/Alb-uPA mice. PLoS Pathog 5(2): e1000291. doi:10.1371/journal.ppat.1000291
129. Fafi-Kremer S, Fofana I, Soulier E et al (2010) Viral entry and escape from antibody-mediated neutralization influence hepatitis C virus reinfection in liver transplantation. J Exp Med 207(9):2019–2031. doi:10.1084/jem.20090766
130. Brown RJ, Hudson N, Wilson G et al (2012) Hepatitis C virus envelope glycoprotein fitness defines virus population composition following transmission to a new host. J Virol 86 (22):11956–11966. doi:10.1128/JVI.01079-12
131. Singaravelu R, Chen R, Lyn RK et al (2014) Hepatitis C virus induced up-regulation of microRNA-27: a novel mechanism for hepatic steatosis. Hepatology 59(1):98–108. doi:10.1002/hep.26634
132. Vassilaki N, Friebe P, Meuleman P et al (2008) Role of the hepatitis C virus core+1 open reading frame and core cis-acting RNA elements in viral RNA translation and replication. J Virol 82(23):11503–11515. doi:10.1128/JVI.01640-08
133. Gottwein JM, Jensen TB, Mathiesen CK et al (2011) Development and application of hepatitis C reporter viruses with genotype 1 to 7 core-nonstructural protein 2 (NS2) expressing fluorescent proteins or luciferase in modified JFH1 NS5A. J Virol 85(17):8913–8928. doi:10.1128/JVI.00049-11
134. Pietschmann T, Zayas M, Meuleman P et al (2009) Production of infectious genotype 1b virus particles in cell culture and impairment by replication enhancing mutations. PLoS Pathog 5(6):e1000475. doi:10.1371/journal.ppat.1000475
135. Kaul A, Woerz I, Meuleman P et al (2007) Cell culture adaptation of hepatitis C virus and in vivo viability of an adapted variant. J Virol 81(23):13168–13179. doi:10.1128/JVI.01362-07
136. Vanwolleghem T, Bukh J, Meuleman P et al (2008) Polyclonal immunoglobulins from a chronic hepatitis C virus patient protect human liver-chimeric mice from infection with a homologous hepatitis C virus strain. Hepatology 47(6):1846–1855. doi:10.1002/hep.22244
137. Law M, Maruyama T, Lewis J et al (2008) Broadly neutralizing antibodies protect against hepatitis C virus quasispecies challenge. Nat Med 14(1):25–27. doi:10.1038/nm1698
138. Meuleman P, Hesselgesser J, Paulson M et al (2008) Anti-CD81 antibodies can prevent a hepatitis C virus infection in vivo. Hepatology 48(6):1761–1768. doi:10.1002/hep.22547
139. Kneteman NM, Weiner AJ, O'Connell J et al (2006) Anti-HCV therapies in chimeric scid-Alb/uPA mice parallel outcomes in human clinical application. Hepatology 43 (6):1346–1353. doi:10.1002/hep.21209
140. Reiser M, Hinrichsen H, Benhamou Y et al (2005) Antiviral efficacy of NS3-serine protease inhibitor BILN-2061 in patients with chronic genotype 2 and 3 hepatitis C. Hepatology 41(4):832–835. doi:10.1002/hep.20612
141. Vanwolleghem T, Meuleman P, Libbrecht L et al (2007) Ultra-rapid cardiotoxicity of the hepatitis C virus protease inhibitor BILN 2061 in the Urokinase-type plasminogen activator mouse. Gastroenterology 133 (4):1144–1155. doi:10.1053/j.gastro.2007.07.007
142. Inoue K, Umehara T, Ruegg UT et al (2007) Evaluation of a cyclophilin inhibitor in hepatitis C virus-infected chimeric mice in vivo. Hepatology 45(4):921–928. doi:10.1002/hep.21587
143. Umehara T, Sudoh M, Yasui F et al (2006) Serine palmitoyltransferase inhibitor suppresses HCV replication in a mouse model. Biochem Biophys Res Commun 346 (1):67–73. doi:10.1016/j.bbrc.2006.05.085
144. Hsu EC, Hsi B, Hirota-Tsuchihara M et al (2003) Modified apoptotic molecule (BID) reduces hepatitis C virus infection in mice

with chimeric human livers. Nat Biotechnol 21(5):519–525. doi:10.1038/nbt817

145. Overturf K, Al-Dhalimy M, Tanguay R et al (1996) Hepatocytes corrected by gene therapy are selected in vivo in a murine model of hereditary tyrosinaemia type I. Nat Genet 12 (3):266–273. doi:10.1038/ng0396-266
146. Shafritz DA (2007) A human hepatocyte factory. Nat Biotechnol 25(8):871–872. doi:10.1038/nbt0807-871
147. Robinet E, Baumert TF (2011) A first step towards a mouse model for hepatitis C virus infection containing a human immune system. J Hepatol 55(3):718–720. doi:10.1016/j.jhep.2011.02.038
148. Gutti TL, Knibbe JS, Makarov E et al (2014) Human hepatocytes and hematolymphoid dual reconstitution in treosulfan-conditioned uPA-NOG mice. Am J Pathol 184 (1):101–109. doi:10.1016/j.ajpath.2013.09.008
149. Strick-Marchand H, Dusseaux M, Darche S et al (2015) A novel mouse model for stable engraftment of a human immune system and human hepatocytes. PLoS One 10(3): e0119820. doi:10.1371/journal.pone.0119820
150. Montagnier L (2010) 25 years after HIV discovery: prospects for cure and vaccine. Virology 397(2):248–254. doi:10.1016/j.virol.2009.10.045
151. Hsiung GD (1987) Perspectives on retroviruses and the etiologic agent of AIDS. Yale J Biol Med 60(6):505–514
152. Collaborators GH, Wang H, Wolock TM et al (2016) Estimates of global, regional, and national incidence, prevalence, and mortality of HIV, 1980–2015: the global burden of disease study 2015. Lancet HIV 3(8): e361–e387. doi:10.1016/S2352-3018(16)30087-X
153. Owen A, Rannard S (2016) Strengths, weaknesses, opportunities and challenges for long acting injectable therapies: insights for applications in HIV therapy. Adv Drug Deliv Rev 103:144–156. doi:10.1016/j.addr.2016.02.003
154. Rahman SM, Vaidya NK, Zou X (2016) Impact of early treatment programs on HIV epidemics: an immunity-based mathematical model. Math Biosci 280:38–49. doi:10.1016/j.mbs.2016.07.009
155. Wainberg MA, Zaharatos GJ, Brenner BG (2011) Development of antiretroviral drug resistance. N Engl J Med 365(7):637–646. doi:10.1056/NEJMra1004180
156. Okoye AA, Picker LJ (2013) CD4(+) T-cell depletion in HIV infection: mechanisms of immunological failure. Immunol Rev 254 (1):54–64. doi:10.1111/imr.12066
157. Denton PW, Garcia JV (2011) Humanized mouse models of HIV infection. AIDS Rev 13(3):135–148
158. Koka PS, Fraser JK, Bryson Y et al (1998) Human immunodeficiency virus inhibits multilineage hematopoiesis in vivo. J Virol 72 (6):5121–5127
159. Mosier DE, Gulizia RJ, MacIsaac PD et al (1993) Resistance to human immunodeficiency virus 1 infection of SCID mice reconstituted with peripheral blood leukocytes from donors vaccinated with vaccinia gp160 and recombinant gp160. Proc Natl Acad Sci U S A 90(6):2443–2447
160. Gauduin MC, Parren PW, Weir R et al (1997) Passive immunization with a human monoclonal antibody protects hu-PBL-SCID mice against challenge by primary isolates of HIV-1. Nat Med 3(12):1389–1393
161. Parren PW, Ditzel HJ, Gulizia RJ et al (1995) Protection against HIV-1 infection in hu-PBL-SCID mice by passive immunization with a neutralizing human monoclonal antibody against the gp120 CD4-binding site. AIDS 9(6):F1–F6
162. van Kuyk R, Torbett BE, Gulizia RJ et al (1994) Cloned human CD8+ cytotoxic T lymphocytes protect human peripheral blood leukocyte-severe combined immunodeficient mice from HIV-1 infection by an HLA-unrestricted mechanism. J Immunol 153 (10):4826–4833
163. Denton PW, Garcia JV (2009) Novel humanized murine models for HIV research. Curr HIV/AIDS Rep 6(1):13–19
164. Bonyhadi ML, Rabin L, Salimi S et al (1993) HIV induces thymus depletion in vivo. Nature 363(6431):728–732. doi:10.1038/363728a0
165. Stoddart CA, Bales CA, Bare JC et al (2007) Validation of the SCID-hu thy/liv mouse model with four classes of licensed antiretrovirals. PLoS One 2(7):e655. doi:10.1371/journal.pone.0000655
166. Policicchio BB, Pandrea I, Apetrei C (2016) Animal models for HIV cure research. Front Immunol 7:12. doi:10.3389/fimmu.2016.00012
167. Brooks DG, Kitchen SG, Kitchen CM et al (2001) Generation of HIV latency during thymopoiesis. Nat Med 7(4):459–464. doi:10.1038/86531

168. Brooks DG, Hamer DH, Arlen PA et al (2003) Molecular characterization, reactivation, and depletion of latent HIV. Immunity 19(3):413–423
169. Korin YD, Brooks DG, Brown S et al (2002) Effects of prostratin on T-cell activation and human immunodeficiency virus latency. J Virol 76(16):8118–8123
170. Berges BK, Rowan MR (2011) The utility of the new generation of humanized mice to study HIV-1 infection: transmission, prevention, pathogenesis, and treatment. Retrovirology 8:65. doi:10.1186/1742-4690-8-65
171. Hofer U, Baenziger S, Heikenwalder M et al (2008) RAG2−/− gamma(c)−/− mice transplanted with CD34+ cells from human cord blood show low levels of intestinal engraftment and are resistant to rectal transmission of human immunodeficiency virus. J Virol 82(24):12145–12153. doi:10.1128/JVI.01105-08
172. Akkina R, Berges BK, Palmer BE et al (2011) Humanized Rag1−/− gammac−/− mice support multilineage hematopoiesis and are susceptible to HIV-1 infection via systemic and vaginal routes. PLoS One 6(6):e20169. doi:10.1371/journal.pone.0020169
173. Choudhary SK, Archin NM, Cheema M et al (2012) Latent HIV-1 infection of resting CD4(+) T cells in the humanized Rag2(−)/(−) gammac(−)/(−) mouse. J Virol 86(1):114–120. doi:10.1128/JVI.05590-11
174. Holt N, Wang J, Kim K et al (2010) Human hematopoietic stem/progenitor cells modified by zinc-finger nucleases targeted to CCR5 control HIV-1 in vivo. Nat Biotechnol 28(8):839–847. doi:10.1038/nbt.1663
175. Halper-Stromberg A, Lu CL, Klein F et al (2014) Broadly neutralizing antibodies and viral inducers decrease rebound from HIV-1 latent reservoirs in humanized mice. Cell 158(5):989–999. doi:10.1016/j.cell.2014.07.043
176. Kirchhoff F (2008) Silencing HIV-1 in vivo. Cell 134(4):566–568. doi:10.1016/j.cell.2008.08.004
177. Kumar P, Ban HS, Kim SS et al (2008) T cell-specific siRNA delivery suppresses HIV-1 infection in humanized mice. Cell 134(4):577–586. doi:10.1016/j.cell.2008.06.034
178. Sun Z, Denton PW, Estes JD et al (2007) Intrarectal transmission, systemic infection, and CD4+ T cell depletion in humanized mice infected with HIV-1. J Exp Med 204(4):705–714. doi:10.1084/jem.20062411
179. Olesen R, Wahl A, Denton PW et al (2011) Immune reconstitution of the female reproductive tract of humanized BLT mice and their susceptibility to human immunodeficiency virus infection. J Reprod Immunol 88(2):195–203. doi:10.1016/j.jri.2010.11.005
180. Watkins RL, Foster JL, Garcia JV (2015) In vivo analysis of Nef's role in HIV-1 replication, systemic T cell activation and CD4(+) T cell loss. Retrovirology 12:61. doi:10.1186/s12977-015-0187-z
181. Denton PW, Long JM, Wietgrefe SW et al (2014) Targeted cytotoxic therapy kills persisting HIV infected cells during ART. PLoS Pathog 10(1):e1003872. doi:10.1371/journal.ppat.1003872
182. Shimizu S, Ringpis GE, Marsden MD et al (2015) RNAi-mediated CCR5 knockdown provides HIV-1 resistance to memory T cells in humanized BLT mice. Mol Ther Nucleic Acids e227:4. doi:10.1038/mtna.2015.3
183. Martin JL, Maldonado JO, Mueller JD et al (2016) Molecular studies of HTLV-1 replication: an update. Virus 8(2). doi:10.3390/v8020031
184. Goncalves DU, Proietti FA, Ribas JG et al (2010) Epidemiology, treatment, and prevention of human T-cell leukemia virus type 1-associated diseases. Clin Microbiol Rev 23(3):577–589. doi:10.1128/CMR.00063-09
185. Manel N, Battini JL, Taylor N et al (2005) HTLV-1 tropism and envelope receptor. Oncogene 24(39):6016–6025. doi:10.1038/sj.onc.1208972
186. Azran I, Schavinsky-Khrapunsky Y, Aboud M (2004) Role of tax protein in human T-cell leukemia virus type-I leukemogenicity. Retrovirology 1:20. doi:10.1186/1742-4690-1-20
187. Tezuka K, Xun R, Tei M et al (2014) An animal model of adult T-cell leukemia: humanized mice with HTLV-1-specific immunity. Blood 123(3):346–355. doi:10.1182/blood-2013-06-508861
188. Feuer G, Zack JA, Harrington WJ Jr et al (1993) Establishment of human T-cell leukemia virus type I T-cell lymphomas in severe combined immunodeficient mice. Blood 82(3):722–731
189. Kondo A, Imada K, Hattori T et al (1993) A model of in vivo cell proliferation of adult T-cell leukemia. Blood 82(8):2501–2509
190. Van Duyne R, Pedati C, Guendel I et al (2009) The utilization of humanized mouse models for the study of human retroviral infections. Retrovirology 6:76. doi:10.1186/1742-4690-6-76

191. Miyazato P, Yasunaga J, Taniguchi Y et al (2006) De novo human T-cell leukemia virus type 1 infection of human lymphocytes in NOD-SCID, common gamma-chain knockout mice. J Virol 80 (21):10683–10691. doi:10.1128/JVI.01009-06
192. Takajo I, Umeki K, Morishita K et al (2007) Engraftment of peripheral blood mononuclear cells from human T-lymphotropic virus type 1 carriers in NOD/SCID/gammac(null) (NOG) mice. Int J Cancer 121 (10):2205–2211. doi:10.1002/ijc.22972
193. Panfil AR, Al-Saleem JJ, Green PL (2013) Animal models utilized in HTLV-1 research. Virology (Auckl) 4:49–59. doi:10.4137/VRT.S12140
194. Villaudy J, Wencker M, Gadot N et al (2011) HTLV-1 propels thymic human T cell development in "human immune system" Rag2 (−)/(−) gamma c(−)/(−) mice. PLoS Pathog 7(9):e1002231. doi:10.1371/journal.ppat.1002231
195. Martin F, Bangham CR, Ciminale V et al (2011) Conference highlights of the 15th international conference on human retrovirology: HTLV and related retroviruses, 4-8 June 2011, Leuven, Gembloux, Belgium. Retrovirology 8:86. doi:10.1186/1742-4690-8-86
196. Tezuka K, Xun R, Tei M et al (2011) Inverse correlation between tax and CD25 expressions in HTLV-1 infected CD4 T-cells in vivo. Retrovirology 8(1):1–1. doi:10.1186/1742-4690-8-s1-a14
197. Peres E, Bagdassarian E, This S et al (2015) From immunodeficiency to humanization: the contribution of mouse models to explore HTLV-1 Leukemogenesis. Virus 7 (12):6371–6386. doi:10.3390/v7122944
198. Feuer G, Fraser JK, Zack JA et al (1996) Human T-cell leukemia virus infection of human hematopoietic progenitor cells: maintenance of virus infection during differentiation in vitro and in vivo. J Virol 70 (6):4038–4044
199. Saito M, Tanaka R, Fujii H et al (2014) The neutralizing function of the anti-HTLV-1 antibody is essential in preventing in vivo transmission of HTLV-1 to human T cells in NOD-SCID/gammacnull (NOG) mice. Retrovirology 11:74. doi:10.1186/s12977-014-0074-z
200. Hiyoshi M, Okuma K, Tateyama S et al (2015) Furin-dependent CCL17-fused recombinant toxin controls HTLV-1 infection by targeting and eliminating infected CCR4-expressing cells in vitro and in vivo. Retrovirology 12:73. doi:10.1186/s12977-015-0199-8

Chapter 2

Zebrafish as a Model for the Study of Host-Virus Interactions

Peng Fei Zou and Pin Nie

Abstract

Zebrafish (*Danio rerio*) has become an increasingly important model for in vivo and in vitro studies on host-pathogen interaction, offering scientists with optical accessibility and genetic tractability, and a vertebrate-type immunity that can be separated into innate and adaptive ones. Although it is shown in previous studies that few species of viruses can naturally infect zebrafish, the spring viraemia of carp virus (SVCV), a rhabdovirus that causes contagious acute hemorrhagic viraemia in a variety of cyprinid fishes, can infect zebrafish by both injection and static immersion methods in laboratory conditions. In addition, SVCV can infect zebrafish fibroblast cell line (ZF4 cells), together with the *Epithelioma papulosum cyprini* (EPC) cell line (EPC cells), a common cell line used widely in fish disease research. The infection and propagation of SVCV in zebrafish and especially in these cell lines can be employed conveniently in laboratory for functional assays of zebrafish genes. The zebrafish, ZF4 and EPC cell, and SVCV can serve as a simple and efficient model system in understanding host-virus interactions. In the present chapter, we provide detailed protocols for the host-virus interaction analysis based on zebrafish embryos, ZF4/EPC cells, and SVCV, including infection methods of zebrafish embryos and cell lines, analyses of immune responses by quantitative PCR (qPCR) and RNA sequencing (RNA-Seq), antiviral assays based on ZF4 and EPC cells, and the analysis of host-virus interaction using luciferase assays. These protocols should provide efficient and typical means to address host-virus interactions in a more general biological sense.

Key words Zebrafish, SVCV, Host-virus interaction, Immunity, ZF4, EPC

1 Introduction

Zebrafish (*Danio rerio*) is a species of vertebrates, which have both innate and adaptive immune systems, and the innate immunity can be investigated separately from the adaptive immunity which is found to be mature at least 3 weeks post-fertilization [1]. As a kind of fish with high fecundity (producing hundreds of embryos from one spawning pair), short spawning span, optical transparency of embryos and larvae, small size and rapid embryonic development, as well as the short life cycle, zebrafish has been an attractive model system to dissect host-pathogen interactions [2, 3]. In addition to the above features, zebrafish has the advantage of its well-

Karen Mossman (ed.), *Innate Antiviral Immunity: Methods and Protocols*, Methods in Molecular Biology, vol. 1656, DOI 10.1007/978-1-4939-7237-1_2, © Springer Science+Business Media LLC 2017

annotated genome [4]. Transient gene knockdown and overexpression can be achieved in vivo by microinjection in one-cell zygotes with designed morpholinos (MOs) and synthetic mRNA or recombinant DNA, respectively [5–7]. Furthermore, recently developed genome-editing approaches based on zinc finger nucleases (ZFNs) [8], transcription activator-like effector nucleases (TALENs) [9, 10], and clustered regularly interspaced short palindromic repeats (CRISPR) [11, 12] can be applied reliably and efficiently in zebrafish to achieve permanent and specific gene manipulation, which makes zebrafish model much more attractive and suitable for biological research in a much wider sense.

Although fish viruses have been studied extensively in relation with aquaculture [13], few viruses are found to infect zebrafish naturally [3, 14]. It has been documented that zebrafish could be experimentally infected with viruses from other fish species, such as Infectious hematopoietic necrosis virus (IHNV) [15, 16], Infectious pancreatic necrosis virus (IPNV) [17], Infectious spleen and kidney necrosis virus (ISKNV) [18, 19], Nervous necrosis virus (NNV) [20], Snakehead rhabdovirus (SHRV) [21, 22], Viral hemorrhagic septicemia virus (VHSV) [23, 24], and Spring viraemia of carp virus (SVCV) [25–30]. Despite this, zebrafish is also used for human viral disease models, such as Herpes simplex virus (HSV) [31, 32], Hepatitis C virus (HCV) [33], Chikungunya virus (CHIKV) [34], and Influenza A virus (IAV) [35]. Notably, most of the infection methods used for the viruses described above are through injection in zebrafish embryos and also in adult fish. However, two viruses, SHRV and SVCV, can infect zebrafish through static immersion [21, 22, 25, 26, 30]. Overall, zebrafish model may serve as the only, or complement other, animal models in examining host-virus interaction and in conducting genetic and chemical or therapeutic screenings, which may facilitate the functional assay of target genes, and the development and testing of new antiviral strategies.

In addition to the wide and successful use of zebrafish model for in vivo studies, zebrafish cell cultures such as embryonic fibroblast cell line (ZF4) and liver cell line (ZFL) are also powerful tools for in vitro analyses, contributing efficiently and sufficiently to the investigation of host immunity and host-pathogen interactions [21, 26, 29, 36, 37]. SVCV can infect not only zebrafish, but also zebrafish cell line (e.g., ZF4) under laboratory conditions [26, 29]. Another important cell line, *Epithelioma papulosum cyprini* (EPC) cells, can be the suitable cells for SVCV propagation. Due to the easy culture and high transfection efficiency, EPC cells have been used widely in functional assay of fish genes and in the study of host-virus interaction, especially in functional assay of genes in zebrafish which also belongs to the Cyprinidae family as the fish from which EPC cells were derived [27, 28, 37, 38]. In combination with the in vivo assays in the zebrafish model system, ZF4 as

well as EPC cells, and SVCV have been used as in vitro host-virus interaction models for understanding host immune responses as well as host-virus association in laboratory.

In this chapter, we provide techniques and detailed protocols for the study of host-virus interaction and for the examination of host immune responses, by using zebrafish embryos, ZF4 and EPC cells, and SVCV as an infection virus. Our main aim is to present essential protocols for researchers to examine host-virus interactions, and to provide useful suggestions in performance of such studies, although some details such as the virus propagation as well as the infection method may not be applicable for other viral pathogens.

2 Materials

2.1 Zebrafish Embryos, Cells, and Virus Preparation

1. Zebrafish rearing facility.
2. Adult wild-type AB fish or specific gene manipulation fish.
3. Spawning tanks.
4. Incubator maintained at 28 °C.
5. Embryo water: 5 mM NaCl, 0.17 mM KCl, 0.33 mM $CaCl_2$, 0.33 mM $MgSO_4$ in sterilized water, supplemented with 0.3 μg/mL methylene blue [39].
6. 100 × 20 and 35 × 10 mm Petri dishes.
7. 25 cm^2, 75 cm^2 flasks.
8. Cell culture plates (6-well and 12-well).
9. CO_2 incubator.
10. Zebrafish embryonic fibroblast cells (ZF4).
11. ZF4 cell culture medium: 1:1 mixed Dulbecco modified Eagle medium (DMEM) and Ham F12 medium supplemented with 10% fetal bovine serum and 100 U/mL penicillin and streptomycin.
12. *Epithelioma papulosum cyprini* (EPC) cells.
13. EPC cell culture medium: Minimum essential medium (MEM) supplemented with 10% fetal bovine serum and 100 U/mL penicillin and streptomycin.
14. 0.25% Trypsin-EDTA.
15. Methylcellulose.
16. Paraformaldehyde.
17. Crystal violet.
18. Spring Viraemia of Carp Virus (SVCV).
19. Centrifuge tubes (2.0 mL and 50 mL).
20. Refrigerated centrifuge.

2.2 Microinjection and Static Immersion Apparatus

1. Microinjector (e.g., Eppendorf, Femto Jet).
2. Mechanical xyz micromanipulator arm (e.g., Narishige, M-152).
3. Microloader pipette tips.
4. Stereo-microscope.
5. Borosilicate glass capillaries.
6. Pipette puller.
7. Phenol red.
8. Agarose.
9. Tricaine.
10. Dumont Watchmaker's forceps No. 5.
11. 100 × 20 and 35 × 10 mm Petri dishes.

2.3 Tools for qPCR and RNA-Seq Analyses

1. Trizol® reagents.
2. Trichloromethane.
3. Isopropanol.
4. Ethanol 75%.
5. Homogenizer.
6. Micro-pipette (e.g., Eppendorf) and tips (10 μL, 200 μL, and 1000 μL).
7. Microtubes (1.5 mL and 200 μL).
8. DNase I, RNase-free.
9. cDNA synthesis kit.
10. qPCR primers with Tm of 58–60 °C.
11. qPCR mix: SYBR Green dye, 50 U/mL Taq DNA polymerase, 0.4 mM each dNTPs, 6 mM $MgCl_2$, 40 mM Tris–HCl pH 8.4, 100 mM KCl, 20 nM fluorescein.
12. Thermal cycler for PCR.
13. Quantitative real-time PCR detection system.

2.4 Tools for Antiviral Assays

1. Plasmids that can express target genes in eukaryotic cells and the desired constructed plasmids (e.g., pcDNA3.1/myc-His(-) A and ptGFP1 [40]).
2. Plasmid purification kit.
3. Cell lines (e.g., ZF4 and EPC).
4. SVCV.
5. Electronical transfection system (e.g., Lonza, Amaxa® Nucleofector® II Device).
6. Electronical transfection reagents (e.g., Lonza, Amaxa™ Cell Line Nucleofector™ Kit V).

7. G418 sulfate.
8. ZF4 cell culture medium.
9. EPC cell culture medium.
10. Opti-MEM medium.
11. 0.25% Trypsin-EDTA.
12. Methylcellulose.
13. Paraformaldehyde.
14. Crystal violet.
15. Lipofectamine™ 2000 transfection reagent.
16. Cell culture plates (12-well, 24-well, and 48-well).
17. 25 cm^2, 75 cm^2 flasks.
18. Microtubes (1.5 and 2.0 mL).

2.5 Tools for Luciferase Assays

1. Constructed plasmids that express host gene as well as viral components.
2. Luciferase reporter plasmids (e.g., IFNφ1pro-Luc, pGL3-Basic, pRL-TK).
3. Cell lines (e.g., EPC).
4. SVCV.
5. Opti-MEM medium.
6. ZF4 cell culture medium.
7. 0.25% Trypsin-EDTA.
8. Lipofectamine™ 2000 transfection reagent.
9. Cell culture plates (24-well).
10. Luminometer (e.g., Promega, GloMax® 20/20).
11. Dual-Luciferase® assay system.

3 Methods

3.1 Zebrafish Embryos, Cells, and Virus Preparation

3.1.1 Preparation of Embryos for Infection

1. Prepare several spawning tanks (containing inner tank with holes that allow laid embryos falling through the holes and preventing adults from eating the embryos) with three to five adult pairs of the breeding wild-type AB zebrafish or specific gene manipulation zebrafish.
2. Collect the zebrafish embryos carefully and rinse with fresh water and transfer the embryos in standard Petri dishes with indicated embryo water.
3. Keep the dishes with embryos in an incubator at 28 °C, remove bad embryos (abnormal developmental embryos) and the remaining waste, and change the culture medium with fresh embryo water every day.

3.1.2 Cell Culture

1. Culture ZF4 cells in a ZF4 cell culture medium at 28 °C in an incubator with 5% CO_2 [36] and EPC cells in an EPC cell culture medium at 25 °C in an incubator with 5% CO_2. The detail methods for cell propagation are as the followings.
2. Maintain the cells in the culture medium as described above in 25 cm^2 or 75 cm^2 flasks.
3. When the cells in the flasks are about 80% confluent, remove the medium and add appropriate 0.25% Trypsin-EDTA (1 mL for 25 cm^2 flask and 2 mL for 75 cm^2 flask) and incubate for 3–5 min to detach the cells from culture flasks.
4. Flutter the flasks gently for detaching the cells completely, add appropriate fresh medium (~ 5 mL), and mix gently.
5. Remove the cell suspension to a 50 mL tube and count the total cell numbers by using hemocytometer.
6. Dilute the cell suspension with fresh medium to an appropriate amount (e.g., 2×10^5 cells in 500 μL plating medium for one well of the 24-well plate), and transfer cell culture into the plates or flasks for later assays such as transfection and infection.

3.1.3 Virus Propagation and Titer Determination for Infection

SVCV could propagate effectively in EPC cells and the virus titer could also be determined by plaque assay on EPC cells. Herein, we describe the detailed procedures used for SVCV propagation and titer determination.

1. Prepare the EPC cells in the 75 cm^2 flask to be about 90% confluent.
2. Thaw SVCV on ice (*see* **Note 1**) and dilute about 2 μL seed virus (*see* **Note 2**) in the 5 mL MEM medium without FBS.
3. Remove the medium of EPC cells and wash the cells once with FBS-free MEM. Remove the medium and gently add the diluted seed virus medium into the flask. Gently shake the flask every 15 min to make sure the virus contact with the cells, and incubate the cells at 25 °C in a CO_2 incubator for 1 h.
4. Remove the seed virus medium and add appropriate volume of normal MEM medium (~15 mL) for cell culture.
5. Check the cell status daily until the appearance of total cytopathic effect (CPE) rising to 80%, put the flask of cells in −80 °C and release the virus from the cells by the repeated freeze-thaw method for three times.
6. Collet the cell lysate and centrifuge at 12,000 × *g* for 20 min to remove the cell debris, transfer the supernatant to new tubes, and store at −80 °C for further analysis.
7. Prepare the EPC cells in 12-well plates for the determination of the virus titer (the cells in plates should be about 90% confluent).

8. Dilute the virus at 1:10, 1:100, 1:1000 and so on with the no-FBS MEM to a volume of 400 μL, and plate the virus dilution in 12-well plates, and then perform as described in Subheading 3.1.3.
9. Remove the virus dilution medium, add 800 μL MEM (with 0.5% methylcellulose and 10% FBS) per well and incubate at 25 °C.
10. Check the cell growth and death everyday using a microscope. When the complete plaque shows up (about 48 h, *see* **Note 3**), fix the cells with a final concentration of 10% paraformaldehyde for 1 h.
11. Remove the mixture and gently wash the cells with fresh water and then stain the cells with 0.5% crystal violet for 2–3 h.
12. Remove the crystal violet medium, gently wash the cells with fresh water, and count the number of plaques. Determine the virus titer by calculating the amount of viruses using the formula: 2.5 × dilution ratio × numbers of plaques emerged at the dilution = total PFU (plaque forming units) of 1 mL virus medium (PFU/mL). Three individual experiments should be performed and data recorded as mean ± standard error (SE).

3.2 Infection with Virus

Zebrafish embryos as well as larvae can be infected with SVCV through static immersion and microinjection [25, 26, 30]. Basically, it is more convenient to infect the embryos by static immersion, whereas the infection by microinjection can be complicated but extremely efficient (the 50% lethal dose is ~2 PFU and 8 PFU for 30- and 54-h post-fertilization (hpf) embryos, respectively) [30]. Although recent genome-editing approaches like ZFNs, TALENs, and CRISPR can generate permanent gene manipulation embryos, transient gene knockdown techniques like MOs still play important roles in such studies [5]. However, MOs knockdown of zebrafish embryos is efficient for not more than 1 week post-fertilization, and zebrafish become susceptible to SVCV until they can swim and open the mouth and gill slits for respiratory movements (about 4 ~ 5 dpf) [5, 30]. It is the fact that only a few viruses can successfully infect zebrafish by immersion, making the infection by microinjection an important method in many research approaches. Herein, we provide the protocols of infecting zebrafish embryos by microinjection and immersion with SVCV, respectively. A typical work plan for infecting zebrafish embryos with SVCV by microinjection is shown in Fig. 1.

3.2.1 SVCV Infection in Zebrafish Embryos by Microinjection

1. Collect and culture zebrafish embryos as described in Subheading 3.1.1. Separate the 48 hpf zebrafish embryos into about 100 per dish for microinjection.

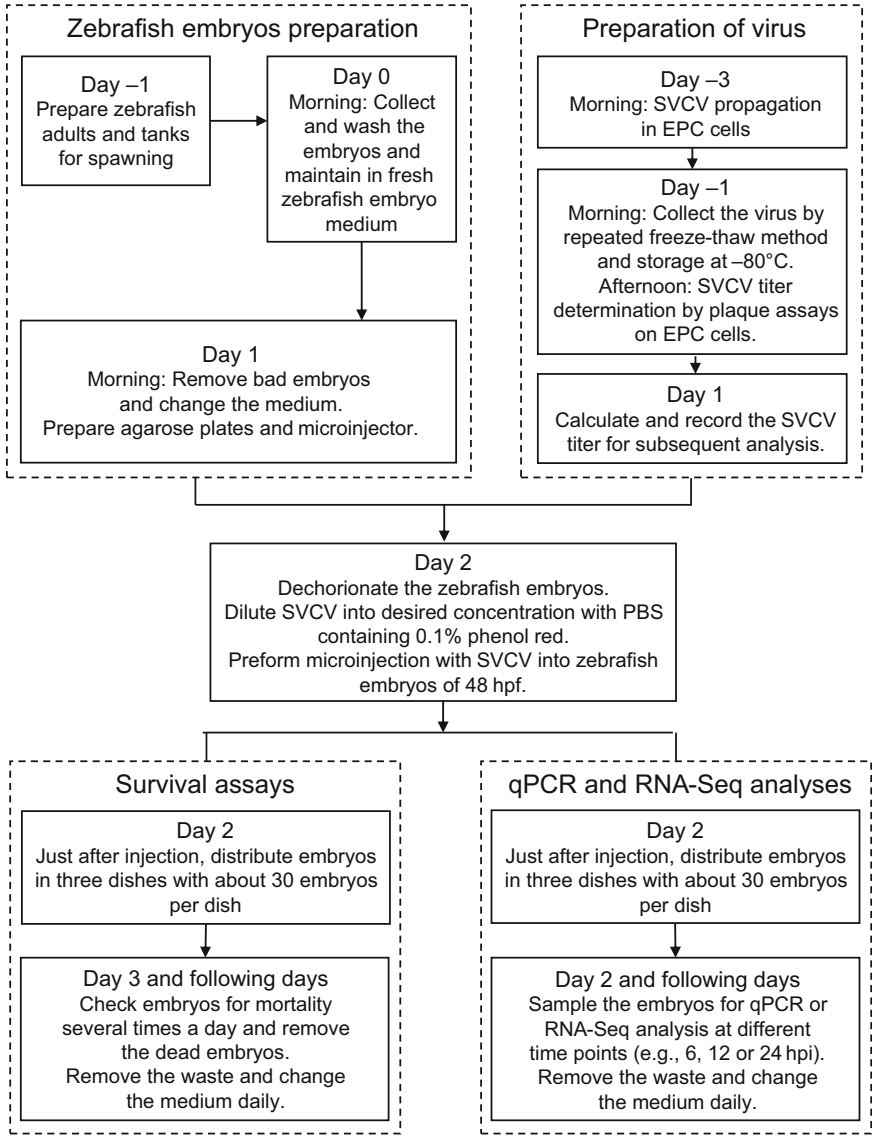

Fig. 1 Typical work plan for infection of zebrafish embryos with SVCV by microinjection. *hpf* hours post-fertilization; *hpi* hours post-infection

2. Manually dechorionate all embryos with Dumont Watchmaker's forceps No. 5 and transfer the embryos into new dishes.
3. Prepare 50 mL embryo water with 200 μg/mL tricaine and move the embryos for microinjection into the dish and incubate for not more than 5 min.
4. Transfer the embryos from the dish with tricaine to a new dish filled with 3% agarose, leaving as little water on the surface of

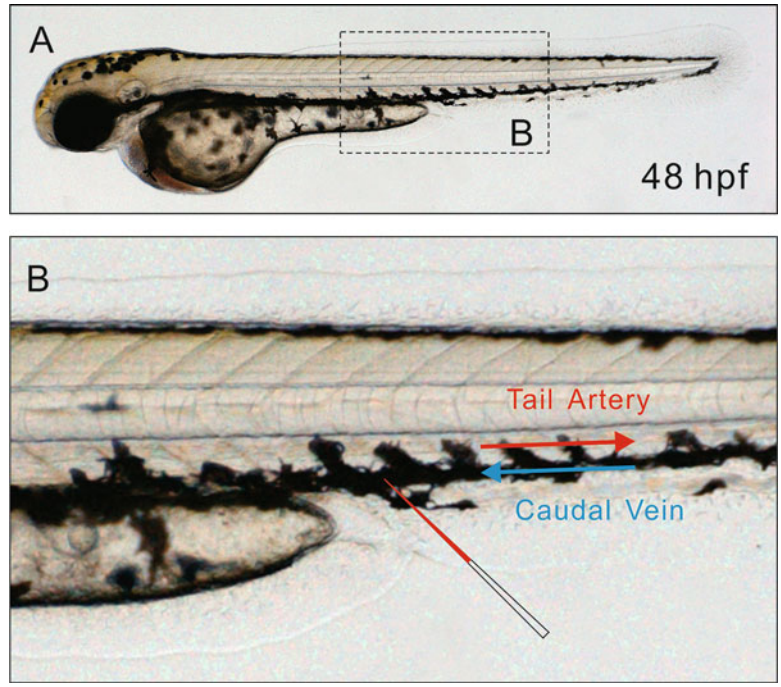

Fig. 2 Microinjection sites of zebrafish embryos. The figure provides the commonly used method for microinjection of SVCV into a 48 hpf zebrafish embryo (**a**). The position of the tail artery and caudal vein of the zebrafish embryo are shown, and the microinjection site is directed with a schematic red needle (**b**)

agarose as possible for aligning the embryos in a same direction.

5. Thaw SVCV on ice and dilute the SVCV titer to reach your desired dose with PBS containing 0.1% phenol red (usually 10^7 PFU/mL).
6. Load 3 ~ 5 μL SVCV dilution into a pulled capillary pipette using a microloader tip and place on the micromanipulator (*see* **Note 4**). Adjust time and pressure of the microinjector to obtain an injection volume of around 2 nl.
7. Locate the capillary needle at the caudal vein and microinject the SVCV dilution with a single pulse with the phenol red to visualize the injection (Fig. 2). Remove the embryos that are poorly injected.
8. Rinse and transfer the embryos into new dishes containing fresh embryo water and maintain at 25 °C (*see* **Note 5**).
9. Separate the embryos into two groups, one for survival experiments and another for gene induction measurements; each group includes three dishes with 30 embryos per dish.

The embryos should be checked daily and dead embryos should be removed, with fresh embryo water added.

10. For control group, the embryos should be microinjected with the same volume of PBS containing 0.1% phenol red at the same position and treated under the same condition.

3.2.2 SVCV Infection in Zebrafish Embryos by Static Immersion

1. Separate the zebrafish embryos into about 100 per dish for infection. At 4 dpf, remove as much embryo water as possible to collect the zebrafish larvae, most of which could swim by then.
2. Immerse the larvae into 10 mL embryo water containing 10^6 PFU/mL SVCV. Control larvae should be exposed to an equal volume of PBS in 10 mL embryo water.
3. Maintain the larvae for 12 h at 25 °C.
4. Wash the larvae carefully with fresh embryo water, transfer the larvae into new dishes of fresh embryo water, and maintain at 25 °C.
5. Separate the infected larvae for two groups, one for survival experiments, and another for gene induction measurements; each group includes three dishes with 30 larvae per dish. The larvae should be monitored daily and dead larvae should be removed, with fresh embryo water added.

3.2.3 SVCV Infection in Zebrafish Cells

Compared with the zebrafish embryos as a model to investigate host-virus interaction in vivo, zebrafish cell lines, like ZF4 and ZFL cells, are also important materials for understanding host-virus interaction in vitro, especially in gene induction measurements and antiviral assays [27–29, 37]. The following section provides the protocols for SVCV infection in ZF4 cells as an example.

1. Transfer the ZF4 cells from the flasks to 6-well plates as described in Subheading 3.1.2. Usually, 1×10^6 cells per well with 2 mL medium should be set up. Then, incubate the cells at 25 °C overnight (*see* **Note 4**).
2. Prepare SVCV for infection in the following day. The specific multiplicity of infection (MOI) of virus to each well must be calculated before infection. Use the formula: (the number of cells) × (desired MOI)/(virus titer (PFU/mL)) = total mL of virus suspension needed to reach your desired dose. For example, you have SVCV with a titer of 1×10^8 PFU/mL and ZF4 cells with 1×10^6 per well, and the desired MOI is 10. Then, the formula is: (1×10^6 cells) × (10 MOI)/(1×10^8 PFU/mL) = 0.1 mL or 100 μL. Therefore, the total volume of virus suspension needed is 100 μL.
3. Dilute the desired volume of SVCV with no FBS added DMEM/F12 medium to a total volume of 2 mL.

4. Remove the culture medium in 6-well plates and add SVCV dilution into the well and incubate at 25 °C for 1 h, with gentle shaking of the plates every 15 min to make sure the virus contacting with the cells.
5. Remove the virus dilution and add 2 mL DMEM/F12 medium with 10% FBS per well for cell culture.
6. Monitor the cell status daily and sample the cells at various time points like 6 or 24 h post-infection (hpi) for further analyses such as gene expression analysis and antiviral assay.

3.3 qPCR and RNA-Seq Analyses

Quantitative real-time PCR (qPCR) is a simple and efficient method to examine the host response such as the induction of immune-related genes under the infection of virus. The following section describes the methodological details for qPCR and RNA-Seq analyses.

3.3.1 qPCR and RNA-Seq Analyses Using Embryos

1. Prepare the primers for qPCR, and the target genes may be immune-related genes, such as interferon, Toll like receptors (TLRs), RIG-I like receptors (RLRs) genes, and so on. The primers for housekeeping genes like GAPDH and β-Actin should also be included.
2. Culture and infect zebrafish embryos with SVCV as described in Subheading 3.2.1.
3. At appropriate time post-infection (e.g., 6, 12, 24 hpi, and so on), collect the embryos (~10 embryos) and transfer them into RNase-free tubes and wash with water.
4. Discard the water and add 1 mL Trizol® reagents for total RNAs extraction. The methodological details are as the followings:
   (a) Homogenize embryos with Trizol using a homogenizer.
   (b) Add 200 μL trichloromethane into the tube containing homogenized embryos with vigorous mixing for 1 min, then incubate at room temperature for 5 min.
   (c) Centrifuge the suspension at 12,000 × *g* for 10 min at 4 °C.
   (d) Transfer the supernatant gently (~400 μL) into a new tube.
   (e) Add 600 μL isopropanol into the tube and mix gently, then incubate at room temperature for 5 min.
   (f) Centrifuge at 12,000 × *g* for 15 min at 4 °C.
   (g) Discard the supernatant and add 1 mL of 75% cold ethanol with the gentle inverting of the tube several times, and then centrifuge at 12,000 × *g* for 10 min at 4 °C.

(h) Discard the liquid and dry the RNA precipitation (usually place the tube at room temperature for 15 min with the lid open).

(i) Add appropriate volume (~30 μL) of RNase-free water to dissolve the RNA precipitation. Determine the quality as well as the concentration by using a spectrophotometer (*see* **Note 6**).

5. Use appropriate amount of total RNA (~1 μg) for cDNA synthesis. Prior to cDNA synthesis, total RNA should be treated with RNase-free DNase I to remove trace amount of DNA as described by the manufacturer.
6. Use the DNase I treated RNA for cDNA synthesis using a cDNA synthesis kit on a thermal cycler for PCR following the instructions of the manufacturer.
7. Perform qPCR on a quantitative real-time PCR detection system with amplifying target genes (e.g., TLRs) as well as housekeeping gene (e.g., GAPDH) transcripts. The gene expression pattern can be presented as fold change relative to the control group, which can be referred to a previous publication [41]. Additionally, the purified RNA could also be used for RNA-Seq analysis to obtain an extensive understanding of the gene transcription under virus infection.

3.3.2 qPCR and RNA-Seq Analyses Using Cell Lines

1. Culture and transfer the cells (e.g., ZF4) into 6-well plates, and on the following day, infect the cells with SVCV at desired MOI as described in Subheading 3.2.3.
2. At different time points post-infection (e.g., 6, 12, 24 hpi, and so on), remove the medium and add 1 mL Trizol® reagents for total RNA extraction. Completely lyse the cell pellet by pipetting the liquid several times.
3. Extract total RNA and synthesize cDNA as described in Subheading 3.3.1.
4. Perform qPCR to analyze the gene expression pattern in a quantitative real-time PCR detection system using the synthesized cDNA, and the RNA-Seq assay could also be used to achieve a full understanding of gene transcription in cells under virus infection.

3.4 Antiviral Assays

To examine the function of genes in zebrafish antiviral response, it is a simple and effective method to overexpress genes in cell lines for further antiviral assays or for checking the induction of downstream molecules [27–29, 37]. The following protocol provides the methods for antiviral assays in vitro by using stably transfected ZF4 cells (ZF4 cells stably transfected with ptGFP1-NOD2 plasmid as an example) and transiently transfected EPC cells (EPC cells transiently transfected with pcDNA3.1-MDA5 as an example)

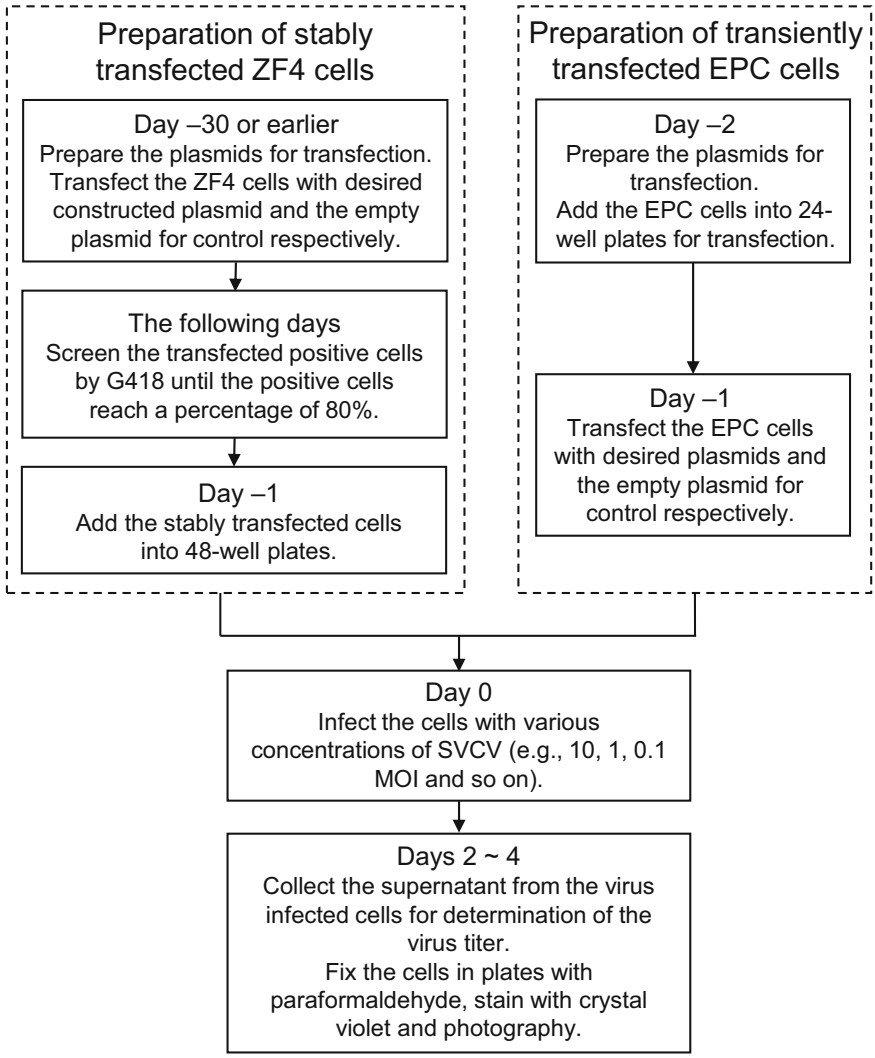

Fig. 3 Typical work plan for antiviral assays using ZF4 and EPC cells. *MOI* multiplicity of infection

respectively [27, 28]. A typical work plan of antiviral assays using stably transfected ZF4 cells as well as transiently transfected EPC cells against SVCV infection can be referred to in Fig. 3.

3.4.1 Antiviral Assays by Stably Transfected ZF4 Cells

1. Prepare the construct plasmids for transfection. The plasmid can be commercial plasmid (e.g., pcDNA3.1/myc-His(-) A), and can also be those constructed by researchers, which can express efficiently the target protein in cells. Herein, we choose ptGFP1 vector for overexpression, which is modified from the commercial plasmid pTurboGFP-N vector (Evrogen), and contains two sets of CMV promoter and SV40 3′ UTR to drive the expression of target gene product and GFP as separate proteins rather than as a fusion protein [40].

2. Construct the target gene (e.g., NOD2) sequence into ptGFP1 vector using molecular cloning technology, and confirm the constructed plasmid by sequencing (*see* **Note 7**).
3. Purify the plasmid by using the commercial plasmid purification kit and measure the purified plasmid concentration by a spectrophotometer.
4. Add the ZF4 cells into a new 25 cm^2 flask as described in Subheading 3.1.2 and culture the cells for 1 ~ 2 days.
5. Transfect the cells with the 2 μg constructed ptGFP1-NOD2 plasmid by using the Amaxa Nucleofector II transfection system (Lonza). Briefly, harvest the cells as described in Subheading 3.1.2 by using 0.25% Trypsin-EDTA and transfer the cells into a new tube and centrifuge at 400 × *g* for 10 min to pellet the cells. Discard the supernatant and resuspend the cells with a 100 μL room-temperature cell line Nucleofector® solution and add a 2 μg constructed ptGFP1-NOD2 plasmid. Transfer the cell/plasmid suspension into the certified cuvette with the cap closed and select Nucleofector® program T20 for transfection. Add ~500 μL medium into the cuvette and gently transfer the cells into a new 25 cm^2 flask with 5 mL medium for culture in an incubator.
6. Remove the medium with the dead cells in the following day, and add 5 mL medium containing 1000 μg/mL G418 sulfate for screening of transfected positive cells.
7. Change the medium with G418 per 3 ~ 5 days and culture the cells with screening for 2 ~ 4 weeks till the transfected positive cells reach a percentage of about 80% (the ptGFP1 plasmid could express GFP separately in transfected cells which could determine as a marker and be examined under a fluorescence microscope). Then, maintain the cell with medium containing 200 μg/mL G418.
8. Harvest the stably transfected ptGFP1-NOD2 cells and transfer into 48-well plates with 1.5 × 10^5 cells per well. The cells stably transfected ptGFP1 empty vector is passed separately and set as control. Incubate the plates of cells at 25 °C.
9. Infect the cells with various concentrations of SVCV (e.g., 10 MOI, 1 MOI, 0.1 MOI, and so on), as described in Subheading 3.2.2.
10. Monitor the cells daily under a microscope till the target cells represent some different status relative to the control cells (e.g., the cells stably transfected ptGFP1-NOD2 cells represent fewer CPE compared to the control cells under the same infection concentration of SVCV), and the time point can be normally 4 days after infection.

11. Collect the supernatant from the target cells and the control cells with the same infection concentration for titer determination by using EPC cells, and fix the plates of ZF4 cells with paraformaldehyde, followed by staining with crystal violet as described in Subheading 3.1.3 and then record by photography.
12. Representative antiviral assay using ZF4 cells stably transfected with ptGFP1 (vector control) or ptGFP1-NOD2 with the infection of SVCV is shown in Fig. 4.

3.4.2 Antiviral Assays by Transiently Transfected EPC Cells

Zebrafish, as a freshwater fish belonging to the Cypriniformes, has a close relationship with common carp (*Cyprinus carpio*) also belonging to this order. It is possible to express zebrafish genes in EPC, which is a cell line from carp [27–29, 37, 38]. In addition, the cell line of EPC has a much higher transfection efficiency and susceptibility to SVCV infection compared to zebrafish cells like ZF4 and ZFL. To some extent, the EPC cell line can be an easy and efficient tool for understanding the function of zebrafish genes in host-virus interaction in vitro. The following section provides the protocols for antiviral assays in transiently transfected EPC cells.

1. Prepare the construct plasmids (e.g., pcDNA3.1-MDA5 for overexpressing MDA5, and empty pcDNA3.1 plasmid for control) for transfection as described in Subheading 3.4.1.
2. Transfer the EPC cells into 24-well plates with 1×10^6 cells per well and incubate the cells at 25 °C overnight.
3. Transfect the cells with 1 μg pcDNA3.1-MDA5 or pcDNA3.1 empty plasmid respectively by using Lipofectamine™ 2000 according to the manufacturer's instructions. Briefly, the methodological details for the transfection of a well in a 24-well plate are as the followings:
   (a) Dilute the plasmids in 50 μL Opti-MEM® and mix gently.
   (b) Dilute appropriate amount (~ 1 μL) of Lipofectamine™ 2000 in 50 μL Opti-MEM® medium and incubate for 5 min at room temperature.
   (c) Combine the diluted plasmid with diluted Lipofectamine™ 2000, mix gently and incubate for 20 min at room temperature.
   (d) Add the 100 μL complex to each well and mix gently by shaking the plate back and forth.
   (e) Change the medium after 4 ~ 6 h incubation at 25 °C.
4. At 24 h post-transfection, infect the transfected EPC cells with various concentrations of SVCV (e.g., 1 MOI, 0.1 MOI, 0.01 MOI, and so on) as described in Subheading 3.2.2.

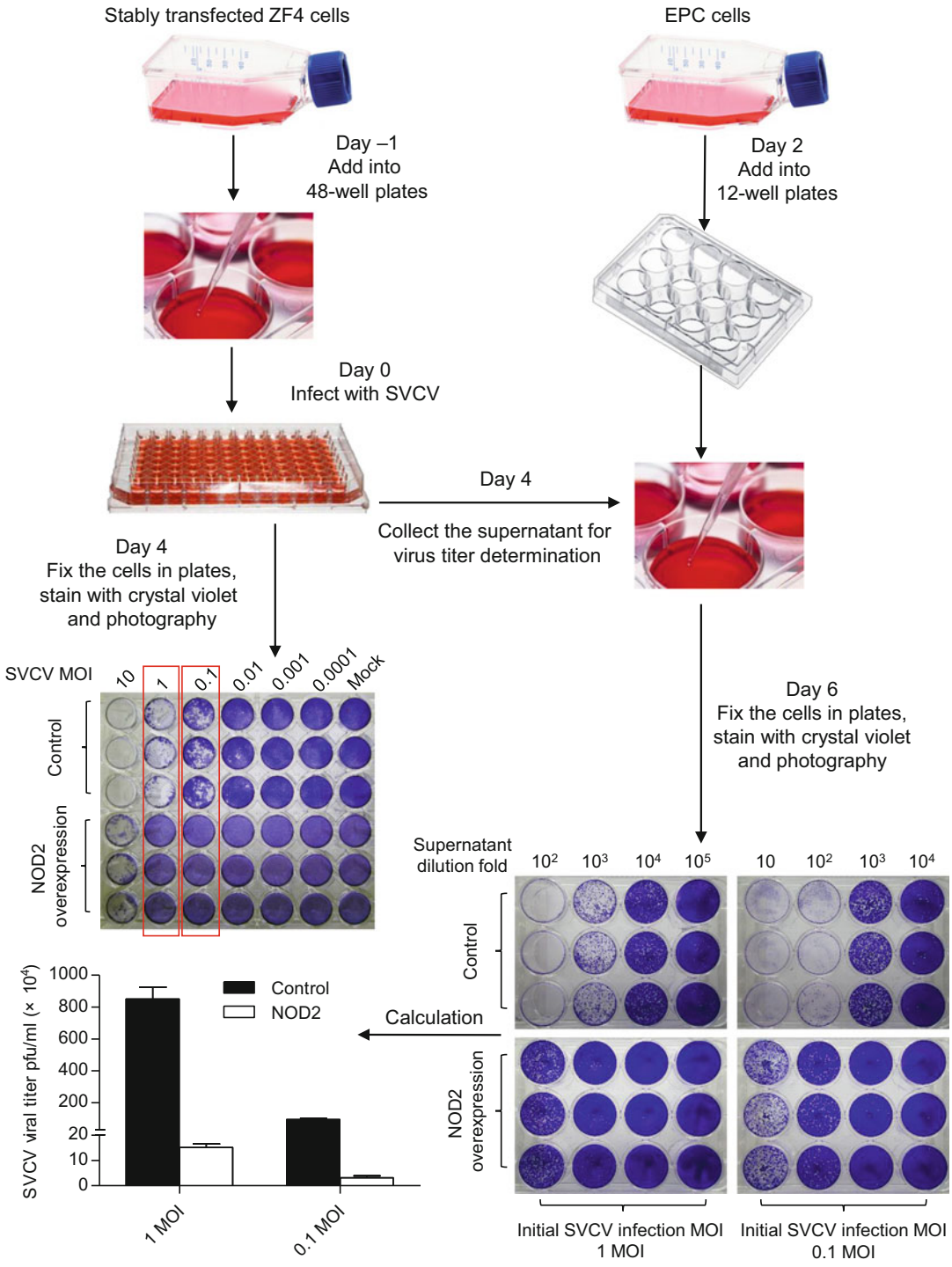

Fig. 4 Antiviral assays of zebrafish NOD2 in ZF4 cells. ZF4 cell line stably transfected with ptGFP1 (vector control) or ptGPF1-NOD2 was transferred into a 48-well plate and infected with tenfold-diluted SVCV for 4 d. The supernatants from stably transfected ZF4 cells with initial SVCV infection at MOI of 1 and 0.1 (marked out with red boxes) were collected and titrated on EPC cells in 12-well plates. The 48-well plates were then fixed with 10% paraformaldehyde, stained with 0.5% crystal violet, washed and photographed. About 2 d after seeding the supernatant dilution on EPC cells in 12-well plates, the plaque can be identified directly with naked vision, then fixed, stained and photographed as described above, and the virus titer can be calculated. Date were expressed as mean ± SE

5. Monitor the cells under a microscope daily till the target cells (cells transfected with pcDNA3.1-MDA5) exhibit obvious different status relative to the control cells (cells stably transfected with pcDNA3.1), such as cells have fewer CPE compared to the control cells under the same infection concentration of SVCV, and the time point for the result should normally be 48 h or less after infection (*see* **Note 2**).
6. Collect the supernatant from the target cells and the control cells with the same infection concentration for titer determination by EPC cells, and fix the plates of EPC cells with paraformaldehyde, followed by staining with crystal violet as described in Subheading 3.1.3 and then record by photography.

3.5 Luciferase Assays for the Study of Host-Virus Interactions

As described above, EPC cells can be transfected with plasmids at high efficiency, and could be used successfully in expressing zebrafish genes even in the promoter assays of zebrafish genes, such as the induction of IFNφ1, IFNφ2, IFNφ3, and IFNφ4 promoters [37]. In addition to the high susceptibility of EPC cells under SVCV infection, EPC cells can be effective tools for understanding host-virus interaction even at the molecular level. We provide a method using EPC cells to investigate the interaction of zebrafish proteins and SVCV proteins. The following section is the details of a method based on luciferase assay to investigate that the N protein of SVCV suppresses zebrafish IFNφ1 production by targeting MAVS as an example.

3.5.1 Luciferase Assay Under Direct Virus Infection to Study Host-Virus Interaction

1. Construct the IFNφ1 promoter reporter plasmid (IFNφ1pro-Luc) using pGL3-Basic luciferase reporter vector, and the plasmid encoding zebrafish MAVS (pcDNA3.1-MAVS) in the pcDNA3.1 vector.
2. Add the EPC cells into 24-well plates with 1×10^6 cells per well and incubate the cells at 25 °C overnight.
3. Transiently transfect the cells with 250 ng IFNφ1pro-Luc, 25 ng pRL-TK plus 250 ng pcDNA3.1-MAVS or pcDNA3.1 (control) using Lipofectamine™ 2000 as described in Subheading 3.4.2.
4. At 6 h post-transfection, cells were infected with SVCV at various concentrations (e.g., 1 MOI or 0.1 MOI) (*see* **Note 8**), and the cells without SVCV infection should be set as mock.
5. At 48 h post-transfection, collect the cells and prepare for luciferase assay by Dual-Luciferase® according to the manufacturer's instructions as the followings:
   (a) Dilute 5 × Passive Lysis Buffer (PLB) into 1 × PLB using distilled water, and mix well.
   (b) Remove the medium from culture cells and gently apply 800 μL PBS to rinse the bottom of the well once.

(c) Remove the PBS and add 100 μL 1 × PLB into each well and shake the culture plates at room temperature for 15 min on a shaker.

(d) Transfer the lysate into a 1.5 mL tube and centrifuge at 12,000 × *g* for 30 s in a centrifuge. Transfer the cleared lysates into a new tube.

(e) Prepare appropriate volume of Luciferase Assay Reagent II (LAR II) (20 μL per assay) and dilute 50 × Stop & Glo® Substrate into 1× with Stop & Glo® buffer to an adequate volume (20 μL per assay).

(f) Programme the luminometer to perform a 2 s premeasurement delay, followed by a 10 s measurement period for each assay.

(g) Transfer 4 μL cell lysate into the luminometer tube containing 20 μL LAR II and mix by pipetting for 3 ~ 5 times. Place the tube in the luminometer, and initiate reading and record the firefly luciferase activity measurement.

(h) Add 20 μL 1× Stop & Glo® Substrate into the luminometer tube and pipet for 3 ~ 5 times to mix. Place the tube in the luminometer, initiate reading, and record the *Renilla* luciferase activity measurement.

(i) Discard the reaction tube and proceed to the next assay.

6. Analyze the results of luciferase assays: relative luciferase activity = the value of firefly luciferase activity/the value of *Renilla* luciferase activity. The relative luciferase activity of cells transfected with pcDNA3.1 (control) or pcDNA3.1-MAVS under the infection of SVCV or without SVCV infection (mock) could be calculated and analyzed, in turn identify whether SVCV infection could affect zebrafish MAVS-mediated IFNφ1 promoter activation.

3.5.2 Luciferase Assay with Virus Components to Study Host-Virus Interaction

The section in Subheading 3.5.1 provides a method to investigate whether a virus could affect the host immune response by luciferase assays (e.g., zebrafish MAVS-mediated IFNφ1 promoter activation could be inhibited by SVCV infection). However, the components that affect the host immune response are still unknown. Herein, we describe a method based on luciferase assay to identify the components of virus which suppresses host immune response.

1. Prepare the plasmids such as IFNφ1pro-Luc, pRL-TK, pcDNA3.1-MAVS, and the plasmids expressing components of SVCV (e.g., pcDNA3.1-N, N protein of SVCV).
2. Add the EPC cells into 24-well plates with 1×10^6 cells per well and incubate the cells at 25 °C overnight.

3. Transiently transfect the cells with 250 ng IFNφ1pro-Luc, 25 ng pRL-TK, 250 ng pcDNA3.1-MAVS plus pcDNA3.1-N or pcDNA3.1 (control) using Lipofectamine™ 2000 as described in Subheading 3.4.2.
4. At 48 h post-transfection, harvest the cells and perform luciferase assay by Dual-Luciferase® as described in Subheading 3.5.1.

4 Notes

1. It is important to store your virus at −80 °C and threw on ice before using it; higher than the temperature may cause the loss of virus titer.
2. EPC cells are very sensitive to SVCV infection, and SVCV propagation could cause mass mortality of the cells. If the cells die faster following the seeding of virus, the virus may not propagate enough. Thus, it is important to use less seeding virus (e.g., 1 ~ 2 μL from the SVCV medium with a titer of 1×10^7 pfu/mL) in order to let the cells survive long enough (usually 2 ~ 3 days after infection with the seeding virus) and make the virus propagate sufficiently to reach a high titer when harvesting.
3. It is necessary to check the cell growth situation frequently to make sure the complete plaque in cells reach appropriate size which can be easily identified and counted with direct observation of naked eyes. If we fix the cells earlier, the plaque size would be too small to be identified, whereas if we fix the cells later, plaques would fuse together, resulting in difficulties to distinguish one plaque from another. We usually choose 48 hpi as the time point to fix the cells. In addition, appropriate density of plaques in wells of 12-well plates is important for the accurate determination of the virus titer (about 50 ~ 150 plaques per well should be sufficient enough). Thus, it is necessary to set various dilutions (such as 1:100, 1:1000, 1:10,000, and so on) to obtain a much more precise data of the virus titer.
4. If there are many zebrafish embryos (more than 200) needed to be microinjected with SVCV, which will take long time (more than 1 h), it is recommended to load some more microinjection capillary needles with SVCV suspension (depending on the number of embryos you need to microinject) and place them on ice whenever possible, change the microinjection capillary needle every 30 min in case that the infectivity of the virus may diminish when left too long in the microinjection capillary needle at room temperature.

5. Since the SVCV infectivity could diminish when the temperature becomes too high, it is recommended to culture the embryos or cells infected with SVCV at a relatively lower temperature. In case that low temperature could also influence the embryonic development, we suggest taking 25 °C for maintaining the embryos or cells that are infected with SVCV.
6. It is important to examine the quality as well as the concentration of the extracted total RNA, especially for RNA-Seq analysis in which highly pure and nondegraded RNA is required. The samples with low quantity of RNA can influence the subsequent cDNA synthesis and qPCR for gene expression analysis. The extracted RNA should be stored at −80 °C for long-time storage.
7. It is of great importance to confirm the constructed plasmids by sequencing since one single base shift could cause the failure in the expression of target genes. In addition, we noticed that in some circumstances, the constructed plasmids, even confirmed by sequencing, could not express the target protein after transfection into the cells. It is recommended that in the preliminary experiment, just transfect the plasmids into the cells and harvest the cells at 24 hpt for Western blotting analysis with the use of appropriate antibody (e.g., antibody for the target protein) to examine whether the target protein could be correctly expressed in cells.
8. Since SVCV infection could cause the cell death of EPC cells, a relatively high infection concentration could result in the complete death of the cells in a very short time span (less than 48 h), leaving no cells for the subsequent luciferase assay. It is recommended to perform a preliminary experiment to determine the appropriate quantity of viruses for infection, which could successfully infect the cells but not cause massive death of cells in 48 h.

Acknowledgments

This work was supported by grants (31402273, 31320103913) from National Natural Science Foundation of China. We thank Dr. Shao Chen Pang in the Institute of Environment and Health, Jianghan University, Wuhan, China for providing a picture in Fig. 2.

References

1. Lam SH, Chua HL, Gong Z et al (2004) Development and maturation of the immune system in zebrafish, *Danio rerio*: a gene expression profiling, *in situ* hybridization and immunological study. Dev Comp Immunol 28:9–28

2. Tobin DM, May RC, Wheeler RT (2012) Zebrafish: a see-through host and a fluorescent toolbox to probe host-pathogen interaction. PLoS Pathog 8:e1002349
3. Levraud JP, Palha N, Langevin C et al (2014) Through the looking glass: witnessing host-virus interplay in zebrafish. Trends Microbiol 22:490–497
4. Howe K, Clark MD, Torroja CF et al (2013) The zebrafish reference genome sequence and its relationship to the human genome. Nature 496:498–503
5. Nasevicius A, Ekker SC (2000) Effective targeted gene 'knockdown' in zebrafish. Nat Genet 26:216–220
6. Hogan BM, Verkade H, Lieschke GJ et al (2008) Manipulation of gene expression during zebrafish embryonic development using transient approaches. Methods Mol Biol 469:273–300
7. Bill BR, Petzold AM, Clark KJ et al (2009) A primer for morpholino use in zebrafish. Zebrafish 6:69–77
8. Miller JC, Holmes MC, Wang J et al (2007) An improved zinc-finger nuclease architecture for highly specific genome editing. Nat Biotechnol 25:778–785
9. Wood AJ, Lo TW, Zeitler B et al (2011) Targeted genome editing across species using ZFNs and TALENs. Science 333:307
10. Cade L, Reyon D, Hwang WY et al (2012) Highly efficient generation of heritable zebrafish gene mutations using homo- and heterodimeric TALENs. Nucleic Acids Res 40:8001–8010
11. Hwang WY, Fu Y, Reyon D et al (2013) Efficient genome editing in zebrafish using a CRISPR-Cas system. Nat Biotechnol 31:227–229
12. De Santis F, Di Donato V, Del Bene F (2016) Clonal analysis of gene loss of function and tissue-specific gene deletion in zebrafish via CRISPR/Cas9 technology. Methods Cell Biol 135:171–188
13. Crane M, Hyatt A (2011) Viruses of fish: an overview of significant pathogens. Virus 3:2025–2046
14. Crim MJ, Riley LK (2012) Viral diseases in zebrafish: what is known and unknown. ILAR J 53:135–143
15. Wang L, Wang L, Zhang HX et al (2006) In vitro effects of recombinant zebrafish IFN on spring viremia of carp virus and infectious hematopoietic necrosis virus. J Interf Cytokine Res 26:256–259
16. Ludwig M, Palha N, Torhy C et al (2011) Whole-body analysis of a viral infection: vascular endothelium is a primary target of infectious hematopoietic necrosis virus in zebrafish larvae. PLoS Pathog 7:e1001269
17. LaPatra SE, Barone L, Jones GR et al (2000) Effects of infectious hematopoietic necrosis virus and infectious pancreatic necrosis virus infection on hematopoietic precursors of the zebrafish. Blood Cells Mol Dis 26:445–452
18. Xu X, Zhang L, Weng S et al (2008) A zebrafish (*Danio rerio*) model of infectious spleen and kidney necrosis virus (ISKNV) infection. Virology 376:1–12
19. Xiong XP, Dong CF, Xu X et al (2011) Proteomic analysis of zebrafish (*Danio rerio*) infected with infectious spleen and kidney necrosis virus. Dev Comp Immunol 35:431–440
20. Lu MW, Chao YM, Guo TC et al (2008) The interferon response is involved in nervous necrosis virus acute and persistent infection in zebrafish infection model. Mol Immunol 45:1146–1152
21. Phelan PE, Mellon MT, Kim CH (2005) Functional characterization of full-length TLR3, IRAK-4, and TRAF6 in zebrafish (*Danio rerio*). Mol Immunol 42:1057–1071
22. Phelan PE, Pressley ME, Witten PE et al (2005) Characterization of snakehead rhabdovirus infection in zebrafish (*Danio rerio*). J Virol 79:1842–1852
23. Novoa B, Romero A, Mulero V et al (2006) Zebrafish (*Danio rerio*) as a model for the study of vaccination against viral haemorrhagic septicemia virus (VHSV). Vaccine 24:5806–5816
24. Encinas P, Rodriguez-Milla MA, Novoa B et al (2010) Zebrafish fin immune responses during high mortality infections with viral haemorrhagic septicemia rhabdovirus. A proteomic and transcriptomic approach. BMC Genomics 11:518
25. Lopez-Munoz A, Roca FJ, Sepulcre MP et al (2010) Zebrafish larvae are unable to mount a protective antiviral response against waterborne infection by spring viremia of carp virus. Dev Comp Immunol 34:546–552
26. Lopez-Munoz A, Roca FJ, Meseguer J et al (2009) New insights into the evolution of IFNs: zebrafish group II IFNs induce a rapid and transient expression of IFN-dependent genes and display powerful antiviral activities. J Immunol 182:3440–3449
27. Zou PF, Chang MX, Xue NN et al (2014) Melanoma differentiation-associated gene 5 in zebrafish provoking higher interferon-promoter activity through signalling enhancing of its shorter splicing variant. Immunology 141:192–202

28. Zou PF, Chang MX, Li Y et al (2015) Higher antiviral response of RIG-I through enhancing RIG-I/MAVS-mediated signaling by its long insertion variant in zebrafish. Fish Shellfish Immunol 43:13–24
29. Zou PF, Chang MX, Li Y et al (2016) NOD2 in zebrafish functions in antibacterial and also antiviral responses via NF-kappaB, and also MDA5, RIG-I and MAVS. Fish Shellfish Immunol 55:173–185
30. Levraud JP, Boudinot P, Colin I et al (2007) Identification of the zebrafish IFN receptor: implications for the origin of the vertebrate IFN system. J Immunol 178:4385–4394
31. Burgos JS, Ripoll-Gomez J, Alfaro JM et al (2008) Zebrafish as a new model for herpes simplex virus type 1 infection. Zebrafish 5:323–333
32. Antoine TE, Jones KS, Dale RM et al (2014) Zebrafish: modeling for herpes simplex virus infections. Zebrafish 11:17–25
33. Ding CB, Zhao Y, Zhang JP et al (2015) A zebrafish model for subgenomic hepatitis C virus replication. Int J Mol Med 35:791–797
34. Palha N, Guivel-Benhassine F, Briolat V et al (2013) Real-time whole-body visualization of Chikungunya virus infection and host interferon response in zebrafish. PLoS Pathog 9: e1003619
35. Gabor KA, Goody MF, Mowel WK et al (2014) Influenza A virus infection in zebrafish recapitulates mammalian infection and sensitivity to anti-influenza drug treatment. Dis Model Mech 7:1227–1237
36. He S, Salas-Vidal E, Rueb S et al (2006) Genetic and transcriptome characterization of model zebrafish cell lines. Zebrafish 3:441–453
37. LF L, Li S, XB L et al (2016) Spring viremia of varp virus N protein suppresses fish IFNphi1 production by targeting the mitochondrial antiviral signaling protein. J Immunol 196:3744–3753
38. Biacchesi S, LeBerre M, Lamoureux A et al (2009) Mitochondrial antiviral signaling protein plays a major role in induction of the fish innate immune response against RNA and DNA viruses. J Virol 83:7815–7827
39. Westerfield M, Streisinger G (1989) The zebrafish book: a guide for the laboratory use of zebrafish (*Brachydanio rerio*). University of Oregon Press, Oregon
40. Chang MX, Collet B, Nie P et al (2011) Expression and functional characterization of the RIG-I-like receptors MDA5 and LGP2 in rainbow trout (*Oncorhynchus mykiss*). J Virol 85:8403–8512
41. Pfaffl MW (2001) A new mathematical model for relative quantification in real-time RT-PCR. Nucleic Acids Res 29:2002–2007

Chapter 3

Northern Blot Detection of Virus-Derived Small Interfering RNAs in *Caenorhabditis elegans* Using Nonradioactive Oligo Probes

Tianyun Long and Rui Lu

Abstract

Northern blot analysis has been widely used as a tool for detection and characterization of specific RNA molecules. When coupled with radioactive probe northern blot allows for robust detection and characterization of small RNA molecules of trace amount. Here, we describe the detection and size characterization of virus-derived small interfering RNAs (vsiRNAs) in *C. elegans* using nonradioactive DNA oligo probes in northern blotting. Our protocol allows for the detection and characterization of not only primary vsiRNAs but also secondary vsiRNAs, a class of single-stranded vsiRNAs that has distinct migration pattern, and can be easily adapted to the detection of vsiRNAs in other organisms.

Key words Northern blot, Nonradioactive, Virus-derived siRNA, DIG-labeled probe, PAGE gel electrophoresis, *Caenorhabditis elegans*

1 Introduction

Northern blot is a molecular biology technique often used for the detection of RNA molecules of certain specific species. Northern blot involves the separation RNA molecules by size through electrophoresis and detection with hybridization probes complementary to the target RNAs. Because its sensitivity and robustness, northern blot has been adopted by many researchers to detect small interfering RNAs (siRNAs) in diverse organism species [1–3]. siRNAs are a class of small RNAs, ranging from 21 to 24 nucleotides, associated with RNA silencing triggered by virus or artificial double-stranded RNA (dsRNA). Accumulating evidence suggests that in antiviral RNA silencing siRNAs are processed from viral dsRNAs, often the replication intermediates, by Dicer, a class III endoribonuclease, and co-factors and will subsequently be loaded into Argonaut proteins to guide the silencing of viral transcripts [4]. In plants, viral dsRNAs are processed into siRNAs of

Karen Mossman (ed.), *Innate Antiviral Immunity: Methods and Protocols*, Methods in Molecular Biology, vol. 1656, DOI 10.1007/978-1-4939-7237-1_3,

different size classes by distinct Dicer proteins [5]. In nematode worms viral dsRNAs are also processed into several size classes of siRNAs although the worm genome only encodes a single Dicer protein [6–10]. Because of the pivotal role they play in antiviral RNA silencing, virus-derived siRNAs (vsiRNAs) are often detected and characterized to address the questions regarding how antiviral silencing is initiated and how viral transcripts are destroyed by RNA silencing.

Probably due to the existence of an siRNA-degrading mechanism vsiRNAs in *Caenorhabditis elegans* accumulate at extremely low level, making it very difficult to detect and characterize vsiRNAs in *C. elegans* through northern blot analysis that utilizes radiolabeled probes [11]. Besides, owing to a unique structure feature, secondary vsiRNA in *C. elegans* migrate faster than 22 nt primary vsiRNAs but slower than 21 nt primary vsiRNAs. As such, detection of such a class of vsiRNAs requires the resolution of northern blot analysis to be high for the visualization of a band that falls between 21 nt and 22 nt vsiRNAs. Recently, deep sequencing, also termed next-generation DNA sequencing, coupled with small RNA library construction has been successfully used for the detection and characterization of vsiRNAs in *C. elegans*. However, the high cost for deep sequencing makes such a strategy not an option for lab with limited funding.

Recently, northern blot protocols utilizing digoxigenin (DIG)-labeled oligonucleotide DNA probes have been successfully developed and used for the detection of various RNA species, including microRNA (miRNA), a class of endogenous small RNAs that shares basic biological properties, such as size and structure features, with vsiRNAs [12–15]. These protocols involve the addition of DIG-labeled nucleotides to the 3′ end of DNA oligos to be used as probes. The labeled probes are then detected using DIG-specific antibodies in a way analogous to western blot analysis. Since each of the DNA oligos can be labeled with multiple DIG-carrying nucleotides, this strategy allows for specific detection of trace amount small RNA molecules with unprecedented sensitivity. Because probes labeled this way can be stored at −20° for a couple of months without losing activity, it is not necessary to repeatedly prepare fresh probes for small RNA detection through northern blot. Besides, since no hazardous radioactive materials are used for probe labeling the whole experiment can be carried out by junior researchers with basic biosafety training and all of the experimental wastes are much more environmentally friendly compared to the conventional northern blot protocol that utilizes isotope-labeled probes.

Here, we describe a northern blot protocol that we have developed for the detection of vsiRNAs in *C. elegans*. Our protocol involves the synthesis and DIG-labeling of short DNA oligos. These labeled DNA oligos are all complementary to the minus-

stranded viral genomic RNA and thus will allow for the detection of both primary and secondary vsiRNAs produced in *C. elegans*. We use isopropanol to enrich small RNAs after total RNA extraction, which is cost effective and much less time consuming. Using this protocol we have successfully detected both primary and secondary vsiRNAs in different genetic backgrounds [6–8, 16]. We believe that such a cost-effective protocol can be easily adapted to other organism systems for the detection of virus or transgene-derived siRNAs.

2 Materials

All stock solutions are prepared using analytical grade reagents and ultrapure water unless otherwise stated.

2.1 Nematode Growth Medium (NGM)

Prepare 1 M stock solution for K_2HPO_4, KH_2PO_4, $MgSO_4$, and $CaCl_2$. Prepare cholesterol stock solution (10 mg/mL in ethanol) and uracil stock solution (2 g/L in H_2O). Then prepare NGM medium following the steps listed below.

1. Prepare potassium phosphate buffer by mixing 132 mL of K_2HPO_4 (1 M) with 868 mL of KH_2PO_4 (1 M). Filter sterilize.
2. Dissolve 3 g/L NaCl and 2.5 g/L bacto peptone in H_2O.
3. Add 17 g/L agar (for 3- and 6 cm plates) or 10 g/L agar and 10 g/L agarose (for 10- and 14.5 cm plates).
4. Autoclave; then cool the solution down to 50 °C.
5. Prepare nematode growth medium: 25 mL potassium phosphate buffer, 1 mL $MgSO_4$ (1 M), 1 mL $CaCl_2$ (1 M), 0.5 mL cholesterol (10 mg/mL in ethanol), 10 mL Uracil (2 g/L) (*see* **Note 1**).
6. Mix the solution well and pour into Petri dishes manually or using Unispense dispenser.

2.2 RNA Extraction

1. TRIZOL Reagent.
2. RNase away (Thermo Fisher).
3. Chloroform.
4. Isopropyl alcohol.
5. 80% ethanol.
6. DEPC-treated water: incubate water with 0.1% diethylpyrocarbonate (DEPC); autoclave to remove DEPC. It can also be purchased.
7. Tissue-tearor (BioSpec).
8. Phase lock gel light tubes (15 mL).

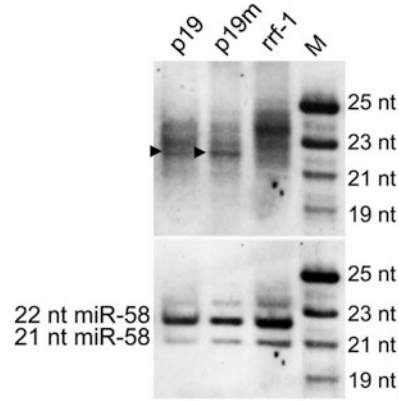

Fig. 1 Northern blot detection of virus-derived siRNAs using nonradioactive oligo probes. In *C. elegans* primary vsiRNAs are produced in several size classes, with the 23 nt class being the most abundant class. The arrows indicate the *rrf-1*-dependent secondary siRNAs that are 22 nt long. Since they carry triphosphate, instead of monophosphate, group at the 5′ end, these secondary siRNAs migrate faster than the 22 nt primary siRNAs but slower than the 21 nt primary siRNAs. p19 and p19m represent the wild-type and corresponding loss of function mutant respectively of the RNAi suppressor p19. The blot was stripped and reprobed to detect worm miRNA miR-58, which served as size reference and equal loading control [1]

2.3 Denaturing PAGE Gel

1. 5× Tris-borate-EDTA (TBE): 450 mM Tris-borate, 10 mM EDTA pH 8.0.
2. Denaturing PAGE gel: 25 mL of 40% Acrylamide: Bis-Acrylamide solution (19:1), 21 g of urea, 5 mL of 5× TBE, 500 μL of 10% ammonium persulfate, 25 μL TEMED, then add DEPC-treated water to a final volume of 50 mL (*see* **Note 2**).
3. Loading gel: 2 mL of 40% Acrylamide: Bis-Acrylamide solution (19:1), 1 mL of 5× TBE, 50 μL of 10% Acrylamide, 10 μL of TEMED and add DEPC-treated water to a final volume of 10 mL (*see* **Note 3**).
4. Small RNA size references: A mixture of four DNA oligonucleotides that are 19, 21, 23, and 25 nt long respectively. These DNA oligos will be loaded in parallel with the small RNA samples (Fig. 1) and will be detected using DIG-labeled matching DNA oligos and used as size references.
5. Semi-Dry Transfer Cell.
6. Spectrolinker UV crosslinker.

2.4 DNA Oligos, Hybridization, Washing, Blocking, and Detection

1. DNA oligos (*see* **Note 4**).
2. PerfectHyb Plus hybridization buffer (Sigma).
3. Hybridization oven and matching hybridization glass bottles.

4. 20× SSC (3 M NaCl, 0.3 M sodium citrate): Per 1 L, add 175.3 g NaCl and 88.3 g sodium citrate to ultrapure water. Adjust the pH to 7.0 with NaOH or HCl. Autoclave sterilize and store at room temperature.
5. Low Stringency Wash Buffer (2× SSC, 0.1% SDS): Add 100 mL of 20× SSC stock solution and 10 mL of 10% SDS stock solution. Adjust volume to 1 L with ultrapure water.
6. High Stringency Wash Buffer (0.5× SSC, 0.1% SDS): Add 25 mL of 20× SSC stock solution and 10 mL of 10% SDS stock solution. Adjust volume to 1 L with ultrapure water.
7. Ultra-High Stringency Wash Buffer (0.1× SSC, 0.1% SDS): Add 5 mL of 20× SSC stock solution and 10 mL of 10% SDS stock solution. Adjust volume to 1 L with ultrapure water.
8. The DIG wash and block buffer set (Roche Applied Science).
9. dATP, dGTP, dTTP mixture.
10. anti-DIG-AP antibody together with the CSPD substrate (Roche Applied Science): Fab fragments from polyclonal anti-digoxigenin antibodies, conjugated to alkaline phosphatase.

3 Methods

3.1 RNA Extraction

1. Use 10 cm plates to grow worms. At least 10 plates of worms of mixed stages will be needed for small RNA preparation for each worm strain.
2. After being washed off the plates the worms are washed three times with ddH_2O to remove residual bacterial cells.
3. Homogenize the worms using Tissue-tearor (BioSpec. Inc) for 1 min in Trizol reagent at a ratio of 1:3 (v/v).
4. Add 0.2 volume of chloroform, mix vigorously.
5. Transfer the homogenized sample to phase lock gel tube.
6. Spin at 12,000 × *g* for 5 min at 4 °C.
7. Transfer the aqueous phase to a new RNase-free tube.
8. Add 0.5 volume of isopropyl alcohol and mix thoroughly.
9. Store at room temperature for 5–10 min.
10. Centrifuge the samples at 1000 × *g* for 10 min at 4 °C to precipitate RNAs of high molecular weight (*see* **Note 5**).
11. Transfer the supernatant to a new tube and add one-third volume of isopropyl alcohol.
12. Mix and precipitate the small RNA samples at −20 °C overnight.
13. Centrifuge 12,000 × *g* for 20 min at 4 °C to collect small RNAs.

14. Wash the small RNA pellet with 80% ethanol.
15. Air dry the RNA pellet for 5–10 min.
16. Dissolve the RNA pellet in DEPC-treated water. The samples can be immediately used for quantity check or can be stored in −80 °C freezer.
17. Measure the concentration of small RNA samples using the BioPhotometer Plus (Eppendorf) following the manufacturer's instruction.

3.2 Denaturing PAGE Gel

1. We use the DASG-250(C.B.S Scientific) vertical gel system with 16.5 × 14.5 cm glass plates and 1.0 mm spacers to prepare gel. Clean the glass plates with DEPC-treated water and RNase Away and assemble the plates following the manufacturer's instructions.
2. Prepare 50 mL of 16% denaturing PAGE gel by mixing 25 mL of 40% Acrylamide: Bis-Acrylamide solution (19:1), 21 g of urea, 5 mL of 5× TBE, 500 μL of 10% ammonium persulfate, 25 μL TEMED and DEPC-treated water. Pour the gel to a level 1 cm below the comb.
3. After gel polymerization, prepare 10 mL of loading gel by mixing 2 mL of 40% Acrylamide: Bis-Acrylamide solution (19:1), 1 mL of 5× TBE, 50 μL of 10% Acrylamide, 10 μL of TEMED add DEPC-treated water.
4. Add loading gel on the top of the denaturing gel.
5. After loading gel polymerization, remove the comb carefully, and set up PAGE apparatus with the gel (*see* **Note 6**).
6. Briefly rinse the wells with 1× TBE to remove excess acrylamide.
7. Prerun the gel at ~200—400 V for 30 min.

3.3 Electrophoresis

1. Prepare small RNA samples of equal amount (10–20 μg each). Add water as needed to make equal volume.
2. Denature the RNA samples (95 °C for 5 min) and quickly chill the denatured samples on ice.
3. Add loading dye that contains both bromophenol blue and xylene cyanol FF to the samples and mix briefly.
4. Load the samples into the wells and run the gel electrophoresis at ~500 V for 2–3 h until the bromophenol blue reaches the bottom of the gel.
5. Disassemble the gel apparatus and cut the gel into lower and upper parts along a line right above the xylene cyanol dye. The upper part should contain tRNAs and some small ribosomal RNAs and lower half contains many small RNA species, including miRNAs and siRNAs. Soak the upper part in 1× TBE containing Ethidium bromide for 15 min with shaking.

6. Use UV transilluminator to record the relative amount of tRNAs in each samples, which will be used as equal loading reference.

3.4 Transfer Gel to Membrane

1. Cut the Hybond N^+ membrane (GE healthcare Inc.) and 6 sheets of 3MM Whatman papers to the size of the gel and thoroughly soak them in 1× TBE for 5 min with shaking.
2. Starting from the side of the positive electrode of semi-dry transfer cell, place three sheets of Whatman papers, nylon membrane, the gel, and an additional three sheets of Whatman papers to form a paper–membrane–gel–paper sandwich.
3. Roll out any bubbles in between the gel, membrane, and papers with plastic sterile pipette. Add more sheets of Whatman papers if needed (*see* **Note 7**).
4. Transfer the RNA to the membrane at ~200 mA for 30 min (*see* **Note 8**).

3.5 Cross-Linking

1. Disassemble the semi-dry transfer apparatus. Carefully remove any gel fragments from the membrane and mark the orientation of the membrane.
2. Place the membrane on a sheet of Whatman 3MM paper with the sample side facing up.
3. Cross-link the RNA to the nylon transfer membrane in a Spectrolinker using 1.8×10^5 μJ /cm^2 as the output power. After cross-linking the membrane can be immediately used for hybridization or wrapped up in a cling film and stored at 4 °C.

3.6 Preparation of DIG-Labeled DNA Probe

1. To prepare probes for the detection of vsiRNA or DNA oligo size references, add 100 pmol oligonucleotide mix in 10 μL H_2O to a 1.5 mL tube.
2. Place the reaction tube on ice and add the following reagents: reaction buffer (5×) 4 μL, $CoCl_2$ 4 μL, DIG-ddUTP solution 1 μL, Terminal Transferase (400 U) 1 μL.
3. Mix thoroughly and centrifuge briefly, incubate at 37 °C for 15 min.
4. Stop the reaction by adding 2 μL 0.2 M EDTA (PH 8.0). The probe can be immediately used for hybridization or stored at −20 °C for future use.

3.7 Hybridization

1. After cross-linking, roll membrane with the sample side facing inward and insert it into a cylindrical glass hybridization bottle.
2. Add 5–10 mL of *PerfectHyb™ Plus* hybridization buffer and prehybridize at 37 °C for at least 30 min in a hybridization oven (*see* **Note 9**).

3. Denature the probe at 95 °C for 1 min and add the probe to the hybridization buffer to achieve a final concentration of ~1 nM.
4. Hybridize at 37 °C overnight with slow rotation.

3.8 Washing, Blocking, and Detection

1. Discard hybridization buffer.
2. Wash the membrane twice with 50 mL of Low Stringent Buffer at 42 °C for 15 min.
3. Wash the membrane twice with 50 mL of High Stringent Buffer at 42 °C for 15 min.
4. Rinse the membrane with 50 mL Washing Buffer at 42 °C for 10 min.
5. Incubate the membrane in 50 mL Blocking Buffer for 3 h at room temperature.
6. Replace the Blocking Buffer with the DIG antibody solution (15 mL) prepared by mixing DIG antibody solution with blocking buffer at a ratio of 1:10,000 and incubate the membrane at room temperature for 30 min.
7. Wash the membrane four times, 15 min each, in 100 mL DIG Washing buffer.
8. Equilibrate the membrane in 20 mL Detection buffer for 5 min.
9. Remove blot from the hybridization bottle with clean forceps and place on Saran wrap. Apply substrate solution (1.0 mL), prepared by mixing CSPD with detection buffer at a ratio of 1:100, to the surface of the membrane.
10. Immediately cover the membrane with another sheet of Saran wrap to spread the substrate evenly. Squeeze out air bubbles in between the membrane and Saran wrap.
11. Incubate the membrane in the dark at 37 °C for 15 min.
12. Expose the membrane to X-ray film (Hyblot CL Autoradiography film). Usually, a few seconds of exposure is sufficient to get strong signals for abundant vsiRNAs in worm mutants defective in secondary vsiRNA production. However, longer exposure time may be needed to detect primary and secondary virus-derived siRNAs in wild-type worms or mutants defective in primary vsiRNA production (*see* **Note 10**).

4 Notes

1. Add more uracil if thicker food lawn is needed. Similarly, use of less uracil will result in a thinner food lawn.
2. Decreasing the acrylamide concentration may yield poor resolution of small RNA bands corresponding to different size classes of vsiRNAs.

3. It is highly recommended to use loading gel for sample loading. Urea at high concentration interferes with the migration of RNA samples. Thus, when loading gel is used the wells can be easily cleaned to ensure a nice-looking result. Also make sure that the PAGE gel is completely polymerized before adding the loading gel.
4. Synthesize DNA oligos, 40 nt each, that are complementary to minus-stranded viral genomic RNA. Each of these DNA oligos, except the ones that cover the ends of viral genome, has 10 nt overlap with adjacent oligos. These DNA oligos will be pooled and labeled with the nonradioactive DIG using End Tailing Kit (Roche Applied Science). We use DNA oligo probes of plus polarity, instead of minus polarity, for the detection of vsiRNAs in *C. elegans* mainly because the secondary vsiRNAs in worms are of minus polarity. For the detection of vsiRNA in plants and insects both plus and minus DNA oligo probes can be used.
5. High molecular weight RNA samples can be collected and used for the detection of viral genomic RNA accumulation in the samples. The information combined with vsiRNA detection can be used to determine if the biogenesis of vsiRNA is compromised.
6. Attach a metal plate (e.g., aluminum alloy) to the gel cassette to reduce heat generated during electrophoresis, which often produces a "smiling" effect. Always turn off the power supply before making any changes to the gel cassette.
7. Ensure that the sandwich is moist by adding small amount of 1× TBE buffer before the transfer. Use constant current, instead of voltage, for the transfer.
8. Use xylene cyanol dye as indication of complete transfer. When all or most of the xylene cyanol dye was transferred to the membrane, all small RNA species should have been transferred to the membrane.
9. Do not use excess amount of hybridization buffer as it will dilute the concentration of the probes. While using PerfectHyb™ Plus, a blocking reagent is not necessary. If the blocking reagent is preferred, it is suggested to use 0.1 mg/mL single-stranded DNA as probe.
10. If noisy background is observed after the exposure, (1) use longer time for the prehybridization; (2) wash the membrane right after transfer using 1× TBE buffer (this will remove residual polyacrylamide on the membrane), which can cause high level background noise by retaining excess probe. If the vsiRNA bands are faint or absent, it may be useful to use only low-stringency washing buffer (e.g., a low-stringency Church and Gilbert hybridization buffer containing 10 mg/mL BSA, 0.5 M sodium phosphate [pH 7.2], 1 mM EDTA, and 7%

SDS) and omit the high-stringency washing step. The blot can be reprobed (after the primary probes being stripped off) to detect miRNAs and the accumulation of miRNAs can be used as equal loading control.

Acknowledgment

This work was supported by NIH grant R01GM119012-01A1 to R.L.

References

1. Hamilton AJ, Baulcombe DC (1999) A species of small antisense RNA in posttranscriptional gene silencing in plants. Science 286 (5441):950–952
2. Li H, Li WX, Ding SW (2002) Induction and suppression of RNA silencing by an animal virus. Science 296(5571):1319–1321
3. Lu R et al (2009) An RIG-I-like RNA helicase mediates antiviral RNAi downstream of viral siRNA biogenesis in *Caenorhabditis elegans*. PLoS Pathog 5(2):e1000286
4. Ding SW, Voinnet O (2007) Antiviral immunity directed by small RNAs. Cell 130 (3):413–426
5. Roghiyh Aliyari S-WD (2009) RNA-based viral immunity initiated by the Dicer family of host immune receptors. Immunol Rev 227 (1):176–188
6. Guo X, Lu R (2013) Characterization of virus-encoded RNAi suppressors in *Caenorhabditis elegans*. J Virol 87(10):5414–5423
7. Guo X et al (2013) Homologous RIG-I–like helicase proteins direct RNAi-mediated antiviral immunity in *C. elegans* by distinct mechanisms. Proc Natl Acad Sci 110:16085–16090
8. Guo X et al (2013) Antiviral RNA silencing initiated in the absence of RDE-4, a double-stranded RNA binding protein, in *Caenorhabditis elegans*. J Virol 87(19):10721–10729
9. Félix M-A et al (2011) Natural and experimental infection of Caenorhabditis Nematodes by novel viruses related to Nodaviruses. PLoS Biol 9(1):e1000586
10. Ashe A et al (2013) A deletion polymorphism in the *Caenorhabditis elegans* RIG-I homolog disables viral RNA dicing and antiviral immunity. elife 2:e00994
11. Kennedy S, Wang D, Ruvkun G (2004) A conserved siRNA-degrading RNase negatively regulates RNA interference in *C. elegans*. Nature 427(6975):645–649
12. Ghildiyal M, Zamore PD (2009) Small silencing RNAs: an expanding universe. Nat Rev Genet 10(2):94–108
13. Ramkissoon SH et al (2006) Nonisotopic detection of microRNA using digoxigenin labeled RNA probes. Mol Cell Probes 20(1):1–4
14. Höltke HJ, Kessler C (1990) Non-radioactive labeling of RNA transcripts in vitro with the hapten digoxigenin (DIG); hybridization and ELISA-based detection. Nucleic Acids Res 18 (19):5843–5851
15. Kim SW et al (2010) A sensitive non-radioactive northern blot method to detect small RNAs. Nucleic Acids Res 38(7):e98–e98
16. Guo X, Li W-X, Lu R (2012) Silencing of host genes directed by virus-derived short interfering RNAs in *Caenorhabditis elegans*. J Virol 86 (21):11645–11653

Chapter 4

Extraction and qPCR-Based Detection of miRNAs from Cultured PBMCs of Bubaline Origin

Chandra S. Mukhopadhyay, Ramneek Verma, and Jasdeep Singh

Abstract

MicroRNAs are small noncoding but functionally important RNA molecules that are involved in regulating diverse cellular, metabolic, and immune processes. Their small size necessitates modification in traditional acid phenol-chloroform based RNA isolation procedures to get highly enriched fraction of small RNA that includes miRNAs and siRNAs. Further, of the different methods available, real-time PCR is a powerful tool for precise and specific detection and quantification of miRNA. Moreover, real-time PCR is used to validate the screening or expression of miRNAs that are discovered during high-throughput sequencing, or microarray analysis. We demonstrate here the method of extraction of miRNAs from cultured PBMCs of bubaline origin followed by the qPCR-based (both SYBR green and TaqMan-based chemistries) identification of miRNAs expressed in response to TLR ligand stimulation.

Key words Small RNAs, PBMCs, TaqMan MicroRNA assay, miScript primer assay

1 Introduction

MicroRNAs are small (~22 bases long), noncoding RNAs that regulate gene expression posttranscriptionally [1, 2]. These are functionally active molecules that regulate various natural as well as disease-related metabolic-, immune-related, and cellular processes [3] such as differentiation [4] and cancer [5]. The sample preparation and extraction of small RNA enriched for miRNAs and siRNAs is quite a challenging process. Traditional methods of extraction of total RNA rely either on chemical extraction (using highly concentrated chaotropic salts in conjunction with acidic phenol-chloroform to inactivate RNases and purify RNA) or solid-phase extraction (i.e., immobilization of RNA on glass and elution by suitable buffer). Although very pure preparations of RNA are yielded by this method, the alcohol precipitation step to concentrate the RNA does not quantitatively recover small nucleic acid molecules. Similarly, the solid phase extraction procedure does not effectively recover the small RNAs (sRNAs) molecules, making

Karen Mossman (ed.), *Innate Antiviral Immunity: Methods and Protocols*, Methods in Molecular Biology, vol. 1656, DOI 10.1007/978-1-4939-7237-1_4,

both the methods ill-suited for the preparation of very small RNAs. Therefore, isolate the RNA fraction enriched for small RNAs (including both miRNAs and siRNAs) from the bubaline cultured PBMCs using the mirVana™ miRNA Isolation Kit. The kit works on the principal of organic extraction followed by immobilization of RNA on glass-fiber filters and subsequent elution in RNAse free water. Moreover, the kit provides an option to purify either the total RNA, or the RNA enriched for small species like miRNAs, siRNAs etc. Furthermore, quantification of microRNAs from this sRNA fraction is again an additional challenge. Different methods have been developed for screening or profiling miRNA viz. next-generation sequencing, DNA microarrays, nanostrings, and quantitative RT-qPCR [6]. Quantitative RT-qPCR is the method of choice when high sensitivity and specific quantification of miRNA is required as well as for validating the data obtained by other methods [7, 8]. Different primer or primer-probe chemistries have been developed for this purpose. Moreover, small size of miRNAs offers additional challenge of designing primers specific to them. In order to provide solutions to these challenges, we describe here the approach that was followed for successfully extracting the small RNA from cultured peripheral blood mononuclear cells, followed by detection and quantification of miRNAs by SYBR green and TaqMan chemistries, with a special emphasis on designing of primers for miRNA quantification.

2 Materials

2.1 Bubaline PBMCs Preparation

1. 0.5 M EDTA: Add: 186.1 g of disodium EDTA (Na_2EDTA) in 800 mL of distilled water. Adjust the pH to 8.0 with caustic soda (~50 mL of NaOH). Bring the final volume to 1 L with distilled water (The disodium salt of EDTA will not dissolve until the pH of the solution is adjusted to 8.0 by the addition of NaOH). Stir vigorously on a magnetic stirrer, then sterilize the solution by autoclaving and finally store at room temperature (25°C).
2. Hisep LSM 1077 iso-osmotic, low viscosity medium.
3. 1× Phosphate Buffer Saline (PBS: pH 7.4): Weigh and dissolve 8 g of sodium chloride (NaCl), 0.2 g of potassium chloride (KCl), 1.44 g of disodium phosphate (Na_2HPO_4), and 0.24 g of monopotassium phosphate (KH_2PO_4) in 800 mL distilled water. Adjust pH to 7.4 with hydrochloric acid (HCl). Adjust the final volume to 1 L with additional distilled water and sterilize by autoclaving.
4. RNA stabilization solution (e.g., RNA *later* from Invitrogen).

2.2 PBMCs Culture

1. RPMI-1640 growth medium: RPMI-1640 media supplemented with 10% fetal bovine serum, 50 μg/mL Gentamicin, 100 IU/mL Penicillin, 100 μg/mL Streptomycin and 0.25 μg/mL Amphotericin.

2. TLR ligands: Poly I:C (synthetic analog of dsRNA), lipopolysaccharide (LPS).
3. 6-well culture plates and 25 mL culture flasks.
4. Phosphate buffer saline.

2.3 Extraction of Small-RNA

1. miRNA Isolation Kit (miRVana™, Ambion or MiRNeasy Mini Kit, Qiagen).
2. Acid phenol:chloroform:isoamyl alcohol (25:24:1), pH 4.0.
3. 1× phosphate buffer saline.
4. Chilled absolute ethanol.

2.4 Quality Checking of sRNA

1. 10× Tris-Borate EDTA (TBE): TBE is generally used at 1× final concentration for preparing gels and/or for gel running buffer. Weigh 109 g of Tris base (i.e., final concentration of 0.9 M), 55 g of boric acid (i.e., final concentration of 0.9 M) and add 40 mL of 0.5 M EDTA (i.e., final concentration of 20 mM) and make up to 1 L using nuclease-free water. First dissolve the components by stirring in approximately 850 mL nuclease-free water and then adjust the final volume to 1 L.
2. 40% acrylamide (acryl:bis acryl = 19:1): Weigh 38 g of acrylamide monomer and 2 g Bis (cross-linker) and transfer to a 100 mL graduated cylinder containing about 40 mL of water. Dissolve by stirring and make up to 100 mL with water. Store at 4 °C, in a bottle wrapped with aluminum foil.
3. Urea.
4. 10% ammonium persulfate (APS).
5. TEMED.
6. Gel Loading Buffer/dye for RNA: 95% deionized formamide, 0.025% (w/v) bromophenol blue, 0.025% (w/v) xylene cyanol FF, 5 mM EDTA (pH 8.0), 0.025% (w/v) SDS. Use distilled deionized formamide and store in small aliquots under nitrogen at −20 °C.
7. sRNALabChip kits (Agilent Technologies, USA) and Agilent's Bioanalyzer.

2.5 Reverse Transcription and qPCR for miRNA

1. miScript II RT kits, miScript Primer Assays, and miScript SYBR Green PCR Kit.
2. TaqMan microRNA reverse transcription kit, Taqman MicroRNA Assays.

3 Methods

The overview of the methodology followed has been presented as flowchart (*see* Fig. 1).

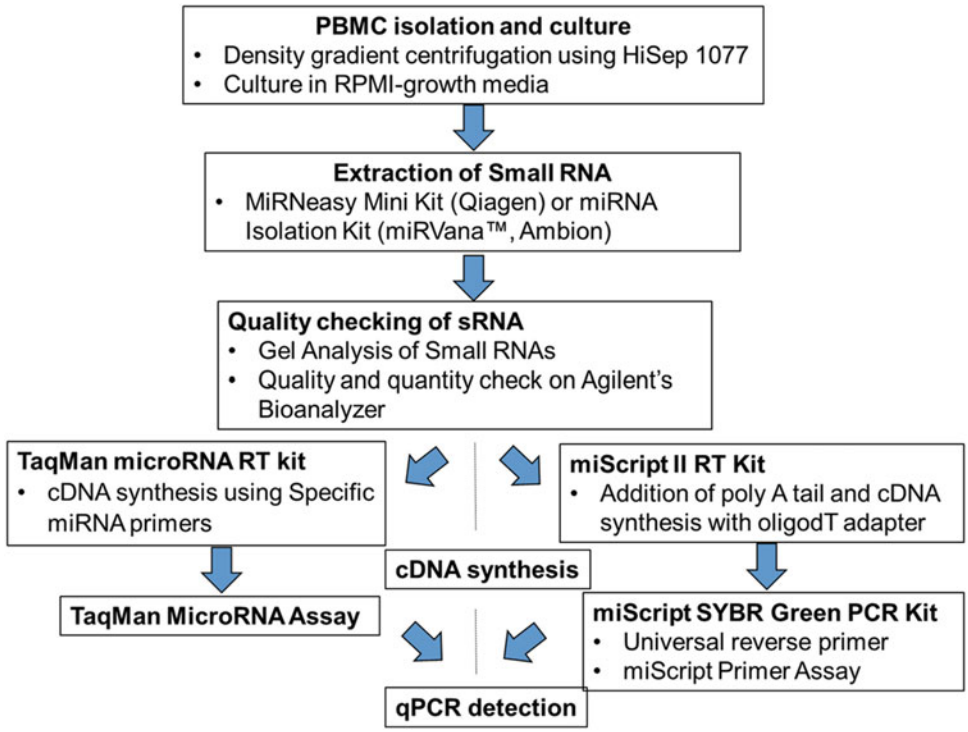

Fig. 1 Flowchart describing steps for detection of miRNAs

3.1 Bubaline PBMCs Isolation

The PBMCs can be isolated from the freshly collected blood following density gradient centrifugation using Hisep LSM 1077 (Himedia) and stored at −80°C in RNA later solution until further use.

1. Collect the peripheral blood (about 30 mL each) aseptically in a 50 mL centrifuge tube, containing 500 μL of 0.5 M EDTA as an anticoagulant, using a 16G sterile needle from the jugular vein of buffaloes.
2. Carry the blood samples in ice packs to the laboratory for further processing (within 2 h).
3. Make 1:2 or 1:3 dilution of blood using phosphate buffer saline.
4. Transfer 10 mL of Hisep LSM 1077 (Himedia) to a 50 mL clean centrifuge tube and slowly overlay with 30 mL of diluted blood. Do not disturb (*see* **Note 1**).
5. Centrifuge (preferably using swinging bucket rotor) at 400 × *g*, at room temperature for 30 min (*see* **Note 2**).
6. Carefully aspirate the lymphocyte/monocyte layer (along with half of the HiSep layer), which appears as a band between the plasma and HiSep LSM, using the clean pasteur pipette and transfer to a clean centrifuge tube.

7. Add equal volume of phosphate buffer saline and mix gently. Centrifuge for 10 min at room temperature at 3000 rpm (aprox 2000 × *g*)(*see* **Note 3**).
8. Repeat the washing of the cells by resuspending in the phosphate buffer saline and centrifuge again.
9. Resuspend the PBMCs in suitable culture or store at −80° in RNA later solution until further use.

3.2 PBMCs Culture and Stimulation with TLR Ligands

1. Count the total number cells and number of viable cells by trypan blue exclusion staining.
2. Culture the PBMCs in 6-well culture plates containing RPMI-1640 growth medium @ 2×10^6 cells per well in 2 mL media and incubate in a CO_2 incubator at 37 °C.
3. Initially, the cultured PBMCs in each well are separately challenged with TLR ligands, such as TLR3 ligand (Poly I:C, synthetic analog of dsRNA), and TLR4 ligand (LPS), in dose- and time-dependent manner so as to find the dosage of ligands at which optimum immune response is generated in the cultured cells (*see* **Note 4**).
4. Next, repeat the experiment with fresh PBMCs culture and challenge with the optimum dose of ligand at optimum incubation period, in a 25 mL culture flask and incubate at 37 °C in a CO_2 incubator.
5. Harvest the PBMCs from the culture by centrifugation at room temperature @ 2500 rpm (aprox. 1300 × *g*)for 10 min and discard the supernatant (culture medium).
6. Wash the cells by resuspending the PBMCs pellet in ~1 mL PBS, and re-pellet as in step 5.
7. Keep the washed cells on ice for small RNA isolation or store −80°C in RNA later solution until further use.

3.3 Extraction of Small RNA

Extraction of Small RNA (enriched for miRNA) for the purpose of miRNA-Seq or miRNA-qPCR assay is performed using the miRNA Isolation Kit (miRVana™, Ambion). The steps are as follows.

3.3.1 Collection of Cells and Washing in PBS

1. Centrifuge the PBMCs (10^2–10^7 cells) from culture medium or PBMCs stored in RNA later at low speed (1500 rpm or 500 × *g*) for 10 min.
2. Discard the supernatant (culture medium or RNA later) and wash the cells by resuspending the pellet in ~1 mL PBS, and re-pellet as in step 1.
3. Place the washed cells on ice.

3.3.2 Cell Disruption

1. Remove the PBS and add 300–600 μL of Lysis/Binding Solution to the pellet.
2. Vortex or pipette vigorously to completely lyse the cells. Obtain a clear homogenous lysate.

3.3.3 Organic Extraction

1. After complete lysis, add miRNA Homogenate solution equaling to the 1/10th amount of the homogenous lysate and vortex to mix properly.
2. Keep the mixture on ice for 10 min.
3. Add Acid-Phenol: Chloroform to the mixture in amount equal to the lysate volume (i.e., before addition of the miRNA Homogenate Additive).
4. Vortex the tubes briefly for 30–60 s to mix and then centrifuge for 10 min at 10,000 rpm (8000 × *g*) at room temperature to get separate layers of the aqueous and organic phases.
5. Collect the aqueous (upper) phase carefully without disturbing the inter phase and transfer to a fresh tube. Note the volume of the aqueous phase recovered.

3.3.4 Final RNA Isolation (Highly Enriched for RNAs Smaller Than ~200 Bases)

1. Preheat the elution solution or nuclease-free water to 95 °C, to be used for final elution of the RNA from the filter at the last step of the procedure.
2. Add 100% ethanol equaling to 1/3rd volume of the aqueous phase (recovered from the organic extraction) and mix thoroughly by inverting the tube several times.
3. Place the filter cartridges (provided in the kit) onto the collection tube and add up to 700 μL of the lysate/ethanol mixture per sample to the filter cartridges (*see* **Note 5**).
4. Centrifuge the tubes shortly (~30 s) at 10,000 rpm (8000 × *g*) to get the mixture pass through the filter and collect the filtrate (*see* **Note 6**).
5. Measure the total volume of the filtrate collected (Pool the filtrates of same sample if multiple passes were done).
6. Add 2/3rd volume 100% ethanol to filtrate (i.e., flow-through) and mixed thoroughly.
7. For each sample, place a second fresh filter cartridge onto the collection tube and add, at a time, up to 700 μL of the filtrate/ethanol mixture, obtained from the previous step, to a cartridge (*see* **Note 7**).
8. Centrifuge at 10,000 rpm (8000 × *g*) for ~30 s to pass the mixture through the filter and discard the flow-through.
9. Next apply 700 μL of miRNA Wash Solution 1 (provided with the kit and working solution prepared by the addition of ethanol) to the filter cartridge.

10. Centrifuge for ~15–30 s to pass the solution through the filter and discard the flow-through wash solution from the Collection Tube.
11. Replace the Filter Cartridge into the same Collection Tube and apply 500 μL of Wash Solution 2/3 (provided by kit and working solution prepared by the addition of ethanol) and pass it through the Filter Cartridge by short centrifugation.
12. Repeat the above Washing step and after discarding the all flow-through, again centrifuge the empty Filter Cartridge for 1 min to remove any residual fluid.
13. Finally, transfer the Filter Cartridge into a fresh Collection Tube and apply 100 μL of preheated (95 °C) Elution Solution or nuclease-free water to the center of the filter.
14. Centrifuge the tubes for ~30 s at maximum speed to recover the final elute containing the RNA enriched for small RNA and store at −20 °C or −80 °C.

3.4 Quality Checking of sRNA

The quality of small RNAs can be analyzed by running an aliquot of sample on a 15% denaturing polyacrylamide gel, i.e., by visualizing the small ribosomal bands or by running samples on Agilent's Bioanalyzer.

3.4.1 Gel Analysis of Small RNAs

1. Prepare 15 mL of gel mix for 15% polyacrylamide gel (with 8 M urea) by adding 7.2 g of urea, 1.5 mL of 10× TBE buffer, 5.6 mL of 40% acrylamide (acryl:bis acryl = 19:1) and make volume up to 15 mL by addition of nuclease-free water (*see* **Note 8**).
2. Stir the components to mix, and then add 75 μL of 10% ammonium persulfate (APS) followed by 15 μL of TEMED.
3. Mix briefly, and pour immediately to cast gel within a 13 cm × 15 cm × 0.75 mm gel cassette.
4. To run the samples on the gel, mix 1–2 μg of the RNA sample with an equal volume Gel LoadingBuffer/dye and heat for 2–5 min at 95–100 °C.
5. Load the samples on a denaturing 15% polyacrylamide gel and electrophorese at 30–45 mA.
6. Stop the electrophoresis when the bromophenol blue dye front migrates to the bottom of the gel.
7. Soak the gel in 0.5–1 μg/mL solution of ethidium bromide for 5 min in 1× TBE. Wash the gel for 2–5 min in 1× TBE and visualize RNA using a UV transilluminator. Alternatively, visualize the RNA by Silver staining method.
8. Observe the clear visible tRNA, 5S rRNA, and 5.8S rRNA bands for good quality small RNA sample (*see* Fig. 2).

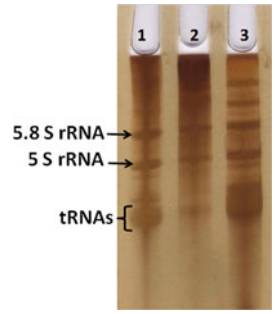

Fig. 2 Small RNA run on 15% denaturing PAGE and silver stained

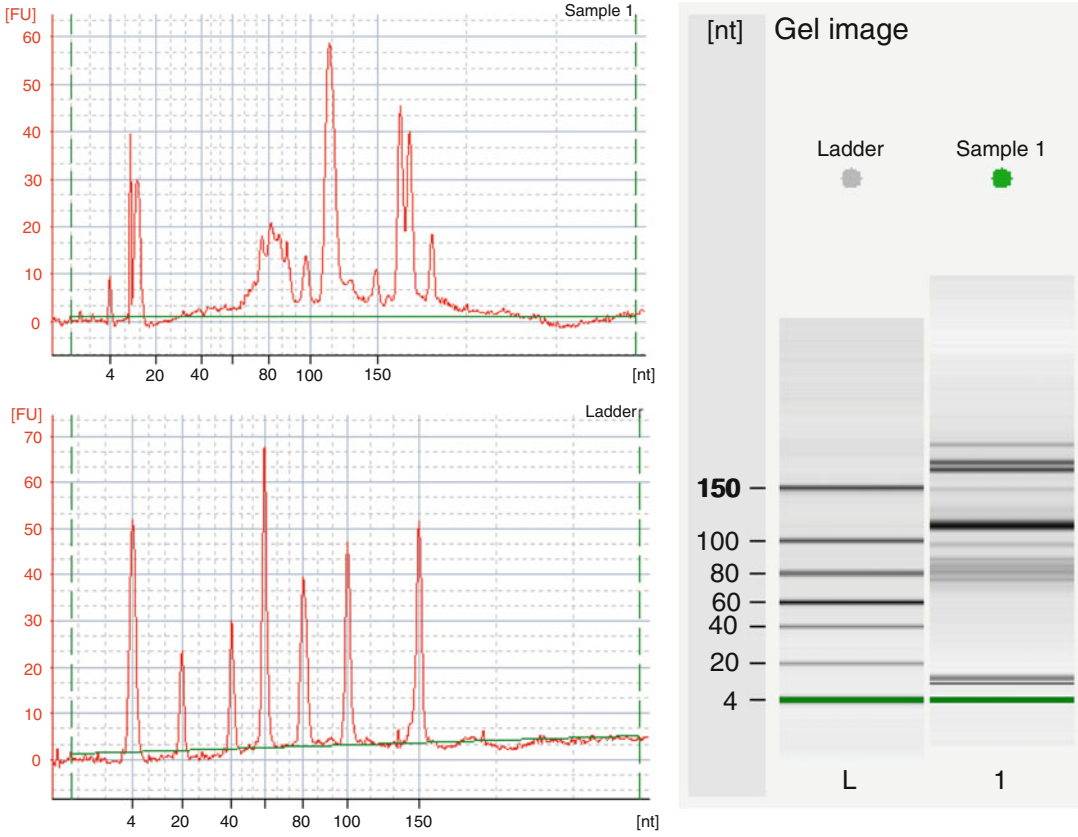

Fig. 3 Electropherograms and gel image of the sRNA sample and ladder being checked on Agilent®2100 Bioanalyzer

3.4.2 Quality and Quantity Check on Agilent's Bioanalyzer

1. Samples can be checked for quality on Agilent's Bioanalyzer using sRNALabChip kits.
2. Obtain the electropherogram profile and the band pattern of each RNA sample and access for degradation of Small RNA (*see* Fig. 3).

3. Obtain, for each sample, Small RNA concentration (pg/μL), miRNA concentration (pg/μL), and miRNA/Small RNA ratio (%).

3.5 Designing miRNA Primers

The short size (~22 nucleotides) of mature miRNAs, which is same as the length of traditional PCR primer, makes it challenging to design of primers for microRNA RT-qPCR. However, several methods have been developed to overcome this problem and commonly all methods rely on elongation of the microRNA producing a template long enough to allow the design of two primers [8]. Moreover, many miRNAs exist as isoforms and have nearly identical mature and precursor sequences, thus complicate the designing of primers that can quantify the specific miRNA [9].

3.5.1 Primer Designing for SYBR Green Based Detection of Mature miRNAs

We can use miScript Primer Assays (commercially available forn Qiagen) for the quantification of mature miRNA expression based on SYBR green chemistry. For the microRNA detection, the miScript Primer Assay acts as the forward primer that is to be used along with the universal reverse primer and other master mix prepared subsequently with miScript SYBR Green PCR Kit. The forward primer can also be easily self-designed. As, for making cDNA (i.e. template for qPCR reaction), miScript II RT kit first adds a poly A tail to the microRNA and then the complementary cDNA version of the miRNA is made with an oligodT adapter attached at the end. Therefore, in the SYBR green –qPCR step, the reverse primer is a universal primer for the dT end, which is generally provided in the SYBR kit, while the forward primer is the DNA version of the miRNA of interest. So to design the forward primer by just replace the U's with T in mature miRNA.

Additional factor that needs to be considered during designing primer is to Match Tm of forward and reverse primer:

1. To increase Tm:
   (a) Add "A" at the 3′ end of primer sequence. (Note: We are adding "A"s, since we did poly "A" tailing and now a stretch of "T"s are at the end of cDNA that was made from the mature miRNA.) No more than 6 "A"s should be added to any one sequence.
   (b) "G" or "C" residues can be added to the 5′ end of primer (Try less than 30 nucleotides).
2. To decrease Tm:
   (a) The sequences at the 5' end can be deleted taking in consideration that at least 18 nucleotides of the primer should exactly match to the target miRNA.
   (b) In most cases, bases can be also deleted from the 3′ end. But the position of deletion and number of nucleiotides to be deleted should be carefully analyzed when isoforms of the miRNAs are present.

3.5.2 TaqMan microRNA Assays

Using SYBR green detection, it is often not possible to design PCR primers that can target hairpin of pre-miRNAs to discriminate among the various isoforms. This issue can be resolved with TaqMan™ minor groove binding (MGB) probes that anneal to the loop portion of the miRNA precursor. Likewise, discrimination of mature miRNAs of closely related families, differing slightly in their 3′ ends, is challenging when using primers relying on SYBR green chemistry.

The TaqMan™ microRNA Assays are quantitative RT-PCR assays and are designed to detect and accurately quantify mature miRNAs in a two step process. In the first step, cDNA is reversed transcribed from the sRNA samples using miRNA specific stem-loop RT- primer. In the second step, PCR products are amplified from the cDNA by using TaqMan miRNA assay i.e. composed of forward primer, reverse primer and a specific detection probe (Fig. 4) [10]. There are several advantages of using stem-loop RT primers. First, by annealing a short RT priming sequence to the 3′ portion of the miRNA, it has better specificity for discriminating similar miRNAs. Second, its double-stranded stem structure inhibits hybridization of the RT primer to miRNA precursors and other long RNAs. Third, the base stacking of the stem enhances the stability of miRNA and DNA hetero-duplexes, improving the RT efficiency for relatively short RT primers (the portion bound to the 3′ end of miRNAs). Finally, the stem-loop structure, when

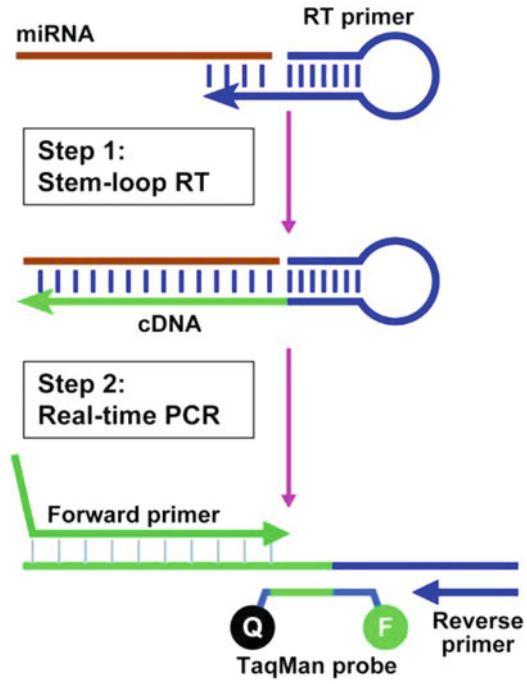

Fig. 4 Schematic description of TaqMan miRNA assays [10]

unfolded, adds sequence downstream of the miRNA after reverse transcription. The resulting longer RT product presents a template more amenable to real-time TaqMan™ assay design. The high sensitivity and specificity is largely contributed by the specific forward PCR primer and TaqMan™ probe.

3.6 qPCR for miRNA

Expression of miRNAs can be validated by real-time PCR using TaqMan or SYBR green chemistry [11].

3.6.1 miRNA Expression Analysis by TaqMan Chemistry: Reverse Transcription (RT) Reaction

1. Convert the Total RNAs (including miRNAs) or sRNAs enriched for miRNA into cDNAs using by TaqMan microRNA reverse transcription kit.
2. This kit converts total RNAs into cDNA using specific miRNA primers which are provided with respective Taqman MicroRNA Assays.
3. For each sample, set up a 15 μL reaction on ice having 7 μL of RT master mix (0.25 mM dNTPs, 3.33 U/μL multiscribe RT enzyme, 1× RT buffer, 0.25 U/μL RNAse inhibitor), 3 μL of specific reverse primer and 5 μL of RNA sample.
4. Incubate the reaction tubes at temperature of 16 °C for 30 min, 42 °C for 30 min and last at 85 °C for 5 min in a thermal cycler.

3.6.2 miRNA Expression Analysis by TaqMan Chemistry: Real Time PCR Detection

1. In the next step, combine 0.8 μL of the product from RT reaction (diluted 1:2) with 0.5 μL of a 20× TaqMan MicroRNA Assay (forward primer, reverse primer, and probe) and 5 μL of 2× TaqMan Universal PCR Master Mix, in a 10 μL final volume.
2. Perform the real-time PCR using suitable system (e.g., BioRAD CFX96 or Applied Biosystems 7500) with the standard TaqMan microRNA assays protocol, i.e., cycling conditions of 95 °C for 10 min, followed by a total of 40 cycles of 95 °C for 15 s and 60 °C for 60 s.
3. Each TaqMan Assay should be run in triplicate or quadruplicate. The relative quantification of mature miRNA expression is normalized to the expression of bovine RNU6, miR-191 or other control assays.
4. For each assay, a no-template control (NTC) reaction should also be included.
5. Determine the threshold cycle (Ct) values with automatic baseline settings at threshold of 0.2.
6. Calibrate the dCt values (Ct values normalized to Ct of each of the endogenous controls) of the samples with the respective dCt of control samples, for each group.
7. Perform relative expression of the miRNA (as fold change) using ΔΔCt method [12].

3.6.3 miRNA Expression Analysis by SYBR Green Chemistry: Reverse Transcription (RT) Reaction

1. For quantifying miRNA expression, reverse transcribe the total RNA or sRNA enriched for miRNA and siRNA into cDNA using miScript II RT kit.
2. For each sample, set up a 20 μL reaction was on ice having 4 μL of 5× miScript Hispec buffer, 2 μL of 10× nucleic mix, 2 μL of miScript RT mix, and 6 μL of RNA sample (1 μg each).
3. Incubate the reaction tubes at 37 °C for 60 min and at 95 °C for 5 min in a thermal cycler.
4. Keep the products of the RT reaction on ice.

3.6.4 miRNA Expression Analysis by SYBR Green Chemistry: Real Time PCR Detection of miRNAs

1. Dilute the product from RT reaction by adding at least 200 μL of RNase-free water.
2. Combine the diluted cDNA (~5 ng) with 5 μL of 2× Quanti-Tect SYBR Green RCR Mix, 1 μL of 10× miScript Universal primer, 1 μL of 10× forward primer, and RNase-free water, in a 10 μL final volume.
3. Perform Real-time PCR was using suitable Real Time PCR System with the following protocol, i.e., initial activation at 95 °C for 15 min, followed by a total of 40 cycles of denaturation (94 °C) for 15 s, annealing (55 °C) for 30 s and extension (70 °C) for 30 s.
4. Run each miRNA assay in triplicate. For each assay, also include a no-template control (NTC) reaction.
5. Determine the threshold cycle (Ct) values with automatic baseline settings at threshold of 0.2.
6. Normalize the relative quantification of mature miRNA expression to the expression of bovine RNU6 control assays.
7. Calibrate the dCt values (Ct values normalized to Ct of each of the endogenous controls) of the samples with the respective dCt of control samples, for each group.
8. Perform relative expression of the miRNA (as fold change) using ΔΔCt method.

4 Notes

1. The quality of the PBMCs separation depends upon the sharpness of the interphase between the blood and HiSep solution. Undiluted blood does not form sharp interphase. Blood should be layered over the solution by dispensing blood very slowly upon the walls of the centrifuge tube rather than directly dispensing over the solution.
2. Swinging bucket centrifuge is preferable, but fixed bucket rotor can also be used for separation of PBMCs. In such a case,

centrifuge at 700 × *g* for 30 min. Also care should be taken to centrifuge with brakes off as it would disturb the layer of leucocytes that will come between the interphase of plasma and HiSep solution. Erythrocytes and other poly-nuclear leucocytes will sediment at the bottom of the centrifuge tubes.

3. Washing with PBS removes the unwanted HiSep and also reduces the number of platelets. If after centrifuge the pellet is red in color (due to presence of erythrocytes), then pellet may be resuspended in 1× RBCs lysis buffer and keep it at room temperature for 10 min and centrifuged again at 3000 rpm (2000 × *g*) for 10 min to get clear white pellet of monocytes.
4. To find the optimum dosage of TLR ligands, expression of the respective TLR gene or other down-stream interleukins of TLR pathway specifically generated in response to respective TLR ligand is measured. For example,
   (a) TLR3 ligand (Poly I: C) stimulation: Stimulate the cultured PBMCs with two or more different doses of poly I: C (@ Final conc. 10 μg/mL and 50 μg/mL) for different time intervals: 1 h, 3 h, 6h, 12, 18, and 24 h. Normal, untreated PBMCs just at the start of incubation time (0 h) and at the end of each interval time should be taken as control.
   (b) TLR4 ligand (LPS) stimulation: Stimulate the PBMCs cultures with four different LPS doses (10 ng/mL, 100 ng/mL, 1000 ng/mL, and 2000 ng/mL). For each treatment group/dose of LPS, incubate the cultures for 2 h, 6 h, 12 h, and 24 h, respectively. Take nonstimulated normal PBMCs cultured for different time intervals, as respective control group.
5. For sample volumes greater than 700 μL, add the mixture in successive applications to the same filter.
6. If the lysate/ethanol mixture was >700 μL, transfer the flow-through to a fresh tube, and repeat centrifugation until all of the mixture passes through using the same filter.
7. If the sample volume exceeds 700 μL, add the mixture in successive applications to the same filter and centrifuge at 10,000 rpm (8000 × *g*) for ~30 s to pass the mixture through the filter
8. 15 mL is enough gel solution for one 13 cm × 15 cm × 0.75 mm gel.

Acknowledgment

The work was supported by SERB-DST (Ministry of Science of Technology, Government of India) sponsored Research Grant SERC-LS-293-2011 (File Number SR/FT/LS-22/2011).

References

1. Bartel DP (2004) MicroRNAs: genomics, biogenesis, mechanism, and function. Cell 116:281–297
2. Huntzinger E, Izaurralde E (2011) Gene silencing by microRNAs: contributions of translational repression and mRNA decay. Nat Rev Genet 12:99–110
3. Baltimore D, Boldin MP, O'Connell RM, Rao DS, Taganov KD (2008) MicroRNAs: new regulators of immune cell development and function. Nat Immunol 9:839–845
4. Ivey KN, Srivastava D (2010) MicroRNAs as regulators of differentiation and cell fate decisions. Cell Stem Cell 7:36–41
5. Farazi TA, Hoell JI, Morozov P, Tuschl T (2013) MicroRNAs in human cancer. Adv Exp Med Biol 774:1–20
6. Kolbert CP, Feddersen RM, Rakhshan F, Grill DE, Simon G, Middha S, Jang JS, Simon V, Schultz DA, Zschunke M, Lingle W, Carr JM, Thompson EA, Oberg AL, Eckloff BW, Wieben ED, Li P, Yang P, Jen J (2013) Multiplatform analysis of microRNA expression measurements in RNA from fresh frozen and FFPE tissues. PLoS One 8:e52517
7. De Planell-Saguer M, Rodicio MC (2013) Detection methods for microRNAs in clinic practice. Clin Biochem 46:869–878
8. Benes V, Castoldi M (2010) Expression profiling of microRNA using real-time quantitative PCR, how to use it and what is available. Methods 50:244–249
9. Varkonyi-Gasic E, Wu R, Wood M, Walton EF, Hellens RP (2007) Protocol: a highly sensitive RT-PCR method for detection and quantification of microRNAs. Plant Methods 3:12. doi:10.1186/1746-4811-3-12. PMCID: PMC2225395
10. Chen C, Ridzon DA, Broomer AJ, Zhou Z, Lee DH, Nguyen JT, Barbisin M, NL X, Mahuvakar VR, Andersen MR, Lao KQ, Livak KJ, Guegler KJ (2005) Real-time quantification of microRNAs by stem-loop RT-PCR. Nucleic Acids Res 33:e179
11. Singh J, Mukhopadhyay CS, Kaur S, Malhotra P, Sethi RS, Choudhary RK (2016) Identification of the MicroRNA repertoire in TLR-ligand challenged bubaline PBMCs as a model of bacterial and viral infection. PLoS One 11 (6):e0156598. doi:10.1371/journal.pone.0156598
12. Schmittgen TD, Livak KJ (2008) Analyzing real-time PCR data by the comparative C(T) method. Nat Protoc 3(6):1101–1108

Chapter 5

Visualizing Virus-Derived dsRNA Using Antibody-Independent and -Dependent Methods

Sarah J. Poynter and Stephanie J. DeWitte-Orr

Abstract

Long double-stranded (ds) RNA molecules are produced as a byproduct of viral replication. Studying virus-derived dsRNA is important for understanding virus replication, understanding host responses to virus infections, and as a diagnostic tool for virus presence and replication. Here, we describe four different techniques for visualizing dsRNA; two antibody-dependent methods (immunoblotting and immunocytochemistry), as well as two antibody-independent methods (differential digestion and acridine orange staining). The benefits and disadvantages of each technique are also discussed.

Key words dsRNA, Immunoblot, Differential digestion, Viral dsRNA, Acridine orange, Immunocytochemistry

1 Introduction

Virus replication leads to the production of dsRNA, either as a genomic fragment, replication intermediate, replicative byproduct, or potentially transcribed from viral DNA by host machinery [1, 2]. These long dsRNA molecules act as an indicator of a viral infection, as healthy host cells do not contain dsRNA molecules >40 bp [3]. Virus-derived (v)dsRNA molecules are recognized by host expressed pattern-recognition receptors (PRRs) and can induce a strong innate antiviral immune response [1]. Many viruses have evolved mechanisms to evade dsRNA-induced innate antiviral mechanisms [4]. Thus studying (v)dsRNA is important for: (1). understanding virus replication, (2). understanding host responses to virus infection, and (3). as a diagnostic tool for virus presence (for dsRNA genome viruses) and replication. Viral dsRNA is clearly an important molecule, worthy of study; however, the methods used to detect these virus-produced molecules can be difficult to execute. There are a number of ways to visualize and distinguish dsRNA from other nucleic acids; four methods have been included here. Differential nuclease digestion can be used as dsRNA is

Karen Mossman (ed.), *Innate Antiviral Immunity: Methods and Protocols*, Methods in Molecular Biology, vol. 1656, DOI 10.1007/978-1-4939-7237-1_5,

sensitive to RNase III but resistant to RNase A and T1 under high salt conditions [3, 5–7]. There are three commercially available dsRNA antibodies, J2, K1, and K2 that can be used for immunoblotting or immunocytochemistry (ICC) [6, 8–10]. Acridine orange (AO) stained agarose gels can be used to look for dsRNA in total RNA extractions from virus-infected cells, as AO stains single-stranded nucleic acids red and double-stranded nucleic acids green [11]; however, AO staining will not differentiate dsDNA and dsRNA so this method alone is not enough to confirm dsRNA presence if there is a possibility of contaminating DNA. Ideally, more than one technique should be employed when looking to confirm the presence of dsRNA. The advantages and disadvantages of these techniques are compared in Table 1.

The dsRNA detection methods described here include both antibody-dependent and -independent assays. As it has a dsRNA genome, we used an aquareovirus, chum salmon reovirus (CSV) as a positive control for virus-derived dsRNA [9]. The antibody-dependent assays include ICC, Fig. 1, and a dsRNA immunoblot, Fig. 2. The strength of these assays includes: providing information of the size of the dsRNA produced (dsRNA immunoblot) and indicating cellular localization (ICC), all while relying on the specificity of a monoclonal antibody. In addition, ICC is the only

Table 1
A summary of select techniques used to visualize dsRNA

Method	*Benefits*	*Disadvantages*
Antibody (J2)-dependent		
Immunoblot	• dsRNA length and amounts can be determined • Does not require digestion to remove ssRNA prior to detection • Specific	• Nucleic acids must be extracted • Specialized equipment needed
Immunocytochemistry	• dsRNA location within cell can be determined • No nucleic acid extraction needed • Specific	• No information on size • Specialized equipment needed
Antibody-independent		
Differential digestion	• No antibody required • No specialized equipment needed	• Possible loss of dsRNA during RNase A inactivation step • Nucleic acids must be extracted
Acridine orange	• Allows for differentiation of RNA strandedness • No specialized equipment needed	• Lower sensitivity than ethidium bromide • Does not differentiate dsDNA from dsRNA • Nucleic acids must be extracted

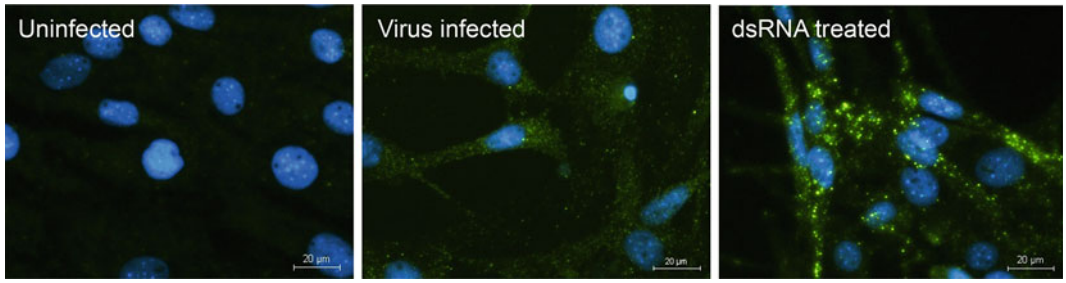

Fig. 1 Immunocytochemistry to detect (v) dsRNA using the J2 antibody. RTG-2 cells were infected with CSV ($TCID_{50}$/mL: 1.5×10^4) for 5 days, treated with media containing 10 μg/mL in vitro transcribed dsRNA for 12 h, or treated with media alone. A 2° only control showed no green signal (data not shown). Cells were counterstained with DAPI (*Green* = dsRNA, *blue* = nuclei). Magnification 200×

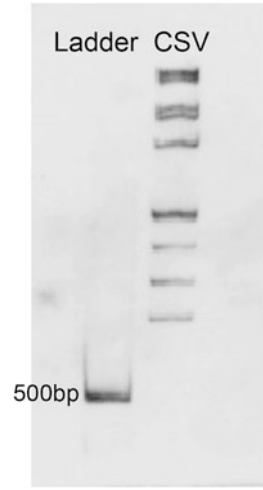

Fig. 2 DsRNA immunoblot to detect (v)dsRNA virus-infected cells using the J2 antibody. CHSE-214 cells were infected with 1.5×10^5 $TCID_{50}$/mL CSV for 7 days prior to RNA extraction. 5 μg of total RNA from CSV-infected cells was used in this experiment. 1 μg of dsRNA ladder was also included. Total RNA from uninfected CHSE-214 cells has no bands (data not shown)

technique described here that does not require extraction of nucleic acids, thus there is no risk of dsRNA being formed during the extraction process. It has been suggested that RNA extraction methods using phenol/chloroform (e.g., TRIzol) can cause dsRNA formation [12]. We have not observed this in our controls, in fact, we have found commercial RNA extraction kits often are ineffective at extracting large (v)dsRNA molecules. Uninfected cells serve as an effective negative control in both these assays, as the J2 antibody cannot detect dsRNA <30 bp [8]. Both the assays have the disadvantages of being time consuming and require specialized equipment.

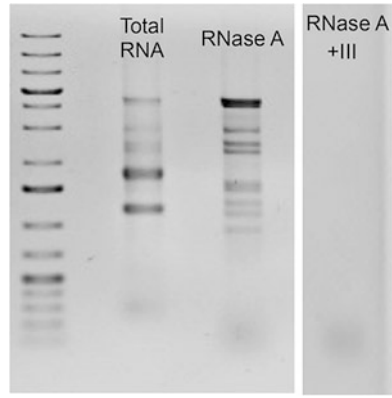

Fig. 3 Differential digestion to detect dsRNA from total RNA extracted from virus-infected cells. CHSE-214 cells were infected with 1.5×10^5 $TCID_{50}$/mL virus for 7 days prior to RNA extraction. 0.5 μg of total RNA, 10 μg of total RNA treated with RNase A or RNase A and RNase III were run on an agarose gel alongside 0.5 μg O'Generuler 1 kb plus. The gel was stained with ethidium bromide and visualized under UV transillumination

The antibody-independent assays use an RNA extraction method (from virus-infected cells; the same RNA used in the immunoblot), combined with either differential nuclease digestion and detection with ethidium bromide (EtBr), Fig. 3, or AO staining, Fig. 4, and require less specialized equipment. AO stain is combined with agarose gel electrophoresis to differentially stain ssRNA red and dsRNA green. The two antibody-independent detection methods for (v)dsRNA have different strengths; differential digestion detected by EtBr is highly sensitive and AO can determine strandedness (Table 1). It should be noted that these two methods could also be combined; a differential digestion can be followed by AO staining in addition to or in place of EtBr. When comparing fluorescence stains, EtBr is a more sensitive stain than AO, but the need to differentiate ssRNA and dsRNA could outweigh sensitivity in some cases. As always, the detection method must be chosen based on the requirements of the researcher.

2 Materials

2.1 RNA Extraction

1. TRIzol reagent.
2. 75% (v/v) Ethanol: Combine 7.5 mL of 100% ethanol with 2.5 mL molecular biology grade water. Store at room temperature.
3. 100% Isopropanol.
4. Chloroform.
5. Nuclease-free molecular biology grade water.

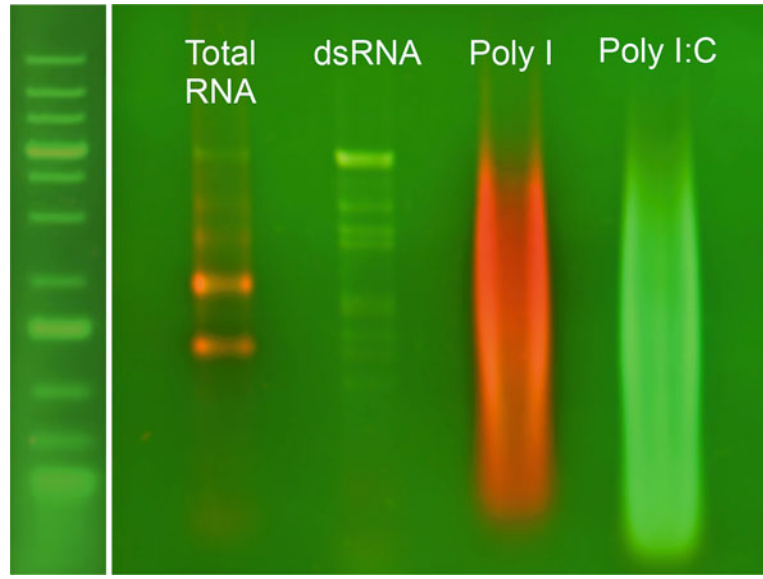

Fig. 4 Acridine orange stain used to visualize nucleic acids with colorimetric indication of strandedness. CHSE-214 cells were infected with 1.5×10^5 $TCID_{50}$/mL chum salmon reovirus (CSV) for 7 days prior to RNA extraction. 0.5 μg of total RNA and dsRNA isolated from 10 μg of total RNA digested with RNase A (dsRNA) were run on an agarose gel alongside 0.5 μg O'Generuler 1 kb plus. 4 μg of poly I (ssRNA) and poly I:C (dsRNA) were run as controls. The gel was stained with acridine orange. Double-stranded nucleic acids stain green and single-stranded nucleic acids stain red with this stain

6. Microcentrifuge tubes.
7. Tabletop centrifuge (speed of at least 12,000 × *g*).

2.2 Immunocytochemistry

1. ICC blocking solution: 3% w/v bovine serum albumin (BSA), 3% v/v goat serum, 0.02% v/v Tween-20 in phosphate-buffered saline (PBS). In a 50 mL Falcon tube dissolve 3 g BSA in 48.49 mL PBS and then add 1.5 mL goat serum and 10 μL Tween-20. Mix thoroughly by inverting tube. Filter through 0.22 μM filter and store at 4 °C (*see* **Note 1**).
2. 10% neutral buffered formalin.
3. Permeabilization solution I: 0.5% v/v Triton-X in PBS. Mix 50 μL Triton-X in 10 mL of PBS. Prepare fresh.
4. Permeabilization solution II: 0.1% v/v Triton-X in PBS: Mix 10 μL Triton-X in 10 mL of PBS. Prepare fresh.
5. 5 mg/mL 4′,6-Diamidine-2′-phenylindole dihydrochloride (DAPI). To prevent product loss reconstitute entire container of DAPI at once. To 10 mg of DAPI add 2 mL of molecular biology grade water. Mix thoroughly by vortexing. Divide into 10 μL aliquots and store at −20 °C protected from light.

6. Circular cover glass 18 mm diameter.
7. Microscope slides 3″ × 1″ × 1 mm.
8. SlowFade Gold Antifade mountant (S36936, Fisher Scientific).
9. 1× PBS with magnesium and calcium.
10. 1× PBS without magnesium and calcium.
11. Goat-anti mouse Dylight 488 antibody (Cedarlane, CLAS09–632).
12. 1 mg/mL J2 monoclonal antibody (Scicons English and Scientific Consulting Kft, Hungary). To 200 µg add 200 µL molecular biology grade water. Mix thoroughly by pipetting and let it sit at room temperature for 15 min. Centrifuge the tube at a max speed in a tabletop centrifuge for 5 min to remove aggregates. Divide into 5 µL aliquots and store at −20 °C.

2.3 dsRNA Immunoblot

2.3.1 Polyacrylamide Gel Electrophoresis (PAGE)

1. 40% (v/v) Acrylamide/Bis solution.
2. 10% (w/v) Ammonium persulfate (APS). Add 1 g of APS solution to 10 mL of MilliQ water; mix by vortexing. Divide into 100 µL aliquots and store at −20 °C.
3. Tetramethylethylenediamine (TEMED).
4. dsRNA ladder.
5. 6× Orange DNA Loading Dye
6. 5× Tris-borate ethylenediaminetetraacetic acid (EDTA) (TBE): 445 mM Tris base, 445 mM borate, 10 mM EDTA. Combine 54 g of Tris base, 27.5 g of boric acid and 20 mL of 0.5 M (pH 8.0) EDTA. Bring up to 1 L with MilliQ water. Mix with a magnetic stir bar until clear. Store at room temperature.
7. Mini-protein electrophoresis system.

2.3.2 Membrane Transfer

1. Trans-Blot Turbo Transfer System.
2. MagnaLift Nylon Membrane 0.45 µm.
3. Extra thick western blotting filter paper.

2.3.3 Immunoblotting

1. 10× Tris-buffered saline (TBS): 200 mM Tris, 1.5 M NaCl (pH 7.6). Dissolve 24 g Tris base and 88 g of NaCl in 1 L of MilliQ water. Adjust pH to 7.6 with concentrated HCl. Store at room temperature.
2. TBS-T: TBS containing 0.1% (v/v) Tween-20. Add 1 mL of Tween-20 to 1 L of TBS. Mix thoroughly by inversion. Store at room temperature.
3. Blocking solution: 5% (w/v) skim milk in TBS-T. Combine 1 g of skim milk powder with 20 mL of TBS-T. Make fresh.

4. 1° Antibody dilution solution: 2% (w/v) BSA in TBS-T. Dissolve 0.2 g of BSA to 10 mL of TBS-T. Make fresh.
5. 2° Antibody dilution solution: 5% (w/v) skim milk in TBS-T. Combine 1 g of skim milk powder with 20 mL of TBS-T. Make fresh.
6. J2 monoclonal antibody (*see* Subheading 2.2).
7. Goat-anti mouse horseradish peroxidase (HRP) antibody.

2.3.4 ECL Detection

1. Western blot ECL detection solution.
2. VersaDoc Imaging System or similar system capable of imaging chemiluminescence.

2.4 Nuclease Digestion

1. RNase A.
2. RNase III and RNase III digestion buffer.
3. Molecular biology grade 5 M NaCl.
4. 10 mg/mL poly inosinic: poly cytidylic acid (poly I:C). To prevent product loss reconstitute entire container of poly I:C at once. To a 25 mg container add 2.5 mL of PBS. Invert bottle to mix solution. Heat in a 55 °C water bath for 15 min and then let it cool at room temperature for 30 min. Divide into 20 μL aliquots and store at −20 °C.
5. 10 mg/mL poly inosinic acid (poly I). To prevent product loss reconstitute entire container of poly I at once. To a 25 mg container add 2.5 mL of molecular biology grade water. Invert bottle to mix solution. Heat in a 55 °C water bath for 15 min. Divide into 20 μL aliquots and store at −20 °C.
6. 1 Kb Plus DNA ladder.

2.5 Agarose Gel

1. Agarose gel apparatus.
2. 6× Orange DNA Loading Dye.
3. 1 Kb Plus DNA ladder.
4. 50× Tris-acetate EDTA (TAE): 2 M Tris, 1 M acetic acid, 50 mM EDTA. Dissolve 242 g Tris base, 18.61 g EDTA, and 57.1 mL of acetic acid in 1liter of MilliQ water. Store at room temperature.
5. 0.5 μg/mL ethidium bromide (EtBr) stain. Dilute 10 μL of 10 mg/mL stock EtBr in 200 mL of MilliQ water. Store at room temperature in the dark for up to 1 month.
6. Agarose (1% w/v in TAE). For a mini-gel combine 40 mL of 1× TAE with 0.4 g of agarose. Microwave for approximately 1.5 min until clear. Swirl under cold water until you are able to touch the container, and then pour into mold.

7. 15 μg/mL Acridine orange (AO) stain. Measure 30 mg of AO in a container big enough to fit the gel you are staining, add 200 mL of MilliQ water. Mix on a rocking platform at a low speed until there are no visible precipitates. Prepare fresh.

3 Methods

Carry out all the steps at room temperature and with room temperature reagents, unless specified. PBS is without magnesium and calcium, unless otherwise specified.

3.1 Immunocytochemistry

All the wash steps will be 500 μL/well for 1 min; to easily remove media or wash solution invert plate over a collection dish.

1. Plate cells of interest at a medium-confluency in 12-well plates containing glass coverslips. For example, for RTG-2 cells [13], plate 200,000 cells/well in a total volume of 1 mL.
2. Incubate overnight at normal growth temperature to allow for re-attachment of cells.
3. Infect cells with a sub-lethal titre of your virus of interest. Treat uninfected control wells with 500 μL of media alone. A positive control can be included (in this case, 10 μg/mL in vitro transcribed dsRNA for 12 h; *see* **Note 2).**
4. Incubate for the required amount of time at a permissive temperature. At this time there may be the beginning signs of cytopathic effects, but the monolayer should be largely intact.
5. Remove media from all wells and wash 1× with PBS (+Mg + Ca).
6. To fix the cells add 500 μL/well 10% neutral buffered formalin and incubate for 10 min.
7. Wash cells 3× with PBS.
8. To permeabilize the cells add 500 μL/well of freshly prepared 0.5% Triton-X in PBS and incubate for 15 min (*see* **Note 3**).
9. Wash cells 3× with PBS.
10. To block nonspecific binding, add 500 μL ICC blocking solution to all wells and incubate for 1 h.
11. Wash cells 1× with PBS.
12. Using a pipette tip, ensure that no coverslips are touching the walls of the well, as this can draw the antibody solution off the coverslip.
13. Dilute J2 (1°) antibody 1:200 in ICC blocking solution and add 40 μL/coverslip; add ICC blocking solution alone to 2° -antibody-only control and no virus, 1° or 2° antibody control wells.

14. Incubate for 1 h in a humidified chamber; a Styrofoam cooler with wet paper towel at the bottom will suffice.
15. Wash cells 3× with PBS.
16. Using a pipette tip to ensure that coverslips are not touching the walls of the well.
17. Dilute goat anti-mouse Dylight 488 (2°) antibody 1:200 in ICC blocking solution and add 40 μL/coverslip; add ICC blocking solution alone to full control well. Incubate for 1 h in a humidified chamber in the dark.
18. Rinse 3× with PBS
19. To counterstain nuclei, dilute DAPI 1:1000 to 5 μg/mL in PBS and add 300 μL/well. Incubate for 5 min in the dark.
20. Wash 3× with PBS and 1× with MilliQ water to remove residual salt.
21. To mount coverslips, add 3 μL of SlowFade Gold Antifade mountant to glass slides and using tweezers place coverslips cell-side down into mounting media.
22. Incubate overnight at room temperature in the dark to cure mounting media.
23. Visualize with a fluorescence microscope at 200× magnification (we use a Nikon Eclipse TiE with Qi1 camera and Nikon NIS-Elements software; *see* **Note 4**).

3.2 Extraction of Viral dsRNA from Cells

The RNA generated in this section is used in Subheadings 3.3–3.5.

1. Infect a T-75 flask of cells with your virus of choice at a sufficient titer, which will need to be determined. For the example shown in Fig. 2, CHSE-214 cells [14] were infected with 1.5×10^5 $TCID_{50}$/mL CSV.
2. Incubate at a permissive temperature until cells are showing advanced cytopathic effects but prior to complete destruction of the monolayer.
3. Aspirate media from the flask.
4. Add 1.2 mL of TRIzol reagent. Coat cell surface with TRIzol by gently tilting the flask. Scrape cells and collect cell/TRIzol mixture in a 1.5 mL microcentrifuge tube. The mix is split into two separate tubes of 600 μL to facilitate processing.
5. To each 600 μL of TRIzol add 0.12 mL of chloroform and shake vigorously for approximately 30 s.
6. Incubate for 3 min at room temperature.
7. Centrifuge at max speed in a tabletop microcentrifuge (13,200 × *g*) for 15 min at 4 °C.
8. Transfer the clear upper aqueous phase (this phase contains RNA) to a new microcentrifuge tube, taking care not to remove any of the white or pink phases.

9. To precipitate the RNA, add 0.3 mL of 100% isopropanol to the aqueous phase. Shake vigorously and incubate at room temperature for 10 min.
10. Centrifuge at max speed in a tabletop microcentrifuge for 10 min at 4 °C. Ensure the hinge of the tube is facing up so the pellet may be easily located. The pellet of RNA may be very small, thus draw off the supernatant by placing a pipette on the opposite side of the tube.
11. To wash the RNA add 0.6 mL of 75% ethanol. Centrifuge at max speed in a tabletop microcentrifuge for 5 min at 4 °C.
12. Remove the 75% ethanol carefully, to avoid displacing the pellet of RNA.
13. Let the tube dry upside down on a KimWipe for 15 min.
14. Resuspend the pellet in 30 μL of molecular biology grade water.
15. Heat at 55 °C for 15 min. Let it cool at room temperature for 15 min.
16. Quantify RNA using a NanoDrop Lite Spectrophotometer (*see* **Note 5**).

3.3 dsRNA Immunoblot

All the steps are performed at room temperature unless otherwise specified; all rinses are for 5 min with gentle rocking.

3.3.1 Polyacrylamide Gel Electrophoresis (PAGE)

1. Prepare a 10% acrylamide gel by combining 3.9 mL MilliQ water, 1.5 mL of 40% acrylamide/Bis solution, 600 μL 10× TBE buffer, 100 μL 10% APS in MilliQ water, and 5 μL of TEMED in a 15 mL Falcon tube, ensuring APS and TEMED are added last.
2. Mix thoroughly but quickly to ensure gel is poured before polymerization occurs in the Falcon tube. Using a P1000 pipette, transfer solution between the mini-protein gel plates, add a comb for wells, and allow it to polymerize (approximately 20–30 min). There is no stacking layer for this gel. Check the leftover gel solution in the Falcon tube; once this solution is solidified the gel should be as well.
3. Assemble the gel apparatus and fill with 1× TBE. Do not use the running buffer meant for a western blot.
4. Load 2 μL (1 μg) of dsRNA ladder mixed with 8 μL of molecular biology grade water and 2 μL of 6× Orange DNA Loading Dye into the dsRNA ladder lane. All the sample lanes should contain 5 μg of RNA mixed with 6X loading dye (*see* **Notes 6–8**).
5. Run gel at 140 V for 2.5–3 h (*see* **Note 9**).

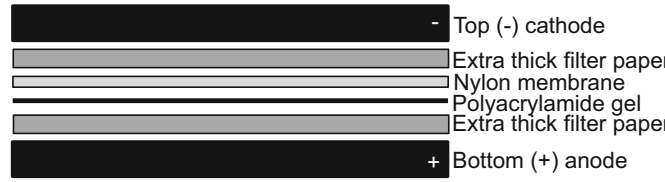

Fig. 5 The order of assembly for a dsRNA immunoblot transfer. From the bottom anode up, the stack should include a layer of extra thick filter paper, a nylon membrane, the polyacrylamide gel, and another layer of extra thick filter paper. The membrane and filter paper should be presoaked in transfer buffer (0.5× TBE)

3.3.2 Transfer

1. Cut two sheets of extra thick paper and a nylon membrane to the size of the gel.
2. Soak paper and membranes in 0.5× TBE for 1–2 min, until saturated.
3. Set up membrane/filter/gel stack with one layer of extra thick paper, nylon membrane, acrylamide gel, one layer extra thick paper (Fig. 5).
4. Roll out any air bubbles using a roller or clean test tube.
5. Using BioRad Turbo Semi-Dry Transfer apparatus, set transfer to 400 mA (max 25 V) for 90 min, the actual transfer will vary between 100 and 200 mA for the majority of the transfer.

3.3.3 Immunoblot

1. Remove membrane from stack carefully using tweezers; transfer to a container of a size to fit the membrane flat, and block in 5% skim milk TBS-T solution for 1 h on a rocking platform set to a low speed.
2. Pour off block solution: rinse 3× with TBS-T.
3. Add J2 antibody diluted 1:2000 in TBS-T with 2% BSA (*see* **Note 10**).
4. Incubate overnight at 4 °C with gentle rocking on a rocking platform set to a low speed.
5. Remove primary antibody solution; collect for reuse.
6. Rinse 3× with TBS-T.
7. Add secondary antibody, goat-anti mouse HRP, 1:2000 in 5% skim milk TBS-T for 1 h on a rocking platform set to a low speed, now at room temperature.

3.3.4 Detection

1. Remove secondary antibody solution, rinse 2× with TBS-T and 1× with TBS.
2. Prepare detection solution as per manufacturer's specifications; a total of 0.5 mL is sufficient for one membrane using this technique. This solution must be made immediately before use.

3. Place blot onto transparent sheet protector, cover with substrate taking care to remove bubbles; incubate for 5 min, keeping the membrane in the dark.
4. Blot along the edges of the membrane using a KimWipe to remove any excess reagent, leaving membrane in sheet protector. Do not touch membrane directly.
5. Image using VersaDoc imager or other imager set to Ultra Chemiluminescence for 30s-1min (*see* **Notes 11** and **12**).

3.4 Differential Digestion + EtBr Stained Agarose Gel Electrophoresis

1. Combine 20 μg of total RNA with 4 μL of 10^{-1} diluted RNase A + 4 μL of 5 M NaCl and bring volume to 40 μL with molecular biology grade water.
2. Incubate for 15 min at room temperature.
3. Add 400 μL of TRIzol (RNase A inactivation step).
4. Perform TRIzol extraction as per manufacturer's instructions, resuspending pellet in 20 μL of molecular biology grade water, *see* Subheading 3.2.
5. Keep RNA on ice until ready for downstream use. For long-term storage store at −80 °C.
6. Take 10 μL of the dsRNA solution and add 5 μL of RNase III + 2 μL of RNase III buffer +3 μL molecular biology grade water.
7. Incubate at 37 °C for 1 h.
8. Mix 10 μL of the single digest with 2 μL of 6× loading dye and 20 μL of the double digest with 4 μL of loading dye. Both the samples will contain the same amount of starting RNA, 10 μg.
9. Run both the single digestion and double digestion on a 1% agarose (w/v) gel in 1× TAE buffer prepared in a horizontal slab gel mold, such as the Wide Mini-Sub Cell GT Cell (BioRad). The gel will use 40 mL of 1% agarose. 4 μL (0.5 μg) of 1 kb plus ladder is also included on the gel (*see* **Note 13**).
10. Run the gel at 80 V for approximately 90 min in 1× TAE buffer.
11. Transfer gel to a container with 200 mL of 0.5 μg/mL EtBr in MilliQ water and incubate for 15 min at room temperature.
12. Transfer to a container with 300 mL of MilliQ water to destain for 15–20 min.
13. Visualize using VersaDoc transilluminator, UV setting for EtBr, exposure time 5 s.

3.5 Acridine Orange Stained Agarose gel

1. Prepare a 1% agarose gel (w/v) in 1× TAE buffer, in a horizontal slab gel mold, such as the Wide Mini-Sub Cell GT Cell (BioRad). The gel will use 40 mL of 1% agaraose.

2. Mix samples with 6× loading dye (to a final 1× loading dye) and add to wells. In Fig. 4 the samples include:
   (a) 0.5 μg O'GeneRuler 1 kb plus.
   (b) 0.5 μg total RNA extracted from virus-infected cells.
   (c) 10 μg of RNaseA-treated total RNA (starting concentration) extracted from virus-infected cells (this treatment should demonstrate dsRNA).
   (d) 4 μg of poly inosinic acid (poly I) (ssRNA control) (*see* **Note 14**).
   (e) 4 μg of poly I:C (dsRNA control) (*see* **Note 15**).
3. Run the gel at 80 V for approximately 90 min in 1× TAE buffer.
4. Stain gel in 200 mL of 15 μg/mL acridine orange in MilliQ water for 10 min at room temperature.
5. Destain for 30–60 min in 300 mL of MilliQ water; checking the gel at 15 min intervals (*see* **Notes 16** and **17**).
6. Visualize using VersaDoc transilluminator, for AO set two custom channels: AO-red: 695 band pass (bp), blue LED, 0.5× gain, 1 × 1bin; AO-green: 530 bp, blue LED, 0.5× gain, 1 × 1bin.
7. Overlap AO images using multi-channel viewer (*see* **Note 18**).

4 Notes

1. Triton-X and Tween-20 are viscous reagents; however, it is very important they are pipetted accurately; to accomplish these we make a 50% solution prior to pipetting (for immunocytochemistry blocking buffer and Triton-X solution the dilution is made in PBS, for immunoblotting the dilution is made in MilliQ water).
2. In vitro dsRNA, in this case a 200 bp molecule made using the MEGAscript RNAi kit (Thermo Fisher Scientific), works as a stronger positive control compared to poly I:C. This is because J2 in some cases can have a 10× lower affinity for poly I:C compared to other forms of dsRNA [8]. If you are interested in looking at poly I:C the K1 antibody may be a better choice.
3. We have found this combination of fixative/permeabilization effective to visualize viral dsRNA in both the cytoplasm and nucleus of fish cells. We have found that 0.1% Triton-X in PBS is best for visualizing in vitro dsRNA. It is entirely possible these concentrations would not be sufficient in some cases; we have not used other methods in our lab but other options for fixation/permeabilization could include using cold methanol,

acetone, or perhaps not permeabilizing to look at surface dsRNA.

4. Fish cells have high autofluorescence in the green spectrum, make sure to use an exposure that does not result in high background in the full control treatment.
5. There could be residual DNA contamination in this RNA, for the immunoblot DNA contamination is not an issue as the antibody is specific, a digestion that is stopped with a second TRIzol extraction will also remove any DNA contamination in our experience. If you are using a downstream application straight from here it strongly recommended to DNase treat the RNA.
6. 5 μg of total RNA was sufficient as the dsRNA in this sample is abundant. If there is a lower amount of dsRNA within the total RNA sample or the abundance is unknown, we recommended running a greater amount of RNA, for example in the past we have found 20 μg necessary.
7. If you want a membrane transfer control, you can also load a prestained protein ladder into an additional well. The dye in the RNA samples will not remain on the membrane but the protein ladder will, this can be useful to ensure you did not make any mistakes such as building your stack upside down.
8. If you think your sample is very large and you are interested in knowing the exact size this ladder will not be helpful as it only has bands up to 500 bp; you can use in vitro transcribed dsRNA of a longer length or a viral genome (preferably segmented), if available.
9. This time will require optimization depending on your sample, usually viral dsRNA length is reflected in the length of the viral genome and as such the molecules are quite large. This time/speed puts a 500 bp dsRNA ladder band at the bottom of the gel.
10. Diluting the antibody in TBS-T with BSA allows the antibody to be frozen, thawed, and reused. This strategy has been very successful for us and we have freeze/thawed a J2 antibody solution three to four times without any apparent decrease in sensitivity.
11. If the dsRNA in your sample is at a very low concentration you may need to do a very long exposure time. If this is the case it may be beneficial to cut off the ladder, as the ladder signal will be strong and might interfere with visualizing a fainter band. The ladder is generally so strong that a visible brown band can be seen with the naked eye.

12. It is recommended to image the gel after the 5 min incubation; however, the membrane can still be imaged several hours after the addition of the substrate.
13. dsRNA migrates slightly slower than dsDNA on an agarose gel [3]; this means the dsDNA ladder such as O'GeneRuler 1 kb plus will not be an entirely accurate means of sizing your dsRNA molecules. For our purposes however it has been sufficient. If you are interested in getting a more accurate ladder you can run the dsRNA marker used in the immunoblot, but the same issues will remain that the ladder does not have a band higher than 500 bp, so once again you will have to create an in vitro dsRNA of known length to accurately assess larger sized (v)dsRNA molecules.
14. ssRNA from total RNA is not always a reliable control because it can have secondary structures that might interfere with the red/green staining. Poly I is a commercially available ssRNA that works well as a ssRNA control.
15. Poly I:C is a commercially available dsRNA molecule that works well as a positive control for dsRNA. The DNA ladder will also function as positive control for double-strandedness. However it is less relevant, as a DNA molecule, for our purposes. An in vitro dsRNA molecule would also be a good control, but these molecules are more expensive to produce and may not be as readily available.
16. Gels can be stained in AO and EtBr, however the AO stain must be completed first as the EtBr seems to interfere with the AO coloring.
17. The destain period can be increased if the background is too high. An overnight destain can drastically reduce the background; however as the nucleic acids will start to diffuse out of gel you lose sensitivity, especially in the smaller and fainter bands. Larger, strong bands look clear and well stained in our experience.
18. If the gel is under stained all nucleic acids will visualize green, this is why it is important to include a single-stranded control.

References

1. Jacobs BL, Langland JO (1996) When two strands are better than one: the mediators and modulators of the cellular responses to double-stranded RNA. Virology 219(2):339–349
2. Ablasser A, Bauernfeind F, Hartmann G, Latz E, Fitzgerald KA, Hornung V (2009) RIG-I-dependent sensing of poly (dA: dT) through the induction of an RNA polymerase III–transcribed RNA intermediate. Nat Immunol 10(10):1065–1072
3. DeWitte-Orr SJ, Mossman KL (2010) dsRNA and the innate antiviral immune response. Future Virology 5(3):325–341
4. Alcami A, Koszinowski UH (2000) Viral mechanisms of immune evasion. Immunol Today 21(9):447–455

5. Edy VG, Szekely M, Loviny T, Dreyer C (1976) Action of nucleases on double-stranded RNA. Eur J Biochem 61(2):563–572
6. Weber F, Wagner V, Rasmussen SB, Hartmann R, Paludan SR (2006) Double-stranded RNA is produced by positive-strand RNA viruses and DNA viruses but not in detectable amounts by negative-strand RNA viruses. J Virol 80 (10):5059–5064
7. Aloni Y (1972) Extensive symmetrical transcription of simian virus 40 DNA in virus-yielding cells. PNAS 69(9):2404–2409
8. Schonborn J, Oberstraβ J, Breyel E, Tittgen J, Schumacher J, Lukacs N (1991) Monoclonal antibodies to double-stranded RNA as probes of RNA structure in crude nucleic acid extracts. Nucleic Acids Res 19(11): 2993–3000
9. Doherty L, Poynter SJ, Aloufi A, DeWitte-Orr SJ (2016) Fish viruses make dsRNA in fish cells: characterization of dsRNA production in rainbow trout (*Oncorhynchus mykiss*) cells infected with viral haemorrhagic septicaemia virus, chum salmon reovirus and frog virus 3. J Fish Dis 39:1133–1137
10. Lukács N (1994) Detection of virus infection in plants and differentiation between coexisting viruses by monoclonal antibodies to double-stranded RNA. J Virol Methods 47(3):255–272
11. Pichlmair A, Schulz O, Tan CP, Rehwinkel J, Kato H, Takeuchi O, Akira S, Way M, Schiavo G, Reis e Sousa C (2009) Activation of MDA5 requires higher-order RNA structures generated during virus infection. J Virol 83 (20):10761–10769
12. Borst P, Weissmann C (1965) Replication of viral RNA, 8. Studies on the enzymatic mechanism of replication of ms2 RNA. PNAS 54 (3):982–987
13. Wolf K, Quimby MC (1962) Established Eurythermic line of fish cells in vitro. Science 23 (3508):1065–1066
14. Lannan CN, Winton JR, Fryer JL (1984) Fish cell lines: establishment and characterization of nine cell lines from salmonids. In Vitro 20 (9):671–676

Chapter 6

RNA PAMPs as Molecular Tools for Evaluating RIG-I Function in Innate Immunity

Renee C. Ireton, Courtney Wilkins, and Michael Gale Jr.

Abstract

Pathogen recognition receptors (PRR)s and their cognate pathogen-associated molecular pattern (PAMP) represent the basis of innate immune activation and immune response induction driven by the host-pathogen interaction that occurs during microbial infection in humans and other animals. For RNA virus infection such as hepatitis C virus (HCV) and others, specific motifs within viral RNA mark it as nonself and visible to the host as a PAMP through interaction with RIG-I-like receptors including retinoic inducible gene-I (RIG-I). Here, we present methods for producing and using HCV PAMP RNA as a molecular tool to study RIG-I and its signaling pathway, both in vitro and in vivo, in innate immune regulation.

Key words RNA, PAMP, Innate immunity, Rig-I, Pathogen recognition receptor

1 Introduction

Pathogen recognition receptors (PRR)s are cellular proteins that serve to recognize nonself pathogen-associated molecular patterns (PAMP)s of microbial origin to alert the body that it is infected with a microbial agent to thus initiate an immune response [1, 2]. A PAMP is defined as a macromolecular motif that is (1) an inherent component of a microbe, (2) present and conserved among all the strains of the microbe, and (3) essential for the viability of the microbe [3, 4]. Eukaryotes have evolved different PRRs to recognize specific PAMPs [5, 6]. During virus infection, PRRs including, but not limited to, Toll-like receptors [7], NOD-like receptors [8], and RIG-I-Like receptors (RLR)s [9] mediate nonself recognition of viral PAMPs. Viral PAMPs include viral nucleic acid, viral protein/lipid complexes, and other macromolecules [4]. In particular, RLRs are a family of PRRs that belong to the RNA helicase superfamily and include retinoic acid inducible gene-I (RIG-I), melanoma differentiation antigen 5 (MDA5), and Laboratory of Genetics and Physiology 2(LGP2) [9]. RLRs are expressed in most cell types in the human body, where they play a major role

Karen Mossman (ed.), *Innate Antiviral Immunity: Methods and Protocols*, Methods in Molecular Biology, vol. 1656, DOI 10.1007/978-1-4939-7237-1_6,

in triggering the immune response against RNA virus infection by recognizing and binding to viral RNA within the infected cell. This process triggers RLR signaling activation to a signal transduction network that activates downstream transcription factors including interferon regulatory factor (IRF)3, IRF7, and NF-Kβ [9].

As a result of signaling by RLRs and other PRRs, cellular gene expression is altered to induce the expression of many genes with antimicrobial actions [10]. Among the RLRs, RIG-I mediates recognition of several different RNA viruses [11, 12]. RIG-I recognizes and binds to viral RNA encoding specific PAMP motifs, including exposed 5′-triphosphate, a poly-uridine motif, double-stranded RNA, or other structures, often present in combination, thus marking the viral RNA as nonself [11]. Viral RNA binding by RIG-I drives its activation to a signaling-on conformation facilitated by RIG-I hydrolysis of ATP and other post-translational modifications [13, 14]. The other RLRs are thought to become activated by a similar process [15]. Activation of RLRs by PAMP engagement results in induction of the expression of a large set of virus-responsive genes within the infected cell, including type 1 and type 3 interferons (IFNs). The IFNs are secreted cytokines that bind to their cognate receptor chains on the surface of the infected cell and surrounding or bystander cells to induce signaling that turns on hundreds of interferon-stimulated genes (ISGs) [16]. The products of virus-induced RLR-dependent genes and of ISGs function to restrict RNA virus replication while also modulating the adaptive immune response to facilitate immunity against RNA virus infection [17].

Molecular studies of RIG-I signaling have provided a framework of how RLRs recognize RNA PAMPs and mediate signal transduction cascades of innate immune activation and antiviral immunity. Specific RNA PAMP motifs have been identified that provide highly useful tools for studying RIG-I structure and function [11]. A major RIG-I PAMP is present with the hepatitis C virus (HCV) genome [18–21]. The HCV PAMP is located with the viral genome RNA 3′ nontranslated region (NTR) that encodes an approximately 100 nucleotide (nt) poly-uridine/cytosine (poly-U/UC) motif. The HCV RNA itself is punctuated by an exposed 5′ ppp to mark the entire HCV RNA as nonself for recognition by RIG-I [21].

The HCV RNA 5′ and 3′ ends form a “kissing loop” [22], which likely brings the 5′ppp into close proximity to the poly-U/UC motifs for the recognition of both 5′ppp and poly-U/UC motif as the PAMP until such time that it is bound by RIG-I [21]. Further processing of this HCV PAMP motif by Ribonuclease L (RNAseL) is shown to produce additional PAMP products for recognition by RIG-I and MDA5 [23, 24]. The HCV poly-U/UC motif lies adjacent to a conserved motif of 3 stem-loop structures

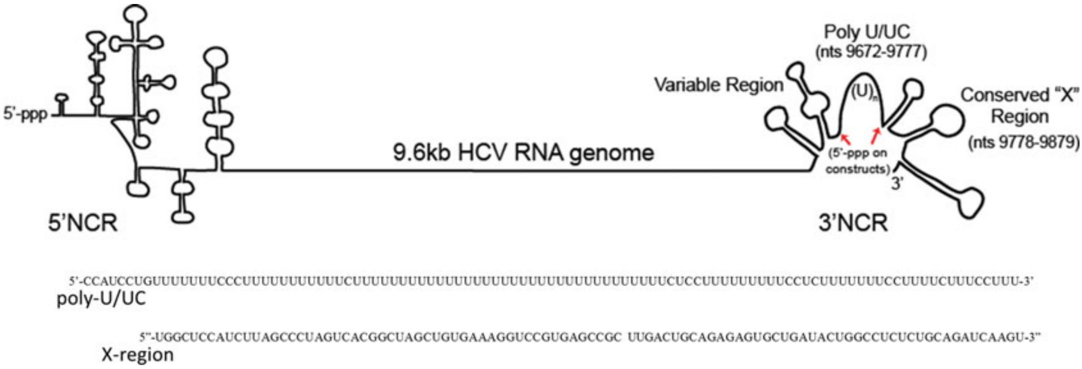

Fig. 1 Hepatitis C virus genome structure. The Hepatitis C virus (HCV) genome consists of a 9.6 kb positive sense RNA. The RNA secondary structure of the 5′ noncoding region (NCR) and 3′ NCR are depicted. The HCV 3′ NCR contains 3 domains: a variable region with 2 RNA stem loops, a single-stranded poly U/UC region, and a conserved "X" region with 3 RNA stem loops. The *red arrows* indicate the positions of the 5′-ppp on the synthetic poly U/UC and "X" region RNA constructs. Nucleotide positions of the poly U/UC and "X" region RNA regions refer to the HCV Con1 genome. **Lower**: Viral genome Con1 sequence of the poly-U/UC PAMP and the X-region RNA motifs

within the HCV RNA 3′ NTR (Fig. 1). Known as the X-region, this 98 nt motif is not recognized by RIG-I, even when appended directly with 5′ppp, and is thus not a RIG-I PAMP [20]. Both poly-U/UC and X-region RNA can be synthesized using in vitro RNA synthesis programmed by specific oligonucleotides encoding RNA polymerase promoter elements and the specific PAMP motif [18, 20, 21]. Alternatively, each can be chemically synthesized by commercial sources [21]. When used as molecular tools to assess RIG-I function, the poly-U/UC and X-region RNAs serve as potent RIG-I PAMP and stringent negative (non-PAMP) controls, respectively, for deciphering the mechanistic actions of the RIG-I pathway [18, 20, 21]. Here, we provide methods of production for each, along with protocols for assessing RIG-I signaling actions toward defining the cellular and biochemical response of RIG-I to PAMP RNA recognition. The poly-U/UC and X-region RNAs can serve as useful tools for assessing novel co-factors of the RLR pathway, assessing the overall cellular response to RIG-I activation, and for testing the RIG-I pathway function in in vivo mouse models of innate immune activation. The following protocols focus on assessing RIG-I activation and signaling through PAMP actions.

2 Materials

2.1 In Vitro Transcription of PAMP RNA

1. PAGE-purified Ultramer primers resuspended in nuclease-free deionized water to a concentration on 1 μg/μL. We purchase our oligos through Integrated DNA Technologies (IDT), Coralville, IA, USA. Sequences in **bold** represent T7 promoter

sequences that have been engineered onto each construct for the purposes of in vitro transcription [20, 21].

(a) PAMP Forward (HCV Con1 poly-U/UC sense): **TAATACGACTCACTATAGG**CCATCCTGTTTTTTTCCCTTTTTTTTTTTCTTTTTTTTTTTTTTTTTTTTTTTTTTTTTTTTT TCTCCTTTTTTTTTCCTCTTTTTTTCCTTTTCTTTCCTTT.

(b) PAMP Reverse (HCV Con1 poly-U/UC antisense): AAAGGAAAGAAAAGGAAAAAAAGAGGAAAAAAAAGGAGAAAAAAAAAAAAAAAAAAAAAAAAAAAAAAAAAAGAAAAAAAAAAAGGGAAAAAAACAGGATGG**CCTATAGTGAGTCGTATTA**

(c) XRNA Forward (Control HCV Con1 X-region sense): **TAATACGACTCACTATAGG**TGGCTCCATCTTAGCCCTAGTCACGGCTAGCTGTGAAAGGTCCGTGAGCCGCTTGACTGCAGAGAGTGCTGATACTGGCCTCTCTGCAGATCAAGT

(d) XRNA Reverse (Control HCV Con1 X-region antisense): ACTTGATCTGCAGAGAGGCCAGTATCAGCACTCTCTGCAGTCAAGCGGCTCACGGACCTTTCACAGCTAGCCGTGACTAGGGCTAAGATGGAGCCA**CCTATAGTGAGTCGTATTA**

2. PCR machine and appropriate PCR tubes for oligo annealing.
3. MEGAshortscript T7 transcription kit (purchased from Thermo Fisher Scientific).
4. TURBO DNase (purchased from Thermo Fisher Scientific).
5. Molecular biology grade phenol, chloroform, and 100% ethanol.
6. Nanodrop spectrophotometer.
7. Denaturing 8 M urea polyacrylamide or 8% formaldehyde agarose gels for quality control of RNA products.

2.2 Assessing PAMP Signaling in Transfected Cells

2.2.1 In Vitro Transient RNA Transfection of PAMP RNA

1. Cells in culture [18].
2. 12-well tissue culture dishes.
3. Cell culture growth medium with serum (*see* **Note 1**).
4. Purified PAMP RNA (*see* **Note 2**).
5. Serum-free medium.
6. Micropipettes.
7. Sterile tube.
8. TransIT-mRNA transfection reagent.
9. mRNA transfection Boost Reagent.
10. CO_2 incubator for cell culture.

2.2.2 Assessment of PAMP Signaling Using Immunoblot Assay

1. Standard reagents used for protein extraction, electrophoresis, and immunoblot assay [18, 20, 21].
2. Antibodies that detect RIG-I, ISG56, IRF-3, and phospho IRF3 Ser 396, Mx-1, and tubulin.

2.2.3 Assessment of PAMP Signaling Using qPCR

1. Standard reagents used for RNA extraction and qPCR analysis [18, 20, 21].
2. Gene-specific primers for IFN-β, TNF-α, ISG56, IL-6, Mx-1, RIG-I, and GAPDH.

2.2.4 Assessment of PAMP Signaling Using Luciferase Reporter Assay

1. Cells in culture [25].
2. 10 cm cell culture dishes.
3. pIFN-beta-luc (firefly luciferase) [25].
4. pCMV-Renilla (Renilla luciferase) [25].
5. Fugene transfection kit.
6. 48-well tissue culture dishes.
7. Cell culture growth medium with serum (*see* **Note 1**).
8. Purified PAMP RNA (*see* **Note 2**).
9. Serum-free medium.
10. Micropipettes.
11. Sterile tube.
12. TransIT-mRNA transfection reagent.
13. mRNA transfection Boost Reagent.
14. CO_2 incubator for cell culture.
15. 48-well cell culture dishes.

2.3 In Vivo Transfection of PAMP RNA

1. Laboratory mice (for example, C57BL/6 compared to matched knockouts within the RLR signaling pathway) and appropriate facilities (*see* **Note 3**) [20, 21].
2. LIPID-based In Vivo Transfection Reagent, Purchased from Altogen Biosciences.
3. RNA*later* Stabilization Solution (Invitrogen).
4. 4% neutral buffered formalin solution for tissue fixation.
5. Tissue paraffin embedding and slicing facilities.
6. EZ DeWax Solution, 10× Antigen Retrieval AR-10 (BioGenex).
7. Phosphate-buffered saline +20% tween (PBST).
8. ProLong Gold Antifade Mountant (Invitrogen).
9. Primary and secondary antibodies for immunostaining, DAPI for nuclear staining.
10. Nikon C2 Confocal inverted microscope or equivalent microscope for imaging.

3 Methods

3.1 In Vitro Transcription of PAMP RNA

1. Anneal sense and antisense oligos for both PAMP and control templates by mixing at a 1:1 ratio. Annealing takes place at 95 °C for 2 min, followed by a gradual decrease in temperature by 1 °C every 30 s until 50 °C, at which time the reaction is held at 4 °C. Annealing is best performed in a PCR machine for accuracy and reproducibility of the cooling process [20].
2. In vitro transcribe RNA off each annealed template using the T7 promoter sequence placed at the beginning of each oligo (*see* **Note 4**). We use the MEGAshortscript kit for synthesis of poly-U/UC and X-RNA constructs. The mixtures are assembled at room temperature per manufacturer's recommendations. Specifically, 2 μL each of the 10× T7 transcription reaction buffer, T7 enzyme mix, annealed DNA template, and each nucleotide solution (ATP, CTP, GTP, and UTP) are added to 6 μL nuclease free water. Incubate at 37 °C for 3–4 h (*see* **Note 5**).
3. Remove the DNA template from transcribed RNA by adding 1 μL TURBO DNase per reaction and incubating at 37 °C for 15 min.
4. Stop all the reactions by adding 115 μL nuclease-free water and 15 μL ammonium acetate stop solution (provided with the MEGAshortscript transcription kit) and mixing thoroughly.
5. Purify transcribed RNA from proteins and unincorporated nucleic acids by phenol-chloroform extraction and ethanol precipitation. Add equal volumes (150 μL each) phenol and chloroform. Mix well and let settle for 5 min. Carefully recover the aqueous phase without disrupting the interphase of the phenol-chloroform mixture. Transfer the recovered aqueous phase containing the RNA product into a clean tube, and add 2 volumes (approximately 300 μL depending on recovery efficiency) 100% ethanol. Chill the aqueous phase-ethanol mixture at −20 °C for at least 15 min. Centrifuge at 4 °C for 15 min at maximum speed in a table-top microcentrifuge to pellet RNA and carefully remove the supernatant. Allow the RNA pellet to air-dry and resuspend in 50 μL nuclease-free water.
6. Determine RNA concentration by absorbance on a Nanodrop or other small volume spectrophotometers. Additionally, confirm the quality of correctly sized RNA by electrophoresis through denaturing 8 M urea polyacrylamide gels. Alternatively, denaturing 2% agarose formaldehyde gels can be used for assessing RNA quality.

3.2 Assessing PAMP Signaling in Transfected Cells

3.2.1 Transient RNA Transfection of PAMP RNA (Adapted from Mirus IT Transfection Manufacturer's Protocol)

1. Plate cells in a 12-well dish (*see* **Note 6**) 18–24 h prior to transfection in 1 mL of cell culture growth medium with serum (*see* **Note 7** for cell numbers per well).
2. Culture cells overnight in an incubator at 37 °C.
3. Allow mRNA Boost and TransIT-mRNA reagents to warm up to room temperature and gently vortex each solution.
4. Pipet 100 μL serum-free media into a sterile tube.
5. Add 25 pmol PAMP RNA.
6. Mix PAMP RNA and serum-free media by gentle pipetting.
7. To the diluted PAMP RNA, add 2 μL mRNA transfection Boost reagent.
8. Mix diluted PAMP RNA and mRNA transfection Boost reagent by gentle pipetting.
9. To the diluted PAMP RNA and mRNA transfection Boost reagent, add 2 μL Trans-IT-mRNA transfection reagent.
10. Mix by gentle pipetting.
11. Allow complexes to form by incubating mixture at room temperature for 2–5 min (*see* **Note 8**).
12. Add above PAMP RNA/transfection mixture dropwise to cultured cells, placing each drop of the mixture in a different part of the plate (*see* **Note 9**).
13. Tilt tissue culture plate back and forth to distribute PAMP/RNA transfection reagent evenly throughout the culture.
14. Place in a CO_2 incubator at 37 °C for 18 h until harvest time to assess for PAMP activity (*see* Subheadings 3.2.2, 3.2.3, 3.2.4, assessment of PAMP activation by qPCR, immunoblot, and luciferase assay respectively).

3.2.2 Assessment of PAMP Signaling in Transfected Cells by Immunoblot

18 h after transfection, protein extracts can be extracted and PAMP signaling can be assessed by standard immunoblot assay using antibodies that detect RIG-I, ISG56, IRF-3, and phospho IRF3 Ser 396, Mx-1, with tubulin used as a loading control for gel electrophoresis [26].

3.2.3 Assessment of PAMP Signaling in Transfected Cells by qPCR

18 h after PAMP transfection, RNA can be extracted, and PAMP signaling can be quantified by qPCR using standard methods with gene-specific primers to measure induction of genes such as IFN-β, tumor necrosis factor alpha (TNF-α), ISG56, interleukin-6 (IL-6), Mx-1, and RIG-I. Primers for GAPDH (glyceraldehyde-3-phosphate dehydrogenase) should be included in these assessments to allow for a normalization standard.

3.2.4 Assessment of PAMP Signaling Using Luciferase Reporter Assay

1. Prior to PAMP RNA transfection, plate cells 10 cm cell culture dishes [21].
2. Incubate cells in an incubator for 24 h at 37 °C.

3. Transfect cells with 5.76 μg pIFN-β-luc (firefly luciferase) and 0.24 μg pCMV-*Renilla*-luc (*Renilla* luciferase) plasmids using the FuGENE 6 transfection reagent and protocol according to manufacturer's instructions by Roche.
4. Incubate cells at 37 °C for 18 h.
5. Split cells into 48-well plates in 263 μL of cell culture media containing serum.
6. Incubate cells in a CO_2 incubator for 12 h at 37 °C.
7. Perform PAMP RNA transfection as described above in Subheading 3.2.1, except using the following volumes of regents: 26 μL of serum-free cell culture medium, 350 ng of PAMP RNA 0.5 μL TransIT-mRNA transfection Reagent, and 0.5 μL of mRNA transfection Boost Reagent.
8. Incubate cells in a CO_2 incubator at 37 °C for 18 h.
9. Harvest cells and conduct standard luciferase assay such as the Dual-Luciferase reporter assay system by Promega.

3.3 In Vivo Transfection of PAMP RNA

1. Prepare the in vitro transcribed PAMP RNA (example poly-U/UC) and matched control RNA (such as HCV X-region RNA and/or phosphatase-treated PAMP RNA) for in vivo transfection. For each mouse to be injected, add 200 μg RNA to 100 μL nuclease-free water and mix well by gentle vortexing.
2. Transfect RNA into each mouse via tail-vein injection per the Altogen LIPID-based in vivo transfection reagent manufacturer's protocol (*see* **Note 10**) [20, 21].
3. Euthanize the mice between 4 and 24 h post-transfection (*see* **Note 11**). Perform systemic PBS perfusion to remove contaminating blood cells prior to collection of mouse liver samples for the detection of innate immune activation.
4. For RNA isolation, tissue samples should be placed immediately into RNA*later* to prevent RNA degradation prior to homogenization of liver tissue. mRNA expression levels of innate immune and inflammatory gene markers can then be assessed by quantitative RT-PCR as described in Subheading 2.2.1.
5. Tissues intended for the purposes of immunohistochemistry should be fixed for 24 h in neutral buffered 4% formalin solution. Prior to immunostaining, paraffin-embed tissues and cut in 4 μm transverse sections. Heat slides on a 60 °C heating block for 5 min and deparaffinize by immersing slides once in EZ DeWax Solution and twice in fresh xylene, each for 5 min at room temperature. Rinse slides in 100% ethanol. After subsequent 5 min immersions in 95% and 70% ethanol, rinse in distilled water and immerse twice in distilled water for 5 min each. Finally, immerse for 5 min in PBST. For antigen retrieval, fill a plastic Coplin jar with 1× Antigen Retrieval AR-10, insert

slides, and cover with a vented lid. Microwave at 100% power for 1 minute or until just bubbling through vent hole. Stop power immediately. Microwave an additional 8 min at 20% power through additional boiling cycles. Top off the solution with cold 1× AR10 solution and cool for 45 min at room temperature. Rinse twice in distilled water and soak for 5 min in PBS. Permeabilize for 5 min in 1% triton X-100 and soak for an additional 5 min in PBS. Allow slides to air dry. Block with 300 μL 10% Normal Goat Serum for 1 h at room temperature, followed by 1 h incubation of primary antibody diluted in 3% Bovine Serum Albumin in PBST (*see* **Note 12**). Wash three times in 300 μL PBST, 5 min each time. Apply secondary antibody for 1 h at room temperature. Wash three more times in PBST for 5 min each. After drying slides, apply ProLong Gold and cover slip. Allow slides to set for 24 h and view on a microscope [20, 27].

4 Notes

1. Use cell culture media best suited for culturing chosen cell line. For this transfection protocol, serum does not impact efficiency and should be used in the media during transfection, unless otherwise noted in the protocol.
2. Use PAMP RNA and/or DNA that has been phenol choroform extracted and ethanol precipitated to ensure RNA and DNA is clean. The use of clean RNA and DNA ensures that the observed downstream responses are indeed from PAMP activation of cytosolic PRRs and not from LPS or other contaminates introduced during synthesis of the PAMP RNA or DNA plasmids.
3. Animal handling and experimental protocols should all be approached according to national and local regulations and Institutional Animal Care and Use Committee (IACUC) and ethics panel approvals. Additionally, personnel handling mice and performing tail vein infections should receive appropriate training.
4. T7 places a 5′-triphosphate (5′-ppp) onto the transcribed RNA, along with a short read-back sequence from the T7 promoter itself. These components are part of the structure recognized by RIG-I during PAMP signaling. Treating the samples with phosphatase will inhibit signaling through RIG-I, which serves as an additional negative control for downstream signaling assays.
5. Increasing incubation time past 4 h has little to no effect on RNA yield. However, decreasing the temperature to 30 °C can result in higher quality poly-U/UC RNA due to higher fidelity read-through of the uridine tract.

6. We have featured transfection in a 12-well dish here, which should provide adequate cell numbers for most downstream PAMP assessment assays (i.e., immunoblotting, or qPCR). If more cells are needed, reagent volumes and cell numbers should be adjusted according to cell culture dish size used. 80% confluency of cells in culture at the time of transfection is optimal.
7. Adherent and non-adherent (suspension) cells require different plating densities for efficient transfection. For adherent cells, plate $0.8–3.0 \times 10^5$ cells/mL. For non-adherent cells, plate $2.5–5.0 \times 10^5$ cells/mL.
8. Do not incubate PAMP RNA/transfection mixture for more than 5 min or transfection efficiency may be severely decreased.
9. Changing growth media prior to the addition of PAMP RNA/transfection reagent mixture is not necessary.
10. We have also successfully used intra-peritoneal injections of PAMP RNA for in vivo transfection. Additionally, the Altogen NANOPARTICLE and POLYMER-based transfection kits are able to transfect PAMP RNA into mice as measured by downstream signaling assays.
11. For comparative analysis of mRNA and protein expression following poly-U/UC RNA transfection, we have found 8 h posttransfection to be an optimal time point for harvest.
12. Primary and secondary antibodies should be optimized in both dilution and time of incubation. We currently use secondary antibodies Alexa488 and Alexa594 (1:100) from Molecular Probes. DAPI (1:1000) is added as a nuclear stain with the secondary antibodies.

References

1. Odendall C, Kagan JC (2017) Activation and pathogenic manipulation of the sensors of the innate immune system. Microbes Infect 19:229–237. doi:10.1016/j.micinf.2017.01.003
2. Sellge G, Kufer TA (2015) PRR-signaling pathways: learning from microbial tactics. Semin Immunol 27(2):75–84. doi:10.1016/j.smim.2015.03.009
3. Luecke S, Paludan SR (2016) Molecular requirements for sensing of intracellular microbial nucleic acids by the innate immune system. Cytokine S1043-4666(16):30543–30549. doi: 10.1016/j.cyto.2016.10.003
4. Collins SE, Mossman KL (2014) Danger, diversity and priming in innate antiviral immunity. Cytokine Growth Factor Rev 25 (5):525–531. doi:10.1016/j.cytogfr.2014.07.002
5. Chisholm ST, Coaker G, Day B, Staskawicz BJ (2006) Host-microbe interactions: shaping the evolution of the plant immune response. Cell 124(4):803–814. doi:10.1016/j.cell.2006.02.008
6. Cook DE, Mesarich CH, Thomma BP (2015) Understanding plant immunity as a surveillance system to detect invasion. Annu Rev Phytopathol 53:541–563. doi:10.1146/annurev-phyto-080614-120114
7. Pasare C, Medzhitov R (2005) Toll-like receptors: linking innate and adaptive immunity. Adv Exp Med Biol 560:11–18. doi:10.1007/0-387-24180-9_2
8. Davis BK, Wen H, Ting JP (2011) The inflammasome NLRs in immunity, inflammation, and associated diseases. Annu Rev Immunol 29:707–735. doi:10.1146/annurev-immunol-031210-101405

9. Loo YM, Gale M Jr (2011) Immune signaling by RIG-I-like receptors. Immunity 34(5):680–692. doi:10.1016/j.immuni.2011.05.003
10. Wilkins C, Gale M Jr (2010) Recognition of viruses by cytoplasmic sensors. Curr Opin Immunol 22(1):41–47. doi:10.1016/j.coi.2009.12.003
11. Kell AM, Gale M Jr (2015) RIG-I in RNA virus recognition. Virology 479-480:110–121. doi:10.1016/j.virol.2015.02.017
12. Ramos HJ, Gale M Jr (2011) RIG-I like receptors and their signaling crosstalk in the regulation of antiviral immunity. Curr Opin Virol 1(3):167–176. doi:10.1016/j.coviro.2011.04.004
13. Chan YK, Gack MU (2015) RIG-I-like receptor regulation in virus infection and immunity. Curr Opin Virol 12:7–14. doi:10.1016/j.coviro.2015.01.004
14. Liu HM, Jiang F, Loo YM, Hsu S, Hsiang TY, Marcotrigiano J, Gale M Jr (2016) Regulation of retinoic acid inducible Gene-I (RIG-I) activation by the histone Deacetylase 6. EBioMedicine 9:195–206. doi:10.1016/j.ebiom.2016.06.015
15. Chiang C, Gack MU (2017) Post-translational control of intracellular pathogen sensing pathways. Trends Immunol 38(1):39–52. doi:10.1016/j.it.2016.10.008
16. Chow KT, Gale M Jr (2015) SnapShot: interferon signaling. Cell 163(7):1808–1808.e1801. doi:10.1016/j.cell.2015.12.008
17. Kawai T, Akira S (2008) Toll-like receptor and RIG-I-like receptor signaling. Ann N Y Acad Sci 1143:1–20. doi:10.1196/annals.1443.020
18. Kell A, Stoddard M, Li H, Marcotrigiano J, Shaw GM, Gale M Jr (2015) Pathogen-associated molecular pattern recognition of hepatitis C virus transmitted/founder variants by RIG-I is dependent on U-Core length. J Virol 89(21):11056–11068. doi:10.1128/JVI.01964-15
19. Uzri D, Gehrke L (2009) Nucleotide sequences and modifications that determine RIG-I/RNA binding and signaling activities. J Virol 83(9):4174–4184. doi:10.1128/JVI.02449-08
20. Schnell G, Loo YM, Marcotrigiano J, Gale M Jr (2012) Uridine composition of the poly-U/UC tract of HCV RNA defines non-self recognition by RIG-I. PLoS Pathog 8(8):e1002839. doi:10.1371/journal.ppat.1002839
21. Saito T, Owen DM, Jiang F, Marcotrigiano J, Gale M Jr (2008) Innate immunity induced by composition-dependent RIG-I recognition of hepatitis C virus RNA. Nature 454(7203):523–527. doi:10.1038/nature07106
22. Friebe P, Boudet J, Simorre JP, Bartenschlager R (2005) Kissing-loop interaction in the 3′ end of the hepatitis C virus genome essential for RNA replication. J Virol 79(1):380–392. doi:10.1128/JVI.79.1.380-392.2005
23. Malathi K, Saito T, Crochet N, Barton DJ, Gale M Jr, Silverman RH (2010) RNase L releases a small RNA from HCV RNA that refolds into a potent PAMP. RNA 16(11):2108–2119. doi:10.1261/rna.2244210
24. Malathi K, Dong B, Gale M Jr, Silverman RH (2007) Small self-RNA generated by RNase L amplifies antiviral innate immunity. Nature 448(7155):816–819. doi:10.1038/nature06042
25. Sumpter R Jr, Loo YM, Foy E, Li K, Yoneyama M, Fujita T, Lemon SM, Gale M Jr (2005) Regulating intracellular antiviral defense and permissiveness to hepatitis C virus RNA replication through a cellular RNA helicase, RIG-I. J Virol 79(5):2689–2699. doi:10.1128/JVI.79.5.2689-2699.2005
26. Loo YM, Owen DM, Li K, Erickson AK, Johnson CL, Fish PM, Carney DS, Wang T, Ishida H, Yoneyama M, Fujita T, Saito T, Lee WM, Hagedorn CH, Lau DT, Weinman SA, Lemon SM, Gale M Jr (2006) Viral and therapeutic control of IFN-beta promoter stimulator 1 during hepatitis C virus infection. Proc Natl Acad Sci U S A 103(15):6001–6006. doi:10.1073/pnas.0601523103
27. Lau DT, Fish PM, Sinha M, Owen DM, Lemon SM, Gale M Jr (2008) Interferon regulatory factor-3 activation, hepatic interferon-stimulated gene expression, and immune cell infiltration in hepatitis C virus patients. Hepatology 47(3):799–809. doi:10.1002/hep.22076

Chapter 7

Methods to Visualize MAVS Subcellular Localization

Christine Vazquez, Dia C. Beachboard, and Stacy M. Horner

Abstract

The mitochondrial antiviral signaling (MAVS) protein is a central adaptor protein required for antiviral innate immune signaling. To facilitate its roles in innate immunity, MAVS localizes to multiple intracellular membranous compartments, including the mitochondria, the mitochondrial-associated ER membrane (MAM), and peroxisomes. Studies of MAVS function therefore often require an analysis of MAVS localization. To detect MAVS protein on intracellular membranes, biochemical fractionation to isolate MAMs, mitochondria, or peroxisomes can be used. Further, immunofluorescence with antibodies against specific membrane markers can be used to visualize MAVS distribution throughout the cell. Here, we describe the biochemical fractionation and immunofluorescence protocols used to detect MAVS subcellular localization.

Key words MAVS, Mitochondria, MAM, Peroxisomes, Endoplasmic reticulum, Fractionation, Immunofluorescence, Interferon

1 Introduction

Mitochondrial antiviral signaling protein (MAVS, has been referred to as VISA, Cardif, or IPS-I) is an innate immune adaptor protein important for the activation of intracellular antiviral innate immunity and subsequent viral clearance. During RNA virus infection, MAVS is activated when a cytosolic pattern recognition receptor, such as RIG-I, binds to MAVS via interactions between the caspase activation and recruitment domains (CARD) for each protein. This initiates a downstream signaling cascade culminating in the transcriptional induction of type I and type III interferon (IFN), as well as IFN-stimulated genes (ISGs) (Reviewed in ([1]). MAVS is a classical C-terminal tail-anchored membrane protein, and its domains are comprised of this C-terminal transmembrane domain, an N-terminal CARD, and a proline-rich region [2]. The transmembrane domain of MAVS tethers it to multiple intracellular membranes, namely the mitochondria, peroxisomes, and a specialized subdomain of the ER called the mitochondrial-associated ER membrane (MAM) [2–5]. This membranous

Karen Mossman (ed.), *Innate Antiviral Immunity: Methods and Protocols*, Methods in Molecular Biology, vol. 1656, DOI 10.1007/978-1-4939-7237-1_7,

localization is critical for MAVS function. Indeed, cleavage of MAVS near its transmembrane domain by the NS3-NS4A protease of hepatitis C virus releases the protein into the cytosol and prevents downstream signaling to type I IFN [6–9].

Multiple techniques have been established that allow for the detection and visualization of MAVS subcellular localization. These include biochemical techniques such as subcellular fractionation to isolate MAM, mitochondria, or peroxisomes, as well as immunofluorescence followed by confocal microscopy. These assays have been crucial in determining where MAVS localizes and in understanding the role of MAVS localization in orchestrating its antiviral signaling function. Further, the MAM/mitochondrial fractionation technique outlined below allows for pure mitochondrial isolation, whereas standard/crude mitochondrial fractionation has contaminating ER, highlighting the importance of the MAM/mitochondrial isolation described herein [4, 10]. Here, we outline the protocols for several assays used to investigate MAVS localization.

2 Materials

2.1 MAM Fractionation

All reagents and equipment should be precooled to 4 °C and kept on ice unless otherwise noted.

1. Cells-eight 15 cm^2 dishes of Huh7 cells plated at 8×10^6 cells/dish the day before (90% confluency when harvested) (*see* **Note 1**).
2. 15 cm^2 tissue culture dishes.
3. Phosphate-buffered saline (PBS).
4. Polyethylene cell lifter with 3 cm blade length.
5. Overhead stirrer.
6. Potter-Elvehjem homogenizer or a 7 ml dounce homogenizer.
7. Tabletop centrifuge (Eppendorf 5430 R) with fixed angle rotor, accommodates tubes up to 2 ml.
8. Ultracentrifuge with SW41 rotor.
9. 14 × 89 mm SW41 ultraclear centrifuge tubes (*see* **Note 2**).
10. Sucrose homogenization buffer: *To 100 ml ultrapure H_2O, add:* 17.1 g sucrose (0.25 M final), 20 ml 100 mM HEPES (10 mM final), adjust to pH 7.4 with 1 N NaOH, add ultrapure H_2O to 200 ml. Sterilize by autoclaving for 20 min using a liquid cycle. It can be stored for 2–3 months at 4 °C.
11. Mannitol buffer A: *To 100 ml ultrapure H_2O*, add: 9.13 g mannitol (0.25 M final), 38 mg EGTA (0.5 mM final), 10 ml 100 mM HEPES (5 mM final), adjust to pH 7.4 with 1 N

NaOH, add ultrapure H_2O to 200 ml. Sterilize by autoclaving for 20 min using a liquid cycle. It can be stored for 2–3 months at 4 °C.

12. Mannitol buffer B: *To 100 ml ultrapure H_2O*, add: 8.22 g mannitol (0.225 M final), 76 mg EGTA (1 mM final), 50 ml 100 mM HEPES (25 mM final), adjust to pH 7.4 with 1 N NaOH, add ultrapure H_2O to 200 ml. Sterilize by autoclaving for 20 min using a liquid cycle. It can be stored for 2–3 months at 4 °C.
13. Stock isotonic Percoll, 90% (v/v): 9 vol Percoll to 1 vol 2.5 M sucrose (0.25 M final). Sterilize by autoclaving for 20 min using a liquid cycle. It can be stored for 2–3 months at 4 °C.
14. 30% (v/v) Percoll suspension in Mannitol buffer B: 1 vol autoclaved 90% (v/v) stock isotonic Percoll to 2 vol autoclaved Mannitol buffer B. It can be stored for 2–3 months at 4 °C.
15. 20-gauge needle.
16. 1 and 3 ml syringes.
17. Amicon Ultra-4 centrifugal Filter Unit with Ultracel-10 membrane.
18. Protease Inhibitor.
19. Halt phosphatase inhibitor.
20. Reagents and equipment for SDS-PAGE analysis.

2.2 Peroxisomal Fractionation

All reagents and equipment should be precooled to 4 °C and kept on ice unless otherwise noted.

1. 15 cm^2 culture dishes.
2. Polyethylene cell lifter with 3 cm blade length.
3. Tabletop centrifuge (Eppendorf 5430 R) with fixed angle rotor, accommodates tubes up to 2 ml.
4. Protease Inhibitor.
5. Halt phosphatase inhibitor.
6. Two chamber gradient maker.
7. MOPS buffer: 4.18 g 3-(*N*-morpholino)propanesulfonic acid (MOPS), add ultrapure water to a final volume of 200 ml. It can be stored at room temperature.
8. Homogenization medium (HM): 0.25 M sucrose, 1 mM disodium EDTA, 5 mM MOPS, 0.1% (v/v) ethanol, adjust to pH 7.2 with 1 M NaOH, add ultrapure water to desired final volume. Store up to 2 days at 4 °C.
9. High-density diluent (HD): 1 mM EDTA, 5 mM MOPS, 0.1% (v/v) ethanol, adjust to pH 7.4 with 1 M NaOH, add ultrapure water to desired final volume. Store up to 2 days at 4 °C.

10. 10% (w/v) Nycodenz in HM.
11. 40% (w/v) Nycodenz in HD.
12. 50% (w/v) Nycodenz in HD.
13. 10^8 Huh7 cells (*see* **Note 3).**
14. Ball-bearing homogenizer.
15. 5–10 ml dounce homogenizer, Wheaton type B.
16. Tabletop centrifuge with swinging bucket rotor, such as the Thermo Scientific Legend XTR to accommodate 15–50 ml tubes.
17. Ultracentrifuge with vertical rotor.
18. Ultraclear sealable tubes compatible with an ultracentrifuge with a fixed angle rotor and can accommodate up to 15 ml.
19. 20-gauge needle.
20. 5 ml syringe with metal cannula.
21. Reagents and equipment for SDS-PAGE analysis.

2.3 Immunofluorescence Assay for MAVS

Images can be obtained using any confocal microscope. Please refer to the specific guidelines for your confocal microscope and its respective computer software.

1. Millicell EZ clear chamber slides for maximum volume of 1.7 ml (*see* **Note 4**).
2. Huh7 cells-cells plated onto chamber slides such that the cells are approximately 60% confluent the following day (*see* **Note 5**).
3. PBS.
4. 4% paraformaldehyde (PFA, methanol-free diluted to 4% in PBS). Keep in light-sensitive container.
5. 0.1% Triton X-100 in PBS. Store at 4 °C.
6. Blocking buffer: 10% fetal bovine serum (FBS) or other blocking reagent diluted into PBS. Store at 4 °C.
7. Antibodies: MAVS (mouse, 1:100); PMP70 (rabbit, 1:100); TOM20 (rabbit, 1:100); Hoechst (1:500); Alexa Fluor rabbit-conjugated secondary (1:500); Alexa Fluor mouse-conjugated secondary (1:500). Primary and secondary antibodies should be diluted in blocking buffer. Store antibodies according to manufacturer's guidelines.
8. Orbital shaker.
9. Confocal microscope.
10. Ultrapure water.
11. Rectangular cover glass.
12. Mounting medium.

3 Methods

3.1 MAM Fractionation

This protocol was adapted from Bozidis et al. Basic Protocol 2 [11]. Antibody companies and dilutions can be found from Horner et al., *PNAS* 2011 [4]. All the procedures and reagents should be kept at 4 °C throughout the protocol.

1. Seed cells 16–24 h before fractionation. For Huh7 cells, seed eight 15 cm^2 dishes at 8×10^6 cells/dish.
2. When cells are 90% confluent, wash cell monolayers with 10 ml PBS per dish. Aspirate PBS.
3. Add 10 ml ice-cold PBS per dish and scrape using a sterile cell lifter.
4. Transfer cells to two 50 ml conical tubes, combining all the dishes (40 ml per conical). Save 1 ml for whole cell lysate and harvest using standard cell lysis buffer.
5. Pellet cells by spinning for 10 min at 1000 × *g* in a tabletop centrifuge at 4 °C.
6. Aspirate the supernatant and resuspend the pellets in a total of 7 ml ice-cold sucrose homogenization buffer containing protease and phosphatase inhibitors (1:100 each).
7. Attach the precooled pestle for the Potter-Elvehjem homogenizer to an overhead stirrer and gently homogenize by 10 up-and-down strokes at 500 rpm. Transfer homogenate to a 15 ml conical tube (*see* **Note 6**).
8. Pellet the nuclei, cell debris, and intact cells by centrifugation at 600 × *g* for 5 min in a tabletop centrifuge. Discard the pellet and keep the supernatant.
9. Transfer the supernatant to 1.5 ml microfuge tubes (~5 per sample) and centrifuge for 10 min at 10,300 × *g* at 4 °C using a tabletop centrifuge with a fixed angle rotor. This pellet contains the mitochondria and MAM—save for **step 14**. Continue to the next step with the supernatant.
10. Centrifuge the supernatant at least two additional times under the same conditions until a pellet is no longer visible. This supernatant contains the microsomes and cytosol fractions (*see* **Note 7**). Discard the pellet after each spin in this step.
11. Pellet the microsomes by pipetting the supernatant from **step 10** into an SW41 ultraclear tube filled to 1 cm from the top and balance to the same weight. Then, spin this for 60 min at 100,000 × *g* at 4 °C using a Beckman SW41 swinging bucket rotor. Keep the resulting microsome pellet for **step 13** and use the supernatant in **step 12** (*see* **Note 8**).

12. Collect the supernatant by pipetting into a 15 ml conical. Concentrate the supernatant using an Amicon protein concentrator according to manufacturer's guidelines to a final volume of ~500 μl. This is the final cytosol fraction (*see* **Note 9**).
13. Resuspend the microsome pellet from **step 11** in 300 μl of Mannitol buffer B. This is the final microsome fraction.
14. Resuspend and combine the pellets from **step 9** in 300 μl of ice-cold Mannitol buffer A.
15. Homogenize using three strokes in a 2 ml Potter-Elvenhjem homogenizer at 500 rpm (*see* **Note 10**).
16. Carefully layer homogenate on the top of 10 ml of 30% Percoll suspension in a 14 × 89 mm SW41 ultraclear tube.
17. Centrifuge for 65 min at 95,000 × *g* at 4 °C in an SW41 rotor (*see* **Note 11**).
18. Collect banded fractions using a 20-gauge needle and a 1 or 3 ml syringe. Collect fractions 1 (mixed membranes) and 2 (MAM) (as seen in Fig. 1a) using a 1 ml syringe by puncturing the wall of the tube above the fraction and slowly suction the fractions with a fan-like movement, avoiding other bands. Collect fraction 3 (mitochondria) by puncturing below the bands and slowly suction using a 3 ml syringe with a fan-like movement, avoiding other bands.
19. Carefully remove the 20-gauge needle from the tube by gently pulling the needle away from the tube. Dispose of the needle in an appropriate biohazard disposal container designated for "Sharps."

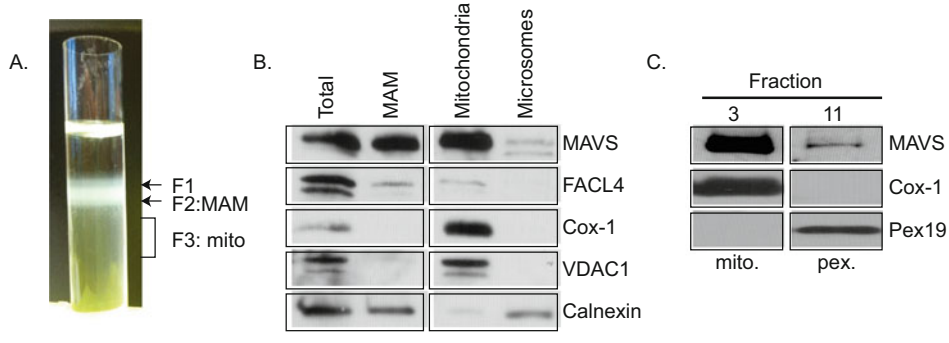

Fig. 1 MAM/mitochondrial and peroxisomal fractionation. (**a**) Percoll gradient showing the fractions obtained in **step 18** following the spin of the MAM/mitochondria through the Percoll gradient. (**b**) Immunoblot of a MAM/mitochondrial fractionation of Huh7 cells, showing MAVS, Cox-1 (mitochondria), tubulin (cytosol), FACL4 (MAM), and calnexin (ER/microsomes). (**c**) Representative immunoblot of fractions 3 and 11 (out of 11 total fractions) from a peroxisomal fractionation of Huh7 cells showing Cox-1 (mitochondria), Pex19 (peroxisomes), and MAVS. Mito, mitochondria; Pex, peroxisomes

20. Transfer each sample (fraction 2 and 3) to a 14 × 89 mm ultraclear SW41 tube. Dilute fractions with ≥5 vol of ice-cold Mannitol buffer B (~10 ml total) to dilute the Percoll.
21. Pellet the MAM and mitochondria (fractions 2 and 3) by centrifuging for 10 min at 6300 × *g* using an SW41 rotor.
22. Aspirate the supernatant and wash an additional time in at least 5 ml ice-cold Mannitol buffer B. Spin for 10 min at 6300 × *g* using an SW41 rotor (*see* **Note 12**).
23. Aspirate the supernatant from **step 22** and resuspend the final mitochondrial pellet in 50 μl of ice-cold Mannitol buffer B.
24. Centrifuge the MAM fraction (fraction 2 from **step 18**) for 60 min at 100,000 × *g* at 4 °C in an SW41 rotor to pellet the MAM.
25. Resuspend the final MAM pellet in 300 μl in ice-cold Mannitol buffer B.
26. Quantify protein concentrations of the fractions using a standard protein quantification assay, such as a bicinchoninic assay (BCA), according to the manufacturer's guidelines.
27. Following protein quantification, fractions can be frozen at −80 °C or used for SDS-PAGE analysis. For SDS-PAGE analysis, load 2 μg of each fraction and 10–20 μg of the whole cell lysate.
28. Immunoblot for Microsomes/ER: calnexin; Mitochondria: Cox-1; Outer membrane of mitochondria: VDAC; MAM: FACL4; cytosol: Tubulin (*see* Fig. 1b).

3.2 Peroxisomal Fractionation

This protocol is slightly modified from this reference [12]. Keep all the reagents and equipment at 4 °C, unless otherwise noted.

1. Collect cells by aspirating off media, washing with cold PBS, and adding 2 ml of cold PBS to the 15 cm^2 culture dishes.
2. Using a cell lifter, scrape the cells and transfer 1.8 ml of the cold PBS + cell suspension to a 15 ml conical tube for fractionation. Also, transfer 200 μl of the cold PBS + cell suspension to a 1.5 ml microfuge tube for whole cell lysate. Spin the cell suspension for fractionation in the 15 ml conical tube for 5 min at 1000 × *g* in a tabletop centrifuge. In the meantime, also spin the suspension for the whole cell lysate in the 1.5 ml microfuge tube for 5 min at 1000 × *g* in a tabletop microfuge.
3. Aspirate off the PBS from both tubes in **step 2**. The pellet in the 1.5 ml microfuge tube will be used for whole cell lysate analysis in SDS-PAGE and can be directly lysed using standard cellular lysis conditions. Proceed with the cell pellet in the 15 ml conical tube.

4. Resuspend this cell pellet in the 15 ml conical tube, which should contain approximately 10^8 cells, with 5 ml of HM containing protease and phosphatase inhibitors (1:100 each) and transfer to an ultraclear centrifuge tube compatible with a vertical rotor ultracentrifuge. Homogenize the cells using five strokes from each handle of the ball-bearing homogenizer.
5. Centrifuge homogenate 5 min at 500 × *g* in a tabletop centrifuge that can accommodate 15 ml tubes.
6. Remove and transfer the supernatant to a new tube. Keep the collected supernatant on ice. Keep the cell pellet for **step 7**.
7. Resuspend the cell pellet in 5 ml of HM using five strokes in a 7 ml dounce homogenizer.
8. Using the homogenate from **step 4**, repeat **steps 5, 6,** and 7.
9. Pool the collected supernatants, which should total 15 ml, and centrifuge for 10 min at 6000 × *g* in a tabletop centrifuge.
10. Collect the supernatant and centrifuge again for 15 min at 20,000 × *g* in an ultracentrifuge with a vertical rotor. There should be a cell pellet at the bottom of the ultracentrifuge tube following centrifugation. This pellet is the light mitochondrial pellet.
11. Aspirate off the supernatant and resuspend the light mitochondrial pellet in 4 ml of HM using four strokes of the pestle of the dounce homogenizer.
12. Prepare a 10 ml linear gradient from equal volumes of the 10% and 40% Nycodenz in a vertical rotor ultracentrifuge-compatible tube using a two-chamber gradient maker.
13. Using a syringe and metal cannula, underlayer the gradient from **step 9** with 0.5 ml of 50% Nycodenz.
14. Add 2 ml of the pellet suspension from **step 10** on the top of the gradient.
15. Centrifuge for 35 min at 75,000 × *g* in an ultracentrifuge with a vertical rotor, using either a controlled acceleration/deceleration centrifugation program or a centrifugation with the brake turned off at 500 × *g*.
16. Collect 750 μl fractions. Hold the ultracentrifuge tube over a microfuge tube, and carefully poke a hole in the bottom of the ultracentrifuge tube with a 20-gauge needle. Allow approximately 750 μl to drip into a microfuge tube, and then collect the subsequent fractions in new microfuge tubes. There should be approximately 11 collected fractions.
17. Dilute the collected fractions with 2 ml of HM and centrifuge for 20 min at 30,000 × *g*. Keep the supernatant.

18. Quantitate total protein of the diluted fractions and adjust the volume of the samples with HM such that the total protein concentration is 1–5 mg/ml.
19. Proceed to SDS-PAGE analysis. Fig. 1c shows the MAVS-containing fractions that contain the peroxisomal marker PMP70 in fraction 11 and the mitochondrial marker Cox-1 in fraction 3.

3.3 Immunofluorescence Assay for MAVS

1. Plate Huh7 cells onto chamber slides such that they are 60% confluent on the following day. If only endogenous protein is being visualized, there is no need for transfection (*see* **Note 13**).
2. The day after plating, harvest the cells, wash with 500 μl of PBS, and aspirate the PBS.
3. Add 400 μl of 4% PFA to each well. Incubate at room temperature for 30 min (*see* **Note 14**).
4. Following incubation, aspirate off PFA, wash twice with 500 μl of PBS (*see* **Note 15**).
5. Add 200 μl of 0.1% Triton X-100 to each well. Gently rock on an orbital rocker at room temperature for 15 min.
6. Wash three times with 500 μl of PBS for 5 min.
7. To each well, add 200 μl of blocking buffer. Gently rock on an orbital shaker at room temperature for 1 h.
8. Aspirate off the blocking buffer and add 200 μl of your desired primary antibody diluted in blocking buffer into the appropriate wells of the chamber slides. Gently rock on an orbital shaker at room temperature for 2 h (*see* **Note 16**).
9. Aspirate off the blocking buffer and wash three times with 400 μl of PBS for 5 min.
10. After the final wash, add 200 μl of Alexa Fluor rabbit-conjugated or mouse-conjugated secondary antibody diluted in blocking buffer to the respective wells. Gently rock on an orbital shaker at room temperature for 1 h (*see* **Note 17**).
11. Wash three times with 500 μl of PBS for 5 min.
12. After the final wash, dismantle the chamber slide such that the plastic wells are removed and only the slide remains. Allow the slide to dry, which should take about 10 min.
13. Mount a glass cover slip onto the chamber slide using a drop of mounting medium onto each corner of the cover slip.
14. Allow the mounting medium to dry overnight in a dark container, such as a drawer. Image using a confocal microscope (*see* **Notes 18** and **19**). Fig. 2 shows representative images of MAVS localized to either mitochondria (Tom20) or peroxisomes (PMP70).

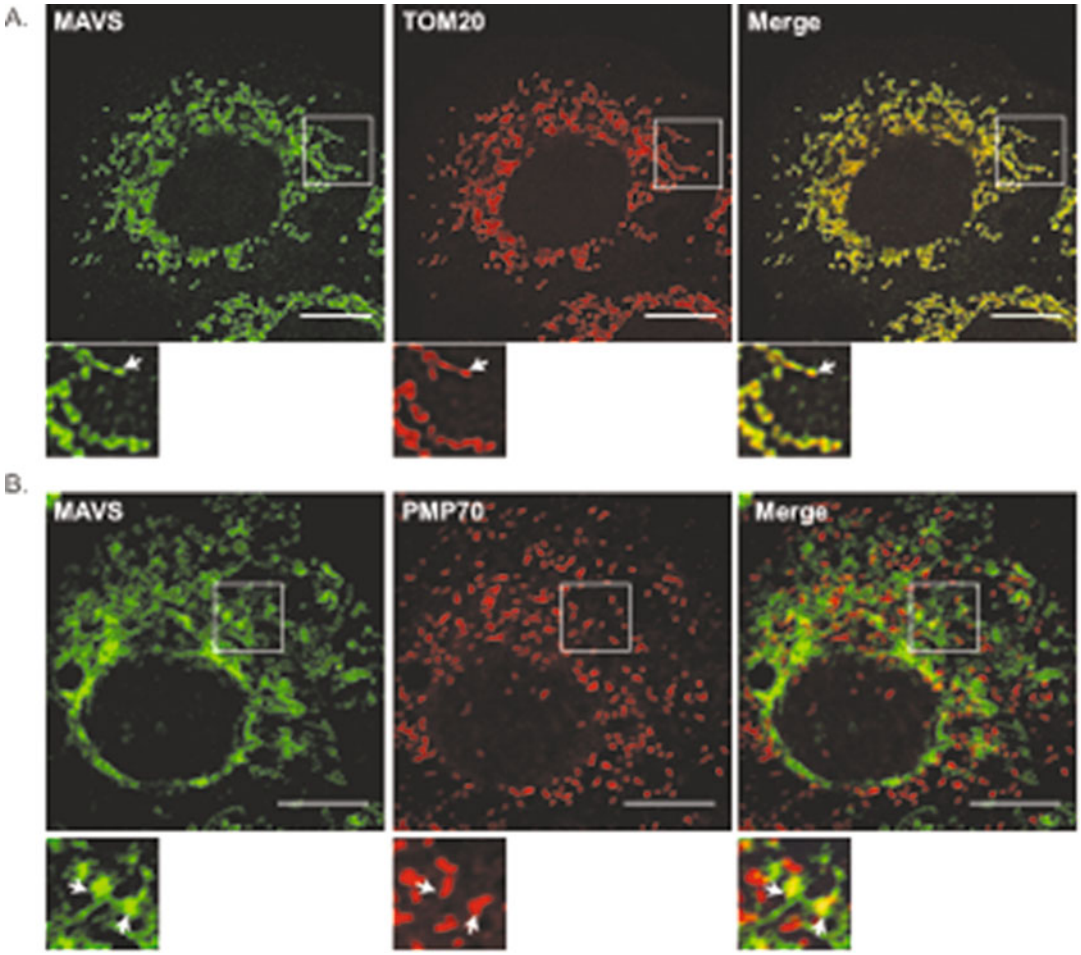

Fig. 2 Confocal microscopy analysis at 63X magnification of Huh7 cells immunostained for (**a**) endogenous MAVS and TOM20 (outer mitochondrial membrane) or (**b**) endogenous MAVS and PMP70 (peroxisomes). *White arrows* indicate colocalization of MAVS with either mitochondria or peroxisomes. Zoom panels below each set are from the area indicated by the white box. Scale bar-10 μm

4 Notes

1. The number of dishes used needs to be optimized according to the cell type used for fractionation, but eight dishes should be enough for most cell lines.
2. An alternative to collecting fractions by pipetting is using a fraction collector. If using a fraction collector, such as the Biocomp gradient station fraction collector, for the biochemical fractionations described here, use 14 × 89 mm open-top polyclear tubes.
3. Any mammalian cell line can be used for this protocol, but the number of cells can be adjusted to increase yield.

4. Alternatively, cover glasses can be used for plating and staining cells. 12 mm round cover glasses can fit into a 24-well tissue culture plate.
5. Mammalian cell lines can be used for immunofluorescence. Determine the cell number to plate that will reach ~60% confluency the next day.
6. Keep cells on ice during homogenization. Check efficiency of homogenization under the microscope by pipetting 10 μl of lysate onto a microscope slide and visualizing homogenization under a microscope. A shiny ring around the nuclei indicates that cells are intact. Cells should be ~90% homogenized, if not repeat homogenization at 1000 rpm. If using a dounce homogenizer, do 20–40 strokes.
7. Additional centrifugation is required to separate microsomes from residual mitochondria and MAM.
8. Pellets can be stored on ice and centrifuged at the same time as the MAM fraction (**step 24**).
9. Amicon concentrators are routinely used for concentrating fractions to increase the protein concentration. Other concentration techniques, such as acetone concentration or methanol/chloroform concentration, can be used as an alternative approach.
10. If using a dounce homogenizer, use ten strokes.
11. To ensure generation of the Percoll gradients, use an acceleration program (e.g., 500 rpm for 3 min) at the start of the spin and a similar deceleration program at the end.
12. Centrifuging the MAM fraction will remove any residual mitochondria.
13. If overexpressed protein is being visualized, the next day following plating, transfect using appropriate transfection reagent and plasmids. Then perform the immunostaining protocol the next day after transfection, as described above.
14. To reduce the risk of cell loss, 10% PFA can be added directly to the culture media, without aspirating and washing with PBS, to a final PFA percentage of 4%.
15. Chamber slides can be stored at 4 °C following fixation in PBS.
16. Alternatively, primary antibodies can be left on overnight, gently shaking on a rocker at 4 °C.
17. Alexa Fluor antibodies can be light-sensitive. Keep chamber slides covered in aluminum foil or turn off the lights in the area the chamber slides are rocking.
18. If you are imaging your cells on the same day as staining them, allow slide to dry for at least 4 h so that the cover slip will not move during focusing adjustments during the confocal imaging.

19. In order to see peroxisomal-MAVS localization, use at least a 63× objective for imaging with multiple averaging and a long pixel dwell.

Acknowledgment

We thank the Duke University Light Microscopy Core Facility for assistance with imaging and analysis. Research in the Horner laboratory is supported by funds from the National Institutes of Health (NIH) (R01AI125416 and R21AI124100) and a Duke School of Medicine Whitehead Scholarship. Additional funding sources include the Ford Foundation (CV) and NIH T32CA009111 (DCB).

References

1. Vazquez C, Horner SM (2015) MAVS coordination of antiviral innate immunity. J Virol 89 (14):6974–6977. doi:10.1128/JVI.01918-14
2. Seth RB, Sun L, Ea CK, Chen ZJ (2005) Identification and characterization of MAVS, a mitochondrial antiviral signaling protein that activates NF-kappaB and IRF 3. Cell 122 (5):669–682. doi:S0092-8674(05)00816-0 [pii]10.1016/j.cell.2005.08.012
3. Kawai T, Takahashi K, Sato S, Coban C, Kumar H, Kato H, Ishii KJ, Takeuchi O, Akira S (2005) IPS-1, an adaptor triggering RIG-I- and Mda5-mediated type I interferon induction. Nat Immunol 6(10):981–988. doi:ni1243 [pii]10.1038/ni1243
4. Horner SM, Liu HM, Park HS, Briley J, Gale M Jr (2011) Mitochondrial-associated endoplasmic reticulum membranes (MAM) form innate immune synapses and are targeted by hepatitis C virus. Proc Natl Acad Sci U S A 108(35):14590–14595. doi:10.1073/pnas.1110133108
5. Dixit E, Boulant S, Zhang Y, Lee AS, Odendall C, Shum B, Hacohen N, Chen ZJ, Whelan SP, Fransen M, Nibert ML, Superti-Furga G, Kagan JC (2010) Peroxisomes are signaling platforms for antiviral innate immunity. Cell 141(4):668–681. doi:S0092-8674(10)00435-6 [pii] 10.1016/j.cell.2010.04.018
6. Li K, Foy E, Ferreon JC, Nakamura M, Ferreon AC, Ikeda M, Ray SC, Gale M Jr, Lemon SM (2005) Immune evasion by hepatitis C virus NS3/4A protease-mediated cleavage of the toll-like receptor 3 adaptor protein TRIF. Proc Natl Acad Sci U S A 102(8):2992–2997. doi:0408824102 [pii]10.1073/pnas.0408824102
7. Li XD, Sun L, Seth RB, Pineda G, Chen ZJ (2005) Hepatitis C virus protease NS3/4A cleaves mitochondrial antiviral signaling protein off the mitochondria to evade innate immunity. Proc Natl Acad Sci U S A 102 (49):17717–17722. doi:0508531102 [pii] 10.1073/pnas.0508531102
8. Meylan E, Curran J, Hofmann K, Moradpour D, Binder M, Bartenschlager R, Tschopp J (2005) Cardif is an adaptor protein in the RIG-I antiviral pathway and is targeted by hepatitis C virus. Nature 437(7062):1167–1172. doi:nature04193 [pii]10.1038/nature04193
9. Loo YM, Owen DM, Li K, Erickson AK, Johnson CL, Fish PM, Carney DS, Wang T, Ishida H, Yoneyama M, Fujita T, Saito T, Lee WM, Hagedorn CH, Lau DT, Weinman SA, Lemon SM, Gale M Jr (2006) Viral and therapeutic control of IFN-beta promoter stimulator 1 during hepatitis C virus infection. Proc Natl Acad Sci U S A 103(15):6001–6006. doi:0601523103 [pii] 10.1073/pnas.0601523103
10. Horner SM, Wilkins C, Badil S, Iskarpatyoti J, Gale M Jr (2015) Proteomic analysis of mitochondrial-associated ER membranes (MAM) during RNA virus infection reveals dynamic changes in protein and organelle trafficking. PLoS One 10(3):e0117963. doi:10.1371/journal.pone.0117963
11. Bozidis P, Williamson CD, Colberg-Poley AM (2007) Isolation of endoplasmic reticulum, mitochondria, and mitochondria-associated membrane fractions from transfected cells and from human cytomegalovirus-infected primary fibroblasts. Curr Protoc Cell Biol Chapter 3: Unit 3 27. doi:10.1002/0471143030.cb0327s37
12. Graham JM (2001) Isolation of peroxisomes from tissues and cells by differential and density gradient centrifugation. Curr Protoc Cell Biol Chapter 3:Unit 3 5. doi:10.1002/0471143030.cb0305s06

Chapter 8

Purification of Cyclic GMP-AMP from Viruses and Measurement of Its Activity in Cell Culture

Alice Mayer, Jonathan Maelfait, Anne Bridgeman, and Jan Rehwinkel

Abstract

Sensing of cytoplasmic DNA by cGAS is essential for the initiation of immune responses against several viruses. cGAS also plays important roles in some autoinflammatory and autoimmune diseases and may be involved in immune responses targeting cancer cells. Once activated, cGAS catalyzes the formation of the di-nucleotide 2′-3′-cyclic GMP-AMP (cGAMP), which propagates a signaling cascade leading to the production of type I interferons (IFNs). Interestingly, cGAMP is incorporated into enveloped viruses and is transferred to newly infected cells by virions. In this article, we describe a method to purify cGAMP from viral particles and a bioassay to measure its activity. This assay takes advantage of a reporter cell line that expresses the genes encoding green fluorescent protein (GFP) and firefly luciferase under the control of the IFNß promoter, allowing the testing of several samples in a single experiment taking not more than 3 days.

Key words Innate immunity, cGAMP, STING, Type I IFN, Bioassay

1 Introduction

Sensing of foreign DNA plays a central role in the detection of viral infections by the immune system. In healthy cells, DNA is restricted to specialized compartments, namely the nucleus and mitochondria. Presence of DNA in other subcellular compartments is detected by specific receptors and triggers different signaling cascades, some of which culminate in the secretion of type I IFNs. These cytokines in turn act on the infected cell and on neighboring cells to induce an antiviral state, leading to a reduction in viral replication and spread. Type I IFNs also play roles in the activation of the adaptive immune response and therefore are crucial to the successful defence of the host against viruses.

In 2013, Sun et al. discovered that the presence of DNA in the cytosol is sensed by the cyclic GMP-AMP synthase (cGAS) [1]. Instead of signaling via protein-protein interactions as often seen for other sensors of virus presence, cGAS—once activated—catalyzes the synthesis of the di-nucleotide 2′-3′-cyclic GMP-AMP

Karen Mossman (ed.), *Innate Antiviral Immunity: Methods and Protocols*, Methods in Molecular Biology, vol. 1656, DOI 10.1007/978-1-4939-7237-1_8,

(hereafter simply cGAMP). cGAMP acts as a second messenger and activates the endoplasmic reticulum-bound secondary receptor STING [2]. Interestingly, STING is also activated by the bacterial dinucleotides cyclic-di-GMP and cyclic-di-AMP [3, 4]. The interaction of cyclic di-nucleotides with STING induces a change of its conformation, which results in recruitment and activation of the kinase TBK1 and the transcription factor IRF3. Once phosphorylated by TBK1, IRF3 dimerizes and translocates to the nucleus to induce the expression of type I IFNs. An interesting feature of this signaling pathway is that cGAMP—being a small molecule—can diffuse from cell to cell via gap junctions [5]. This allows rapid propagation of the signal in cells connected by gap junctions as soon as one cell is infected. Another consequence of cGAMP's nature as a small, diffusible molecule is that it can be incorporated into enveloped viral particles during budding and is transferred from one cell to another cell by viruses [6, 7]. This may allow newly infected cells to respond faster during secondary rounds of infection.

The cGAS pathway not only plays a critical role in the initiation of immune responses against several DNA viruses (including Herpes viruses, Vaccinia virus, adenovirus, Hepatitis B virus, mouse, and human cytomegaloviruses), retroviruses (including HIV), and bacteria (including *Mycobacterium tuberculosis*), but also in antitumor immunity [8, 9]. Of note, injection of cGAMP directly into solid tumors enhances the immune response targeting both the injected tumor and distal tumors [10, 11]. Moreover, cGAMP has been successfully used as an adjuvant in several vaccination models [12–14]. However, uncontrolled activation of cGAS by endogenous ligands can also lead to the development of inflammatory pathologies such as Aicardi-Goutières Syndrome [8, 9].

Because of the central role of cGAS in the development of immune responses in a broad range of pathological conditions, measuring its product, cGAMP, is important in studies aimed at understanding the physiopathology of infectious and inflammatory diseases. The methods currently available to detect cGAMP are (1) reverse phase HPLC followed by tandem mass spectrometry analysis [2, 6, 7, 15, 16] or by NMR spectroscopy [15, 17, 18] and (2) bioassays in which the activation of STING is assessed after incubation of mildly permeabilized cells with samples containing cyclic dinucleotides [2, 3]. The first approach may be more sensitive, but it also requires specialized equipment and expertise and has limitations in terms of the number of samples that can be processed. Bioassays have the advantage of being fast and requiring only standard tissue culture facilities, and can also be adapted to large sample numbers. Importantly, bioassays also provide information on the biological activity of the tested samples, and can therefore be used not only to detect the presence of cGAMP, but also to test the

ability of different cellular, viral, or synthetic components to modulate STING signaling.

In this chapter, we describe a step-by-step protocol to purify cGAMP from viral particles and a bioassay to detect and quantify its activity. The method for small molecule extraction from virions was adapted from [16]. Briefly, viral particles are lysed in a buffer containing 1% Triton X-100 and nucleic acids are degraded by the treatment with an endonuclease that degrades both DNA and RNA (benzonase). Proteins are then removed by two successive rounds of phenol-chloroform extraction, followed by a chloroform wash to remove all traces of phenol. The extract is then filtered through a 3 kDa centrifugal filter and the filtrate is concentrated by centrifugation under vacuum. With this method, we typically recover 36% of the cGAMP present in the original sample. The bioassay used to quantify cGAMP activity has been adapted from [2, 3] and takes advantage of a reporter cell line we have generated. These cells were derived from the monocytic cell line THP-1 and express firefly luciferase and GFP under the control of the human IFNß promoter. Overnight incubation in the presence of PMA induces the differentiation of these THP-1 reporter cells into macrophage-like cells. This step is important to increase the sensitivity to stimulation with cGAMP. The bioassay involves incubation of the cells with samples diluted in an isotonic buffer containing a very low concentration of digitonin. This mild detergent causes the formation of small holes in the plasma membrane, such that small molecules can diffuse into the cell but proteins and intracellular organelles stay in place (Fig. 1a). After half an hour, the stimulus is washed away and cells are incubated in normal media for 6–24 h, at which point firefly luciferase activity or GFP fluorescence is measured with a luminometer (Fig. 1b) or by flow cytometry (Fig. 1c), respectively. The lower detection limit of this bioassay using luciferase as readout typically ranges from 0.05 to 0.2 ng per well (2–8 ng/mL, Fig. 1b). Taken together, this bioassay allows the measurement of cGAMP concentration in several samples in only 3 days.

2 Materials

2.1 cGAMP Purification from Viral Particles

1. X-100 lysis buffer: 1 mM NaCl, 3 mM MgCl2, 1 mM EDTA, 1% Triton X-100, 10 mM Tris ph 7.4.
2. Optional: (2′-3′) cGAMP: Cyclic (guanosine- (2′ − > 5′)-monophosphate- adenosine- (3′ − > 5′)-monophosphate (Biolog or Invivogen; *see* **Note 1**).
3. Benzonase.
4. P:I:C [phenol:chloroform:isoamyl alcohol 25:24:1].
5. Chloroform.

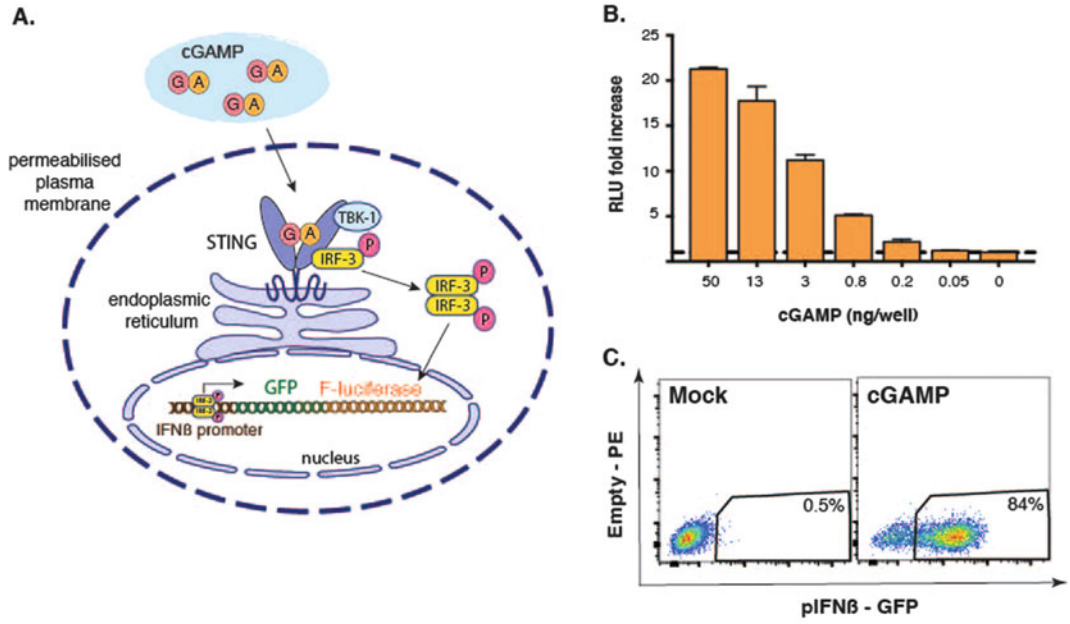

Fig. 1 (**a**) Illustration of the bioassay. (**b**) Representative luciferase assay: PMA-treated p125-THP1 cells were stimulated with graded doses of cGAMP. Luciferase activity was measured 24 h post simulation. Data represent the fold increase of firefly luciferase activity relative to the unstimulated mock control. Error bars indicate SD from four technical replicates. (**c**) Representative FACS plots: GFP expression in PMA-treated cells stimulated for 6 h with 25 ng of cGAMP per well or mock treated (gated on DAPI-negative single cells)

6. Amicon Ultra 3 K filter.
7. Sterile nuclease-free distilled water.
8. Ultracentrifuge to pellet viruses and associated tubes.
9. Standard table top centrifuge.
10. Chemical hood for handling of phenol-chloroform.
11. Speed vac to dry samples.

2.2 cGAMP Bioassay

2.2.1 Seeding and Differentiation of THP-1 Reporter Cells

1. Cells: p125-THP1 clone 9. These reporter cells were generated as follows: THP-1 cells were lentivirally transduced with a construct coding for GFP and firefly luciferase under control of the human IFNß promoter and were then cloned by limiting dilution (cells available upon request, *see* **Note 2**).
2. R10 media: 1× RPMI media, 10% fetal calf serum (FCS), 2 mM L-glutamine, 50 µM 2-mercapto-ethanol.
3. PMA (Phorbol 12-myristate 13-acetate).
4. Sterile flat-bottom 96-well plates.

5. Basic tissue-culture devices: centrifuge, 5% CO_2 incubator, laminar flow hood, material for counting cells, 50 mL conical tubes, pipettes and multichannel pipettes.

2.2.2 Stimulation of THP-1 Reporter Cells

1. R10 media and basic tissue-culture devices (hood, centrifuge, incubator, etc.).
2. Optional: sterile v-bottom 96-well plates.
3. 2× permeabilization (2xPERM) buffer: 100 mM Hepes-HCl (pH 7.4), 200 mM KCl, 6 mM MgCl2, 0.4% BSA, 170 mM sucrose, 2 mM ATP, 0.2 mM GTP, 0.002% digitonin (*see* **Note 3**).
4. Sterile nuclease-free distilled water.
5. (2′-3′) cGAMP: Cyclic (guanosine-(2′ − > 5′)-monophosphate- adenosine-(3′ − > 5′)-monophosphate (*see* **Note 1**).

2.2.3 Luciferase Assay

1. R10 media and multichannel pipettes.
2. OneGlo luciferase assay system.
3. Optiplate 96-white microplate.
4. Luminometer.

3 Methods

3.1 cGAMP Purification from Viral Particles

1. Resuspend pelleted viruses in 500 µL of X-100 lysis buffer, transfer to 1.5 mL tubes, and incubate 20 min on ice, vortex regularly (*see* **Note 4**).
2. Centrifuge for 10 min at 1000 × *g* at 4 °C.
3. Optional: Spike 1 µg cGAMP into 500 µL X-100 lysis buffer as a positive control (to test the efficiency of the purification process).
4. Collect the supernatant, add 50 U/mL of benzonase and incubate for 45 min on ice.
5. Add 500 µL of P:I:C, vortex vigorously, spin for 5 min at 17,000 × *g* (*see* **Note 5**).
6. Take off upper aqueous layer by pipetting carefully without disturbing the lower layer.
7. Add 500 µL P:I:C, vortex vigorously, spin 5 min at 17,000 × *g*.
8. Take off upper aqueous layer by pipetting carefully without disturbing the lower layer.
9. Add 500 µL chloroform, vortex vigorously, spin 5 min at 17,000 × *g*.

10. Transfer the upper aqueous layer onto Amicon 3 K filter column and centrifuge 30′ at 14,000 × *g*.
11. Dry the samples using a Speed Vac, resuspend pellets in 20 μL H_2O, and store at −80 °C.

3.2 cGAMP Bioassay

50,000 p125-THP1 cells are seeded per well in the presence of 5 ng/mL of PMA. *See* **Note 6** for an estimation of the number of wells to seed.

3.2.1 Seeding and Differentiation of THP-1 Reporter Cells (Day 0 of the Bioassay)

1. Harvest the THP-1 reporter cells, centrifuge, resuspend in R10 media, and count.
2. Adjust the cell concentration to 5×10^5 cells per mL.
3. Add PMA to a final concentration of 5 ng/mL.
4. Dispatch 100 μL per well in a flat-bottom 96-well plate.
5. Place in a tissue culture incubator (37 °C, 5% CO_2) and incubate overnight (*see* **Note 7**).

3.2.2 Stimulation of THP-1 Reporter Cells (Day 1 of the Bioassay)

1. Warm some R10 media to 37 °C and bring nuclease-free distilled water to room temperature.
2. Thaw the 2× PERM buffer, the samples containing the cGAMP to dose and some cGAMP for the standard.
3. Dilute the cGAMP-containing samples in nuclease-free distilled water to a total of 55 μL for duplicate measurements or 80 μL for triplicates (see **Notes 8** and **9**).
4. Further dilute samples 1:2 with 2× PERM buffer, then titer down in twofold dilution series in 1× PERM buffer. We usually do between 4 and 6 dilutions per sample (*see* **Note 6**).
5. Dilute the (2′-3′) cGAMP standard in 1× PERM buffer, from 50 ng/well to 0.02 ng/well in two-fold dilution series. Prepare 80 μL of each dilution (triplicates). Do not forget to keep 80 μL of 1× PERM buffer only as a negative control (blank).
6. Wash the reporter cells by removing the medium and by replacing it with 100 μL of fresh R10 (*see* **Note 10**).
7. Remove all medium.
8. Gently overlay the cells with 25 μL of sample or standard dilutions.
9. Incubate for 30 min in a tissue culture incubator.
10. Wash the cells by adding 100 μL of fresh R10 per well, and then remove all medium.
11. Add 100 μL of fresh R10 media and incubate between 6 and 24 h in a tissue culture incubator.

*3.2.3 Luciferase Assay (Day 2 of the Bioassay, See **Note 11**)*

1. Dilute the One Glo reagent 1:2 with R10 media, protect from light, and wait until it reaches room temperature.
2. Flick off the media from the plates containing the THP1 cells and replace with 100 μL of the diluted One Glo reagent.
3. Incubate for 3 min at room temperature in the dark.
4. Pipette up and down to homogenize and transfer 75 μL to a white 96-well plate.
5. Read with a luminometer according to the manufacturer's instructions.

4 Notes

1. It is important to use cGAMP molecules with a (2′-5′) link between the guanosine and the adenine and a (3′-5′) link between the adenine and the guanosine (here referred to as (2′-3′) cGAMP). cGAMP with (3′-5′) links in both positions has a lower affinity for human STING and is not as efficient at inducing its activation [15–18].
2. The growth of p125-THP1 clone 9 is similar to parental, unmodified THP-1 cells. These cells are suspension cells grown in R10. We suggest passaging them by diluting cells once or twice per week by adding fresh R10 media. Typically, we dilute these cells 1:3 to 1:5 when they reach 10^6/mL. We do not split them if there are less than 6×10^5 cells/mL. This clone is available upon request.
3. The 2× PERM buffer can be made in advance, filtered, aliquoted, and stored at −20 °C.
4. We typically analyze pelleted virus stocks corresponding to at least 10^6 infectious units, although this will depend on the type of virus and the amount of cGAMP incorporated during budding. For highly concentrated samples, it is advisable to increase the volume of X-100 lysis buffer, in which case the volumes of P:I:C and chloroform need to be adjusted accordingly. It is noteworthy that we have not been able to detect cGAMP activity in extracts when using this protocol to recover cGAMP from DNA-stimulated cells. Nevertheless, it may be possible to use this method to purify cGAMP from cells overexpressing cGAS [16].
5. All the steps involving P:I:C and chloroform should be performed in a chemical hood. These reagents, and also the tubes and pipette tips that have been in contact with them, should be disposed of in an appropriate way. Phase lock tubes can be used for these extractions.

6. The number of wells to seed depends on the number of samples, the number of dilutions of each sample, and the number of technical replicates (ideally triplicates). The number of dilutions depends on the expected concentration of cGAMP in the sample, taking into account that the assay usually saturates around 10 or 20 ng/well. We typically analyze between 4 and 6 dilutions per sample. Ideally, 30 wells for the standard (9 dilutions and a blank, all in triplicate) and 18 wells per sample are required.
7. The cells should be incubated with PMA for at least 18 h, and this incubation can be extended up to 24 h. Shorter and longer incubation periods have not been tested with the luciferase readout; however, using flow cytometry, 12 h or 42 h incubation gave rise to a diminished fraction of GFP-positive cells.
8. We typically prepare the dilutions of the standard and the samples in sterile v-bottom 96-well plates, and then transfer these to the cells with a multichannel pipette.
9. We typically use only half of our samples (10 μL). If the sample contains a concentration of cGAMP very close to the lower detection limit, we suggest using all of it without serial dilution. In this case, add 7.5 μL of water to the 20 μL of sample and do the experiment in duplicate.
10. In all the wash steps, media can be removed with a multichannel pipette or flicked off the plate.
11. The activation of the IFNß promoter can also be assessed by flow cytometry. This method takes more time, but is an alternative if you do not have access to the equipment needed for luciferase assays. In that case, the cells should be harvested 6 h after stimulation as follows: (1) flick off the supernatant and add 200 μL of ice-cold FACS buffer (PBS, 2 mM EDTA, 1% FCS, and 0.02% sodium azide), (2) incubate for a minimum of 2 minutes on ice, (3) detach the cells by pipetting up and down and transfer to a v-bottom 96-well plate, (4) centrifuge 5 min at 500 × *g*, (5) flick off the supernatant and resuspend the cells in 100 μL of FACS buffer containing 1 ng/mL of DAPI. The fold increase of the GFP median fluorescence intensity (gated on DAPI-negative cells) is comparable to the luciferase assay.

References

1. Sun L, Wu J, Du F, Chen X, Chen ZJ (2013) Cyclic GMP-AMP synthase is a cytosolic DNA sensor that activates the type I interferon pathway. Science 339(6121):786–791. doi:10.1126/science.1232458
2. Wu J, Sun L, Chen X, Du F, Shi H, Chen C, Chen ZJ (2013) Cyclic GMP-AMP is an endogenous second messenger in innate immune signaling by cytosolic DNA. Science 339(6121):826–830. doi:10.1126/science.1229963
3. Woodward JJ, Iavarone AT, Portnoy DA (2010) C-di-AMP secreted by intracellular *Listeria monocytogenes* activates a host type I

interferon response. Science 328 (5986):1703–1705. doi:10.1126/science.1189801

4. Burdette DL, Monroe KM, Sotelo-Troha K, Iwig JS, Eckert B, Hyodo M, Hayakawa Y, Vance RE (2011) STING is a direct innate immune sensor of cyclic di-GMP. Nature 478 (7370):515–518. doi:10.1038/nature10429
5. Ablasser A, Schmid-Burgk JL, Hemmerling I, Horvath GL, Schmidt T, Latz E, Hornung V (2013) Cell intrinsic immunity spreads to bystander cells via the intercellular transfer of cGAMP. Nature 503(7477):530–534. doi:10.1038/nature12640
6. Gentili M, Kowal J, Tkach M, Satoh T, Lahaye X, Conrad C, Boyron M, Lombard B, Durand S, Kroemer G, Loew D, Dalod M, Thery C, Manel N (2015) Transmission of innate immune signaling by packaging of cGAMP in viral particles. Science 349(6253):1232–1236. doi:10.1126/science.aab3628
7. Bridgeman A, Maelfait J, Davenne T, Partridge T, Peng Y, Mayer A, Dong T, Kaever V, Borrow P, Rehwinkel J (2015) Viruses transfer the antiviral second messenger cGAMP between cells. Science 349(6253):1228–1232. doi:10.1126/science.aab3632
8. Ablasser A, Gulen MF (2016) The role of cGAS in innate immunity and beyond. J Mol Med (Berl) 94:1085–1093. doi:10.1007/s00109-016-1423-2
9. Chen Q, Sun L, Chen ZJ (2016) Regulation and function of the cGAS-STING pathway of cytosolic DNA sensing. Nat Immunol 17 (10):1142–1149. doi:10.1038/ni.3558
10. Demaria O, De Gassart A, Coso S, Gestermann N, Di Domizio J, Flatz L, Gaide O, Michielin O, Hwu P, Petrova TV, Martinon F, Modlin RL, Speiser DE, Gilliet M (2015) STING activation of tumor endothelial cells initiates spontaneous and therapeutic antitumor immunity. Proc Natl Acad Sci U S A 112 (50):15408–15413. doi:10.1073/pnas.1512832112
11. Corrales L, Glickman LH, McWhirter SM, Kanne DB, Sivick KE, Katibah GE, Woo SR, Lemmens E, Banda T, Leong JJ, Metchette K, Dubensky TW Jr, Gajewski TF (2015) Direct activation of STING in the tumor microenvironment leads to potent and systemic tumor regression and immunity. Cell Rep 11 (7):1018–1030. doi:10.1016/j.celrep.2015.04.031
12. Wang J, Li P, Wu MX (2016) Natural STING agonist as an "ideal" adjuvant for cutaneous vaccination. J Invest Dermatol 136:2183–2191. doi:10.1016/j.jid.2016.05.105
13. Li XD, Wu J, Gao D, Wang H, Sun L, Chen ZJ (2013) Pivotal roles of cGAS-cGAMP signaling in antiviral defense and immune adjuvant effects. Science 341(6152):1390–1394. doi:10.1126/science.1244040
14. Blaauboer SM, Mansouri S, Tucker HR, Wang HL, Gabrielle VD, Jin L (2015) The mucosal adjuvant cyclic di-GMP enhances antigen uptake and selectively activates pinocytosis-efficient cells in vivo. Elife 4. doi:10.7554/eLife.06670
15. Zhang X, Shi H, Wu J, Zhang X, Sun L, Chen C, Chen ZJ (2013) Cyclic GMP-AMP containing mixed phosphodiester linkages is an endogenous high-affinity ligand for STING. Mol Cell 51(2):226–235. doi:10.1016/j.molcel.2013.05.022
16. Ablasser A, Goldeck M, Cavlar T, Deimling T, Witte G, Rohl I, Hopfner KP, Ludwig J, Hornung V (2013) cGAS produces a 2′-5′-linked cyclic dinucleotide second messenger that activates STING. Nature 498(7454):380–384. doi:10.1038/nature12306
17. Diner EJ, Burdette DL, Wilson SC, Monroe KM, Kellenberger CA, Hyodo M, Hayakawa Y, Hammond MC, Vance RE (2013) The innate immune DNA sensor cGAS produces a noncanonical cyclic dinucleotide that activates human STING. Cell Rep 3(5):1355–1361. doi:10.1016/j.celrep.2013.05.009
18. Gao P, Ascano M, Zillinger T, Wang W, Dai P, Serganov AA, Gaffney BL, Shuman S, Jones RA, Deng L, Hartmann G, Barchet W, Tuschl T, Patel DJ (2013) Structure-function analysis of STING activation by c[G(2′,5′)pA(3′,5′)p] and targeting by antiviral DMXAA. Cell 154 (4):748–762. doi:10.1016/j.cell.2013.07.023

Chapter 9

cGAMP Quantification in Virus-Infected Human Monocyte-Derived Cells by HPLC-Coupled Tandem Mass Spectrometry

Jennifer Paijo, Volkhard Kaever, and Ulrich Kalinke

Abstract

Upon virus infection, cells of the innate immune system such as dendritic cells and macrophages can mount type I interferon (IFN-I) responses that restrict viral dissemination. To inform host cells of virus infection, detection of cytosolic DNA is one important mechanism. Inappropriate sensing of endogenous DNA and subsequent induction of IFN-I responses can also cause autoimmunity, highlighting the need to tightly regulate DNA sensing. The cyclic GMP-AMP synthase (cGAS) was recently identified to be the major sensor of cytosolic DNA that triggers IFN-I expression. Upon DNA binding, cGAS synthesizes the second messenger cyclic guanosine-adenosine monophosphate (cGAMP) that induces IFN-I expression by the activation of the stimulator of interferon genes (STING). Notably, cGAMP does not only act in infected cells, but can also be relocated to noninfected bystander cells to there trigger IFN-I expression. Thus, direct quantification of cGAMP in cells of the innate immune system is an important approach to study where, when, and how DNA is sensed and IFN-I responses are induced. Here, we describe a method that allows specific quantification of cGAMP from extracts of virus-infected human myeloid cells by HPLC-coupled tandem mass spectrometry.

Key words cGAMP, cGAS, Macrophage, Dendritic cell, Type I interferon, HPLC, Tandem mass spectrometry

1 Introduction

Early detection of pathogens by triggering of pattern recognition receptors (PRR) is a hallmark of innate immunity. Determinants associated with groups of pathogens trigger PRR and thus activate innate immune cells to mount cytokine responses. The rapid induction of anti-viral cytokines such as type I interferons (IFN-I) is essential to control the infection with many different viruses. The induction of IFN-I is mainly triggered by sensing of nucleic acids that inform of virus infection when present in too high quantities, located at the wrong subcellular location, or containing certain structures that are not common in the vertebrate host (reviewed

Karen Mossman (ed.), *Innate Antiviral Immunity: Methods and Protocols*, Methods in Molecular Biology, vol. 1656, DOI 10.1007/978-1-4939-7237-1_9,

in [1]). In 2000, it was discovered that CpG-rich DNA can be sensed in endolysosomal compartments by the Toll-like receptor 9 (TLR9) [2]. While in the murine system TLR9 expression is found in a broad range of different cells [3], in the human system the expression of this receptor is more restricted and is found, e.g., on plasmacytoid dendritic cells (pDC), which mount abundant IFN-I responses upon TLR9 triggering [4–6]. Cytosolic DNA sensing received increased attention since 2006 when cytosolic double-stranded DNA (dsDNA) was described as a strong IFN-I stimulus [7, 8]. Initially, many potential cytosolic receptors were described such as ZBP1 (DAI) [9], DDX41 [10], and IFI16 [11] that were proposed to signal via the adaptor protein stimulator of interferon genes (STING), which was identified to be essential for DNA-dependent IFN-I induction [12]. However, a distinct mechanism for the activation of STING by these receptors could not be identified and also in vivo studies could not confirm their relevance for IFN-I induction [9, 13].

Finally, in 2013 the cyclic GMP/AMP synthase (cGAS) was identified as a major component in cytosolic DNA sensing and IFN-I induction [14, 15]. cGAS binds dsDNA as well as RNA:DNA hybrids in a sequence-independent manner that induces a conformational switch of cGAS, which changes the catalytic core to its active conformation. This active conformation is further stabilized by cGAS dimerization [16–19]. Active cGAS catalyzes the formation of the noncanonical cyclic dinucleotide cGAMP, which contains an adenosine monophosphate (AMP) unit and a guanosine monophosphate (GMP) unit with a mixed phosphodiester linkage [Gp(2′-5′)Ap(3′-5′)] (2′,3′ cGAMP) [18, 20, 21]. cGAMP can directly bind and activate STING, which recruits tank-binding kinase 1 (TBK1) and interferon regulatory factor 3 (IRF3) to induce IFN-I expression [14, 15, 21, 22]. Moreover, cGAMP was also found to be transferred via gap junctions, virus particles, or cell-cell fusion into neighboring cells to activate STING signaling even in the absence of cGAS [23–26]. Since its first description, many viruses such as herpes simplex virus-1 [14], murine gamma herpes virus-68 [27], modified vaccinia virus Ankara (MVA) [28], human cytomegalovirus (HCMV) [13, 29, 30], and even human immunodeficiency virus [31], as well as bacteria such as *Mycobacterium tuberculosis* [32–34] and *Listeria monocytogenes* [35] have been shown to induce IFN-I responses in a cGAS/cGAMP/STING-dependent manner. However, uncontrolled or inappropriate activation of the cGAS/STING axis can also cause autoimmunity [36–39]. Therefore, the activity and stability of cGAS and STING are tightly regulated by mechanisms such as phosphorylation [40, 41], glutamylation [42], or sumoylation [43] (reviewed in [44]).

Many studies addressing cGAS-dependent recognition of DNA are focusing on myeloid cells such as macrophages and dendritic

cells, which are major components of the innate immune system that upon stimulation can express abundant levels of cytokines, activate and regulate immune responses, and activate cells of the adaptive immune system by antigen presentation. In the murine system, cGAS-dependent recognition of DNA by myeloid cells was analyzed using cells from cGAS-deficient mice [27, 28, 32, 34]; however, in the human system similar experiments are difficult to carry out with primary human cells and thus many studies addressing the role of cGAS in human myeloid cells were performed using cell lines [14, 19, 33, 35].

Quantification of intracellular cGAMP is a direct approach to verify the involvement of cGAS and to determine its activity in cells that are difficult to genetically modify. As a specific anti-cGAMP antibody is not yet available, conventional immunological quantification methods such as ELISA are not applicable. Initial studies identified cGAMP by mass spectrometry or visualized it by liquid chromatography or thin-layer chromatography of ^{32}P-labeled cGAMP [15, 17–21, 31, 41, 42, 45, 46]. Furthermore, attempts to quantify cGAMP from cell lysates often rely on indirect detection methods such as transfer of cell lysates on STING expressing cells and determination of subsequently induced IFN-I responses [15, 25, 47, 48]. In contrast, we adapted a method to directly quantify cGAMP from virus-infected human monocyte-derived cells by using high pressure liquid chromatography-coupled tandem mass spectrometry (HPLC-MS/MS). By this method, we found that different subsets of human monocyte-derived cells produced cGAMP upon infection with HCMV or MVA, thus directly revealing activation of cGAS [29]. Moreover, the direct quantification of the cGAMP responses can give additional information on cell-subset-specific recognition properties. For instance, our results showed that cGAMP responses did not correlate with the amount of IFN-I that was produced by different virus-infected cell subsets [29]. Thus, regulatory mechanisms or the varying abundance of STING might restrict cGAMP-dependent IFN-I induction in a subset-specific manner. Notably, we also found that pDC expressed high levels of cGAS and STING and that they were stimulated by cGAMP transfection to mount IFN-I responses [29, 49]. However, upon virus stimulation no cGAMP synthesis was detected in pDC, suggesting that cGAS activity was either modulated or that cGAS was not sufficiently stimulated. These data further highlighted the major differences in DNA recognition of pDC and monocyte-derived myeloid cells. In this example cGAMP detection not only proved the activation of cGAS in cell systems that are difficult to genetically manipulate such as primary human cells, but also revealed deeper insights into fine tuning mechanisms deployed by different innate immune cell subsets to recognize DNA.

2 Materials

2.1 Isolation and Differentiation of Human Myeloid Cells

1. Blood samples: Lymphocyte concentrates from 500 mL whole blood donations, always stored at room temperature (RT) (*see* **Notes 1** and **2**).
2. Biocoll separating solution (pre-warmed to RT; Biochrom).
3. 50 mL reaction tubes.
4. Phosphate-buffered saline (PBS) (pre-warmed to RT).
5. Magnetic-activated cell sorting (MACS) buffer (precooled to 4 °C): 2 mM EDTA, 0.1% BSA, in PBS.
6. Counting chamber.
7. CD14 human MicroBeads (Miltenyi Biotec).
8. Differentiation medium: Serum-free CellGro DC medium (CellGenix) (*see* **Note 3**) supplemented with 1000 U/mL granulocyte-macrophage colony-stimulating factor (GM-CSF) and interleukin 4 (IL-4), or 80 U/mL GM-CSF, or 100 ng/mL macrophage colony-stimulating factor M-CSF.

2.2 cGAMP Extraction and Calibration Curves

1. Extraction reagent: 2/2/1 [v/v/v] methanol, acetonitrile, and water mixture (*see* **Note 4**).
2. Extraction reagent with internal tenofovir standard: dissolve 25 ng/mL tenofovir (obtained through the NIH AIDS Research and Reference Reagent Program) in extraction reagent.
3. Device to vaporize samples: We used the Concentrator plus from Eppendorf.
4. Water (HPLC-grade).
5. Thread bottles with screw caps and 200 µL glass micro-inserts (Macherey-Nagel).
6. Safe-lock tubes (Eppendorf).
7. Defined amounts of 2′,3′ cGAMP.
8. cGAMP calibration solutions: add 0.0262, 0.0655, 0.164, 0.410, 1.024, 2.56, 6.4, 16, 40, 100, and 250 pmol cGAMP per 10 µL HPLC-grade water

2.3 Liquid Chromatography, Mass Spectrometry, and Analysis

1. Identification and quantification of cGAMP was performed by HPLC-MS/MS. The HPLC and MS/MS instrumentation is specified in Table 1.
2. Analyst software (version 1.5.2, SCIEX) was applied for control of the HPLC and MS/MS systems as well as for data generation.

Table 1
HPLC and MS/MS parameters of standard method for quantification of 2′,3′ cGAMP and 3′,3′ cGAMP

Instrumentation				
HPLC (Shimadzu)	Controller: CBM-20A Autosampler: SIL-30AC Pump: LC-30AD Oven: CTO-20AC Degasser: DGU-20A5			
HPLC column	ZORBAX Eclipse XDB-C18 1.8 μ, 50 × 4.6 mm (Agilent)			
Security guard	C18, 4 × 2 mm (Phenomenex)			
Column saver	2 μm (Supelco)			
Mass spectrometer (SCIEX)	5500QTRAP®			
HPLC parameters				
Sample solvent	H_2O (HPLC-grade)			
Injection volume	20 μL			
Flow rate	0.4 mL/min			
Eluent A	3/97 (v/v) MeOH/H_2O; 50 mM NH_4Ac; 0.1% HAc			
Eluent B	97/3 (v/v) MeOH/H_2O; 50 mM NH_4Ac; 0.1% HAc			
Needle flushing	H_2O			
Temperature (column oven)	Ambient temperature			
Temperature (autosampler)	4 °C			
Maximal column pressure	2040 PSI			
HPLC gradient	Total time 0 min 5 min 5.1 min 8 min	Flow rate 0.4 mL/min 0.4 mL/min 0.4 mL/min 0.4 mL/min	A [%] 100 50 100 100	B [%] 0 50 0 0
Valve setup	Time 0 min 2 min 4.5 min	Position Waste Elution Waste		
Average retention times	Analyte cGAMP (2′,3′) cGAMP (3′,3′) Internal standard (Tenofovir)	 2.4 min 2.9 min 3.3 min		

(continued)

Table 1
(continued)

MS/MS parameters								
Ionization mode	positive							
Ion source parameters	Temperature: 400 °C Curtain gas: 45 Collision gas: 9 Ion spray voltage: 4500				Ion source gas 1: 60 Ion source gas 2: 75			
Analyte parameters	**Analyte**	**m/z precursor**	**m/z fragments**	**Dwell time [ms]**	**DP [V]**	**EP [V]**	**CE [V]**	**CXP [V]**
	cGAMP	338.1*	152.0	40	86	10	21	16
		338.1*	136.0	40	86	10	23	20
		675.0**	136.0	40	66	10	45	14
	Tenofovir	288.0**	176.0	40	16	10	35	14
		288.0**	159.1	40	16	10	43	12

*: $[M + 2H]^{2+}$, **: $[M + H]^{+}$

3 Methods

3.1 Isolation and Differentiation of Human Myeloid Cells

All the steps are performed at RT if not otherwise indicated (*see* **Note 1**) (*see* Fig. 1).

1. Dilute blood samples (lymphocyte concentrate) 1:4 with PBS (*see* **Note 2**). Overlay 15 mL of sterile Biocoll with 25 mL of the blood/PBS mixture in 50 mL reaction tubes. Centrifuge without brakes for 20 min at 900 × *g*. This separates the mixture in four phases: plasma, peripheral blood mononuclear cells (PBMC), Biocoll, erythrocytes, and granulocytes (top to bottom).
2. Gently remove the layer containing the PBMC with a 10 mL pipette and transfer it into a new 50 mL reaction tube. Wash two times with 50 mL MACS-buffer. In between, pellet the cells by centrifugation at 300 × *g* for 10 min. Determine the cell number.
3. Of PBMCs, 5–10% monocytes can be isolated by MACS sorting using the CD14 MicroBeads Kit. Therefore, resuspend cells in 40 µL MACS-buffer per 10^7 PBMC and add 10 µL CD14 MicroBeads per 10^7 cells (*see* **Notes 5** and **6**). Incubate for 20 min at 4 °C. Separate with the AutoMACS Pro Seperator using the program Posseld. Determine cell number of $CD14^+$ monocytes, centrifuge at 300 × *g* for 10 min, and resuspend cells in the CellGro serum-free DC medium at a concentration of 10^6 cells/mL (*see* **Note 3**).
4. Supplement the medium with 1000 U/mL GM-CSF and 1000 U/mL IL-4, or 80 U/mL GM-CSF, or 100 ng/mL

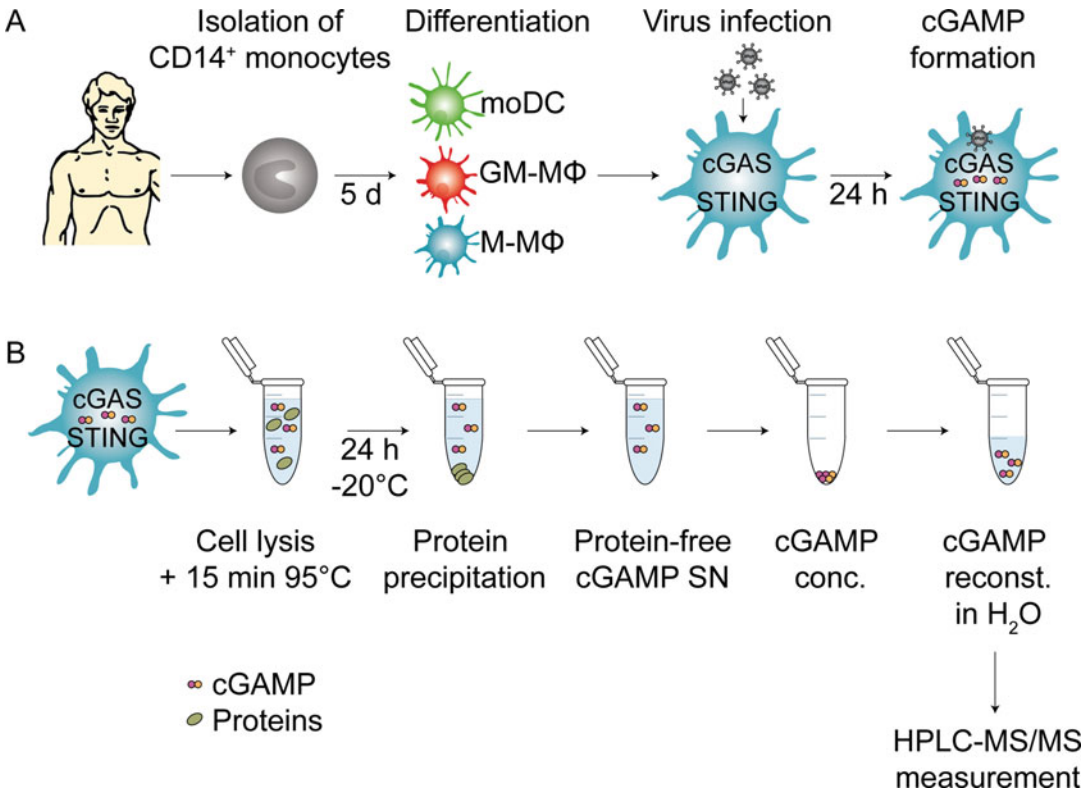

Fig. 1 Workflow to (**a**) induce cGAMP formation in human monocyte-derived cells by virus infection and (**b**) to extract cGAMP from these cells for HPLC-MS/MS quantification. (moDC: monocyte-derived dendritic cells, GM-MΦ: GM-CSF macrophages, M-MΦ: M-CSF macrophages, SN: supernatant, conc.: concentration, reconst.: reconstitution)

M-CSF to obtain monocyte-derived dendritic cells (moDC), GM-CSF macrophages (GM-MΦ), or M-CSF macrophages (M-MΦ), respectively. Seed cells in 48-well plates in a final volume of 500 µL per well (5×10^5 cells) and incubate for 5 days at 37 °C to differentiate them (*see* **Note 7**).

5. To stimulate cGAMP production, infect cells with virus (*see* **Notes 8** and **9**).

3.2 cGAMP Extraction

All the steps are performed on ice if not otherwise indicated (*see* Fig. 1).

1. Transfer the culture supernatant into 2 mL safe-lock tubes and centrifuge at 300 × *g* for 10 min at 4 °C to collect cells that might have come loose from the plates and are present in the supernatant. Subsequently, remove the supernatant completely and keep the cell pellet.
2. Scrape off and lyse cells, which are remaining in the 48-wells, by the addition of 300 µL extraction reagent with internal standard (*see* **Notes 4** and **10**).

3. Transfer the lysed cells in 300 µL extraction reagent with internal standard into the 2 mL safe-lock tubes, which contain the cell pellets of the centrifuged supernatants (**step 1**).
4. Rinse wells twice with 400 µL extraction reagent without internal standard and combine those two 400 µL aliquots with the cell lysates in the 2 mL safe-lock tubes.
5. Heat samples to 95 °C for 15 min and cool down on ice (*see* **Note 11**).
6. Precipitate proteins of the cell lysates by incubating at −20 °C overnight. Subsequently, centrifuge at 20,000 × *g* for 15 min to pellet down protein precipitates. Transfer protein-free supernatants (contain cGAMP) into new reaction tubes (*see* **Notes 12** and **13**).
7. Vaporize protein-free supernatants completely until only a small, dry, white/red pellet remains. If using the Concentrator plus (Eppendorf) vaporize for approximately 4 h using the "alcoholic solution" program.
8. Dissolve the pellet in 150 µL HPLC-grade water (*see* **Note 14**). Vortex samples two times for 10 s and transfer 75 µL of the solution into the glass micro-inserts of the thread-bottles for HPLC-MS/MS measuring (injection volume 20 µL) (*see* **Note 15**).
9. Store samples at −20 °C until measurement.

3.3 Calibration Curve

1. Prepare cGAMP calibration solutions.
2. Mix 10 µL of each cGAMP solution with 800 µL extraction reagent and 300 µL extraction reagent with internal standard (*see* **Note 3**).
3. Proceed as described in **step 5–9** of Subheading 3.2.

3.4 Analysis of cGAMP by Tandem Mass Spectrometry

1. The applied mass spectrometer is operated in positive ionization mode. In Table 1 the ion source (electrospray ionization) parameters, mass-to-charge ratios (m/z) for the precursor ions and specific fragment ions, and mass spectrometer-specific parameters are listed (*see* **Note 16**). The most intensive mass transitions ($[M + 2H]^{2+}$ for cGAMP and $[M + H]^{+}$ for the internal standard tenofovir) are used as quantifiers. Additional fragment ions serve as qualifiers (*see* Fig. 2).
2. Calibration curves are generated for cGAMP by calculating the ratios of the peak areas of the cGAMP calibrators and samples in relation to the respective peak areas of the internal standard tenofovir (*see* **Note 17**).
3. Misinterpretation of false-positive cGAMP peaks should be avoided by recording specific quantifier and qualifier mass transitions.

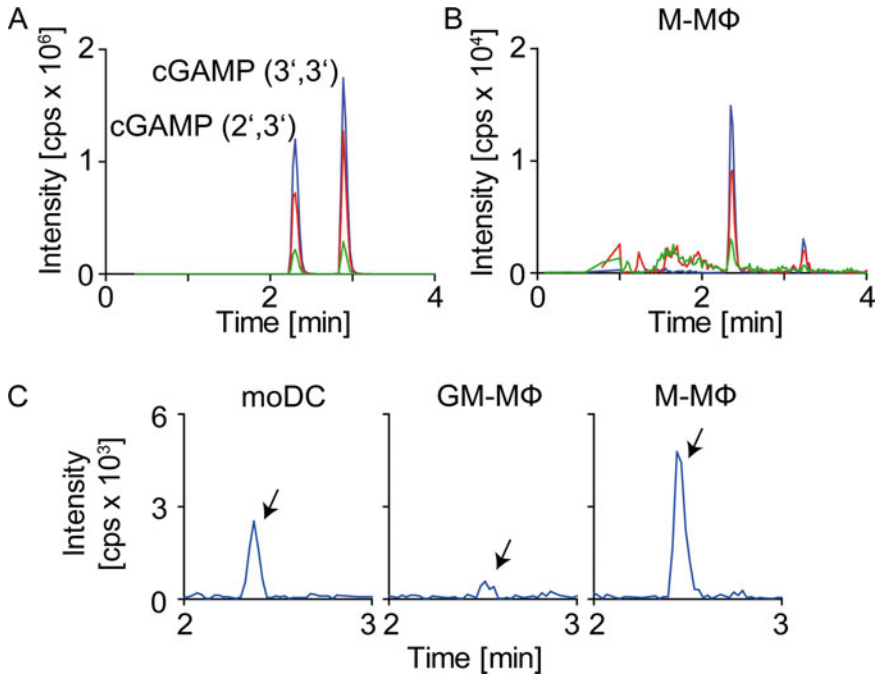

Fig. 2 cGAMP formation in monocyte-derived dendritic cells and macrophages upon HCMV infection. Chromatograms (quantifier and 2 qualifiers) from the HPLC-MS/MS quantification of cGAMP are shown. (**a**) synthetic cGAS-derived 2′,3′ cGAMP, which contains a mixed phosphodiester linkage can be distinguished from 3′,3′ cGAMP, which is produced by some bacteria species such as *Vibrio cholerae* [50]. Human monocyte-derived cells were infected with HCMV at MOI 3 for 24 h and (**b**) quantifier and 2 qualifiers of the cGAMP measurement from M-MΦ are shown and (**c**) an enlarged visualization of the quantifier between 2–3 min retention time is depicted for moDC, GM-MΦ, and M-MΦ. (Reproduced from reference [29])

4 Notes

1. The source and handling of the blood may have an impact on the phenotype and function of the myeloid cells you generate and might therefore also influence your cGAMP responses. We found that myeloid cells are very sensitive to handling at lower temperatures and then are less viable and active with regard to the production of cytokines. Therefore, blood samples should ideally be kept at RT and not at 4 °C over longer periods of time prior to cell isolation.
2. Do not use glass containers to store or mix the blood samples, as this might preactivate the cells.
3. Data derived from primary human cells often show some variability. To increase reproducibility and consistency of the results, it is important to use defined differentiation and cultivation conditions. Therefore, the usage of serum-free media is recommended.

4. Ingredients of the extraction reagent (acetonitrile and methanol) are highly toxic and volatile. Therefore, take care to perform all the steps involving these reagents on ice and under the fume hood, if possible.
5. The CD14 MicroBeads, human, isolation kit from Miltenyi Biotec can be used according to the manufacturer's instructions to ensure the isolation of sufficient numbers of cells. Nevertheless, to minimize costs it is also possible to use 40 μL of MACS buffer and 10 μL of beads per 10^7 PBMC instead of 80 μL of MACS buffer and 20 μL of beads per 10^7 PBMC as stated in the manual.
6. We found that the yield of $CD14^+$ cells was higher when using fresh MACS columns instead of used ones for isolation.
7. In addition to using monocyte-derived cells for cGAMP quantification, we were also able to quantify low amounts of cGAMP in virus-infected THP-1 cells (analyzing 5×10^5 cells, unpublished), in virus-infected murine tissue (unpublished), and upon generating cGAMP by activating recombinant cGAS with viral or synthetic DNA in a cell-free in vitro assay [29].
8. To obtain measurable cGAMP levels it is of major importance to have an effective infection of the cells. In our hands GM-MΦ that were only moderately infected by HCMV (appr. 2% of HCMV-GFP infected GM-MΦ were GFP positive) mounted cGAMP responses which were hardly measurable, whereas highly infected M-MΦ (35%) or moDC (20%) synthesized high amounts of cGAMP (*see* Fig. 2) [29]. Therefore, it is very important to assure the percentage of infected cells in the culture in order to correctly interpret the results. If needed infectivity with some viruses can be enhanced by centrifugation at $300 \times g$ for 30 min after the addition of the virus to the cells.
9. The time point of cGAMP extraction is important. We found that cGAMP levels increased in the first 24 h post virus infection, presumably because cGAS abundance was upregulated in a positive feedback reaction upon endogenous IFN-I production. Although cGAMP was detectable already 2–4 h post HCMV infection of myeloid cells, amounts increased over time and were highest and best quantifiable at later time points [29].
10. Directly start scraping off the cells after the addition of the 300 μL extraction reagent with internal standard, as cells might be fixed to the bottom of the well by the extraction reagent upon longer incubation times.
11. We found it helpful to place a heavy block on the tops of the safe-lock tubes, since unwanted explosions/spill overs during this step might happen due to the heating (also shortly after heating) even when using safe-lock tubes. Therefore, always wear goggles until the samples have cooled down to RT.

Notably, the components of the extraction reagent dissolve most markings, which might be written on your tube. Thus, it is always helpful to note down which sample is at which position in your heating block, so you can identify your sample even if spillovers happen. This step inactivates phosphodiesterases as well as remaining virus.

12. Protein pellets can be very fluffy and often detach from the bottom of the tubes after a short time. Therefore, only small numbers of samples should be processed at once (less than approx. 20). It might even be needed to centrifuge the samples again for 15 min at 20,000 × *g* to not transfer enhanced amounts of protein together with the cGAMP sample. Transfer of the protein pellet or parts of it with the cGAMP sample should be avoided since protein contamination might increase background signals.
13. Protein precipitates can be kept, dried, and dissolved by the addition of 0.1 N NaOH and heating for 15 min at 95 °C to determine the protein content.
14. Samples might also be taken up in less volume to increase the cGAMP concentration of the samples before measuring. However, since this also increases the concentration of the components causing background signals overall measuring of cGAMP was not improved in our hands. Nevertheless, if using other volumes than 150 μL of water to reconstitute the cGAMP samples, take care to also adjust the volume in which the calibration curve is reconstituted.
15. Take care to not encase air bubbles in the tip of the glass micro-inserts, as these might disrupt the HPLC-MS/MS measurement.
16. Instrument-specific parameters may vary between tandem mass spectrometers of different vendors and have, therefore, to be adapted.
17. All the established HPLC-MS/MS methods should be validated at least in terms of precision and accuracy. The lower limit of detection (LOD) is defined as a signal-to-noise ratio of 3. The lower limit of quantification (LLOQ) is specified by a signal-to-noise ratio of 10.

Acknowledgments

We gratefully acknowledge the skillful technical assistance of Annette Garbe. This study was supported by funding from the Helmholtz Virtual Institute (VH-VI-424 Viral Strategies of Immune Evasion, VISTRIE) and from the Helmholtz-Alberta Initiative, Infectious Diseases Research (HAI-IDR SO-073) to UK.

References

1. Schlee M, Hartmann G (2016) Discriminating self from non-self in nucleic acid sensing. Nat Rev Immunol 16(9):566–580. doi:10.1038/nri.2016.78
2. Hemmi H, Takeuchi O, Kawai T, Kaisho T, Sato S, Sanjo H, Matsumoto M, Hoshino K, Wagner H, Takeda K, Akira S (2000) A toll-like receptor recognizes bacterial DNA. Nature 408(6813):740–745. doi:10.1038/35047123
3. Edwards AD, Diebold SS, Slack EM, Tomizawa H, Hemmi H, Kaisho T, Akira S, Reis e Sousa C (2003) Toll-like receptor expression in murine DC subsets: lack of TLR7 expression by CD8 alpha+ DC correlates with unresponsiveness to imidazoquinolines. Eur J Immunol 33(4):827–833. doi:10.1002/eji.200323797
4. Lund J, Sato A, Akira S, Medzhitov R, Iwasaki A (2003) Toll-like receptor 9-mediated recognition of herpes simplex virus-2 by plasmacytoid dendritic cells. J Exp Med 198 (3):513–520. doi:10.1084/jem.20030162
5. Ito T, Kanzler H, Duramad O, Cao W, Liu YJ (2006) Specialization, kinetics, and repertoire of type 1 interferon responses by human plasmacytoid predendritic cells. Blood 107 (6):2423–2431. doi:10.1182/blood-2005-07-2709
6. Kadowaki N, Ho S, Antonenko S, Malefyt RW, Kastelein RA, Bazan F, Liu YJ (2001) Subsets of human dendritic cell precursors express different toll-like receptors and respond to different microbial antigens. J Exp Med 194 (6):863–869
7. Ishii KJ, Coban C, Kato H, Takahashi K, Torii Y, Takeshita F, Ludwig H, Sutter G, Suzuki K, Hemmi H, Sato S, Yamamoto M, Uematsu S, Kawai T, Takeuchi O, Akira S (2006) A toll-like receptor-independent antiviral response induced by double-stranded B-form DNA. Nat Immunol 7(1):40–48. doi:10.1038/ni1282
8. Stetson DB, Medzhitov R (2006) Recognition of cytosolic DNA activates an IRF3-dependent innate immune response. Immunity 24 (1):93–103. doi:10.1016/j.immuni.2005.12.003
9. Takaoka A, Wang Z, Choi MK, Yanai H, Negishi H, Ban T, Lu Y, Miyagishi M, Kodama T, Honda K, Ohba Y, Taniguchi T (2007) DAI (DLM-1/ZBP1) is a cytosolic DNA sensor and an activator of innate immune response. Nature 448(7152):501–505. doi:10.1038/nature06013
10. Zhang Z, Yuan B, Bao M, Lu N, Kim T, Liu YJ (2011) The helicase DDX41 senses intracellular DNA mediated by the adaptor STING in dendritic cells. Nat Immunol 12(10):959–965. doi:10.1038/ni.2091
11. Unterholzner L, Keating SE, Baran M, Horan KA, Jensen SB, Sharma S, Sirois CM, Jin T, Latz E, Xiao TS, Fitzgerald KA, Paludan SR, Bowie AG (2010) IFI16 is an innate immune sensor for intracellular DNA. Nat Immunol 11 (11):997–1004. doi:10.1038/ni.1932
12. Ishikawa H, Ma Z, Barber GN (2009) STING regulates intracellular DNA-mediated, type I interferon-dependent innate immunity. Nature 461(7265):788–792. doi:10.1038/nature08476
13. Gray EE, Winship D, Snyder JM, Child SJ, Geballe AP, Stetson DB (2016) The AIM2-like receptors are dispensable for the interferon response to intracellular DNA. Immunity 45 (2):255–266. doi:10.1016/j.immuni.2016.06.015
14. Sun L, Wu J, Du F, Chen X, Chen ZJ (2013) Cyclic GMP-AMP synthase is a cytosolic DNA sensor that activates the type I interferon pathway. Science 339(6121):786–791. doi:10.1126/science.1232458
15. Wu J, Sun L, Chen X, Du F, Shi H, Chen C, Chen ZJ (2013) Cyclic GMP-AMP is an endogenous second messenger in innate immune signaling by cytosolic DNA. Science 339(6121):826–830. doi:10.1126/science.1229963
16. Zhang X, Wu J, Du F, Xu H, Sun L, Chen Z, Brautigam CA, Zhang X, Chen ZJ (2014) The cytosolic DNA sensor cGAS forms an oligomeric complex with DNA and undergoes switch-like conformational changes in the activation loop. Cell Rep 6(3):421–430. doi:10.1016/j.celrep.2014.01.003
17. Civril F, Deimling T, de Oliveira Mann CC, Ablasser A, Moldt M, Witte G, Hornung V, Hopfner KP (2013) Structural mechanism of cytosolic DNA sensing by cGAS. Nature 498 (7454):332–337. doi:10.1038/nature12305
18. Gao P, Ascano M, Wu Y, Barchet W, Gaffney BL, Zillinger T, Serganov AA, Liu Y, Jones RA, Hartmann G, Tuschl T, Patel DJ (2013) Cyclic [G(2′,5′)pA(3′,5′)p] is the metazoan second messenger produced by DNA-activated cyclic GMP-AMP synthase. Cell 153(5):1094–1107. doi:10.1016/j.cell.2013.04.046
19. Mankan AK, Schmidt T, Chauhan D, Goldeck M, Honing K, Gaidt M, Kubarenko AV, Andreeva L, Hopfner KP, Hornung V (2014) Cytosolic RNA:DNA hybrids activate the cGAS-STING axis. EMBO J 33(24):2937–2946. doi:10.15252/embj.201488726

20. Diner EJ, Burdette DL, Wilson SC, Monroe KM, Kellenberger CA, Hyodo M, Hayakawa Y, Hammond MC, Vance RE (2013) The innate immune DNA sensor cGAS produces a noncanonical cyclic dinucleotide that activates human STING. Cell Rep 3(5):1355–1361. doi:10.1016/j.celrep.2013.05.009
21. Ablasser A, Goldeck M, Cavlar T, Deimling T, Witte G, Rohl I, Hopfner KP, Ludwig J, Hornung V (2013) cGAS produces a 2′-5′-linked cyclic dinucleotide second messenger that activates STING. Nature 498(7454):380–384. doi:10.1038/nature12306
22. Zhang X, Shi H, Wu J, Zhang X, Sun L, Chen C, Chen ZJ (2013) Cyclic GMP-AMP containing mixed phosphodiester linkages is an endogenous high-affinity ligand for STING. Mol Cell 51(2):226–235. doi:10.1016/j.molcel.2013.05.022
23. Ablasser A, Schmid-Burgk JL, Hemmerling I, Horvath GL, Schmidt T, Latz E, Hornung V (2013) Cell intrinsic immunity spreads to bystander cells via the intercellular transfer of cGAMP. Nature 503(7477):530–534. doi:10.1038/nature12640
24. Bridgeman A, Maelfait J, Davenne T, Partridge T, Peng Y, Mayer A, Dong T, Kaever V, Borrow P, Rehwinkel J (2015) Viruses transfer the antiviral second messenger cGAMP between cells. Science 349(6253):1228–1232. doi:10.1126/science.aab3632
25. Gentili M, Kowal J, Tkach M, Satoh T, Lahaye X, Conrad C, Boyron M, Lombard B, Durand S, Kroemer G, Loew D, Dalod M, Thery C, Manel N (2015) Transmission of innate immune signaling by packaging of cGAMP in viral particles. Science 349(6253):1232–1236. doi:10.1126/science.aab3628
26. Xu S, Ducroux A, Ponnurangam A, Vieyres G, Franz S, Müsken M, Zillinger T, Malassa A, Ewald E, Hornung V, Barchet W, Häussler S, Pietschmann T, Goffinet C (2016) cGAS-mediated innate immunity spreads Intercellularly through HIV-1 Env-induced membrane fusion sites. Cell Host Microbe 20:443–457. doi:10.1016/j.chom.2016.09.003
27. Schoggins JW, MacDuff DA, Imanaka N, Gainey MD, Shrestha B, Eitson JL, Mar KB, Richardson RB, Ratushny AV, Litvak V, Dabelic R, Manicassamy B, Aitchison JD, Aderem A, Elliott RM, Garcia-Sastre A, Racaniello V, Snijder EJ, Yokoyama WM, Diamond MS, Virgin HW, Rice CM (2014) Pan-viral specificity of IFN-induced genes reveals new roles for cGAS in innate immunity. Nature 505(7485):691–695. doi:10.1038/nature12862
28. Dai P, Wang W, Cao H, Avogadri F, Dai L, Drexler I, Joyce JA, Li XD, Chen Z, Merghoub T, Shuman S, Deng L (2014) Modified vaccinia virus Ankara triggers type I IFN production in murine conventional dendritic cells via a cGAS/STING-mediated cytosolic DNA-sensing pathway. PLoS Pathog 10(4):e1003989. doi:10.1371/journal.ppat.1003989
29. Paijo J, Doring M, Spanier J, Grabski E, Nooruzzaman M, Schmidt T, Witte G, Messerle M, Hornung V, Kaever V, Kalinke U (2016) cGAS senses human cytomegalovirus and induces type I interferon responses in human monocyte-derived cells. PLoS Pathog 12(4):e1005546. doi:10.1371/journal.ppat.1005546
30. Lio CW, McDonald B, Takahashi M, Dhanwani R, Sharma N, Huang J, Pham E, Benedict CA, Sharma S (2016) cGAS-STING signaling regulates initial innate control of cytomegalovirus infection. J Virol 90(17):7789–7797. doi:10.1128/jvi.01040-16
31. Gao D, Wu J, YT W, Du F, Aroh C, Yan N, Sun L, Chen ZJ (2013) Cyclic GMP-AMP synthase is an innate immune sensor of HIV and other retroviruses. Science 341(6148):903–906. doi:10.1126/science.1240933
32. Collins AC, Cai H, Li T, Franco LH, Li XD, Nair VR, Scharn CR, Stamm CE, Levine B, Chen ZJ, Shiloh MU (2015) Cyclic GMP-AMP synthase is an innate immune DNA sensor for Mycobacterium tuberculosis. Cell Host Microbe 17(6):820–828. doi:10.1016/j.chom.2015.05.005
33. Wassermann R, Gulen MF, Sala C, Perin SG, Lou Y, Rybniker J, Schmid-Burgk JL, Schmidt T, Hornung V, Cole ST, Ablasser A (2015) Mycobacterium tuberculosis differentially activates cGAS- and Inflammasome-dependent intracellular immune responses through ESX-1. Cell Host Microbe 17(6):799–810. doi:10.1016/j.chom.2015.05.003
34. Watson RO, Bell SL, MacDuff DA, Kimmey JM, Diner EJ, Olivas J, Vance RE, Stallings CL, Virgin HW, Cox JS (2015) The cytosolic sensor cGAS detects Mycobacterium tuberculosis DNA to induce type I interferons and activate autophagy. Cell Host Microbe 17(6):811–819. doi:10.1016/j.chom.2015.05.004
35. Hansen K, Prabakaran T, Laustsen A, Jorgensen SE, Rahbaek SH, Jensen SB, Nielsen R, Leber JH, Decker T, Horan KA, Jakobsen MR, Paludan SR (2014) *Listeria monocytogenes* Induces IFNbeta expression through an IFI16-, cGAS- and STING-dependent pathway. EMBO J 33(15):1654–1666. doi:10.15252/embj.201488029
36. Ablasser A, Hemmerling I, Schmid-Burgk JL, Behrendt R, Roers A, Hornung V (2014)

TREX1 deficiency triggers cell-autonomous immunity in a cGAS-dependent manner. J Immunol 192(12):5993–5997. doi:10.4049/jimmunol.1400737

37. Gao D, Li T, Li XD, Chen X, Li QZ, Wight-Carter M, Chen ZJ (2015) Activation of cyclic GMP-AMP synthase by self-DNA causes autoimmune diseases. Proc Natl Acad Sci U S A 112 (42):E5699–E5705. doi:10.1073/pnas.1516465112
38. Mackenzie KJ, Carroll P, Lettice L, Tarnauskaite Z, Reddy K, Dix F, Revuelta A, Abbondati E, Rigby RE, Rabe B, Kilanowski F, Grimes G, Fluteau A, Devenney PS, Hill RE, Reijns MA, Jackson AP (2016) Ribonuclease H2 mutations induce a cGAS/STING-dependent innate immune response. EMBO J 35(8):831–844. doi:10.15252/embj.201593339
39. Pokatayev V, Hasin N, Chon H, Cerritelli SM, Sakhuja K, Ward JM, Morris HD, Yan N, Crouch RJ (2016) RNase H2 catalytic core Aicardi-Goutieres syndrome-related mutant invokes cGAS-STING innate immune-sensing pathway in mice. J Exp Med 213(3):329–336. doi:10.1084/jem.20151464
40. Konno H, Konno K, Barber GN (2013) Cyclic dinucleotides trigger ULK1 (ATG1) phosphorylation of STING to prevent sustained innate immune signaling. Cell 155 (3):688–698. doi:10.1016/j.cell.2013.09.049
41. Seo GJ, Yang A, Tan B, Kim S, Liang Q, Choi Y, Yuan W, Feng P, Park HS, Jung JU (2015) Akt kinase-mediated checkpoint of cGAS DNA sensing pathway. Cell Rep 13(2):440–449. doi:10.1016/j.celrep.2015.09.007
42. Xia P, Ye B, Wang S, Zhu X, Du Y, Xiong Z, Tian Y, Fan Z (2016) Glutamylation of the DNA sensor cGAS regulates its binding and synthase activity in antiviral immunity. Nat Immunol 17:369–378. doi:10.1038/ni.3356
43. MM H, Yang Q, Xie XQ, Liao CY, Lin H, Liu TT, Yin L, Shu HB (2016) Sumoylation promotes the stability of the DNA sensor cGAS and the adaptor STING to regulate the kinetics of response to DNA virus. Immunity 45 (3):555–569. doi:10.1016/j.immuni.2016.08.014
44. Chen Q, Sun L, Chen ZJ (2016) Regulation and function of the cGAS-STING pathway of cytosolic DNA sensing. Nat Immunol 17 (10):1142–1149. doi:10.1038/ni.3558
45. Liang Q, Seo GJ, Choi YJ, Kwak MJ, Ge J, Rodgers MA, Shi M, Leslie BJ, Hopfner KP, Ha T, BH O, Jung JU (2014) Crosstalk between the cGAS DNA sensor and Beclin-1 autophagy protein shapes innate antimicrobial immune responses. Cell Host Microbe 15 (2):228–238. doi:10.1016/j.chom.2014.01.009
46. Kranzusch PJ, Lee AS, Berger JM, Doudna JA (2013) Structure of human cGAS reveals a conserved family of second-messenger enzymes in innate immunity. Cell Rep 3 (5):1362–1368. doi:10.1016/j.celrep.2013.05.008
47. Li XD, Wu J, Gao D, Wang H, Sun L, Chen ZJ (2013) Pivotal roles of cGAS-cGAMP signaling in antiviral defense and immune adjuvant effects. Science 341(6152):1390–1394. doi:10.1126/science.1244040
48. Orzalli MH, Broekema NM, Diner BA, Hancks DC, Elde NC, Cristea IM, Knipe DM (2015) cGAS-mediated stabilization of IFI16 promotes innate signaling during herpes simplex virus infection. Proc Natl Acad Sci U S A 112(14):E1773–E1781. doi:10.1073/pnas.1424637112
49. Bode C, Fox M, Tewary P, Steinhagen A, Ellerkmann RK, Klinman D, Baumgarten G, Hornung V, Steinhagen F (2016) Human plasmacytoid dentritic cells elicit a type I interferon response by sensing DNA via the cGAS-STING signaling pathway. Eur J Immunol 46:1615–1621. doi:10.1002/eji.201546113
50. Davies BW, Bogard RW, Young TS, Mekalanos JJ (2012) Coordinated regulation of accessory genetic elements produces cyclic di-nucleotides for V. Cholerae virulence. Cell 149 (2):358–370. doi:10.1016/j.cell.2012.01.053

Chapter 10

Methods of Assessing STING Activation and Trafficking

Vladislav Pokatayev and Nan Yan

Abstract

The signaling adapter protein STING is crucial for the host immune response to cytosolic DNA and cyclic dinucleotides. Under basal conditions, STING resides on the endoplasmic reticulum (ER), but upon activation, it traffics through secretory pathway to cytoplasmic vesicles, where STING activates downstream immune signaling. Classical STING activation and trafficking are triggered by binding of cyclic dinucleotide ligands. STING signaling can also be activated by gain-of-function mutations that lead to constitutive trafficking of STING. These gain-of-function mutations are associated with several human diseases such as STING-associated vasculopathy with onset in infancy (SAVI), systemic lupus erythematosus (SLE), or familial chilblain lupus (FCL). This dynamic activation pathway presents a challenge to study. We describe methods here for measuring ligand-dependent and ligand-independent activation of STING signaling in HEK293T cells. We also describe a retroviral-based reconstitution assay to study STING protein trafficking and activation in immune competent cells such as mouse embryonic fibroblasts (MEF), which avoids the use of plasmid DNA. These methods will expedite research regarding STING trafficking and signaling dynamics in the settings of infection and autoimmune diseases.

Key words Sting, Interferon response, Innate immunity, Cytosolic DNA sensing

1 Introduction

Extracellular and intracellular innate immune receptors alert the host of infection or self-damage. STING is an intracellular protein indispensable for the pathway involved in detecting cytosolic DNA of viral, bacterial, or self-origin [1]. Under basal conditions, STING resides on the endoplasmic reticulum (ER) as a transmembrane protein. Upon the introduction of DNA into the cellular cytosol, the intracellular DNA-sensor, cGAS, binds to the DNA ligand, and converts ATP and GMP to produce the STING ligand cyclic di-GMP-AMP (cGAMP). cGAMP diffuses throughout the cell and binds to the cytosolic carboxy-terminal-domain of STING. After cGAMP binding, STING translocates from the ER to the ER-Golgi intermediate compartment (ERGIC) and the Golgi, then to cytoplasmic vesicles, during which time it recruits TBK1 and IRF3 and activates downstream type I IFN signaling [2, 3]. The cGAS-

Karen Mossman (ed.), *Innate Antiviral Immunity: Methods and Protocols*, Methods in Molecular Biology, vol. 1656, DOI 10.1007/978-1-4939-7237-1_10,

STING pathway is critical for sensing a variety of microbial pathogens, including DNA viruses such as herpes simplex virus 1 (HSV-1), bacterial pathogens such as *Listeria monocytogenes*, *Shigella flexneri*, and *Mycobacterium tuberculosis*, and retroviruses such as human immunodeficiency virus 1 (HIV-1) [3–9].

STING may also be activated independently of upstream activator cGAS or cyclic dinucleotide binding, through gain-of-function mutations in the gene encoding for STING, *TMEM173*. Several STING mutations have been reported in STING-associated vasculopathy with onset in infancy (SAVI), patients with SLE-like syndromes or familial chilblain lupus [10–12]. These STING mutations constitutively activate STING trafficking and type I IFN signaling and are associated with high childhood morbidity and mortality.

Here, we describe a HEK293T cell-based assay to measure ligand-dependent and ligand-independent activation of STING signaling. We also describe a retroviral-based reconstitution assay to study STING-GFP trafficking and activation in immune competent cells to avoid the use of plasmid DNA for the expression of STING.

2 Materials

2.1 Cells

1. HEK293T cells.
2. *Sting−/−* mouse embryonic fibroblasts (MEF).
3. Lenti-X 293T cells (Clontech).

2.2 Plasmids

1. pGL3-IFNβ-firefly.Luc (IFNβ-Luc), reporter plasmid, IFNβ promoter-driven firefly luciferase.
2. pRL-CMV-renilla.Luc (CMV-Luc), reporter plasmid, CMV promoter-driven renilla luciferase.
3. pMCSV-hSTING, mammalian expression plasmid for human STING.
4. pMRX-ibsr, retroviral expression plasmid.
5. pCMV-VSV-G (VSVG), retroviral packaging plasmid.
6. pCMV-Gag-Pol (Gagpol), retroviral packaging plasmid.

2.3 Media and Reagents

1. Opti-MEM reduced serum media.
2. Cell culture medium: Dulbecco's modified Eagle medium (DMEM) supplemented with 10% fetal bovine serum.
3. Dual luciferase assay system.
4. Microplate reader with dual injection system.
5. Lipofectamine 2000.

6. 2′3′-cGAMP.
7. Blasticidine S hydrochloride.
8. Lenti-X Concentrator.
9. Sterile syringe filter, 0.45 μm, PVDF.
10. Hexadimethrine bromide (Polybrene).

3 Methods

3.1 Ligand-Dependent STING Activation

3.1.1 Day 1 (STING Plasmid Transfection)

1. Plan to have at least the following conditions in each experiment, with at least two duplicates. Each experimental transfection will require its own 1.5 mL tube when setting up the transfection:

   293T cells alone.

   293T cells + IFNβ-Luc + CMV-Luc plasmids.

   293T cells + IFNβ-Luc + CMV-Luc + STING plasmid.

   293T cells + IFNβ-Luc + CMV-Luc + STING plasmid + cGAMP.
2. Utilize Table 1 to calculate amounts of each reagent required for 1 well in a 24-well plate. Scale up or down as necessary.
3. Create a single master mix consisting of Opti-MEM media and the reporter plasmids, IFNβ-Luc and CMV-Luc. Count the total number of wells which will be transfected and calculate the volumes of Opti-MEM and reporter plasmids to add into a single tube. Take into account pipetting errors. Mix homogenously and distribute appropriate amounts to separate 1.5 mL tubes to be used for distinct transfection conditions.

Table 1
Reagents required for ligand-dependent STING plasmid transfection

Reagent	Amount needed/well
293T cells	200,000 cells
DMEM + 10%FBS media	400 μL
Opti-MEM media for plasmid Opti-MEM media for lipofection	50 μL 50 μL
Lipofectamine 2000	1 μL
IFNβ-Luc plasmid	100 ng
CMV-Luc plasmid	20 ng
MCSV-hSTING plasmid	50 ng
cGAMP	0.5–2 μg/mL

4. To each prepared tube containing reporter plasmids, add the appropriate amount of STING plasmid, to account for the number of wells to be transfected.
5. Count the total number of wells to be transfected, and in a separate tube, add a scaled amount of Opti-MEM. Scale the amount of lipofectamine-2000 to add by this same factor. Take into account for pipetting errors. Mix well.
6. Incubate the tubes with plasmids and the tube with lipofectamine separately for 5 min at room temperature.
7. After 5 min of incubation, add in a 1:1 ratio the lipofectamine and Opti-MEM mixture to each tube with reporter plasmids. Mix and incubate for 20 min at room temperature.
8. Prepare 293T cells for reverse plasmid transfection during plasmid and lipofectamine incubation. Trypsinize 293T cells, wash with PBS, and then plate 200,000, 293T cells per well in a 24-well plate. Bring the final volume to 0.4 mL in DMEM +10% FBS. Incubate cells at a 37 °C incubator (*see* **Note 1**).
9. After 20 min plasmid and lipofectamine incubation, carefully pipette 100 μL of the incubated transfection mixture to each well containing 293T cells. Incubate for 18–24 h at 37 °C.

3.1.2 Day 2 (cGAMP Transfection)

1. The following day, ensure cells are 75–90% confluent prior to beginning transfection of cGAMP. Change media to 0.4 mL fresh media (*see* **Note 2**).
2. In separate tubes incubate a scaled amount of Opti-MEM with cGAMP, and Opti-MEM with lipofectamine. Calculate the amount of cGAMP to utilize given the final concentration to be 0.5–2 μg/mL (1–4 μg per well of the 24-well plate).
3. Perform separate 5 min incubation, then combine in a 1:1 ratio the lipofectamine and Opti-MEM mixture to the tube with cGAMP and Opti-MEM. Incubate for 20 min, then add 100 μL of the reaction per well of the 24-well plate. Incubate for 18–24 h at 37 °C.

3.1.3 Day 3 (Measuring Luciferase Activity)

1. The following day, thaw the Dual Luciferase Kit's reagents prior to removing cells from the incubator. Follow the manufacturer's protocol to reconstitute the kit components.
2. Aspirate media from cells, and add 100 μL of 1× lysis buffer (diluted 1:5 with nuclease-free H_2O) to each well of the plate.
3. Place the plate on a shaker at room temperature for 15 min.
4. Transfer cell lysates to 1.5 mL tubes and spin at top speed at room temperature for 1 min.
5. Transfer the supernatant to PCR tubes (*see* **Note 3**).

Table 2
Reagents required for ligand-independent STING plasmid transfection

Reagent	Amount needed/well
293T cells	200,000 cells
DMEM + 10%FBS media	400 μL
Opti-MEM media for plasmid Opti-MEM media for lipofection	50 μL 50 μL
Lipofectamine 2000	1 μL
IFNβ-Luc plasmid	100 ng
CMV-Luc plasmid	20 ng
MCSV-hSTING plasmid (wild type or mutants)	50–200 ng

6. Pipette 20 μL with a multi-channel pipette to an opaque 96-well plate. Pipette in technical duplicates.
7. Follow the Dual-Luciferase Kit protocol and plate reader instructions to measure firefly and renilla luciferase activities.
8. Normalize IFNβ-Luc to CMV-Luc values to calculate specific activation of IFNβ promoter (*see* **Note 4**).

3.2 Ligand-Independent STING Activation

1. Plan to have at least the following conditions in each experiment, with at least two duplicates. Each experimental transfection will require its own 1.5 mL tube when setting up the transfection (*see* **Note 5**):

   293T cells alone.

   293T cells + IFNβ-Luc + CMV-Luc plasmids.

   293T cells + IFNβ-Luc + CMV-Luc + STING plasmid (wild type or mutants).
2. Utilize Table 2 to calculate amounts of each reagent required for 1 well in a 24-well plate. Scale up or down as necessary.
3. **Steps 3**–9 are the same as above in Subheading 3.1.
4. Follow the steps above in Subheading 3.1.3.

3.3 Establish Stable STING-GFP Expressing Cells for Microscopy Studies of STING Trafficking

3.3.1 Generate Retrovirus Expressing Wild-Type or Mutant STING-GFP

1. Day 1: Plate Lenti-X 293T cells onto a 10 cm dish so that they will be 60–75% confluent the next day (*see* **Note 6**).
2. Day 2: Obtain pCMV-VSV-G, pCMV-Gag-Pol, and pMRX-STING-GFP (wild-type or mutant) plasmids and calculate the volume needed to transfect 4 μg of VSVG +6 μg of Gagpol +6 μg of pMRX-STING plasmids into one 10 cm dish of Lenti-X 293T cells.
3. Add the calculated amount into 0.5 mL Opti-MEM media in a 1.5 mL tube. In a separate tube, add 0.5 mL Opti-MEM media and 15 μL of lipofectamine-2000.

4. Incubate both tubes separately for 5 min, then combine into one tube and incubate for 20 min.
5. Pipette the entire 1 mL of mixture carefully onto 293T Lenti-X cells so as to not disrupt the monolayer. Incubate for 18–24 h at 37 °C.
6. Day 3: In the morning, discard the cell media and add 8 mL fresh media per 10 cm plate.
7. Day 4: Collect media in the morning by pipetting it into a 15 mL centrifuge tube and spin at 1500 × *g* for 5 min to pellet any suspending cells. Transfer supernatant media containing retroviruses into a 50 mL centrifuge tube and store in 4 °C. Add 8 mL fresh media to cell culture. Repeat these steps in the evening, and once again the next day in the morning (*see* **Note 7**).
8. Day 5: After three collections of virus, use a 30 mL syringe and a 0.45 syringe filter to filter the ~24 mL media containing retrovirus.
9. (*Optional*) To this filtered media, add 1/3 the volume of Lenti-X concentrator and incubate in 4 °C for 12–24 h.
10. (*Optional*) At 4 °C, spin the media with viral concentrator for 45 min at 1500 × *g*. After spin a white pellet will be visible. Resuspend in approximately 1/10 of original media or less depending on desired viral concentration.
11. Aliquot virus and store in −80 °C.

3.3.2 Establish Sting−/− MEFs Stably Expressing Wild-Type or Mutant STING-GFP

1. Infect *Sting−/−* MEFs with wild-type or mutant STING-GFP virus supplemented with 1 μg/mL of polybrene. Incubate for 24 h, then remove media and add new media containing the 15 μg/mL of BSH. Maintain cells for 2–3 days to ensure complete killing of control untransduced cells (*see* **Note 8**).
2. (*Optional*) Using FACS, sort for GFP-positive cells with a narrow window of GFP fluorescence intensity. Expand sorted cells and freeze aliquots. This will help to achieve uniform STING-GFP expression for microscopy.
3. Cell line expressing STING-GFP is now available for microscopy, flow cytometry, and other biochemical studies (*see* **Note 9**).

4 Notes

1. If the 20 minimum incubation time is insufficient for preparing the cells, 293T cells can be prepared before assembling the plasmid DNA/lipofectmine complex. We found that reverse transfection yields higher efficiency than conventional transfection.

2. Be very gentle when changing the media because 293T cells can easily detach after overnight transfection.
3. Clear cell lysate from this step can be stored at −20 °C for luciferase activity measurement at a later time.
4. Make sure the reading for both luciferases are within range of the instrument. If the readings are too high or too low, adjust sensitivity of the instrument accordingly or adjust amount of each luciferase plasmid.
5. This protocol for ligand-independent STING activation essentially removes cGAMP transfection from previous protocol ligand-dependent STING activation.
6. Other HEK293T cells can also be used for producing pseudotyped retrovirus, although the efficiency may not be as good as Lenti-X 293T cells.
7. We recommend three collections to maximize production of retrovirus from each plate of cells. The first collection usually contains the highest titer virus. The viral titer usually declines substantially 3 days after plasmid transfection.
8. We recommend testing the dose of BSH required for complete kill of parent cell line of interest. 15 μg/mL BSH is usually sufficient to kill untransduced MEFs in 2 days.
9. For microscopy studies, wild-type STING-GFP will localize to the ER at basal state, and translocates to vesicles after DNA or cGAMP transfection within a few hours. Gain-of-function STING constitutively localize to the ERGIC and Golgi at basal state. An example can be seen at [3].

Acknowledgment

This work is supported by US National Institute of Health (AI098569, AR067135 to N.Y.), UT Southwestern Immunology graduate program training grant (2T32AI005284 to V.P.), and Burroughs Wellcome Fund (N.Y.). The authors have no conflict of interest.

References

1. Barber GN (2015) STING: infection, inflammation and cancer. Nat Rev Immunol 15:760–770. doi:10.1038/nri3921
2. Barber GN (2011) STING-dependent signaling. Nat Immunol 12:929–930. doi:10.1038/ni.2118
3. Dobbs N, Burnaevskiy N, Chen D et al (2015) STING activation by translocation from the ER is associated with infection and Autoinflammatory disease. Cell Host Microbe 18:157–168. doi:10.1016/j.chom.2015.07.001
4. Gao D, Wu J, Wu Y-T et al (2013) Cyclic GMP-AMP synthase is an innate immune sensor of HIV and other retroviruses. Science 341:903–906. doi:10.1126/science.1240933
5. Li X-D, Wu J, Gao D et al (2013) Pivotal roles of cGAS-cGAMP signaling in antiviral defense

and immune adjuvant effects. Science 341:1390–1394. doi:10.1126/science.1244040

6. Stetson DB, Medzhitov R (2006) Recognition of cytosolic DNA activates an IRF3-dependent innate immune response. Immunity 24:93–103. doi:10.1016/j.immuni.2005.12.003
7. Collins AC, Cai H, Li T et al (2015) Cyclic GMP-AMP synthase is an innate immune DNA sensor for Mycobacterium tuberculosis. Cell Host Microbe 17:820–828. doi:10.1016/j.chom.2015.05.005
8. Watson RO, Bell SL, Macduff DA et al (2015) The cytosolic sensor cGAS detects Mycobacterium tuberculosis DNA to induce type I Interferons and activate autophagy. Cell Host Microbe 17:811–819. doi:10.1016/j.chom.2015.05.004
9. Waßermann R, Gulen MF, Sala C et al (2015) Mycobacterium tuberculosis differentially activates cGAS- and Inflammasome-dependent intracellular immune responses through ESX-1. Cell Host Microbe 17:799–810. doi:10.1016/j.chom.2015.05.003
10. Liu Y, Jesus AA, Marrero B et al (2014) Activated STING in a vascular and pulmonary syndrome. N Engl J Med 371:507–518. doi:10.1056/NEJMoa1312625
11. Jeremiah N, Neven B, Gentili M et al (2014) Inherited STING-activating mutation underlies a familial inflammatory syndrome with lupus-like manifestations. J Clin Invest 124:5516–5520. doi:10.1172/JCI79100
12. König N, Fiehn C, Wolf C et al (2016) Familial chilblain lupus due to a gain-of-function mutation in STING. Ann Rheum Dis 76:468–472. doi:10.1136/annrheumdis-2016-209841

Chapter 11

Genome-Wide CRISPR/Cas9 Screening for High-Throughput Functional Genomics in Human Cells

Shiyou Zhu, Yuexin Zhou, and Wensheng Wei

Abstract

It is highly desirable to identify gene's function in a high-throughput fashion, and the CRISPR/Cas9 system has been harnessed to meet such a need. Here, we describe a general method to generate genome-scale lentiviral single-guide RNA (sgRNA) library and conduct a pooled function-based screening in human cells. This protocol would be of interest to researchers to rapidly identify genes in a variety of biological processes.

Key words CRISPR-Cas9 system, High-throughput, Knockout, Screening, sgRNA

1 Introduction

The CRISPR/Cas9 system is commonly used as a defense system in archaea and bacteria [1] The most widely used engineered CRISPR/Cas system is composed of the Cas9 nuclease and a single guide RNA (sgRNA). A~20-bp sequence at the 5′ terminus of the sgRNA recognizes the targeted sequence via Watson-Crick base pairing, which recruits Cas9 protein to the targeted locus to produce double-stranded DNA breaks (DSBs) and modulate endogenous gene expression [2–4] The high efficiency and easy programmability of the CRISPR/Cas9 system make it possible to create large-scale loss-of-function mutations in mammalian cells. The CRISPR/Cas9 system has been harnessed to produce pooled gene knockout libraries through lentivirus infection for the functional screening of genes in a certain biologic process, aided by deep-sequencing technology [5–8] Here, we describe the design of sgRNAs targeting all human genes, with six different sgRNAs targeting each gene. sgRNA-coding sequences were generated by array-based synthesis and cloned into a lentiviral vector. An

Shiyou Zhu and Yuexin Zhou contributed equally to this work.

Karen Mossman (ed.), *Innate Antiviral Immunity: Methods and Protocols*, Methods in Molecular Biology, vol. 1656, DOI 10.1007/978-1-4939-7237-1_11,

sgRNA-expressing cartridge was introduced into a cell line stably expressing Cas9 by lentiviral infection at a low multiplicity of infection (MOI $\leq$ 0.3), followed by selection with antibiotics or fluorescence-activated cell sorting (FACS). After library screening, sgRNA-coding sequences were PCR-amplified from genomes, followed by deep-sequencing analysis. Candidate gene targets were then selected for further validation.

2 Materials

2.1 sgRNA Library Synthesis, Primers, and Plasmids

1. Oligo B3 Synthesizer (CustomArray, Inc.).
2. SpeedVac (Thermo Fisher Scientific).
3. Primers for the amplification of oligos for sgRNA library construction (*see* Table 1).
4. Primers for PCR amplification of sgRNA-coding sequences in genome for deep-sequencing analysis (*see* Table 1).
5. sgRNA expressing vector: pLenti-sgRNA-Lib [5].
6. Virus packaging plasmid: pVSVG, pR8.74.

2.2 Enzymes, Chemicals, and Kits

1. TransTaq DNA polymerase High Fidelity.
2. Phusion Hot Start Flex DNA polymerase.
3. dNTP mix (2.5 mM each).
4. PCR product purification kit.
5. BsmBI restriction enzyme.
6. Tango buffer: 33 mM Tris-acetate pH 7.9, 10 mM magnesium acetate, 66 mM potassium acetate, 0.1 mg/mL BSA (or buffer compatible with BsmBI restriction enzyme).
7. T4 DNA ligase.
8. 10 mM ATP.
9. 50 mM DTT.

Table 1
Primers for PCR amplification of synthesized oligos and sgRNA-coding sequences in the genome

Primer	Sequence
Oligo-F	5′-TTGTGGAAAGGACGAAACCG-3′
Oligo-R	5′-TGCTGTCTCTAGCTCTACGT-3′
Lib-F	5′-TATCTTGTGGAAAGGACGAAACACC-3′
Lib-R	5′-AATACGGTTATCCACGCGGC-3′

10. Trans1-T1 competent cells.
11. LB broth: to 800 mL dH_2O add 10 g tryptone, 5 g yeast extract and 5 g NaCl. Adjust pH to 7.5 with NaOH. Adjust volume to 1 L with dH_2O; autoclave to sterilize.
12. Endo free plasmid Maxi kit.
13. TIANamp genomic DNA kit (TIANGEN).
14. NGS Fast DNA Library Prep Set for Illumina.

2.3 Cell Culture and Transfection

1. HEK293T cell line.
2. Mammalian cell line of interest (HeLa in this protocol).
3. Complete culture medium, e.g., Dulbecco's modified Eagle medium (DMEM) with 10% FBS and 1% Penicillin-Streptomycin solution.
4. 0.25% Trypsin-EDTA solution.
5. Phosphate-buffered saline (PBS).
6. X-tremeGENE HP or other DNA transfection reagent.

3 Methods

3.1 sgRNA Library Design

1. For each targeting gene, 5′-end coding sequence is preferred for the design of sgRNAs (*see* **Note 1**).
2. Six sgRNAs are designed for each gene (*see* **Note 2**).
3. For genome-scale sgRNA library, at least 1000 nontarget sgRNAs are included as negative controls (*see* **Note 3**).

3.2 PCR Amplification for Synthesized DNA Oligo

1. For each PCR reaction, mix the followings into a 0.2 mL PCR tube: synthesized oligo template, forward primer (10 μM, 2.5 μL), reverse primer (10 μM, 2.5 μL), Phusion Hot Start Flex DNA polymerase (0.5 μL), HF buffer (5×), dNTP mix (1 μL), ddH_2O to a total volume of 50 μL. No less than 24 tubes are needed (*see* **Note 4**).
2. Perform PCR reaction as follows: 98 °C, 30 s for hot start; thermal cycling (98 °C, 10 s; 58 °C, 20 s; 72 °C, 10 s; 26 cycles); 72 °C, 10 min; and hold at 4 °C.
3. Optional step: DNA electrophoresis with 1 ~ 2 μL PCR product for quality check. The size of PCR product is about 80 bp (*see* **Note 5**).
4. Purify the PCR products using kit of choice.

3.3 BsmBI Digestion, DNA Ligation, and Transformation

1. Mix the purified PCR fragments with the following into one tube: BsmBI (7.5 units), T4 DNA ligase (100 units), ATP (10 nmol), DTT (10 nmol), Tango buffer (10×), sgRNA expressing vector (~20 ng), and ddH_2O to a total volume of 10 μL (*see* **Note 6**).

2. Perform thermo cycles (37 °C, 5 min; 16 °C, 5 min; 16 cycles); 37 °C, 5 min; and hold at 4 °C.
3. Transform 2 μL product into each tube of 50 μL Trans1-T1 competent cells, then add 1 mL liquid LB without antibiotics and culture the mixture overnight at 37 °C (*see* **Note 7**).
4. Mix all the bacterial liquid together, and extract the plasmids using Endo free plasmid Maxi kit.

3.4 Lentivirus Package

1. Culture HEK293T cells in complete culture medium at 37 °C and 5% CO_2 in a humidified incubator. Seed 4×10^6 HEK293T cells onto 10 cm plates 24 h before transfection.
2. Co-transfect 0.4 μg pVSVG plasmid, 4 μg of pR8.74, and 4 μg of Cas9 expressed plasmid or sgRNA library plasmids into HEK293T cells.
3. Collect the media and centrifuge at 395 RCF for 10 min to pellet cell debris 72 h posttransfection.
4. Calculate the virus titer.

3.5 Cas9 Stably Expressed Cell Line Construction

1. Culture HeLa cells in complete culture media at 37 °C and 5% CO_2 in a humidified incubator. Seed 2×10^6 cells into 10 cm plates 24 h before viral infection.
2. Add polybrene into DMEM at a final concentration of 8 μg/mL. Infect cells with Cas9-producing virus.
3. Add 5 μg/mL of Blasticidin onto cells 48 h after virus infection to enrich Cas9-expressing cells. Isolate the best single clones that show high efficiency in the indel analysis (*see* **Note 8**).

3.6 sgRNAs Delivery and Cell Library Construction

1. Culture HeLa cells stably expressing Cas9 in complete culture medium at 37 °C and 5% CO_2 in a humidified incubator. For each repeat, seed at least 3.6×10^7 cells (15 cm plate, total of 9 plates) 24 h before viral infection.
2. Add polybrene into DMEM at a final concentration of 8 μg/mL, and then add sgRNA library virus into cells with MOI ≤ 0.3 (*see* **Note 9**).
3. Collect cells expressing sgRNA by FACS or antibiotic selection 48 h after virus infection. Keep culturing these cells for 14 days before splitting them into four cell libraries (at least 1.2×10^7 cells per library), one for control and three replicates for the screening (*see* **Notes 10** and **11**).

3.7 Library Screening and Deep-Sequencing Analysis

1. Perform library screen.
2. Extract genomic DNA from 1.2×10^7 of control library cells and experimental library cells.
3. PCR-amplify sgRNA-coding regions from cell genome. For each PCR reaction, mix the following material into 0.2 mL

PCR tube: genomic DNA (4 μg), primer Lib-F (10 μM, 2 μL), primer Lib-R (10 μM, 2 μL), dNTP mix (2.5 nM, 8 μL), Taq DNA polymerase buffer (10×, 10 μL), Taq DNA polymerase (5 units/μL, 2 μL), and ddH_2O to a total volume of 50 μL.

4. Perform PCR reaction as follows: 94 °C 5 min for hot start; thermal cycling (95 °C 30 s; 62 °C 30 s; 72 °C 30 s; 26 cycles); 72 °C 10 min; hold at 4 °C. For each sample, perform 20 separate 100-μL reactions with 4 μg genomic DNA in each.
5. Pool and purify PCR products (20 tubes total) of each replicate, followed by high-throughput sequencing analysis. Index control library and different experimental library replicates with barcodes.
6. Use DESeq2 (R software package from Bioconductor) to perform a statistical analysis of the sequencing data. Rank the enrichment of sgRNA by the average fold change of normalized counts ($reads_{Exp}/reads_{Ctrl}$) and the adjusted *P* value ≤ 0.05. Select candidate sgRNAs and their targeted genes for further validation (*see* **Note 12**).

4 Notes

1. The basic design principles are consistent across different libraries. First, the reading frame could be disrupted by indels mediated by DSBs at target sites of sgRNAs. One should design sgRNAs targeting 5′ end of coding sequences for gene knockout as much as possible to maximize the chance of gene knockouts. Second, one should select sgRNAs with the best efficiency based on certain sequence features and criteria to minimize the off-target effect and maximize on-target activity. For instance, the GC content should be in the range of 20% ~ 70%, and sequences containing homopolymer stretches (e.g., TTTT, GGGG) should be avoided [9, 10].
2. We suggest designing six sgRNAs for each gene in this protocol. Although one report has shown that only one sgRNA for each gene is enough through the optimized design [9], designing 4 ~ 6 sgRNAs for each gene would have a better chance at target identification and the statistical analysis of screening data.
3. For negative controls in the library, one could also design sgRNAs targeting safe locus on genome, such as *AAVS1*.
4. To minimize both the mutation rate and the amplification bias, fewer PCR cycles and more PCR reactions are recommended. We usually conduct 26 cycles with no less than 24 tubes for each library sample.

5. If there are other nonspecific amplified bands, one should perform gel purification on the PCR products.
6. Make sure that the BsmBI enzyme works at 37 °C.
7. Before culturing bacteria overnight, plate 1 μL mixture onto solid LB medium with 25 μg/mL of ampicillin to count the colony number for each reaction. We perform multiple tubes of transformation to ensure that the total colony numbers exceed 200-fold coverage of the sgRNA library size.
8. To maximize the gene knockout efficiency, one should select the best Cas9-expressing single clones to construct the sgRNA library, those that have the highest efficiency in generating Cas9-mediated DSBs.
9. Low MOI is used to lower the odd that more than one sgRNA enters the same cell.
10. One should keep culturing cells for 7 ~ 14 days after lentiviral infection in order to maximize the gene knockouts in the cell library [5, 11].
11. To ensure library complexity, one should maintain the number of cells in each library at least 100-fold. For the whole-genome sgRNA library containing ~10^5 sgRNAs, at least 1.2×10^7 cells should be harvested for each passage.
12. Other bioinformatics tools could also be used for the analysis of deep-sequencing data [12].

Acknowledgments

We thank J. Xi for providing the Cas9-encoding construct, and D. Trono for aid with the lentivirus packaging system. We thank Peking University High-throughput Sequencing Center operated by BIOPIC. This work was supported by funds from the National Basic Research Program of China (2010CB911800), the National Science Foundation of China (NSFC31170126, NSFC31070115), and the Peking-Tsinghua Centre for Life Sciences. Shiyou Zhu and Yuexin Zhou contributed equally to this work.

References

1. Barrangou R et al (2007) CRISPR provides acquired resistance against viruses in prokaryotes. Science 315:1709–1712
2. Jinek M et al (2012) A programmable dual-RNA-guided DNA endonuclease in adaptive bacterial immunity. Science 337:816–821
3. Cong L et al (2013) Multiplex genome engineering using CRISPR/Cas systems. Science 339:819–823
4. Mali P et al (2013) RNA-guided human genome engineering via Cas9. Science 339:823–826
5. Zhou Y et al (2014) High-throughput screening of a CRISPR/Cas9 library for functional genomics in human cells. Nature 509:487–491
6. Wang T, Wei JJ, Sabatini DM, Lander ES (2014) Genetic screens in human cells using the CRISPR-Cas9 system. Science 343:80–84

7. Shalem O et al (2014) Genome-scale CRISPR-Cas9 knockout screening in human cells. Science 343:84–87
8. Koike-Yusa H, Li Y, Tan EP, Velasco-Herrera Mdel C, Yusa K (2014) Genome-wide recessive genetic screening in mammalian cells with a lentiviral CRISPR-guide RNA library. Nat Biotechnol 32:267–273
9. Doench JG et al (2016) Optimized sgRNA design to maximize activity and minimize off-target effects of CRISPR-Cas9. Nat Biotechnol 34:184–191
10. Doench JG et al (2014) Rational design of highly active sgRNAs for CRISPR-Cas9-mediated gene inactivation. Nat Biotechnol 32:1262–1267
11. Peng J, Zhou Y, Zhu S, Wei W (2015) High-throughput screens in mammalian cells using the CRISPR-Cas9 system. FEBS J 282:2089–2096
12. Li W et al (2014) MAGeCK enables robust identification of essential genes from genome-scale CRISPR/Cas9 knockout screens. Genome Biol 15:554

Chapter 12

High-Throughput Screening for Identification of Novel Innate Immune Activators

Bryan J. Gall and Victor R. DeFilippis

Abstract

Modern drug discovery has embraced in vitro platforms that enable investigation of large numbers of compounds within tractable timeframes and for feasible costs. These endeavors have been greatly aided in recent years by advances in molecular and cell-based methods such as gene delivery and editing technology, advanced imaging, robotics, and quantitative analysis. As such, the examination of phenotypic impacts of novel molecules may only be limited by the size of the compound collection. Innate immune signaling processes in mammalian cells are especially amenable to high-throughput screening platforms since the cellular responses elicited by their activation often result in high level transcription that can be harnessed in the form of bioluminescent or fluorescent signal. In addition, targeted activation of innate immune pathways represents a valuable therapeutic strategy applicable to multiple chronic and acute human diseases. Herein, we describe the optimization and utilization of a high-throughput screening method using human reporter cells reactive to stimulation of the type I interferon response. Importantly, the principles and methods described can be applied to adherent reporter cells of diverse derivation and innate signaling pathway readouts.

Key words STING, Drug discovery, High-throughput screening, Innate immunity, Signaling

1 Introduction

Activation of innate immune signaling in mammalian cells culminates in the synthesis and release of factors such as cytokines, chemokines, and effector molecules that confer key immunological outcomes. These include establishment of tissue inflammation [1], direct impairment of microbial replication [2], and potentiation of adaptive immune responses [3]. As such, molecules capable of triggering these pathways are being sought with the intent to develop novel immunotherapeutic drugs to treat infectious diseases and cancer but also to enhance vaccination and even to investigate novel cellular processes [4]. Conventional innate immune signaling is initiated through the engagement of pattern recognition receptors (PRRs) including Toll like receptors (TLRs), NOD like

Karen Mossman (ed.), *Innate Antiviral Immunity: Methods and Protocols*, Methods in Molecular Biology, vol. 1656, DOI 10.1007/978-1-4939-7237-1_12,

receptors (NLRs), RIG-I-like receptors (RLRs), C-type lectin receptors (CLRs), and AIM2-like receptors (ALRs) by biologically derived ligands such as pathogen- or danger-associated molecular patterns (i.e., PAMPs, DAMPs) [5]. PRR-dependent signaling can lead to the activation of transcription factors especially interferon regulatory factors (IRFs) and nuclear factor κB (NF-κB) that induce synthesis of multiple crucial immune mediators including the type I interferons (IFNs), proinflammatory interleukins (IL-1β, IL-6, IL-8), and antiviral effector genes (IFIT1/2, ISG15, Viperin). Alternatively, signaling from some ALRs and NLRs activates a Caspase 1 complex termed the inflammasome that proteolytically processes immature forms of IL-18, IL-33, and IL-1β to enable their secretion. Many innate cytokines, in turn, can feed back and amplify transcriptional signaling via paracrine and autocrine loops. Fundamentally, however, the terminal factors induced and phenotypes elicited by innate immune signaling are determined by the cell type exposed, chemical structure of the stimuli, the PRR(s) activated, and the downstream signaling molecules expressed.

PRRs have evolved to optimally interact with specific molecular patterns and many molecular patterns (e.g., dsRNA, dsDNA) can activate multiple PRRs. Importantly, numerous small molecule agonists have been discovered and subsequently optimized that stimulate innate immune reactivity via PRR-dependent pathways with specificity. The number of cellular pathways potentially targeted for therapeutic benefit has increased dramatically in recent years in parallel with access to large and highly diverse molecule libraries. As such, efficient exploration of this resource for discovering molecules that stimulate desirable cellular responses necessitates experimental strategies amenable to high volume interrogation. Pharmaceutical and academic laboratories now routinely apply in vitro high-throughput screening (HTS) techniques as a molecular and drug discovery platform. The feasibility of cell-based HTS has been augmented by the development and optimization of novel bioluminescent enzymes [6] and fluorescent proteins [7] as cell-based signals that are measured using increasingly sensitive detection devices [8]. In addition, transgenic technologies such as lentivectors, transposons, and CRISPR/Cas9-mediated genome editing have facilitated the construction of cell lines that function as quantifiable indicators of pathway activation. In fact, many such lines are currently commercially available along with the vectors and reagents for constructing them as well as the reagents for reading and optimizing their signal emission.

The purpose of this protocol is to provide a generalized strategy for growing, stimulating, optimizing, and evaluating innate reporter cell lines for the purpose of screening chemical libraries to identify novel inducers of innate immune pathways. We describe the use of life-extended human fibroblasts that contain a firefly (*Photinus pyralis*) luciferase open reading frame driven by

an IFN-dependent response element [9]. However, it is important to note that most of the methods presented here will be applicable to adherent cell types of diverse origin. This should therefore be treated as a general guide for cell-, stimulus-, and innate pathway-specific molecule screening. For a more detailed description of HTS guidelines, the reader is referred to the *NCGC Assay Guidance Manual and HTS Guidance Criteria* (https://www.ncbi.nlm.nih.gov/books/NBK53196/). The HTS process requires a number of additional considerations beyond conventional assays, including signal optimization, miniaturization, and reproducibility. Due to the large number of molecules that must be examined, many HTS experiments test compounds in either duplicate or singlet. A high degree of accuracy, precision, and sensitivity is therefore required to identify active compounds (i.e., "hits" or "lead compounds"). Consequently, it is critical that HTS assays are properly **optimized** to minimize experimental variability and achieve the greatest signal-to-noise ratio to minimize false positives and negatives. Importantly, Z-factor is a robust statistic incorporating both dynamic range and variability of the assay making it possible to determine how manipulation of assay dependent variables affects the quality of the HTS assay. In particular, it is important to determine the optimal treatment duration, positive control and test compound concentrations, and reporter cell density. The number of compounds needed to be screened may also necessitate **miniaturization** of the assay in such a way that minimizes the use of costly reagents, and often are ultimately performed in 384- or even 1536-well plates, which must be independently validated by the Z' factor. Additionally, it is important to address assay **reproducibility** by comparing results well-to-well, plate-to-plate, and day-to-day.

The purpose of this chapter will be to describe optimization of a screening assay to identify small molecule agonists of IRF3- or IFN-dependent signaling using adherent mammalian reporter cells although the principles and methods are broadly applicable to other innate immune pathways.

2 Materials

2.1 Equipment

1. CO_2 tissue culture incubator for cell growth and maintenance.
2. Platform rocker.
3. Multi-mode plate reader or luminometer.
4. 12-well multichannel pipette.
5. Water bath.
6. Hemocytometer.

2.2 Reagents and Solutions

1. Dimethyl sulfoxide (DMSO).
2. Trypsin.
3. Culture medium: cell type compatible media (e.g., DMEM, RPMI 1640), 10% heat inactivated fetal bovine serum (FBS), 100 I.U./mL penicillin, 100 μg/mL streptomycin.
4. Maintenance media: cell type compatible media (e.g., DMEM, RPMI 1640), 2% heat inactivated fetal bovine serum (FBS), 100 I.U./mL penicillin, 100 μg/mL streptomycin.
5. Recombinant purified human type I IFNβ.
6. Sendai virus (Cantell strain; Charles River).
7. High-throughput quantitation of firefly (*Photinus pyralis*) luciferase expression kit (e.g., Promega SteadyGlo® reagent).
8. High-throughput quantification of cell viability kit (e.g., Promega CellTiter Glo® reagent).

2.3 Consumables

1. 96-well flat clear-bottom white polystyrene tissue culture-treated plates.
2. 96-well clear polystyrene tissue culture-treated plates for limiting dilutions.
3. 225cm^2 tissue culture-treated flask for expansion of cells.
4. Low-binding 96-well polypropylene Microwell™ plates.

3 Methods

3.1 Optimizing Positive Control Stimuli Conditions

1. Trypsinize and count reporter cells. Resuspend at 400 cells per μL in culture medium.
2. Using multichannel pipette add 50 μL cell suspension per well (2×10^4 cells per well) to a white 96-well plate and incubate at 37 °C and 5% CO_2.
3. After 18 h remove media and, in quadruplicate, carefully (*see* **Note 1** and Fig. 1) replace with 50 μL pre-warmed maintenance media (*see* **Note 2**) containing the following stimuli: maintenance media alone (negative control); IFNβ at 1000 U, 500 U, 200 U, 100 U, 50 U, 25 U, 10 U, 5 U, or 1 U per mL; Sendai virus (SeV) at 160, 80, 40, 20, or 10 HA units per mL (*see* **Note 3**).
4. Rock slowly at 37 °C and 5% CO_2 for 8 h.
5. Thaw SteadyGlo luciferin to room temperature and add 50 μL directly to all treated wells using multichannel pipette (*see* **Note 4**).
6. Set luminometer or plate reader to detect luminescence with a 1 s integration time and auto-gain turned on (*see* **Note 5**). Acquire luminescence signal per well within 30 m according to the manufacturer's instructions.

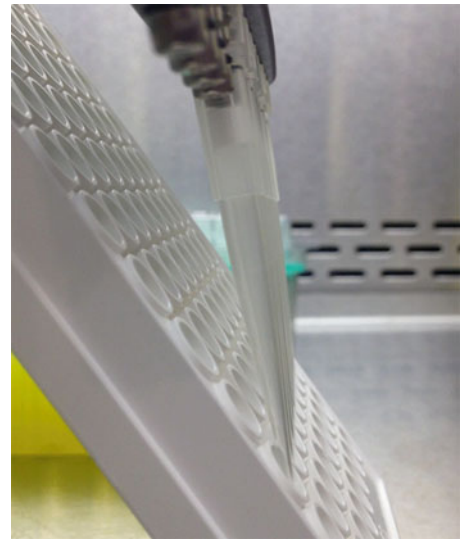

Fig. 1 General suggestion for addition of solutions to a 96-well plate containing cells. Tilt the plate at a 75° angle and keep the multichannel pipet vertical. Add media at the slowest possible dispense rate to minimize disruption of the cell monolayer

7. **Z factor calculation** – use the values from the quadruplicate treatments to calculate the Z factor as:

$$\textbf{Z factor} = 1 - \left[3\left(\sigma_p + \sigma_n\right)/\left|\mu_p + \mu_n\right|\right]$$

σ_p = standard deviation of stimulus-treated sample

σ_n = standard deviation of negative control

μ_p = mean luminescence of stimulus-treated sample

μ_n = mean luminescence of negative control

8. Select concentration of control stimulus for future assays that have a Z factor value closest to 1 in accord with these quality criteria ranks [10]:

Z Factor	Interpretation
1.0	Ideal assay
0.5 to <1.0	Excellent assay
>0.0 to <0.5	Marginal assay
0.0	Poor assay

9. In the event that Z factors between 0.5 and 1 are not observed, it may be necessary to identify alternate assay parameters. For example, alternate positive control stimuli, mono- or oligoclonal reporter cells that exhibit improved dynamic range, altering cell number, or varying treatment time.

	1	2	3	4	5	6	7	8	9	10	11	12
A	5×10^3	5×10^3	1×10^4	1×10^4	1.5×10^4	1.5×10^4	2×10^4	2×10^4	2.5×10^4	2.5×10^4	3×10^4	3×10^4
B	5×10^3	5×10^3	1×10^4	1×10^4	1.5×10^4	1.5×10^4	2×10^4	2×10^4	2.5×10^4	2.5×10^4	3×10^4	3×10^4
C	5×10^3	5×10^3	1×10^4	1×10^4	1.5×10^4	1.5×10^4	2×10^4	2×10^4	2.5×10^4	2.5×10^4	3×10^4	3×10^4
D	5×10^3	5×10^3	1×10^4	1×10^4	1.5×10^4	1.5×10^4	2×10^4	2×10^4	2.5×10^4	2.5×10^4	3×10^4	3×10^4
E	5×10^3	5×10^3	1×10^4	1×10^4	1.5×10^4	1.5×10^4	2×10^4	2×10^4	2.5×10^4	2.5×10^4	3×10^4	3×10^4
F	5×10^3	5×10^3	1×10^4	1×10^4	1.5×10^4	1.5×10^4	2×10^4	2×10^4	2.5×10^4	2.5×10^4	3×10^4	3×10^4
G	5×10^3	5×10^3	1×10^4	1×10^4	1.5×10^4	1.5×10^4	2×10^4	2×10^4	2.5×10^4	2.5×10^4	3×10^4	3×10^4
H	5×10^3	5×10^3	1×10^4	1×10^4	1.5×10^4	1.5×10^4	2×10^4	2×10^4	2.5×10^4	2.5×10^4	3×10^4	3×10^4

Fig. 2 Suggested 96-well plate format for optimizing cell number per well. IFNβ or SeV is added to red wells as a positive control and media to blue wells as negative controls

10. Repeat protocol treating the cells with the optimal concentration of IFNβ or SeV in a checkerboard pattern, with media treatment in alternate wells. Plot the data from each well on a XY scatterplot. Although "significance" of edge effect is dependent on the assay, we recommend maintaining a CV ≤10% (*see* **Note 6**; Fig. 3).

3.2 Optimizing Cell Numbers and Assay Timing

1. Plate cells at 5×10^3, 1×10^4, 1.5×10^4, 2×10^4, 2.5×10^4, or 3×10^4 per well in four replicate white 96-well plates in 50 μL culture medium and incubate in a tissue culture incubator at 37 °C and 5% CO_2 as indicated in Fig. 2.
2. After 18 h remove media and replace with 50 μL maintenance media (negative control) or containing IFNβ or SeV at ideal concentrations as identified above in replicates of eight.
3. Read luminescence from one 96-well plate per time point as described above (3.1D-E) at 8 h, 16 h, 24, and 48 h posttreatment (*see* **Note 7**).
4. Calculate Z factors as described above (3.1 #7) for each time point and cell density grouping. The combination leading to the optimal Z factor should be utilized for future assays.
5. Optimization of cell numbers for 384-well format can be performed similarly by assuming growth area of these plates per well is approximately 17.5% that of standard 96-well plates and thus cell numbers to be examined should be decreased accordingly.

3.3 Primary Screen

3.3.1 Prepare Cells

1. Plate cells in 50 μL of culture medium at optimal cell number determined above and incubate overnight at 37 °C and 5% CO_2.
2. Using a multichannel aspirator, carefully remove medium from cells.
3. Slowly add 50 μL of pre-warmed (*see* **Note 8**) maintenance medium to the cells (*see* **Note 1** and Fig. 1).

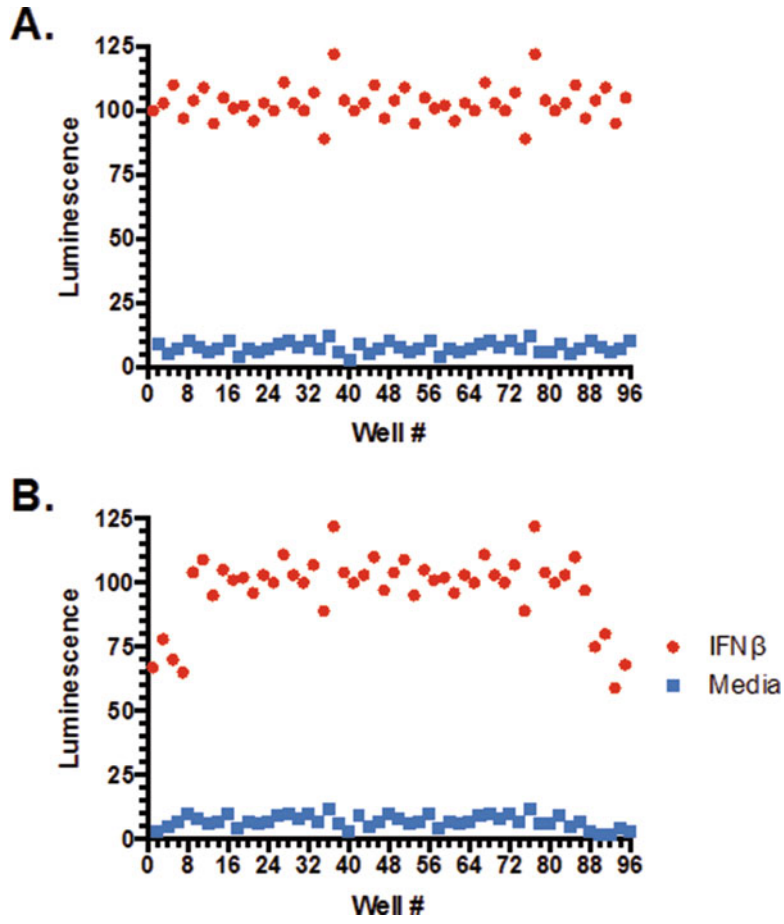

Fig. 3 Results indicating (**a**) a lack of edge effect with similar results across all 96 wells, or (**b**) clear edge effect with columns on the left and right of the plate having lower results

4. Optional: Serum-starve the cells with maintenance medium for optimal time, as previously determined, at 37 °C and 5% CO_2 (*see* **Note 2**).
5. During incubation proceed to compound dilutions (Subheading 3.3.2).

3.3.2 Compound Dilutions

1. Resolubilize test molecules to 10 mM in DMSO (*see* **Note 9**).
2. Make multiple aliquots of each at a volume that is sufficient for future experiments.
3. In a separate 96-well plate dilute the test molecules 1:5 in DMSO to obtain a concentration of 2 mM (100% DMSO).
4. In a separate 96-well dilution plate, dilute the 2 mM stock 1:50 in pre-warmed maintenance media to obtain a concentration of 40 μM (2% DMSO). This is the 2× stock solution. Also make

	1	2	3	4	5	6	7	8	9	10	11	12
A	Positive control	1	9	17	25	33	41	49	57	65	73	81
B	Positive control	2	10	18	26	34	42	50	58	66	74	82
C	Positive control	3	11	19	27	35	43	51	59	67	75	83
D	Positive control	4	12	20	28	36	44	52	60	68	76	84
E	Negative control	5	13	21	29	37	45	53	61	69	77	85
F	Negative control	6	14	22	30	38	46	54	62	70	78	86
G	Negative control	7	15	23	31	39	47	55	63	71	79	87
H	Negative control	8	16	24	32	40	48	56	64	72	80	88

Fig. 4 Suggested 96-well plate format for HTS of 88 molecules per plate

negative control wells with 2% DMSO (*see* **Note 10**). Recommended compound and control plating is indicated in Fig. 4.

3.3.3 Treatment and Readout

1. Using a multichannel pipet, gently transfer 50 μL of the 2× stock solutions from the dilution plate to the reporter cells. This results in a final concentration of 20 μM (1% DMSO) (*see* **Note 11**).
2. Incubate cells at 37 °C and 5% CO_2 for the time period determined during assay optimization.
3. Bring SteadyGlo® reagent to room temperature, avoiding prolonged exposure to light.
4. Set luminometer to detect luminescence with a 1 s integration time and auto-gain turned on.
5. Remove 96-well test plates from the incubator.
6. Using a multichannel pipettor, add 100 μL of the 2× SteadyGlo® reagent directly to the 100 μL of culture media in each well.
7. Incubate the plate at room temperature for at least 5 min to allow cell lysis.
8. Read plate in luminometer following the manufacturer's instructions.

*3.3.4 Identify Lead Compounds (See **Note 12**)*

1. Calculate the mean (μ_{DMSO}) luminescence and standard deviation (σ_{DMSO}) of the 1% DMSO treated wells.

2. Lead compounds will ideally have elicited a mean luminescence greater than $\boldsymbol{\mu_{DMSO} + 3(\sigma_{DMSO})}$.
3. Secondary screens on lead compounds can include the following:
   (a) *Toxicity*: using Promega CellTiter-Glo® cell viability assay. Follow the same protocol as outlined with the following exceptions: [1] equilibrate assay plate with cells to room temperature, [2] add the 2× CellTiter-Glo® reagent in place of the 2× SteadyGlo® reagent, and [3] incubate for 10 min at room temperature before reading luminescence.
   (b) *Pathway Specificity*: using the same protocol outlined above using cells with the signaling pathway of interest knocked out (e.g., ΔIRF3). Small molecules acting on that pathway should not induce luminescence in these knockout cells
   (c) *Potency*: using the same protocol outlined above, treat cells with a range of concentrations of each lead compound.

4 Notes

1. Be careful not to disturb cell monolayer by avoiding physical contact of aspirator with cells and dispensing solutions slowly by adding media using a multichannel pipettor at the slowest dispense rate to the side of the 96-well plate by tilting the 96-well plate at a 75° angle and dispensing media from the pipette at a 0° angle (Fig. 1). Confirm the cell layer is not disturbed by microscopic examination.
2. Undefined solutions, like serum, are discouraged because they may contain cytokines that interfere with assay readout. Using low serum media reduces background signaling due to cytokines present in the fetal bovine serum, which may increase the background signal and affect the assay Z factor. Lot-to-lot variability in serum may also lead to experimental variability. Serum levels can be adjusted from 0 to 2% to minimize background signal, and an additional serum-starvation prior to addition of compounds may further reduce background signal. Serum-starving (0–2% FBS) cells for 1–16 h prevents the activation of signaling pathways by cytokines present in serum, and minimizes lot-to-lot variability caused by serum. If cells are sensitive to serum-starvation, chemically defined serum-free media, like OptiMEM or X-Vivo, can be used in place of serum-free culture media.
3. It is also important that a positive control is selected that most closely mimics the desired mechanism of action of identified hits.

For example, if looking for a direct STING agonist, the optimal positive control would be cyclic guanosine monophosphate-adenosine monophosphate (cGAMP), which activates STING via direct interaction. Inappropriate positive controls may work through other pathways and have different kinetics.

4. SteadyGlo reagent can be diluted in equal parts PBS pH 7.4 prior to addition to cell culture media without loss of signal. The 2× SteadyGlo® reagent is photosensitive and therefore should be protected from light using aluminum foil.
5. Auto gain function will automatically adjust the voltage sent to the photomultiplier tube detector. This adjusts the sensitivity of the instrument to the intensity of the signal coming from the well, and prevents saturation by intense luminescence and minimizes risk of weak signals being below detectable range.
6. Edge effects are often a result of differential evaporation of media in wells on the edges of the plate. Evaporation of media results in a concentration of compounds and media components that may differentially affect the response of cells in those wells. Steps to minimize this effect include [1] using plastic lids with condensation rings or commercially available plates with an additional reservoir to maintain homogeneous humidity or [2] plate cell-free media in wells with consistent edge effect and exclude them from your experimental design.
7. Read each plate individually. We have observed that the addition of the SteadyGlo reagent affects the pH of media in adjacent wells, which may alter readout.
8. Pre-warming media to 37 °C prevents stress to cells and activation of a cold-shock response, both of which can alter readout.
9. Insure proper homogenization of test compounds by pipetting the media repetitively until no visible particulates remain. The solution may require brief warming to 37 °C and continued agitation to solubilize. If necessary, further dilutions can be made adjusting the volume of stock added in the following steps accordingly. Adjust concentrations and dilution methods of test molecules to best suit your experimental system.
10. Insure compounds have not precipitated in serum-free media by macroscopic and/or microscopic examination for particulates. The solution may require brief warming to 37 °C and continued agitation to solubilize. If necessary, further dilutions can be made adjusting the volume of stock added in the following steps accordingly.
11. Avoid using DMSO concentrations in excess of 1%. If necessary confirm cell viability and use the appropriate negative control.

12. Some of the compounds that induce luminescence may be false positives or induce nonspecific increases in transcription. It is important to follow up with these lead compounds with a secondary assay, like Western blot or qPCR.

References

1. Qian C, Liu J, Cao X (2014) Innate signaling in the inflammatory immune disorders. Cytokine Growth Factor Rev 25:731–738
2. McNab F, Mayer-Barber K, Sher A, Wack A, O'Garra A (2015) Type I interferons in infectious disease. Nat Publ Group 15:87–103
3. Schenten D, Medzhitov R (2011) The control of adaptive immune responses by the innate immune system. Adv Immunol 109:87–124
4. Ulevitch RJ (2004) Therapeutics targeting the innate immune system. Nat Rev Immunol 4:512–520
5. Brubaker SW, Bonham KS, Zanoni I, Kagan JC (2015) Innate immune pattern recognition: a cell biological perspective. Annu Rev Immunol 33:257–290
6. Kaskova ZM, Tsarkova AS, Yampolsky IV (2016) 1001 lights: luciferins, luciferases, their mechanisms of action and applications in chemical analysis, biology and medicine. Chem Soc Rev 45:6048–6077
7. Chudakov DM, Matz MV, Lukyanov S, Lukyanov KA (2010) Fluorescent proteins and their applications in imaging living cells and tissues. Physiol Rev 90:1103–1163
8. Roda A, Mirasoli M, Michelini E, Di Fusco M, Zangheri M, Cevenini L, Roda B, Simoni P (2016) Progress in chemical luminescence-based biosensors: a critical review. Biosens Bioelectron 76:164–179
9. Defilippis VR, Sali T, Alvarado D, White L, Bresnahan W, Früh KJ (2010) Activation of the interferon response by human cytomegalovirus occurs via cytoplasmic double-stranded DNA but not glycoprotein B. J Virol 84:8913–8925
10. Zhang J, Chung T, Oldenburg K (1999) A simple statistical parameter for use in evaluation and validation of high throughput screening assays. J Biomol Screen 4:67–73

Chapter 13

Chromosome Conformation Capture for Research on Innate Antiviral Immunity

Yoon Jung Kim and Tae Hoon Kim

Abstract

Chromosome conformation capture (3C) technology has revolutionized our knowledge on chromatin folding and nuclear organization. This *cis*-loop detection approach can be used to identify candidate regulatory elements interacting with target gene of interest. This chapter introduces the application of 3C technique to investigate a dynamic alteration in the chromosome folding structure or genomic architecture resulting from interaction changes between the enhancer and its target gene. Innate antiviral immunity is one of the well-known gene induction systems, involving rapid first-line response to virus or pathogen to trigger gene expression changes in order to protect cells and to limit further infection. Thus, the 3C technique can be a powerful tool for exploring how enhancers control expression of immunity genes during virus infection. 3C assay consists of four major steps: Cross-linking with formaldehyde, restriction enzyme digestion, ligation of cross-linked DNA fragments, and quantitative data analysis. Here, we discuss in detail the design, application, and data analysis of a 3C experiment.

Key words Chromosome conformation, Cross-linking, Dilution limited ligation, Quantitative PCR, Relative interaction frequency

1 Introduction

Long-range enhancers of transcription are a fundamental component of the genomic regulatory architecture. They play critical roles in developmental patterning [1, 2], direct cell-type-specific gene expression [3], and can play a causative role in human diseases [4]. Recent advances in functional genomics approaches have revealed multiple mechanisms that enhancers employ to regulate their target genes, including specialized histone marks at enhancers that distinguish them from the other genomic regions, protein complexes that assemble on the enhancers, long-range chromosomal looping with the target promoters, and generation of transcripts known as enhancer RNAs (eRNAs). However, the details and dynamics of these mechanisms remain to be determined.

Karen Mossman (ed.), *Innate Antiviral Immunity: Methods and Protocols*, Methods in Molecular Biology, vol. 1656, DOI 10.1007/978-1-4939-7237-1_13,

Virus infection leads to considerable changes in the nucleus. Nucleosome remodeling and redistribution of open chromatin and histone modifications [5–8] result from virus infection. These changes are coordinated with chromosome folding changes that bring about appropriate interactions between enhancers and target genes to induce expression of genes necessary for innate antiviral immunity [9, 10]. Thus, transcriptional regulation is critical for innate immunity. Viral infection can be detected by nearly all cell types through pathogen recognition receptors (PRRs) and initiates a signaling cascade that culminates in the activation of the TFs, IRF3, and NFκB (Fig. 1) [11, 12]. In most cells, these TFs activate transcription of Type I IFN family [13]. Type I IFNs are secreted and bind a common receptor, IFNAR [14]. Engagement of IFNAR with IFNs activates a JAK-STAT signaling cascade activating ISGF3 [14, 15], which mediates activation of a host of interferon-stimulated genes (ISGs) that ultimately confer an antiviral state on the cell. A broader transcriptional profile of this cellular antiviral response includes enrichment of genes for antiviral, immune modulation, inflammation, and host defense [16]. Identification of relevant distal enhancers induced by viral infection will provide critical insights into long-range gene regulation that may underlie

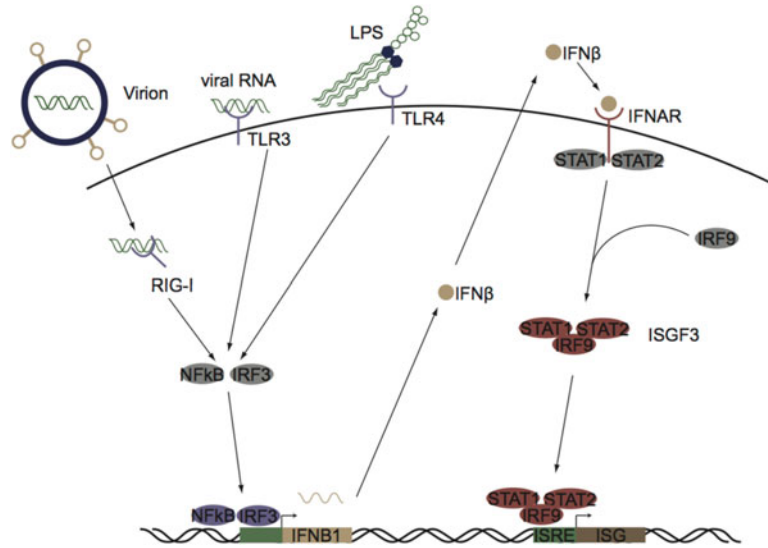

Fig. 1 Outline of Type I IFN activation and signaling. Schematic: Three key PRRs are RIG-I, TLR3 and TLR4. Cytosolic viral RNA is detected by RIG-I, while extracellular viral RNA is detected by TLR3. LPS is detected by TLR4. Pathogen pattern recognition leads to the activation NFκB and IRF3, which activate IFNβ production. IFNβ is secreted, binds to IFNAR, which activates STAT1 and STAT2. These TFs interact with IRF9 to form active ISGF3, which activates ISG expression

specific antiviral responses in different cell types and tissues against distinct pathogens.

Actively engaged *cis*-regulatory elements are known to form chromosomal loops with their target genes [17]. Chromosome Confirmation Capture (3C) technology was developed by Job Dekker and colleagues in 2002, and provided for the first time ability to study chromosomal folding and consequently contributed significantly to our understanding of nuclear organization and function [18, 19]. Over a decade later, the 3C technique still remains a major molecular approach used to interrogate physical proximity of two genomic regions within the nucleus. 3C interrogates interactions between selected pairs of DNA sites and is referred to as one-versus-one method, in contrast to one-versus-all (4C) or all-versus-all (HiC) [19]. The strategy relies on formaldehyde cross-linking of proteins to proteins or to DNA, the subsequent digestion of cross-linked DNA by restriction enzymes, the ligation of these ends, and quantitative frequency assessment of selected ligation junctions by PCR (Fig. 2a). If two distal sites on the linear chromosome form more ligation junctions with each other than with intervening sequences, a chromatin loop is demonstrated to exist between these sites in vivo [20]. 3C has been used to identify candidate regulatory elements that are physically associated with target genes in various developmental and disease contexts.

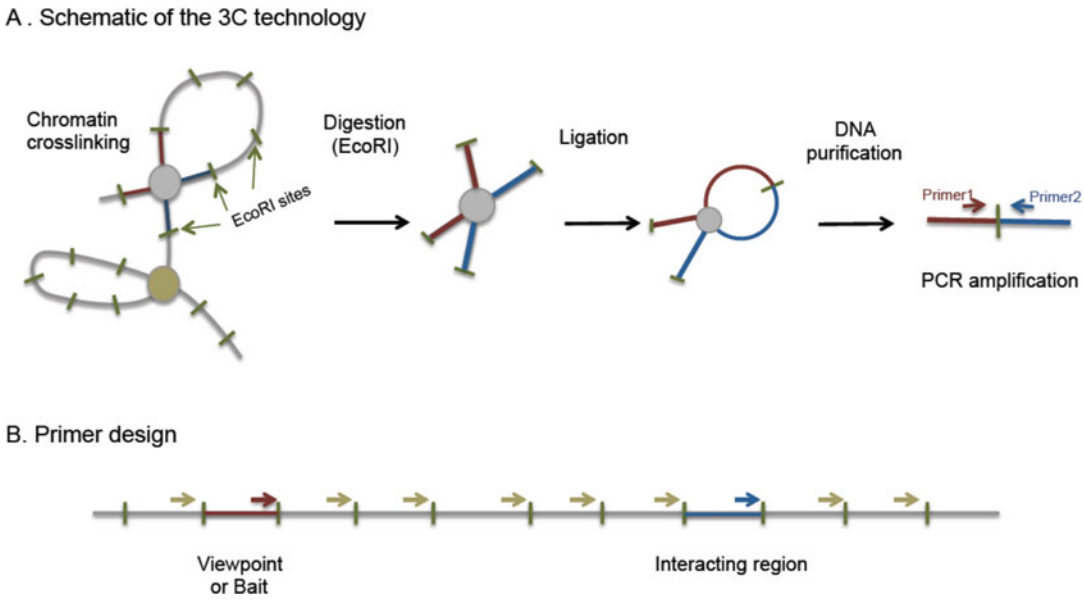

Fig. 2 Schematic of 3C assay. (**a**) 3C analyzes excised DNA fragments generated from formaldehyde cross-linked, then restriction enzyme digested chromatin to find interacting region where selected DNA regions are connected through a protein complex. The frequency and identity of these fragments are then determined by quantitative PCR (qPCR). (**b**) For 3C primer design, the forward direction sequences should be selected inside of the region less than 150 bp from the 3′ end of the digested DNA fragment

A recent paper from our laboratory demonstrated a successful use of 3C to find and characterize a novel long-range enhancer of IFNB1 upon the virus infection [9]. This chapter highlights the application of the 3C technique to investigate the alteration in chromosome structure or architecture upon virus infection [18, 20].

2 Materials

2.1 Reagents

1. 5–10 million cells (GM12878K or IMR90, etc.).
2. Cell culture medium: appropriate medium supplemented with 10% fetal bovine serum.
3. BAC (bacterial artificial chromosome) DNA.
4. 11% Formaldehyde solution: 50 mM Hepes pH 8.0, 0.1 M NaCl, 1 mM EDTA, 0.5 mM EGTA, 11% formaldehyde.
5. 1× phosphate-buffered saline (PBS).
6. 10 mM Tris (pH 8.0).
7. 3C Lysis buffer for cell lysis A: 10 mM Tris pH 8.0, 10 mM NaCl, 0.2% NP-40, 1× Protease Inhibitor.
8. 3C lysis buffer for cell lysis B: 50 mM Tris pH 8.0, 150 mM NaCl, 0.5% NP-40, 5 mM EDTA, 1% Triton X-100, 1× Protease Inhibitor.
9. 3C Restriction buffer: 100 mM Tris pH 7.5, 50 mM NaCl, 10 mM MgCl2, 0.3% SDS.
10. Protease inhibition cocktail 50× (e.g., Complete Protease Inhibitor tablets from Roche).
11. 10× ligation buffer.
12. 10% Triton X-100.
13. 300 mM NaOAc.
14. 5 M NaCl.
15. T4 DNA Ligase 400,000 unit/mL.
16. High concentrated EcoRI 100,000 unit/mL.
17. Glycogen.
18. 10% SDS.
19. Proteinase K (20 mg/mL).
20. RNase A (10 μg/mL).
21. Phenol: Chloroform:Isoamyl or phenol (Tris saturated).
22. Chloroform.
23. Ethanol 100% and 70%.
24. 0.8% Agarose gel containing EtBr.
25. LB media and plate containing 12.5 μg/mL chloramphenicol.
26. 2× SYBR qPCR mix (e.g., Roche).

27. Qubit DNA concentration measuring kit.
28. PCR primers (Primer1: viewpoints, Primer2: target regions).

2.2 Equipment

1. Agarose gel electrophoresis equipment.
2. Falcon tubes (15 mL and 50 mL).
3. Centrifuge (up to 18,514 × *g*, 4 °C or room temperature).
4. Dounce homogenizer and pestle.
5. Stirrer.
6. Incubators (37 °C and 65 °C).
7. Shaking incubator (37 °C).
8. Rotator.
9. Micro centrifuge.
10. Vortex machine.
11. Freezer.
12. Qubit machine and kit.
13. qPCR machine with 96-well setup.
14. PCR plates (96 well).
15. Nanodrop.
16. Gel image and quantification machine (e.g., Gel Doc-it from UVP or ChemDoc from BioRad).

3 Method—Chromosome Confirmation Capture (3C)

3.1 Cross-Link

1. Take 10 million cells and centrifuge for 3–5 min at 289 × *g* at room temperature.
2. Discard the supernatant and resuspend the pellet in 10 mL PBS or cell culture medium.
3. Add 1 mL of 11%-formaldehyde solution to a 1% final concentration.
4. Incubate for 15 min (should not incubate more than 15 min, ≤15 min) with rotating at room temperature.
5. Add 550 μL of 2.5 M Glycine to quench the cross-linking reaction by formaldehyde and incubate for 5 min at room temperature.
6. Centrifuge 1,575 × *g* for 5 min at 4 °C and discard the supernatant.

3.2 Cell Lysis

3.2.1 Cell lysis A

1. Resuspend the cell pellet in 10 mL cold lysis buffer with freshly added protease inhibitors.
2. Add a small magnetic stirrer and incubate on ice for 90 min with stirring on a stirrer plate.

3. Remove the magnetic bar, centrifuge for 15 min at 3,500 rpm at 4 °C and discard the supernatant.
4. Resuspend nuclei pellet in 5 mL of 1× PBS and count nuclei using a hemocytometer.
5. Centrifuge for 10 min at 3,500 rpm and remove the supernatant.

3.2.2 Cell lysis B

1. Resuspend the cell pellet in 500 μL mL cold lysis buffer with freshly added protease inhibitors.
2. Incubate for 15 min on ice.
3. Transfer the cell mixture to a dounce homogenizer. Break cells open on ice 15 stroke using pestle. Repeat another 15 stroke.
4. Transfer the lysate to a 1.7 mL microcentrifuge tube.
5. Centrifuge for 10 min at 3,500 rpm at 4 °C and remove the supernatant.

3.3 Digestion of Cross-Linked Chromatin

1. Resuspend the nuclei pellet in 500 μL of 3C restriction buffer with 0.3% SDS.
2. Centrifuge for 10 min at 3,500 rpm, 4 °C and discard the supernatant.
3. Resuspend the nuclei pellet in 500 μL of 3C restriction buffer with 0.3% SDS.
4. Incubate 1 h at 37 °C with shaking.
5. Add 100 μL of Triton X-100 to a final concentration 1.8% to sequester the SDS contained in 3C restriction buffer (*see* **Note 1**).
6. Incubate for 1 h at 37 °C with shaking.
7. Add 4000 U EcoRI (40 μL of 100 U/μL) and mix well (*see* **Notes 2–4**).
8. Digest overnight at 37 °C with shaking.

3.4 Ligation of Digested Chromatin

1. Add 120 μL 10% SDS to a final volume of 1.6% to inactivate the restriction enzyme.
2. Incubate at 65 °C for 20 min (*see* **Notes 5** and **6**).
3. Take 160 μL and divide in 4 aliquots of chromatin (around 2.5 million nuclei) in 15 mL falcon tube and then add the reagent below to dilute the digested chromatin in 8 mL ligase reaction solution:
   (a) 800 μL 10× ligation buffer.
   (b) 800 μL Triton-X-100 (1% final).
   (c) Distilled-water 6.24 mL to total volume 8 mL.

   The ligation is performed under large volume dilute conditions. These conditions allow intra-molecular ligation to occur more than inter-molecular ligation.

4. Incubate for 1 h at 37 °C with shaking.
5. Lower temperature to 16 °C and add 2000 U T4 DNA ligase (5 μL of 400 cohesive end units/μL).
6. Incubate for 2–4 h at 16 °C (*see* **Note 7**).

3.5 3C Ligation Purification

1. Split each 8 mL of 3C ligation into two 4 mL in 15 mL Falcon tubes.
2. Add 20 μL proteinase K (100 μg/mL final with 20 mg/mL Proteinase K stock solution) to each 4 mL tube and incubate at 65 °C overnight (*see* **Notes 8** and **9**).
3. Add 200 μL with RNase A (0.5 μg/mL final with 10 μg/mL RNase A stock solution) to each tube.
4. Incubate for 30 min at 37 °C.
5. Add 4 mL of phenol and mix vigorously by vortexing for 1 min at room temperature.
6. Centrifuge the 15 mL falcon tubes containing 8 mL mixture of 3C ligation and phenol for 15 min at 2,057 × *g* at room temperature.
7. Transfer the aqueous phase (~4 mL) in each tube to new 15 mL falcon tubes (*see* **Note 10**).
8. Repeat phenol extraction steps (**steps 5**–**7**).
9. Add 4 mL of chloroform into new tubes containing phenol extracted aqueous phase and mix vigorously by vortexing at room temperature.
10. Centrifuge for 15 min at 4,000 rpm at room temperature and transfer the aqueous phase (~4 mL) to a new 15 mL falcon tube (*see* **Note 11**).
11. Add 160 μL 5 M NaCl and 8 μL Glycogen.
12. Add 10 mL ice cold 100% ethanol to precipitate the DNA and mix gently by inverting the tubes.
13. Incubate −20 °C overnight or −80 °C at least for 30 min.
14. Centrifuge at 12,857 × *g* for 40 min at 4 °C.
15. Discard the supernatant and add 2–5 mL of 70% ethanol to cover the DNA pellet.
16. Centrifuge at 3,214 × *g* for 10 min at 4 °C (*see* **Note 12**).
17. Remove the supernatant and air dry for 2–5 min at room temperature.
18. Resuspend DNA pellet in 50 μL of 10 mM Tris buffer (pH 8.0).
19. Combine DNA solution together from 8 falcon tubes to be 400 μL total volume and store it at −20 °C before use (*see* **Note 13**).

3.6 3C BAC DNA Plasmid Preparation

See **Notes 14–17** before starting plasmid preparation.

1. Digest BAC DNA with EcoRI restriction enzyme (the same enzyme used for 3C sample preparation).
   (a) 50 μL DNA (100 μg of purified BAC plasmid).
   (b) 10 μL 10× EcoRI reaction buffer.
   (c) 5 μL EcoRI enzyme (100 U/μL).
   (d) 35 μL water (total volume up to 100 μL).
2. Incubate for more than 2 h at 37 °C.
3. Incubate 65 °C for 20 min to inactivate the enzyme and cool it down to 16 °C.
4. Ligate the digested BAC DNA by adding the belows:
   (a) 40 μL of 10× ligase buffer.
   (b) 5 μL of T4 DNA ligase (400 U/μL).
   (c) 255 μL of distilled water (up to 400 μL total).
5. Incubate overnight at 16 °C.
6. Add 20 μL of RNase A (0.5 μg/mL final with 10 μg/mL stock solution) to BAC control ligation solution and mix well.
7. Incubate for 30 min at 37 °C.
8. Add 400 μL of phenol and mix vigorously by vortexing for 1 min at room temperature.
9. Centrifuge for 5 min at 18,407 × *g* at room temperature.
10. Transfer the aqueous phase (~400 μL) to a new microcentrifuge tube.
11. Repeat phenol extraction steps (**steps 5–7**).
12. Add 400 μL of chloroform into the aqueous phase extracted by phenol and mix vigorously by vortexing at room temperature for 1 min.
13. Centrifuge for 5 min at 14,000 rpm at room temperature and transfer the aqueous phase (~400 μL) to a new tube.
14. Add 16 μL 5 M NaCl, 1 μL Glycogen.
15. Add 1 mL ice-cold absolute ethanol to precipitate the DNA and mix gently by inverting the tubes.
16. Incubate −20 °C overnight or −80 °C at least for 30 min.
17. Centrifuge at 14,000 rpm for 30 min at 4 °C.
18. Discard the supernatant and add 500 μL of 70% ethanol.
19. Centrifuge at 14,000 rpm for 10 min at 4 °C.
20. Remove the supernatant and air dry for 2–5 min at room temperature.
21. Resuspend DNA pellet in 50 μL of 10 mM Tris buffer (pH 8.0).
22. Store at −20 °C before use.

3.7 Quality and Quantity Check of 3C Library

1. To determine the quality of 3C library, run 1–5 μL of tenfold diluted 3C library on a 0.8% agarose TBE gel. The average DNA size digested by 6 bp-cutter restriction enzyme is around 4–5 kb. 3C library should be bigger than 8 Kb (*see* **Note 18**).
2. To determine the quantity of 3C library and BAC control library Qubit or picogreen kit should be used (*see* **Note 19**).
3. Test the 3C library by detecting PCR product with target primers.

3.8 Primer Design and qPCR

1. Decide on the genomic sites of interests (these are referred to as "viewpoints" or "baits").
2. Decide the target genomic regions or locus that you want to observe the interaction with the "viewpoints."
3. Based on the genomic information from **Step 1** to **Step 2**, determine a proper BAC DNA control plasmid or BACs, which should contain both "viewpoints" and its interacting target region.
4. Extract the DNA sequences digested by EcoRI restriction enzyme, which includes the viewpoints and target regions.
5. Design the forward direction primers inside of the region less than 150 bp from 3′ end of digested DNA fragment (Fig. 2b 3C primer design).
6. Test the primers using BAC control library by qPCR and redesign the primer if you cannot efficiently obtain positive PCR products (Ct value >25).

   (a) qPCR sample preparation.

	Volume
BAC DNA library	1 or 2 μL of 50 ng/μL DNA (Qubit concentration)
2× SYBR qPCR master mix (Roche)	5 μL
Primer 1 (viewpoint fragment)	1 μL of 10 μM
Primer 2 (target fragment)	1 μL of 10 μM
Distilled water	Up to 10 μL

(b) qPCR condition.

Step 1	98 °C	10 min
Step 2	98 °C	30 s
Step 3	60 °C	45 s
Cycle	Go to **step 2**	30 cycles
Melting curve		

7. Quantitative PCR with 3C and BAC library (*see* **Note 20**).
   (a) qPCR reaction sample preparation.

	Volume
3C sample or BAC DNA library	1 or 2 μL of 50 ng/μL DNA (Qubit concentration)
2× SYBR qPCR master mix (Roche)	5 μL
Primer 1 (viewpoint fragment)	1 μL of 10 μM
Primer 2 (target fragment)	1 μL of 10 μM
Distilled water	Up to 10 μL

   (b) qPCR condition.

Step 1	98 °C	10 min
Step 2	98 °C	30 s
Step 3	60 °C	45 s
Cycle	Go to **step 2**	45 cycles

3.9 Data Analysis

In this 3C assay, the aim is to measure the frequency with which two loci interact within cells. Individual 3C ligation DNA library or control library can be detected by qPCR using locus-specific primers. We can use the equation below to calculate interaction frequency:

3C interaction frequency = 3C ligation junction/whole genome ligation junctions.

However, whole genome ligation is technically difficult (~10^{12} possible junctions).

Therefore, BAC DNA containing the genomic locus of interest is used for a random ligation pool of control library.

$$\Delta Ct = \mathrm{Ct(3C)} - \mathrm{Ct(BAC)}$$

3C interaction frequency = $2^{-\Delta \mathrm{Ct}}$.

4 Notes

1. Triton X-100 sequesters the SDS and prevents SDS from inactivating the restriction enzyme.
2. 6 bp-cutter restriction enzymes, EcoRI, HindIII, or BglII are often used for 3C assay. Further digestion for 4C assay is performed by 4 bp-cutter restriction enzymes, DpnII, NlaIII, or Csp6I (CviQ1). This protocol uses EcoRI (GAATTC) for 3C library preparation.

3. Enzyme volume should not be larger than 10% of total reaction volume.
4. If you want to use 1 million cells only, you can take 60 μL of nuclei and scale down all reagent volume tenfolds.
5. The incubation at 65 °C with SDS effectively inactivates the restriction enzyme. Do not incubate more than 30 min at 65 °C. It would reverse the cross-links and loss of captured chromatin interaction.
6. You can stop at this step and store the digested chromatin sample at −80 °C.
7. If you want to apply this 3C library to 4C assay, you should extend the ligation time to 24 h or even 72 h to ensure complete circularization of ligation products.
8. Incubation with proteinase K at 65 °C overnight results in degradation of proteins and reversal of cross-links.
9. You can repeat the Proteinase K treatment (add 20 μL additionally and incubate for 2 h at 65 °C) if you want to increase the yield of 3C DNA.
10. You should take the aqueous phase as much as possible in this phenol/chloroform extraction steps. It will determine the yield of 3C DNA.
11. When the aqueous phase of the phenol/chloroform extraction is not clear, repeat phenol/chloroform extraction steps [5–10] until you get the clear aqueous phase. The relatively high concentration of the detergent (Triton X-100 and SDS) in the restriction buffer, and dithiothreitol (DTT) from 3C ligation buffer can result in the cloudy aqueous phase after first phenol/chloroform extraction.
12. To get rid of all of the salt from the DNA pellet, multiple washes (~five times, **steps 15–16**) with 70% ethanol are required.
13. Here you can apply another phenol/chloroform extraction steps.

    Add 400 μL of phenol solution into 1.7 mL microcentrifuge tube containing 400 μL of DNA solution from **step 19** and vortex vigorously. Centrifuge for 10 min at 14,000 rpm at room temperature. Transfer the aqueous phase (~400 μL) to a new 1.7 mL microcentrifuge tube. Add 400 μL of chloroform and vortex vigorously. Centrifuge for 10 min at 14,000 rpm at room temperature. Transfer 400 μL of the aqueous phase to a new tube. Add 40 μL of 3 M sodium acetate (pH 5.2) to each tube, mix, and add 1 mL of ice-cold absolute ethanol to precipitate DNA. Mix gently and incubate for at least 30 min at −80 °C or overnight at −20 °C. Centrifuge at 14,000 rpm for 20 min at 4 °C and discard the supernatant. Add cold 70%

ethanol to the DNA pellet, mix gently, and centrifuge for 5 min at 14,000 rpm at 4 °C. Discard the supernatant and dry pellet for 2 min at room temperature. Resuspend the DNA pellet in 400 μL of 10 mM Tris buffer (pH 8.0).

14. Select a BAC DNA containing the genomic locus of interest using the UCSC genome browser (https://genome.ucsc.edu/). For large genomic regions, several BAC clones would be required to span the entire region.
15. Before the preparation of the BAC DNA control library, integrity of the clones should be confirmed by restriction fingerprint of the BAC clones (e.g., BamHI) compared to its virtual fingerprint generated from the genomic sequence obtained from UCSC genome browser. The virtual restriction digest map of the BAC clone insert (fragment sizes and gel image) can be obtained from the NEB cutter website (http://nc2.neb.com/NEBcutter2/).
16. To get single colonies, streak the cell from agar stock from the source (Invitrogen or BACPAC resource center) on an LB plate with 12.5 μg/mL chloramphenicol and incubate overnight at 37 °C. Next day pick a single colony of BAC clone and cultivate it in 2–3 mL of LB media with 12.5 μg/mL chloramphenicol overnight at 37 °C in the shaking incubator. Purify BAC plasmid DNA followed by BamHI digestion. Add 2 μL of 10× restriction buffer 3 (Red buffer in NEB) and 2 μL of restriction enzyme BamHI into the 10 μL of purified BAC DNA and incubate for 2 h at 37 °C. Run the digested plasmid DNA on 0.8% agarose/TBE gel for around 1 h at constant 80 v and compare to the size of DNA fragments of the BAC DNA digested with BamHI.
17. BAC plasmid purification—5 mL cell culture in LB media with 12.5 μg/mL chloramphenicol is spin down to get cell pellet and discard the supernatant. Add 250 μL of cold cell resuspension buffer (P1, 50 mM Tris–HCl pH 8.0, 10 mM EDTA, 100 μg/mL RNase A) and resuspend cell pellet and then add 250 μL of cell lysis buffer (P2, 200 mM NaOH, 1% SDS) and mix gently. Incubate not more than 5 min. Add 300 μL of cold neutralization buffer (P3, 3.0 M potassium acetate pH 5.5) and mix well by inverting the tube. Incubate on ice for 15 min and centrifuge at 14,000 rpm for 15 min at 4 °C. Transfer the supernatant carefully to a new tube containing 0.67 μL of cold isopropanol and mix well. Incubate at least for 5 min on ice (or overnight at −20 °C) and centrifuge at 14,000 rpm for 20 min. Discard the supernatant and wash the plasmid DNA pellet with 70% ethanol. Resuspend the pellet in 50 μL of 1 0 mM Tris buffer (pH 8) and check OD of the BAC plasmid DNA using Nanodrop.

18. Multiple bands of less than 8 Kb or a large amount of smear could indicate inefficient ligation. In this case, one can extend the incubation time at 16 °C.
19. DNA concentration of 3C library measured by Nanodrop is not accurate.
20. Before qPCR, DNA concentration of 3C BAC library should be determined by using Qubit or Picogreen DNA concentration measuring kit. Make 50 ng/μL of each DNA template from 3C and BAC library (50 ng/μL or 100 ng/μL can be used for qPCR depending on the PCR efficiency).

References

1. Chan YF, Marks ME, Jones FC, Villarreal G Jr, Shapiro MD, Brady SD, Southwick AM, Absher DM, Grimwood J, Schmutz J et al (2010) Adaptive evolution of pelvic reduction in sticklebacks by recurrent deletion of a Pitx1 enhancer. Science 327:302–305
2. Sagai T, Hosoya M, Mizushina Y, Tamura M, Shiroishi T (2005) Elimination of a long-range cis-regulatory module causes complete loss of limb-specific Shh expression and truncation of the mouse limb. Development 132:797–803
3. Heintzman ND, Hon GC, Hawkins RD, Kheradpour P, Stark A, Harp LF, Ye Z, Lee LK, Stuart RK, Ching CW et al (2009) Histone modifications at human enhancers reflect global cell-type-specific gene expression. Nature 459:108–112
4. Visel A, Rubin EM, Pennacchio LA (2009) Genomic views of distant-acting enhancers. Nature 461:199–205
5. Decque A, Joffre O, Magalhaes JG, Cossec JC, Blecher-Gonen R, Lapaquette P, Silvin A, Manel N, Joubert PE, Seeler JS et al (2016) Sumoylation coordinates the repression of inflammatory and anti-viral gene-expression programs during innate sensing. Nat Immunol 17:140–149
6. Jankowski A, Obara P, Mathur U, Tiuryn J (2016) Enhanceosome transcription factors preferentially dimerize with high mobility group proteins. BMC Syst Biol 10:14
7. Wang Y, Zhong H, Xie X, Chen CY, Huang D, Shen L, Zhang H, Chen ZW, Zeng G (2015) Long noncoding RNA derived from CD244 signaling epigenetically controls CD8+ T-cell immune responses in tuberculosis infection. Proc Natl Acad Sci U S A 112:E3883–E3892
8. Avgousti DC, Herrmann C, Kulej K, Pancholi NJ, Sekulic N, Petrescu J, Molden RC, Blumenthal D, Paris AJ, Reyes ED et al (2016) A core viral protein binds host nucleosomes to sequester immune danger signals. Nature 535:173–177
9. Banerjee AR, Kim YJ, Kim TH (2014) A novel virus-inducible enhancer of the interferon-beta gene with tightly linked promoter and enhancer activities. Nucleic Acids Res 42:12537–12554
10. Sarkar D, Leung EY, Baguley BC, Finlay GJ, Askarian-Amiri ME (2015) Epigenetic regulation in human melanoma: past and future. Epigenetics 10:103–121
11. Theofilopoulos AN, Baccala R, Beutler B, Kono DH (2005) Type I interferons (alpha/beta) in immunity and autoimmunity. Annu Rev Immunol 23:307–336
12. Yoneyama M, Kikuchi M, Natsukawa T, Shinobu N, Imaizumi T, Miyagishi M, Taira K, Akira S, Fujita T (2004) The RNA helicase RIG-I has an essential function in double-stranded RNA-induced innate antiviral responses. Nat Immunol 5:730–737
13. Gobl AE, Funa K, Alm GV (1988) Different induction patterns of mRNA for IFN-alpha and -beta in human mononuclear leukocytes after in vitro stimulation with herpes simplex virus-infected fibroblasts and Sendai virus. J Immunol 140:3605–3609
14. Darnell JE Jr, Kerr IM, Stark GR (1994) Jak-STAT pathways and transcriptional activation in response to IFNs and other extracellular signaling proteins. Science 264:1415–1421
15. Taniguchi T, Ogasawara K, Takaoka A, Tanaka N (2001) IRF family of transcription factors as regulators of host defense. Annu Rev Immunol 19:623–655
16. de Veer MJ, Holko M, Frevel M, Walker E, Der S, Paranjape JM, Silverman RH, Williams BR (2001) Functional classification of interferon-stimulated genes identified using microarrays. J Leukoc Biol 69:912–920

17. Tolhuis B, Palstra RJ, Splinter E, Grosveld F, de Laat W (2002) Looping and interaction between hypersensitive sites in the active beta-globin locus. Mol Cell 10:1453–1465
18. Dekker J (2006) The three 'C' s of chromosome conformation capture: controls, controls, controls. Nat Methods 3:17–21
19. Dekker J, Marti-Renom MA, Mirny LA (2013) Exploring the three-dimensional organization of genomes: interpreting chromatin interaction data. Nat Rev Genet 14:390–403
20. Dekker J, Kim TH (2012) Cross-linking technologies for analysis of chromatin structure and function. CSH press, Cold spring harbor, New York

Chapter 14

Discovery of Variants Underlying Host Susceptibility to Virus Infection Using Whole-Exome Sequencing

Gabriel A. Leiva-Torres, Nestor Nebesio, and Silvia M. Vidal

Abstract

The clinical course of any viral infection greatly differs in individuals. This variation results from various viral, host, and environmental factors. The identification of host genetic factors influencing inter-individual variation in susceptibility to several pathogenic viruses has tremendously increased our understanding of the mechanisms and pathways required for immunity. Next-generation sequencing of whole exomes represents a powerful tool in biomedical research. In this chapter, we briefly introduce whole-exome sequencing in the context of genetic approaches to identify host susceptibility genes to viral infections. We then describe general aspects of the workflow for whole-exome sequence analysis together with the tools and online resources that can be used to identify and annotate variant calls, and then prioritize them for their potential association to phenotypes of interest.

Key words Host genetics, Antiviral immunity, Exome, Whole-exome sequencing, Sequence alignment, Read depth, Variant calling, Variant annotation, Gene annotation

1 Introduction

1.1 Value and Genetic Approaches to Identify Host Susceptibility Genes to Virus Infection

A characteristic feature of human infections, including virus infections, is that just a proportion of exposed individuals develop clinical disease. Even during the 1918 influenza pandemic, the more recent human immunodeficiency virus (HIV) epidemic or severe acute respiratory syndrome coronavirus (SARS-CoV) pandemic, only a proportion of individuals succumbed to infection [1, 2]. On the contrary, widespread pathogens that are innocuous for the most of the population, such as herpes simplex virus type 1 (HSV-1), can be fatal only to a very few [3]. It is now well established that host genetic variation is an important component of the varied onset, severity, and outcome of infectious disease. Such data have provided important insights into the pathogenesis of virus infections shedding light into antiviral mechanisms required for host defense.

Karen Mossman (ed.), *Innate Antiviral Immunity: Methods and Protocols*, Methods in Molecular Biology, vol. 1656, DOI 10.1007/978-1-4939-7237-1_14,

Several different, yet complementary approaches to the identification of genetic variation important in infectious disease progression have been taken. By far the most common approach has been to look for association in candidate genes using case–control studies. These studies have highlighted a few common, high-penetrance (*see* Table 1 for the definition of the terms) human genetic variants associated with infection and disease resistance due to virus receptor polymorphism. A homozygous 32 base-pair deletion in the chemokine receptor 5 (CCR5 Δ32) gene provides near complete protection against HIV-1 infection [4], whereas homozygous individuals with nonsense mutations in the fucosyltransferase 2, or FUT2, gene are almost completely protected from experimental and natural infections with norovirus [5]. In a second approach, genome-wide linkage analyses paired with candidate-gene approaches have led to the identification of rare large-effect genetic variants in susceptibility to infection against pathogens segregating in families. An excellent example is the dissection of the genetic architecture of childhood herpes simplex encephalitis (HSE), a rare life-threatening complication of primary infection with HSV-1 [6]. A body of elegant studies have revealed that children with mutations in the TLR3-UNC93B-TRIF-TBK1-TRAF3-IRF3 pathway are particularly susceptible to HSE [7], due to impaired CNS-intrinsic TLR3-dependent IFN-α/β and IFN-λ immunity to HSV-1 [8]. Candidate gene approaches, however, have been limited by their reliance on hypothesis based on—often incomplete—biological knowledge.

The sequencing of the human genome and the international HapMap project [9–11] led the way to Genome Wide Association

Table 1
Definition of terms (in alphabetic order)

Term	Meaning
Haplotype	A set of alleles that commonly segregate together and are defined as regions of extended linkage disequilibrium, which in humans is often up to 100 kb in length.
Indel	Insertions and deletions in a genome; the second most common type of variation after SNPs.
Minor allele frequency (MAF)	Refers to the frequency at which the second most common allele occurs in population.
Penetrance	Describes the proportion of individuals with a mutation or risk variant who have the disease. Incomplete penetrance is said when individuals carrying pathogenic mutations manifest no disease phenotype.
Rare allele	Allele present with MAF <1% (PMID: 19293820)
SNP	Single nucleotide polymorphism. Variation of a single nucleotide base, with the minor allele present in at least 1% of alleles in the population.
SNV	Single nucleotide variant. Minor allele frequency undefined.

Studies (GWAS) [12]. This approach does not require a prior hypothesis. Using large well-characterized cohorts of cases and controls, the whole genome is interrogated with a large set of genetic variants to possible association between a variant and the disease trait. One of the most remarkable successes of GWAS in infection diseases was the identification of *IFNL3* variants in association with the clearance of hepatitis C virus (HCV) following treatment (ribavirin and IFN-α) [13–15] or with spontaneous HCV clearance [16, 17], highlighting the importance of IFN-λ3 signaling in innate control of HCV [18].

GWAS applied to other viral infections have confirmed a major role for HLA genes in host susceptibility against HIV, Dengue and hepatitis B viruses and identified several new risk loci [19–21]. However, except for HCV mentioned before, non-HLA loci often span numerous linked genes and have modest effect size challenging their identification. Interestingly, these loci seem to behave in a pathogen-specific fashion, possibly delineating host-pathogen interactions that are specific to a given virus infection.

1.2 Power and Constraints of Whole-Exome Sequencing

In the past few years, the advent of next-generation sequencing technologies (NGS)—such as whole-exome sequencing (WES)—has revolutionized the biomedical field, including the discovery of many new mutations in patients with unexplained infections often seen at the immunodeficiency clinic [22–24]. WES provides a one-step simultaneous interrogation of virtually all exonic and adjacent intronic sequences, which has been remarkably successful both in a diagnostic setting sequencing and as a discovery tool (research exome sequencing) [25, 26].

These studies have been most effective for the discovery of rare, high-penetrance protein-coding variants for presumed monogenic disorders. A recent report counted that out of about 300 primary immuno-deficiencies characterized at the single gene level, close to 1/3 have been identified by NGS in the past 5 years [27]. WES discoveries have provided fresh insights into the mechanisms that control the development, function, and regulation of immune cells during response to infection (recently reviewed in [26, 28]). Notably, they have highlighted (1) pathways that are required for general protection against infection, generally involving genetic block in the T/B-lymphocyte differentiation program or result in absence of specific immune cells, and (2) pathways that are required for response to narrow groups of pathogens, somewhat reminiscent of infection-specific risk loci mapped by GWAS. An example of the latter was the discovery of compound heterozygous mutations in *IRF7* in a child suffering from life-threatening influenza [29]. Each parent was heterozygous for a single mutated allele, indicating autosomal-recessive segregation for the *IRF7*-deficiency. Detailed biochemical analysis indicated that both alleles were loss-of-function mutations, consistent with the mode of inheritance. Mechanistically, *IRF7*-deficiency was linked to both, lack of IFN-α

production in the patient's plamocytoid cells challenged with influenza virus and lack of intrinsic anti-viral immunity in patient-specific fibroblasts or pulmonary epithelial cells derived from induced pluripotent stem cells (iPSC). This study represented the first demonstration of a genetic cause for severe influenza in humans and may well pave the way for the discovery of other influenza susceptibility genes in the IRF7 pathway, akin to mutations in the TLR3-pathways underlying HSE.

The example above illustrates critical requirements for the successful application of WES, including variant prioritization and variant validation. The study design requires a substantial body of previous knowledge about the phenotype including the prevalence in the general population and the penetrance to help in surmising the mode of inheritance [27, 30]. This will dictate the selection samples (*see* **Note 1**). For situations in which there is a single affected case and no family history, sequencing the unaffected parents (as for IRF7-deficiency) permits efficient discovery of de novo mutations and compound heterozygous genotypes. The availability of multiple families with very similar clinical phenotypes substantially increases power for gene discovery.

However, prioritization of disease-causing variants by WES remains one of the main challenges due to the sheer number of variants found in individual exomes. The exome has been defined traditionally as the sequence encompassing all exons of protein-coding genes in the genome and covers between 1 and 2% of the genome [31–33]. Yet this portion houses 85% of the known disease causing variants [34, 35]. An individual exome typically harbors thousands of variants, compared to a reference genome, which are predicted to lead to nonsynonymous amino acid substitutions, alterations of conserved splice site residues, or small insertions or deletions. As presented below, various methods exist to identify which variants deleteriously affect the function of individual proteins. However, each genome is thought to harbor about 100 genuine loss-of-function variants with about 20 genes completely inactivated [36, 37]. Hence, rigorous criteria, including the absence of the candidate variant genotype in individuals without the clinical phenotype together with robust experimental validation, have been proposed to validate disease-causing variants [38]. Whereas study design and experimental approaches need to be developed in a case-by-case situation, below we will present the reagents and methodology for the discovery of and validation of candidate genetic variants in a typical exome-sequencing pipeline.

2 Materials

In addition to DNA samples from cases, their families, and the appropriate controls, the materials required for WES are a well-annotated reference genome, whole-exome capture DNA libraries, and computing facilities.

2.1 Annotated Reference Genome

The human reference assembly defines a standard upon which other whole genome studies are based. The last build of the human reference genome provided by the Genome Reference Consortium reports ~3×10^9 bases having coding and noncoding sequences. The exome is defined as all the exons for the 20,000 protein-coding genes in the human genome and all the exons pertaining to microRNA, small nucleolar RNA, and large intergenic noncoding RNA genes [39]. This information is not static and projects such as GENCODE [40] and RefSeq [41] continue to provide comprehensive annotation of both protein-coding genes and noncoding transcripts. The last assembly of human reference genome (GRCh38) can be accessed via the European Bioinformatics Institute and the Wellcome Trust Sanger Institute (Ensembl) [42] or the University of California Santa Cruz (UCSC) [43] genome browsers.

2.2 Whole-Exome Capture Library

Exome capture essentially consists of the steps of fragmenting a DNA sample, hybridizing the DNA to complementary oligonucleotide baits whose sequence has been designed to hybridize to exon regions. After binding to genomic DNA, these probes are pulled down and PCR amplified through the addition of adapters, allowing exon regions to be selectively sequenced. The most common and efficient strategies are in-solution capture methods offered by Roche/NimbleGen's SeqCap EZ Human Exome Library and Agilent's SureSelect Human All Exon. Several publications have compared the specificity and sensitivity of these platforms [44–46]. The NimbleGen's kit has the greatest bait density of any of the platforms and uses short (55 – 105 bp), overlapping baits to cover the target region [46]. This approach has been found to be an efficient method to cover the target region, sensitively detect variants and has a high level of specificity. Indeed, NimbleGen's kit shows fewer off-target reads than other platforms [46]. Importantly, this bait design has been found to show greater genotype sensitivity than the other platforms in difficult to sequence regions, such as areas of high GC content [44]. The Agilent's kit is the only platform to use RNA probes. The baits are longer than those used in NimbleGen's platform (114 – 126 bp) and the corresponding target sequences are adjacent to one another rather than overlapping. This design has been found to be good at identifying insertions and deletions (indels), because longer baits can tolerate larger mismatches [45].

2.3 High-Performance Computing Facility/Network for Data Storage and Maintenance of Pipelines for WES Analysis

Massively parallel short-read sequencing on NGS platforms typically results in the production of ~50–100 million reads per exome. This large volume of reads needs to be analyzed and stored. Moreover, software packages work best when tools and sequencing data are immediately available in the same network as accessing an external storage location for sequencing data slows down the process. High-performance computing infrastructure (HPC) and IT professionals are needed to access and storage of the generated and analyzed data. The most common infrastructure components

include HPC resources ranging from high-performance computing clusters to cloud computing resources, equipped with batch (queuing) systems, and commonly connected to shared-network-attached storage. Academic researchers have access to these services through national infrastructures, which provide HPC, storage, and ultra-high-speed network connectivity and remote access to research data. These systems are equipped with actively maintained bioinformatics suites for automation of WES analysis. The most widely used variant callers include the Sequence Alignment/Map (SAM) tools [47] and the Genome Analysis Tool Kit (GATK) [48, 49] developed by the Broad Institute. The latter was found the most efficient NGS variant caller in comparative studies [50] (*see* Table 2 for commonly used tools for WES and their weblinks).

3 Methods

A typical pipeline of WES analysis consists of the main following steps: (1) raw data QC and preprocessing, (2) sequence alignment mapping, (3) post-alignment processing, (4) variant analysis, (5) variant prioritization, and (6) variant validation (Fig. 1).

3.1 Raw Data Quality Control (QC) and Preprocessing

An effective QC is critical for a reliable data analysis, since this may affect downstream analysis results. The raw sequence output format for NGS is the FASTQ format (*see* Table 3 for commonly used file formats in WES), which incorporates (1) a text-based representation of sequences (FASTA format) and (2) a per-base quality score of the read provided by the sequencing instrument. The latter is a Phred-like score [51] assigned by an algorithm of the sequencing instrument that estimates the probability that a base is called incorrectly. Several tools have been developed for QC of raw sequence data. The most commonly used is the java script FastQC [52]; it can generate diagnosis plots such as distributions of base quality scores and GC content, N content, and sequence duplication levels. FastQC can also perform standard preprocessing procedure including adapter removal and trimming of low-quality bases at the ends of the reads.

3.2 Sequence Alignment Mapping

After raw data QC and preprocessing, the next step is to map the reads to the reference genome. This is arguably the most crucial step and most time-consuming operation of most WES analysis pipelines. The computational challenge resides in finding an alignment algorithm that is tolerant to imperfect matches, where genomic variations may occur, while being able to align millions of reads at a reasonable speed. To achieve high-speed most alignment algorithms are based on an effective compression algorithm, the Burrows–Wheeler Transformation (BWT) [53]. Many short-read

Table 2
Commonly used tools and weblinks for whole-exome sequence data analysis pipeline

Tool	weblink
Genome browser	
Ensembl	www.ensembl.org
UCSC	http://genome.ucsc.edu
Quality control	
FastQC	http://www.bioinformatics.babraham.ac.uk/projects/fastqc/
Short read mapping	
Bowtie	http://bowtie-bio.sourceforge.net/index.shtml
Bfast	http://bfast.sourceforge.net
Mosaik	https://github.com/wanpinglee/MOSAIK
BWA	http://bio-bwa.sourceforge.net/
Manipulate NGS data (mark duplicates, merge files)	
Picard tools	https://broadinstitute.github.io/picard/index.html
SAMTools	http://www.htslib.org/doc/samtools.html
Variant calling	
GATK	https://software.broadinstitute.org/gatk/
SAMTools	http://www.htslib.org/doc/samtools.html
Variant annotation: (1) Coding effect predictions	
SnpEff	http://snpeff.sourceforge.net/
VEP	http://ensembl.org/info/docs/tools/vep/index.html
SIFT	http://sift.jcvi.org/
PolyPhen2	http://genetics.bwh.harvard.edu/pph2/
Variant annotation: (2) Conservation	
PhyloP	http://compgen.bscb.cornell.edu/phast
GERP++	http://gvs.gs.washington.edu/GVS147/
CADD	http://cadd.gs.washington.edu/
Variant annotation: (3) Gene-level	
MSC	http://lab.rockefeller.edu/casanova/MSC
GAVIN	https://molgenis20.gcc.rug.nl/
Variant annotation: (4) integrative	
ANNOVAR	http://annovar.openbioinformatics.org/en/latest/user-guide/download/
Knowledge-based annotation	
HGPS	http://hgc.rockefeller.edu/
KEGG	www.genome.jp/kegg/
REACTOME	www.reactome.org/
MPO	www.informatics.jax.org/humanDisease.shtml
GEO	www.ncbi.nlm.nih. gov/geoprofiles
GXA	www.ebi.ac.uk/gxa
BioGPS	http://biogps.org
STRING	http://string-db.org
ToppGene	https://toppgene.cchmc.org
GeneMania	http://genemania.org

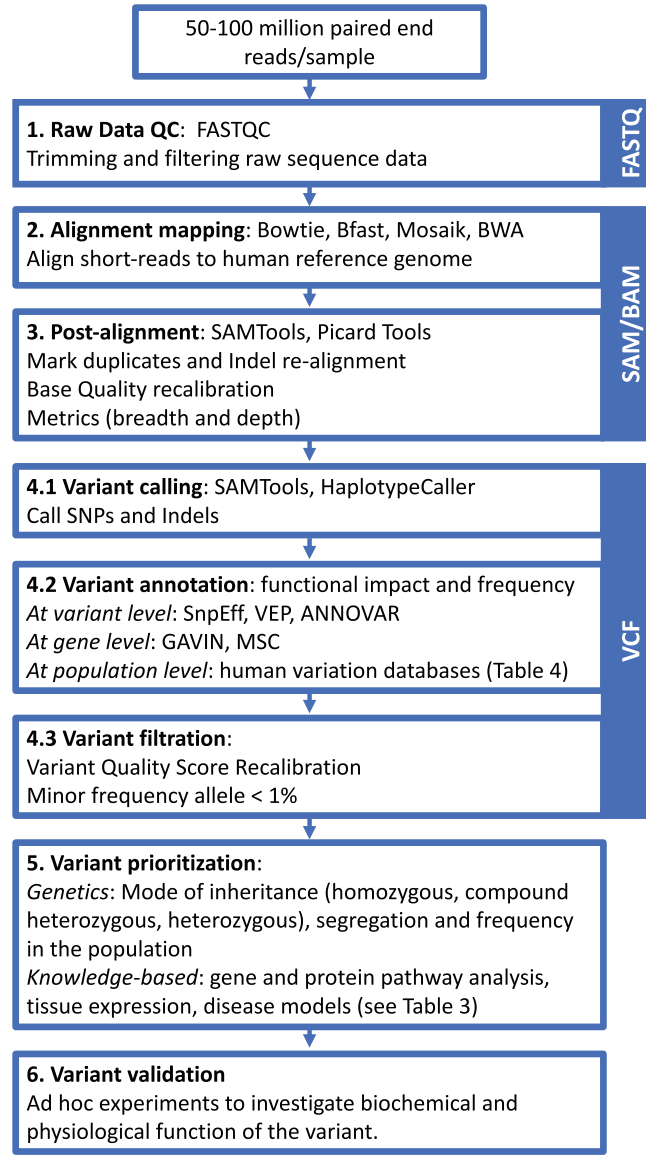

Fig. 1 Basic workflow and tools for whole-exome sequencing project. Following sequencing, reads undergo quality assessment and read alignment against a reference genome, followed by variant identification. The detected variants are annotated to infer their biological relevance. Then, variants are filtered based on quality of the read and frequency on the population. Then variants are prioritized based on the genetic hypothesis for the trait under study and knowledge about the candidate gene/protein. Ultimately, experimental validation is required to ascertain variant discovery. On the right the format outputs are indicated

aligners have been developed using this method: Bowtie [54], Bfast [55], Mosaik [56], and BWA [57]. They vary a lot in speed and accuracy, which are likely to affect the identification of structural variations and influence variant calling. BWA is the most common

Table 3
Description of commonly used file formats in WES workflows

Format	Characteristics
FASTQ file (.fastq)	Text file that stores nucleotide sequence and quality score for downstream analysis. There are typically four lines in a FASTQ file: (1) sequence identifier initialized "@"; (2) biological sequence of nucleotide reads (ACTG); (3) sequence identifier initialized "+"; (4) quality score of corresponding sequencing read, which is coded with ASCII characters.
Sequence alignment/map (SAM) file (.sam)	Text file that stores alignment information of short reads to reference genome. The SAM file contains multiple lines including a header initialized "@" and multiple lines for the sequence alignment.
Binary alignment/map (BAM) file (.bam)	Binary file (stored in a format that is only computer readable) containing the same information as the SAM file, the content of which has been compressed to reduce storage disk space and increase performance.
Browser extensible data (BED) file (.bed)	Tab-delimited text file that consists of several lines each representing a single genomic region, such as an exon. BED files provide the coordinates of those regions including chromosome, start and end positions, and additional fields can be added.
Variant call format (VCF) file (.vcf)	Text file containing meta-information lines (i.e., file format, date, or other information about the overall experiment), a header line naming the columns (chromosome #, position, ID, reference allele, alternative allele, quality, filte, infor), and then data lines each containing information about a position in the genome. It is a standardized text file format for representing SNP, indel, and structural variation calls.

choice of WES alignment [58]. It allows gapped alignment, using very little memory. It performs separated alignment on both strands of a paired-end lane, in multi-threaded execution, unifying results in a single mapping file in the Sequence Alignment Map (SAM) format [47].

3.3 Post-Alignment Processing

To enhance the quality of the alignments for more accurate variant detection, the pipeline carries out three "cleanup" procedures. They consist of read duplicate removal, base quality score recalibration (BQSR), and indel realignment. A final, intermediate step provides important metrics to assess the quality of the data.

3.3.1 Read Duplicate Removal

Many of the reads from massively parallel sequencing instruments are identical—same sequence, start site, and orientation—indicating PCR artefacts [59]. These duplicates may introduce a bias in estimating variant allele frequencies, thus it is advisable that they are removed prior to the variant calling. Programs such as the function rmdup from SAMTools [47] or PicardMarkDuplicates integrated in Picard Tools [49] apply optimal fragment-based duplicate identification and provide unique identifiers for each read group, i.e.,

the set of reads generated from a single run of an instrument. This allows minimizing of experimental noise, reducing the number of false calls and improving the accuracy in the search of the variants.

3.3.2 *Indel Re-Alignment*

Small insertions or deletions (Indels) in coding regions have been strongly associated with human diseases but accurate Indel calling remains difficult [60, 61]. The local realignment around Indels is an important step. This process searches a consensus alignment among all the reads spanning a deletion or an insertion or both (1) to improve Indel detection sensitivity and accuracy, and (2) to reduce variant false calls due to misalignment of the flanking bases. The alignment is improved by increasing the number of sequences in their local context. The program Haplotype Caller from GATK offers an efficient solution to Indel detection by generating local de novo assembly of aligned reads prior to Indel calling, improving Indel detection [62]. As presented in Subheading 4, the HaplotypeCaller is capable of calling variants and indels simultaneously, which improves Indel detection while producing more accurate variant calls.

3.3.3 *BQSR*

The per-base quality scores (Phred-score), which convey the probability that the called base in the read is the true sequenced base [51], are quite inaccurate and co-vary with features like sequencing technology, machine cycle, and sequence context. These inaccurate quality scores propagate into faulty SNP discovery [51]. BQSR is a process in which machine learning tools are applied to model these errors empirically and adjust the quality scores accordingly. One of the most commonly used BQSR programs is BaseRecalibrator from the GATK suite, which takes alignment files and for each unknown base, a re-calibrated quality score is calculated to be used for variant calling. Recalibrated scores better reflect the empirical probability of mismatches to the reference genome, and by doing so provide more accurate quality scores [48, 62].

3.3.4 *Metrics*

Biases in sample preparation, sequencing, genomic alignment, and assembly can result in genomic regions lacking coverage (i.e., gaps) or in regions with much higher coverage than theoretically expected. Hence to evaluate the quality of data to discover variants with reasonable confidence, two important metrics are the breadth and the depth of coverage of a target genome. Breadth of coverage denotes the percentage of bases that are sequenced a given number of times. Depth of coverage represents the number of reads that align at a given position, which is often quoted as average raw or aligned read depth. For example, a genome sequencing study may sequence a genome to 50× average depth and achieve a 95% breadth of coverage of the reference genome at a minimum depth of ten reads. The flagstat command from SAMtools [47] or DepthOfCoverage from GATK [48, 62] provides the calculation

of the fraction of reads that successfully mapped to the reference, with number and percentages of the read mapped and unmapped.

3.4 Variant Analysis

Following these treatment steps of the read, variant analysis consists of three independent steps: variant calling, annotation, and prioritization. Several open source tools are available for variant calling (Table 4).

3.4.1 Variant Calling

Variant calling implies identifying the sites in the sample that statistically differ from the reference genomic sequence. Single nucleotide polymorphisms (SNPs) and Indels are detected where the reads collectively provide evidence of variation (*see* **Note 2**). As with alignment tools, several open source tools are available to identify a high-quality set of variants in WES projects [63]. SAMtools [47] and GATK HaplotypeCaller [48, 62] are widely used in genomic variant analyses. HaplotypeCaller has been found to have high sensitivity for SNP detection and outperform other pipelines for

Table 4
Databases of human genetic variation

Name	Weblink and description
Combined annotation dependent depletion database (CADD)	http://cadd.gs.washington.edu/ Catalog of precomputed scores for all possible SNPs or small Indels of the reference genome and the 1000 Genomes obtained by combining 63 annotations (e.g., SIFT, GERP, others) through a machine-learning framework.
Single nucleotide polymorphism database (dbSNP)	https://www.ncbi.nlm.nih.gov/projects/SNP/ Broad collection of SNPs and Indels submitted by investigators worldwide and curated by NCBI.
Human gene mutation database (HGMD)	http://www.hgmd.org A catalog of all published gene lesions responsible for human inherited disease.
Exome aggregation consortium (ExAC)	http://exac.broadinstitute.org/ Catalogue of exome variation in 60706 individuals some with adult onset diseases (Type 2 Diabetes, schizophrenia) patients presenting severe pediatric diseases have been excluded.
1000 Genomes project	http://www.internationalgenome.org/ Catalogue of genome variation with at least 1% frequency in the population based on whole-genome sequencing of 2504 individuals from 26 populations (including study cohorts for adult onset diseases).
NHLBI exome sequencing project (ESP6500)	http://evs.gs.washington.edu/EVS/ Catalogue of variation within 6500 exomes from well-phenotyped populations from various projects, e.g. Severe Asthma Research Project; Pulmonary Arterial Hypertension population; Acute Lung Injury cohort; Cystic Fibrosis cohort.

Indels [50, 63]. HaplotypeCaller runs a "reading window" along the reference genome, comparing the reference to sequenced reads counting mismatches and Indels. These variations from the reference are used as a measure of entropy, or disorder in the read data. If the level of entropy within the reading window surpasses a cutoff score (default value can be changed), the window is marked as an Active Region, which is inspected to generate the plausible haplotypes. Then, HaplotypeCaller uses a Bayesian statistical model for the calculation of the probability of the genotype, estimating the accuracy of the call with a score of Phred-like quality. The results are reported in a standard Variant Call Format (VCF) file.

3.4.2 *Variant Annotation*

Annotation of disease-causing variants involves determining (1) the effect they have on the protein-coding sequence, including synonymous and non-synonymous changes, stop-gained or stop-lost, consensus splice site changes for SNPs, frame-shift or other structural impacts on transcript structure for Indels, (2) the frequency of the variant in the population, as disease-causing variants are expected to be rare.

1. Three major tools are used to classify variants functionally: SnpEff (**SNP Eff**ects) [64], VEP (Variant Effect Predictor) [65], and ANNOVAR (**Anno**tate **Var**iation) [66, 67]. SnpEff annotates variants based on their genomic location and predicts coding effects [64], as does VEP, a tool available from the genome browser, Ensembl [65]. Besides annotating functional effects of variants with respect to genes, ANNOVAR has many additional functionalities, such as integrating information from up to 4000 different databases and external resources to annotate the variants [67]. For SNPs, these include (1) calculating their predicted functional importance scores using SIFT (**S**orting **I**ntolerant **F**rom **T**olerant) [68] and PolyPhen2 (**Poly**morphisms **Phen**otyping v**2**) [69] and (2) reporting their conservation levels by PhyloP (**Phylo**genetic ***P***-values) [70, 71] and GERP++ (**G**enomic **E**volutionary **R**ate **P**rofiling) [72]. The CADD (**C**ombined **A**nnotation **D**ependent **D**epletion) database is another useful external linked for deleterious prediction of a variant. The CADD score combines information from several resources to score both protein-altering and regulatory variants [73].

   New tools are being developed for variant annotation that considers gene-level metrics (e.g., conservation at the gene-level, accumulation of mutational load) and provides more sensitive scoring of variants [74]. GAVIN (**G**ene-**A**ware **V**ariant **IN**terpretation for medical sequencing) classifies variants as benign, pathogenic, or a variant of uncertain significance [75]. The MSC (**M**utation **S**ignificance **C**utoff) [76] generates a quantitative score that provides gene-level and gene-specific phenotypic impact cutoff values above which a variant is considered pathogenic with 98% true positive detection rate.

2. To determine variant frequency, ANNOVAR links to external databases such as dbSNP database [77, 78] or the Human Gene Mutation Database [79] to identify the presence or absence of a variant (*see* Table 4 for commonly used databases of human genetic variation). Large-scale genomic studies such as 1000 Genomes Project [36], the US National Institutes of Health–National Heart, Lung, and Blood Institute (NIH-NHLBI), ESP6500 exome-sequencing project [80], and the Exome Aggregation Consortium [37, 81] have catalogued sequence variants from thousands of exomes and genomes, which serve as a valuable resource for allele frequency estimations. These resources are integrated in ANNOVAR, which can find the alternative allele frequency for newly discovered variants in a WES project. The GATK pipeline also integrates ANNOVAR as an external option for variant annotation and can use the tool VariantAnnotator, which is enriched with additional features such as gene set enrichment analysis for downstream analysis.

3.4.3 Variant Filtration

There are two aspects to variant filtration (1) filtering low-quality variants; (2) filtering common variants, which are represent in the general population.

1. Low-quality variants are those including variants with low coverage, low quality, strand biased, as well as those mapping to low-complexity regions or incomplete regions of the reference genome [82]. GATK uses machine learning algorithms (VQSR or variant quality score recalibration) to learn from each dataset what is the annotation profile of "good" and "bad" variants [48, 62]. The tool assigns scores (VQSLOD for variant quality score log-odds) which can be used to set the filtering of "bad" variants. There is tradeoff in the process in which increasing the specificity will decrease the sensitivity of the filtering. VQSR can be applied to SNPs or indels. The availability of in-house databases for WES variants obtained with the same sequencing technology and analysis pipeline is recommended to exclude variants resulting from systematic errors (*see* **Note 3**).
2. Under the assumption that common variants are less likely to cause disease than rare ones, it is important to set a minor allele frequency (MAF) threshold based on disease model of the study. A variant with a MAF greater than 1% is regarded as common; the remainder are considered rare or private to the subject or the kindred studied. Setting the MAF threshold at 1% is recommended, usually filters out over 70% of the variants [83].

3.4.4 Variant Prioritization

At this point the output is a subset of high-quality, low-frequency, predicted pathogenic variants, which require customized filtering process depending on the disease trait. The more information

gathered both on (1) the phenotype and (2) the gene in which the variant resides, the greater the likelihood to accurately assess the functional significance of a variant.

1. A deep knowledge of the clinical and cellular phenotype, the prevalence of the trait in the general population together with an understanding of the familial segregation are essential in the prioritization of gene variants. For example, a recessively inherited disease variant is likely homozygous whereas a dominant disease variant is heterozygous. In general, a dominant allele should be absent in a variant database based on healthy controls or exceedingly rare to allow for reduced penetrance. However, there can be exceptions to these rules. For instance, recessive disease variants can be compound heterozygous. In a cohort, the search for either identical variants or additional rare variants in the same gene can further strengthen the evidence for causality. Variants found in a gene in which other variants have already been associated with a certain phenotype are more likely to be associated with the same phenotype, although this is not always the case.

   Segregation of the variant with disease status is another key criterion for variant prioritization. This requires appropriate WES control data obtained with the same method from healthy subjects, ideally of the same ethnic origin as the patients. In case of complete penetrance, the candidate disease-causing variants found in patients cannot be present in unaffected subjects. In case of incomplete penetrance, the situation is more complex because these hypothetical disease-causing variants can also be present in asymptomatic subjects, including unaffected subjects of the same pedigree.

2. At the gene level, it is reasonable to first review variants found in genes that participate in its related pathways. This is also true when a phenotypically similar disease exists, and related pathways are known. The HGPS (**H**uman **G**ene **C**onnectome) ranks genes by their biological distance to core genes (known to be associated with phenotype), and provides the distances and all possible biological connections between all pairs of human genes based on protein-protein interaction prediction [74, 84]. Genes can be mapped online to KEGG (**K**yto **E**ncyclopedia of **G**enes and **G**enomes) pathways [85] or REACTOME pathways [86]. It is useful to find information about candidate genes-knockout phenotypes. For this, the Mouse Genome Informatics database enables queries for human–-mouse disease and MPO (**M**ammalian **P**henotype **O**ntology) connections using gene symbols as an input [87]. Expression of candidate gene in the tissues or organs of interest is an important criterion for prioritization. GEO (**G**ene **E**xpression **O**mnibus) profiles [88], the ExA (**Ex**pression **A**tlas [89], and the BioGPS gene annotation portals [90] are excellent resources

for this purpose. Knowledge about protein structure, function, and interactions also can help rank candidate genes. The UniprotKB (**Uniprot k**nowledge**b**ase) collects information from several databases including curated protein sequences and structures with links to annotations of genomic variants [91]. The STRING database and associated search tools [92] are powerful resources for identifying interacting partners of a candidate gene's product or for identifying interactions between the products of a set of genes that bear functional variants. The ToppGene [93] and GeneMania [94] web portals are other resources that perform candidate gene prioritization based on the interactome.

3.4.5 *Variant Validation*

With all the tools available and new ones emerging monthly, variant filtration and prioritization are becoming more automated. A similar trend is also observed in other parts of variant analysis such as the detection and annotation. Regardless, a deep understanding of the biological questions being asked and the etiology of the disease being studied is crucial for properly choosing tools and parameters that suit a study the best.

Ultimately, variant validation requires experimental confirmation at the level of protein, cell and—if possible—animal model to establish causality. This necessitates solid knowledge of physiology and pathology of the phenotype at the study for the design of appropriate experiments relevant to the nature of the protein. The recent breakthrough of genetic manipulation of human-induced pluripotent stem cells [95], CRISPR genome-editing tools [96, 97] permits establishing the causal relationship between the candidate genotype and the clinical phenotype in relevant cell types [98] or organoids [99] representing relevant tissues, even for isolated cases.

4 Notes

1. Broadly, the mode of inheritance can be recessive, dominant, or X-linked. Recessive mutations are easier to identify by filtering for homozygosity, or compound heterozygous mutations. Dominant inherited mutations will be either inherited from one of the parents or be de novo mutations, in both cases dominant mutations should be absent in unaffected family members or matched unrelated controls.
2. Joint application of variant calling software to multiple samples is recommended to reduce false positive variants. We can also improve variant calling in regions with fewer reads by utilizing reads from multiple samples concurrently. This increases the confidence of any given variant and allele bias and strand bias are much easier to sort.

3. The evaluation of family trios can also eliminate low-quality variants as the majority of variants detected in the child and absent from the parents most likely result from sequence artifacts. Moreover, the accuracy of error detection and variant identification increases with the number of relatives and generations sequenced per family.

References

1. Casanova JL (2015) Human genetic basis of interindividual variability in the course of infection. Proc Natl Acad Sci U S A 112(51): E7118–E7127
2. Herrington CS, Coates PJ, Duprex WP (2015) Viruses and disease: emerging concepts for prevention, diagnosis and treatment. J Pathol 235 (2):149–152
3. Zhang SY, Abel L, Casanova JL (2013) Mendelian predisposition to herpes simplex encephalitis. Handb Clin Neurol 112:1091–1097
4. Dean M et al (1996) Genetic restriction of HIV-1 infection and progression to AIDS by a deletion allele of the CKR5 structural gene. Hemophilia growth and development study, multicenter AIDS cohort study, multicenter hemophilia cohort study, San Francisco City cohort, ALIVE study. Science 273 (5283):1856–1862
5. Lindesmith L et al (2003) Human susceptibility and resistance to Norwalk virus infection. Nat Med 9(5):548–553
6. Whitley RJ (2006) Herpes simplex encephalitis: adolescents and adults. Antiviral Res 71(2-3):141–148
7. Rozenberg F (2013) Acute viral encephalitis. Handb Clin Neurol 112:1171–1181
8. Lafaille FG et al (2012) Impaired intrinsic immunity to HSV-1 in human iPSC-derived TLR3-deficient CNS cells. Nature 491 (7426):769–773
9. International HapMap, C (2005) A haplotype map of the human genome. Nature 437 (7063):1299–1320
10. Lander ES et al (2001) Initial sequencing and analysis of the human genome. Nature 409 (6822):860–921
11. Venter JC et al (2001) The sequence of the human genome. Science 291(5507): 1304–1351
12. Manolio TA (2010) Genomewide association studies and assessment of the risk of disease. N Engl J Med 363(2):166–176
13. Ge D et al (2009) Genetic variation in IL28B predicts hepatitis C treatment-induced viral clearance. Nature 461(7262):399–401
14. Suppiah V et al (2009) IL28B is associated with response to chronic hepatitis C interferon-alpha and ribavirin therapy. Nat Genet 41 (10):1100–1104
15. Tanaka Y et al (2009) Genome-wide association of IL28B with response to pegylated interferon-alpha and ribavirin therapy for chronic hepatitis C. Nat Genet 41 (10):1105–1109
16. Rauch A et al (2010) Genetic variation in IL28B is associated with chronic hepatitis C and treatment failure: a genome-wide association study. Gastroenterology 138 (4):1338–1345. 1345 e1-7
17. Thomas DL et al (2009) Genetic variation in IL28B and spontaneous clearance of hepatitis C virus. Nature 461(7265):798–801
18. Sheahan T et al (2014) Interferon lambda alleles predict innate antiviral immune responses and hepatitis C virus permissiveness. Cell Host Microbe 15(2):190–202
19. Abel L, Alcais A, Schurr E (2014) The dissection of complex susceptibility to infectious disease: bacterial, viral and parasitic infections. Curr Opin Immunol 30:72–78
20. Loeb M (2013) Genetic susceptibility to West Nile virus and dengue. Public Health Genomics 16(1-2):4–8
21. McLaren PJ, Carrington M (2015) The impact of host genetic variation on infection with HIV-1. Nat Immunol 16(6):577–583
22. Conley ME, Casanova JL (2014) Discovery of single-gene inborn errors of immunity by next generation sequencing. Curr Opin Immunol 30:17–23
23. Fodil N, Langlais D, Gros P (2016) Primary Immunodeficiencies and inflammatory disease: a growing genetic intersection. Trends Immunol 37(2):126–140
24. Stoddard JL et al (2014) Targeted NGS: a cost-effective approach to molecular diagnosis of PIDs. Front Immunol 5:531
25. Boycott KM et al (2013) Rare-disease genetics in the era of next-generation sequencing: discovery to translation. Nat Rev Genet 14 (10):681–691

26. Casanova JL (2015) Severe infectious diseases of childhood as monogenic inborn errors of immunity. Proc Natl Acad Sci U S A 112(51): E7128–E7137
27. Meyts I et al (2016) Exome and genome sequencing for inborn errors of immunity. J Allergy Clin Immunol 138(4):957–969
28. Chou J, Ohsumi TK, Geha RS (2012) Use of whole exome and genome sequencing in the identification of genetic causes of primary immunodeficiencies. Curr Opin Allergy Clin Immunol 12(6):623–628
29. Ciancanelli MJ et al (2015) Infectious disease. Life-threatening influenza and impaired interferon amplification in human IRF7 deficiency. Science 348(6233):448–453
30. Wu L et al (2015) Case-only exome sequencing and complex disease susceptibility gene discovery: study design considerations. J Med Genet 52(1):10–16
31. Ezkurdia I et al (2014) Multiple evidence strands suggest that there may be as few as 19,000 human protein-coding genes. Hum Mol Genet 23(22):5866–5878
32. Ezkurdia I et al (2014) Analyzing the first drafts of the human proteome. J Proteome Res 13(8):3854–3855
33. Sakharkar MK, Chow VT, Kangueane P (2004) Distributions of exons and introns in the human genome. In Silico Biol 4(4):387–393
34. Majewski J et al (2011) What can exome sequencing do for you? J Med Genet 48 (9):580–589
35. Ng SB et al (2009) Targeted capture and massively parallel sequencing of 12 human exomes. Nature 461(7261):272–276
36. Genomes Project, C et al (2012) An integrated map of genetic variation from 1,092 human genomes. Nature 491(7422):56–65
37. Lek M et al (2016) Analysis of protein-coding genetic variation in 60,706 humans. Nature 536(7616):285–291
38. Casanova JL et al (2014) Guidelines for genetic studies in single patients: lessons from primary immunodeficiencies. J Exp Med 211 (11):2137–2149
39. Consortium GR (2017) https://www.ncbi.nlm.nih.gov/grc/human
40. Pruitt KD et al (2014) RefSeq: an update on mammalian reference sequences. Nucleic Acids Res 42(Database issue):D756–D763
41. Harrow J et al (2012) GENCODE: the reference human genome annotation for the ENCODE project. Genome Res 22 (9):1760–1774
42. Aken BL et al (2016) The Ensembl gene annotation system. Database (Oxford) 2016. doi:10.1093/database/baw093
43. Hung JH, Weng Z (2016) Visualizing genomic annotations with the UCSC genome browser. Cold Spring Harb Protoc 2016(11). doi:10.1101/pdb.prot093062. p. pdb prot093062
44. Bodi K et al (2013) Comparison of commercially available target enrichment methods for next-generation sequencing. J Biomol Tech 24 (2):73–86
45. Chilamakuri CS et al (2014) Performance comparison of four exome capture systems for deep sequencing. BMC Genomics 15:449
46. Clark MJ et al (2011) Performance comparison of exome DNA sequencing technologies. Nat Biotechnol 29(10):908–914
47. Li H et al (2009) The sequence alignment/map format and SAMtools. Bioinformatics 25 (16):2078–2079
48. DePristo MA et al (2011) A framework for variation discovery and genotyping using next-generation DNA sequencing data. Nat Genet 43(5):491–498
49. McKenna A et al (2010) The genome analysis toolkit: a MapReduce framework for analyzing next-generation DNA sequencing data. Genome Res 20(9):1297–1303
50. Liu X et al (2013) Variant callers for next-generation sequencing data: a comparison study. PLoS One 8(9):e75619
51. Ewing B, Green P (1998) Base-calling of automated sequencer traces using phred. II. Error probabilities. Genome Res 8(3):186–194
52. Andrews S (2010) FastQC: a quality control tool for high throughput sequence data. Available online at: http://www.bioinformatics.babraham.ac.uk/projects/fastqc
53. Burrows M, Wheeler DJ, (1994) A block-sorting lossless data compression algorithm. Technical report–CaliforniaDigital Equipment Corporation, Palo Alto, 124
54. Langmead B et al (2009) Ultrafast and memory-efficient alignment of short DNA sequences to the human genome. Genome Biol 10(3):R25
55. Homer N, Merriman B, Nelson SF (2009) BFAST: an alignment tool for large scale genome resequencing. PLoS One 4(11):e7767
56. Lee WP et al (2014) MOSAIK: a hash-based algorithm for accurate next-generation sequencing short-read mapping. PLoS One 9 (3):e90581
57. Li H, Durbin R (2009) Fast and accurate short read alignment with Burrows-Wheeler transform. Bioinformatics 25(14):1754–1760

58. Shang J et al (2014) Evaluation and comparison of multiple aligners for next-generation sequencing data analysis. Biomed Res Int 2014:309650
59. Koboldt DC et al (2010) Challenges of sequencing human genomes. Brief Bioinform 11(5):484–498
60. Mills RE et al (2006) An initial map of insertion and deletion (INDEL) variation in the human genome. Genome Res 16 (9):1182–1190
61. Mullaney JM et al (2010) Small insertions and deletions (INDELs) in human genomes. Hum Mol Genet 19(R2):R131–R136
62. Van der Auwera GA et al (2013) From FastQ data to high confidence variant calls: the genome analysis toolkit best practices pipeline. Curr Protoc Bioinformatics 43:11 10 1–11 1033
63. Huang HW et al (2015) Evaluation of variant detection software for pooled next-generation sequence data. BMC Bioinformatics 16:235
64. Cingolani P et al (2012) A program for annotating and predicting the effects of single nucleotide polymorphisms, SnpEff: SNPs in the genome of *Drosophila melanogaster* strain w1118; iso-2; iso-3. Fly (Austin) 6(2):80–92
65. Flicek P et al (2010) Ensembl's 10th year. Nucleic Acids Res 38(Database issue): D557–D562
66. Wang K, Li M, Hakonarson H (2010) ANNOVAR: functional annotation of genetic variants from high-throughput sequencing data. Nucleic Acids Res 38(16):e164
67. Yang H, Wang K (2015) Genomic variant annotation and prioritization with ANNOVAR and wANNOVAR. Nat Protoc 10 (10):1556–1566
68. Kumar P, Henikoff S, Ng PC (2009) Predicting the effects of coding non-synonymous variants on protein function using the SIFT algorithm. Nat Protoc 4(7):1073–1081
69. Adzhubei I, Jordan DM, Sunyaev SR (2013) Predicting functional effect of human missense mutations using PolyPhen-2. Curr Protoc Hum Genet 76:7.20.1–7.20.41
70. Siepel A, Pollard KS, Haussler D (2006) New methods for detecting lineage-specific selection. In: Apostolico A, Guerra C, Istrail S, Pevzner P, Waterman M (eds) Proceedings of the 10th international conference on research in computational molecular biology. Springer, Germany, pp. 190–205
71. Pollard KS et al (2010) Detection of nonneutral substitution rates on mammalian phylogenies. Genome Res 20(1):110–121
72. Cooper GM et al (2010) Single-nucleotide evolutionary constraint scores highlight disease-causing mutations. Nat Methods 7 (4):250–251
73. Kircher M et al (2014) A general framework for estimating the relative pathogenicity of human genetic variants. Nat Genet 46(3):310–315
74. Itan Y et al (2015) The human gene damage index as a gene-level approach to prioritizing exome variants. Proc Natl Acad Sci U S A 112 (44):13615–13620
75. van der Velde KJ et al (2017) GAVIN: Gene-aware variant INterpretation for medical sequencing. Genome Biol 18(1):6
76. Itan Y et al (2016) The mutation significance cutoff: gene-level thresholds for variant predictions. Nat Methods 13(2):109–110
77. Day IN (2010) dbSNP in the detail and copy number complexities. Hum Mutat 31(1):2–4
78. Sherry ST et al (2001) dbSNP: the NCBI database of genetic variation. Nucleic Acids Res 29 (1):308–311
79. Stenson PD et al (2014) The human gene mutation database: building a comprehensive mutation repository for clinical and molecular genetics, diagnostic testing and personalized genomic medicine. Hum Genet 133(1):1–9
80. Fu W et al (2013) Analysis of 6,515 exomes reveals the recent origin of most human protein-coding variants. Nature 493 (7431):216–220
81. Karczewski KJ et al (2017) The ExAC browser: displaying reference data information from over 60 000 exomes. Nucleic Acids Res 45 (D1):D840–D845
82. Li H (2014) Toward better understanding of artifacts in variant calling from high-coverage samples. Bioinformatics 30(20):2843–2851
83. Bao R et al (2014) Review of current methods, applications, and data management for the bioinformatics analysis of whole exome sequencing. Cancer Inform 13(Suppl 2):67–82
84. Itan Y et al (2014) HGCS: an online tool for prioritizing disease-causing gene variants by biological distance. BMC Genomics 15:256
85. Kanehisa M et al (2017) KEGG: new perspectives on genomes, pathways, diseases and drugs. Nucleic Acids Res 45(D1):D353–D361
86. Croft D et al (2014) The reactome pathway knowledgebase. Nucleic Acids Res 42(Database issue):D472–D477
87. Bello SM, Smith CL, Eppig JT (2015) Allele, phenotype and disease data at mouse genome informatics: improving access and analysis. Mamm Genome 26(7-8):285–294

88. Sayers EW et al (2010) Database resources of the national center for biotechnology information. Nucleic Acids Res 38(Database issue): D5–16
89. Petryszak R et al (2016) Expression atlas update–an integrated database of gene and protein expression in humans, animals and plants. Nucleic Acids Res 44(D1):D746–D752
90. Wu TD, Nacu S (2010) Fast and SNP-tolerant detection of complex variants and splicing in short reads. Bioinformatics 26(7):873–881
91. The UniProt, C (2017) UniProt: the universal protein knowledgebase. Nucleic Acids Res 45 (D1):D158–D169
92. Szklarczyk D et al (2015) STRING v10: protein-protein interaction networks, integrated over the tree of life. Nucleic Acids Res 43(Database issue):D447–D452
93. Chen J et al (2009) ToppGene suite for gene list enrichment analysis and candidate gene prioritization. Nucleic Acids Res 37(Web Server issue):W305–W311
94. Zuberi K et al (2013) GeneMANIA prediction server 2013 update. Nucleic Acids Res 41(Web Server issue):W115–W122
95. Takahashi K et al (2007) Induction of pluripotent stem cells from adult human fibroblasts by defined factors. Cell 131(5):861–872
96. Cong L et al (2013) Multiplex genome engineering using CRISPR/Cas systems. Science 339(6121):819–823
97. Makarova KS et al (2011) Evolution and classification of the CRISPR-Cas systems. Nat Rev Microbiol 9(6):467–477
98. Hamazaki T et al (2017) Concise review: induced pluripotent stem cell research in the era of precision medicine. Stem Cells 35(3):545–550
99. Nie J, Hashino E (2017) Organoid technologies meet genome engineering. EMBO Rep 18 (3):367–376

Chapter 15

Isolation, Purification, and Culture of Primary Murine Sensory Neurons

Sarah Katzenell, Jorge R. Cabrera, Brian J. North, and David A. Leib

Abstract

Cultured primary neurons have been of extraordinary value for the study of neuronal anatomy, cell biology, and physiology. While use of neuronal cell lines has ease and utility, there are often caveats that arise due to their mitotic nature. This methods article presents detailed methodology for the preparation, purification, and culture of adult murine sensory neurons for the study of herpes simplex virus lytic and latent infections. While virology is the application for our laboratory, these cultures also have broad utility for neurobiologists and cell biologists. While these primary cultures have been highly informative, the methodology is challenging to many investigators. Through publication of this highly detailed protocol, it is our hope that the use of this culture system can spread in the field to allow more rapid progress in furthering our understanding of neurotropic virus infection.

Key words Primary neuron culture, Neuron purification, Neurotropic virus infection

1 Introduction

Herpes simplex virus 1 (HSV-1) establishes lifelong infection in the neurons of the trigeminal ganglia (TG), where it may remain latent for extended periods of time. Periodic reactivation events result in the formation of cold sores, herpetic keratitis, or herpetic encephalitis [1]. In vivo models of infection can provide insight into viral pathogenesis, and have demonstrated that neuronal innate immune responses are crucial for control of HSV-1 [2]. However, the involvement of epithelial and immune cells confounds the analysis of specific neuronal contributions to this process.

To study neuronal innate immune responses specifically, it is useful to use cultured primary neurons. For the study of HSV-neuron interactions, there has been significant recent focus on the sensory trigeminal ganglion or TG [3–6]. To achieve this, the TG must be dissected, enzymatically digested to liberate the neurons, and the neurons isolated by gradient separation. This yields a mixed neuronal culture that accurately represents the neuronal

Karen Mossman (ed.), *Innate Antiviral Immunity: Methods and Protocols*, Methods in Molecular Biology, vol. 1656, DOI 10.1007/978-1-4939-7237-1_15,

subpopulations observed in the intact adult TG. To further isolate specific neuronal subpopulations, it is possible to perform secondary enrichment using flow cytometry.

These methods provide several important advantages: (1) use of adult mice ensures the neuronal innate immune responses are fully mature; (2) it is possible to isolate neurons from transgenic mouse strains; (3) long-term culture (up to 3–4 weeks) facilitates long-term experimental procedures. Thus, this model lends itself to a diverse range of inquiries into neuronal innate immune responses. In this chapter, we will describe our detailed methodology for the isolation, purification, and culture of these murine adult sensory neurons.

2 Materials

2.1 Equipment

1. CO_2 for euthanasia.
2. Biosafety hood (*see* **Note 1**).
3. Rotator at 37 °C (in an incubator or a water bath).
4. Centrifuge suitable for 15 ml and 50 ml conical tubes, achieving 800 × *g*, with the option of slow acceleration and deceleration.

2.2 Plastic Ware, Glassware, and Tools

1. Coverslips (12 mm, autoclaved).
2. 100 mm plastic petri dish, sterile.
3. Parafilm.
4. Large scissors.
5. Small scissors.
6. Micro-scissors.
7. Large forceps.
8. Fine forceps.
9. Large curved hemostat.
10. Small curved hemostat.
11. 10 ml plastic syringe, with luer-lock tip.
12. 20-gauge needle, bevel removed (*see* **Note 13**).
13. Disposable absorbent bench paper.
14. Raised perforated stage + tray (optional, *see* **Note 19**).
15. Plastic ziptop bags.
16. Ice + bucket.
17. 6-well plate, or small plastic dishes, sterile.
18. 50 ml and 15 ml screw cap tube with conical base.
19. 0.22 μm filter, ×2.

20. Glass Pasteur pipettes, sterile.
21. Rubber bulb for Pasteur pipette.
22. Plastic Pasteur pipettes, sterile.
23. Hemocytometer.
24. 24-well plate.
25. Pipettes and sterile tips (p10, p200, p1000).

2.3 Chemicals and Reagents

1. Hank's Buffered Salt Solution (HBSS): 0.137 M NaCl, 5.4 mM KCl, 0.25 mM Na_2HPO_4, 0.1 g glucose, 0.44 mM KH_2PO_4, 1.3 mM $CaCl_2$, 1.0 mM $MgSO_4$, 4.2 mM $NaHCO_3$
2. 20 μg/ml Poly-D-lysine (PDL) in HBSS. Prepare 150 μl per coverslip.
3. 180 μg/ml mouse laminin in HBSS. Prepare 150 μl per coverslip.
4. Sterile distilled H_2O.
5. Mice: 6–10 weeks old.
6. Phosphate-buffered saline (PBS).
7. Papain solution: 120 units papain (*see* **Notes 2** and **3**), 1 μg L-cysteine, 1 mM $NaHCO_3$, in 3 ml HBSS. The papain will lower the pH of the solution, and the $NaHCO_3$ will raise it. The solution will appear cloudy, but will clarify over several minutes. For best results, prepare 1–2 h before use and incubate at 37 °C for at least 1 h. Filter-sterilize immediately before use.
8. Collagenase/Dispase solution (C/D): 210 units collagenase type II, 1.1 units neutral protease, in 3 ml HBSS (*see* **Note 4**). Prepare 1-2 h before use, store at 4 °C, and then bring up to 37 °C for use. Filter-sterilize immediately before use.
9. Opti-work solution: 0.66 g/ml OptiPrep in 0.8% w/v sodium chloride. Use this to prepare the Optiprep gradient layers.
10. Optiprep gradient layers: Opti-work diluted in NBA-W to the following densities: 0.3 g/ml (1st layer), 0.23 g/ml (2nd layer), 0.16 g/ml (3rd layer), 0.1 g/ml (4th layer, *see* **Note 5**). Each gradient requires 1 ml of each layer.
11. Neurobasal A Medium (NBA).
12. Neurobasal-A Work (NBA-W): 2% B27 in NBA.
13. Neurobasal-A Complete (NBA-C): 2% B27, 1% GlutaMAX, 50 ng/ml Neurturin, 50 ng/ml Neuronal growth factor, 50 ng/ml Glial-derived neurotrophic factor. Make FRESH for each media change.
14. NBA-FUDR: NBA-C supplemented with 60 μM 5′-fluoro-2′-deoxyuridine (FUDR).

2.4 Additional Materials and Solutions for Sorting by FACS

1. Collagenase/Dispase solution (C/D): 420 units collagenase type II, 1.1 units neutral protease, in 3 ml HBSS. Prepare 1-2 h before use, store at 4 °C, then bring up to 37 °C for use. Filter-sterilize immediately before use. This solution replaces the lower dose C/D solution listed in Subheading 2.3.
2. 40 μm cell strainer.
3. Percoll gradient layers: 28% and 12%, in NBA-W. Prepare 4 ml of each gradient layer per gradient.
4. Phenol Red-free NBA.
5. Fluorescent stains for appropriate cell surface markers, or else endogenously expressed fluorescent markers.
6. Flow cytometry device capable of sorting live cells under sterile conditions, fitted with a 100 mm nozzle and a 2.0 neutral density filter.

2.5 Additional Materials and Solutions for Microfluidics

1. 150 μm microfluidic devices—sonicate them for 10 min in distilled water in a bath sonicator, then submerge them in 70% ethanol for at least 30 min, and then air dry.
2. Glass coverslips, 24 × 50 mm (1 per microfluidic device)—submerge the coverslips in 70% ethanol for at least 30 min, and then allow them to partially air dry.
3. 100 mm dish, lined with parafilm.
4. Basal medium (any type) supplemented with 10% FBS.
5. 500 μg/ml PDL in HBSS.
6. 10 μg/ml laminin in HBSS.

3 Methods

This protocol takes approximately 4 h if performed by an experienced scientist (Fig. 1). It includes the following general stages: preparing the reagents and workstation, mouse euthanasia, mouse dissection, transcardial perfusion, TG dissection, enzymatic digestion, counting and plating the neurons (*see* **Note 1**). A video demonstration of the perfusion process can be found in the Journal of Visual Experiments [7]; the neuron isolation process is based on descriptions by Malin and Bertke [3, 4].

3.1 Prepare Coated Coverslips

1. Start preparing 1–2 days before neuron isolation.
2. Prepare a 100 mm sterile petri dish lined with parafilm (ethanol wiped, air dried).
3. Take 12 mm coverslips (autoclaved) and arrange them on the parafilm, with at least 2–3 mm left between slips. This setup encourages liquids to form a bubble on the coverslips, rather than spilling off them.

Fig. 1 Steps in the neuron isolation process. Coverslips should be coated with PDL and Laminin the day before neuron isolation. This will take a few minutes, followed by >3 h and overnight incubation, respectively. Neuron isolation should take a total of ~4 h. This will include ~1 h of setup, <1 h to isolate the TGs, <1 h of enzymatic digestions (20 min each, with some additional time for spin down), and ~1 h to separate, wash, count, and seed the neurons. This is followed by >1 h incubation, and then 3–4 days culturing, at which point the neuron cultures are ready for use in experiments

4. Apply 150 μl PDL per coverslip. Close the dish and incubate at 37 °C for at least 3 h, or as long as overnight (*see* **Note 6**).
5. Remove the PDL, and wash the coverslips three times with sterile distilled H_2O. It is convenient to use the vacuum to remove the liquids during this process. However, be sure to use a sterile tip or Pasteur pipette, and make sure there are no residual liquids in the vacuum tube, which might drip onto the coverslips.
6. Allow the coverslips to air-dry in the hood.
7. Apply 150 μl laminin per coverslip. Close the dish and incubate at 37 °C overnight.
8. The next day, wash the coverslips once in NBA-W. They are now ready for use.
9. Do not allow laminin-coated coverslips to dry, as laminin will crystalize.
10. Coated coverslips should be used the day after laminin is applied, and never store for later use.

3.2 Prepare Enzymes and NBA-W

Prepare within 1 h of the time you expect to start isolating TGs. For 10 mice, prepare 3 ml of papain, 3 ml of C/D, and 50 ml of NBA-W (*see* **Notes 2–4**). Use some NBA-W to prepare your workstation. Incubate the remainder at 37 °C until needed.

3.3 Prepare Your Workstation

1. It is convenient to have three work areas: a mouse euthanasia area, a perfusion area, and a dissection area. The euthanasia area may be in or out of the hood, as space permits. The perfusion and dissection areas must be in the hood (*see* **Note 1**). If hood-space is limited, it is possible to perform perfusion and dissection in the same area.

2. Mouse euthanasia area: It is most convenient to have the mouse euthanasia area in the hood; however, it can be out of the hood if space is limited. Mice should be euthanized one at a time, never in batches (*see* **Note 9**). Therefore, use an empty mouse cage to expose individual mice to CO_2. Make sure that this station is in compliance with your institution's animal welfare protocols.
3. Perfusion area: lay out disposable absorbent bench paper (*see* **Note 19**), and the following instruments: small scissors, large hemostat, small hemostat, large forceps, large scissors, ziptop bag. Take a 10 ml syringe and attach a 20-gauge needle to it. Use the large hemostat to grasp the beveled edge of the needle, then bend it gently back and forth until it breaks off—you now have a blunted needle (*see* **Note 13**). Make sure to deposit the broken-off beveled edge in the sharps waste. Fill the syringe with ice-cold sterile PBS, and set it next to the surgery tools.
4. Dissection area: lay out disposable absorbent bench paper and the following instruments: small scissors, micro-scissors, fine forceps, small ice bucket with ice, small petri dish or 6-well plate with 2–3 ml NBA-W (on ice, for isolated TGs, *see* **Notes 7** and **8**), 50 ml conical tube with PBS (on ice, for re-fills of the syringe), a larger bottle with PBS (on ice, for re-fills of the 50 ml conical tube).

3.4 Mouse Euthanasia and Dissection

1. Expose one mouse to CO_2 according to your institution's animal welfare protocols (*see* **Note 9**). When agonal gasping has ceased squeeze the footpad to confirm the mouse is unconscious. DO NOT perform a secondary method of euthanasia, such as cervical dislocation. Transfer the mouse to the dissection area, and proceed to the next step.
2. Pinch the abdominal skin above the diaphragm, and use the small scissors to make a small incision in the abdominal skin. Pinch the skin above and below the cut and pull firmly toward the head and tail, respectively. This will widen the cut, exposing the abdominal muscles and the lower portion of the ribcage. Pull until the cut has reached the back of the mouse, so you have unobstructed access to the diaphragm (Fig. 2a).
3. Use the large forceps to pinch the abdominal muscles directly below the ribcage and cut to left and right, along the lowest rib (Fig. 2a).
4. Use the large forceps to grasp the xiphoid cartilage (at the bottom of the rib cage), and pull slightly up. This will cause the viscera to fall away from the ribcage, exposing the diaphragm.
5. Using the small scissors, puncture the diaphragm at one side of the mouse, and cut along the ribcage to the other side

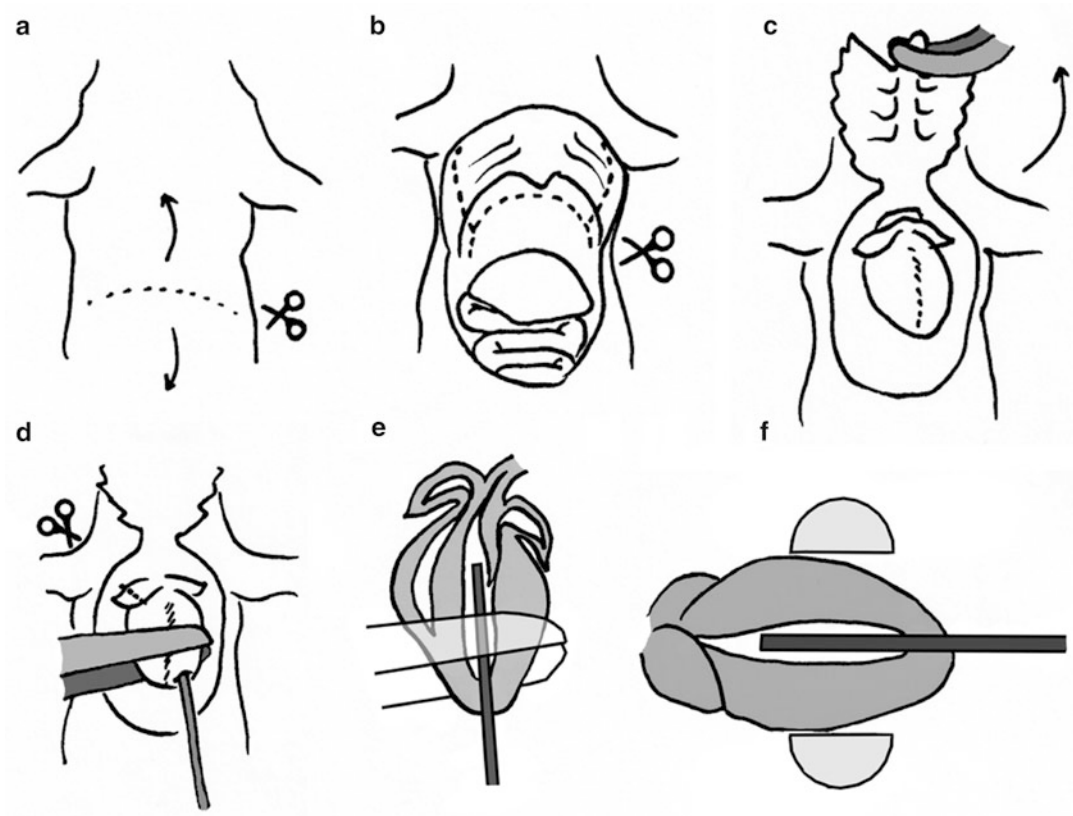

Fig. 2 Transcardial perfusion. Lay the mouse on its back, with the tail toward you, and the head away from you. (**a**) Use small scissors to cut the skin and muscle right below the ribcage. (**b**) Cut the diaphragm and ribcage, then (**c**) fold the ribcage up and away, exposing the heart. Use large forceps to grasp the heart while inserting the needle into the left ventricle, taking care not to punch clear through (**d–f**). Use a small hemostat (locked) to secure the needle in the heart, and then cut a hole in the right atrium (**d**). Begin perfusing with PBS

(Fig. 2b). Take great care not to accidentally puncture or cut the lungs and heart, since this would compromise the perfusion process.

6. Using the small scissors cut the rib cage at left and right, from the lowest rib toward the head (Fig. 2b). The front of the rib cage is now attached to the carcass only at the top.
7. Using the large hemostat, grasp the xiphoid cartilage, lock the hemostat, and fold toward the head. The heart and lungs are now fully exposed (Fig. 2c). The heart may be encased in a thin layer of connective tissue and fat. This is normal. Use the large forceps to gently peel away the fat, fully exposing the ventricles and atria.

3.5 Transcardial Perfusion (See Notes 10–12)

1. Use the forceps to grasp the heart in the middle, with the atria left free at the top, and the apex of the ventricles extending 2–3 mm out at the bottom (Fig. 2d). The grip should be firm

enough to hold the heart while you insert the needle, but not so firm as to damage the tissue or block the needle.

2. While holding the heart in place, position the blunted needle tip slightly to the right of the apex, so as to enter the left ventricle (Fig. 2d). Push the needle slowly and firmly into the heart (*see* **Notes 13** and **14**). You will encounter some initial resistance because the needle is blunted. However, once you punch through the muscle wall and into the ventricle the needle should slide in smoothly. Insert ~5–7 mm of the needle, depending on the size of the heart. Take care to insert the needle toward the aorta, without swiveling it to left and right, or pitching it up or down (Fig. 2e, f).
3. Keep the needle and syringe steady as you set aside the large forceps, and pick up the small hemostat. Use the hemostat to clamp the heart onto the needle (*see* **Notes 15** and **16**). Lock the hemostat, and gently put it down.
4. Use the small scissors to cut a hole in the right atrium (Fig. 2d). A little blood may flow out.
5. Slowly press the plunger on the syringe (*see* **Note 17**). This will push PBS into the mouse vasculature, pushing blood out of the organs and perfusing them with PBS. Blood, and eventually PBS, will flow out of the right atrium. The liver and paws may turn pale, the lungs may inflate and turn white, and PBS may drip out of the nose and mouth (*see* **Notes 18** and **19**). Perfuse the mouse with 5–10 ml PBS over the course of ~60 s.
6. Once the mouse is perfused, unlock the hemostat and remove the needle.
7. Use the large scissors to remove the head from the carcass (*see* **Note 20**). Discard the carcass (into the ziptop bag), and transfer the head to the dissection area.

3.6 TG Dissection

1. Using the small scissors, cut the skin on the top of the head, from the base of the spine to between the eyes. Fold the skin flaps under the chin of the mouse and use them to hold the head securely while you work.
2. The brain should be visible through the thin layer of bone at the top of the skull. Cut the skull along the left and right, with the cuts meeting a point between the eyes. The skull top can now be flipped up and away from you, exposing the brain (Fig. 3a).
3. Insert the large or small forceps between the frontal lobe and the skull, and flip the brain back toward you, exposing the base of the skull and the TGs (Fig. 3b, c). The optic chiasm will be exposed and ripped during this process. The pituitary gland also rests on the base of the skull, perpendicular to the TGs. Discard it by scraping the gland down and away from the TGs.

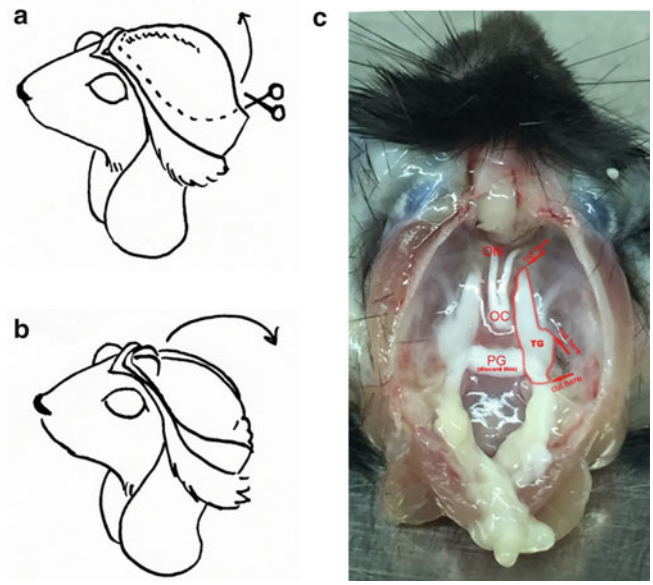

Fig. 3 TG isolation. After separating the head from the carcass, cut the skin from neck to between the eyes, and fold the skin flaps under the mouse's chin (**a**). Cut the exposed skull along left and right, to between the eyes, then lift the bone up and away (**a**). Pull the brain out toward you (**b**), exposing the base of the skull (**c**). TG dissection: Picture shows a mouse head after brain removal. Trigeminal ganglion is double lined. *Arrows* indicate cutting sites and the orientation of the cutting. Abbreviations: *TG* trigeminal ganglion, *ON* optic nerve, *OC* optic chiasm, *PG* pituitary gland. The optic nerves and chiasm should be visible at the top, the TGs along the base to either side, and the pituitary gland along the base between the TGs. Cut the connective tissue anchoring the TGs to the skull, and sever the nerve where it enters the skull—you should now be able to lift out the TGs (C)

4. The TGs are laid on the top of the skull, to left and right. Each TG has two branches threaded through holes in the base of the skull and extending toward the nose and eyes (*see* **Note 21**). Snip the branches at the point where they thread into the skull. Slide the micro-scissors under and along the TGs to cut the connective tissue which anchors the TG to the skull (Fig. 3c).
5. Use the fine forceps to gently lift the TGs out and place them in the ice cold NBA-W (*see* **Note 22**).

3.7 Enzymatic Digestion

1. Filter-sterilize the papain through a 0.22 μm filter.
2. Collect the TGs and papain in a 50 ml conical tube, making sure that all the TGs are in the enzyme solution.
3. Place the 50 ml conical tube, slightly tilted, on a rotator set to ~200 rpm (the gentle agitation improves the enzymatic digestion), and incubate at 37 °C for 20 min.

4. During this time, warm the C/D solution to 37 °C ten minutes before use.
5. At the end of the incubation spin down the TGs (200 g, 1 min), and remove the supernatant (*see* **Note 23**).
6. Filter-sterilize the C/D directly onto the TG pellet, and incubate as before (tilted, ~200 rpm, 37 °C, 20 min).
7. During this time, prepare the gradient (*see* Subheading 3.8 and **Notes 10** and **26**).
8. At the end of the incubation, spin down the TGs (400 g, 4 min), and remove the supernatant.
9. Add 1 ml of NBA-W to the TGs and triturate gently through a p-1000 pipette tip (~10 times). The TGs should dissociate fully, resulting in a cloudy suspension of cells (*see* **Notes 24** and **25**).
10. Add NBA-W for a final volume of 3 ml per gradient (*see* Subheading 3.8).

3.8 Gradient Separation

1. Each gradient can be loaded with up to 10 dissociated TGs (isolated from 5 mice). The volume loaded onto each gradient should always be 3 ml. Therefore, if you have isolated more than 10 TGs, prepare the appropriate number of gradients (up to 4, *see* **Note 10**) and bring the volume of tissue homogenate to 6, 9, or 12 ml (3 ml per gradient).
2. For each gradient you intend to layer, prepare the 4 Optiprep dilutions as described in Subheading 2.3 (*see* **Note 5**). Layer the gradient in a 15 ml conical tube (*see* **Notes 26–28**), with the densest (1st) layer at the bottom, and the least dense (4th) layer at the top. Handle carefully so as not to disturb the gradient.
3. Layer 3 ml of cell suspension (containing up to 10 dissociated TGs) on the top of the gradient.
4. Load the gradient into the centrifuge (*see* **Note 28**), and spin the gradient at 800 × *g* for 20 min, with a slow acceleration and a slow deceleration.
5. During this time, wash the coverslips with NBA, if not already washed.
6. Once the gradient spin is complete, remove the 15 ml conical tubes to the hood. As before, handle carefully so as not to disturb the gradient.
7. Inspect the gradient (Fig. 4). The NBA-W that contained the dissociated TGs should be clear. The lightest (uppermost) layer of the gradient may contain some debris, and there should be a thick band of debris at the junction between this layer and the next. Further down, there should be two distinct bands at the

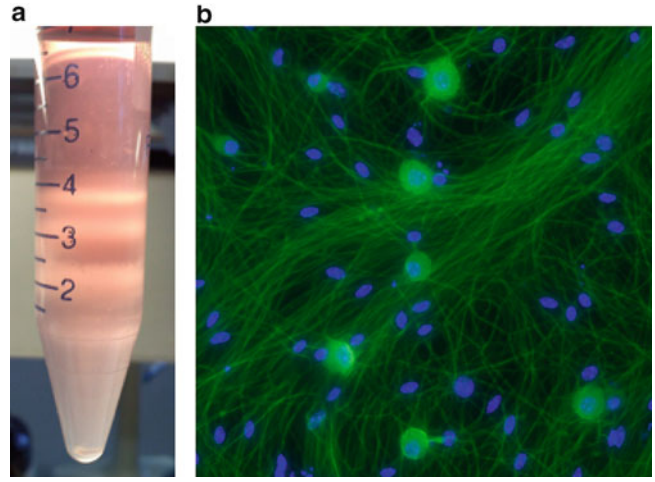

Fig. 4 Gradient separation and culture. (**a**) After the gradient has been spun, there should be four visibly distinct cell suspension layers and a pellet. Collect the liquid and two cell suspension layers from just above the 2.5 ml line to just below the 1 ml line, a total of ~2 ml. Discard the remainder. (**b**) Fluorescence microscopy of cultured TG neurons for 4 days stained with β-3 tubulin (green) and Dapi (*blue*)

junctures between the gradient layers. Both the bands contain neurons (small neurons and glial cells in the upper band, large neurons in the lower). The bottom layer of the gradient should be clear, with a small pellet at the bottom (*see* **Note 29**).

8. If desired, you may remove some of the NBA-W and some of the first band, though this is not necessary.
9. Use a p200 or p1000 pipette to collect the lower two bands, as well as the second gradient layer, and most of the third. Avoid collecting the thick band of debris in the third band. Collect this liquid (~2 ml in total) into a new 15 ml conical tube. It is sometimes useful to move the tip gently in circular motions while collecting, so as to collect cells from all the areas of the band.
10. Wash the OptiPrep away: Add 5 ml of NBA-W, then spin at 670 g for 4 min to pellet. Discard the supernatant, resuspend in 1 ml of NBA-W, then add 5–10 ml NBA-W, spin at 400 g for 2 min, and discard the supernatant.
11. Resuspend the neurons in NBA-W (100 μl per mouse). At this point, it is possible to combine the output of several gradients, if appropriate.

3.9 Seeding and Culturing Neurons

1. Count the neurons using a hemocytometer according to the manufacturer's instructions (*see* **Note 30**). Neurons will appear phase-bright and quite large, and their size will also be apparent

over a range of focal distances. The sample will also contain debris and supporting cells (which will appear much smaller and flatter than the neurons).

2. The expected yield is ~15,000–20,000 neurons per mouse (or 4–6 coverslips per mouse). This may vary between mouse strains (e.g., C57B/6 J yields are slightly lower than 129SVEV yields) (*see* **Notes 31–33**).
3. Add NBA-W to dilute the neuron suspension to a concentration of 60 neurons per μl.
4. Aspirate the NBA from the coverslips, and seed 60 μl per coverslip (a total of 3600 neurons per coverslip, seeded at an approximate density of 32 cells per mm^2).
5. Incubate the coverslips at 37 °C for 1–2 h. During this time the neurons settle and attach. A pad of debris will settle on the top of the cells, and will be visible to the naked eye. This debris will eventually slough off as the cultures are fed. Do not try to tap, scrape, or aspirate the pad off—this is likely to result in significant neuronal loss.
6. During this time prepare NBA-C with FUDR (400 μl per coverslip) and warm it to 37 °C.
7. If desired, gently aspirate the seeding media from the coverslips (some of the debris pad might also come off—this is ok).
8. Using fine forceps, transfer the coverslips to a 24-well plate, and add 400 μl NBA-FUDR to each well (*see* **Note 34**). The FUDR will inhibit glial cell division and will prevent them from overrunning the culture.
9. Incubate at 37 °C for 3–4 days; then replace media with NBA-C (no FUDR). The neurons are now ready for experimentation.
10. For continued culturing, replace neuron media every 3–4 days with 400 μl freshly prepared NBA-C. Appearance of cultures should resemble Fig. 4b.

3.10 Culturing Neurons (See Notes 35–38)

1. Once seeded, the neurons will rapidly grow neurites (Fig. 4b). These will be visible within ~4–8 h, and will form a dense mat at the coverslip surface within ~24 h. The neurites often form whorls, and any scratches in the PDL + laminin coating will be evident in the pattern of neurite growth. The pattern of neurite growth will also appear different on precoated coverslips (which can be purchased).
2. The neurons will appear to be unevenly seeded, with very sparse seeding toward the edges of the coverslip. Nonetheless, over most of the coverslip area neurons should be evenly distributed. It is normal to observe 2–6 neurons which have settled together. If the coverslip is tapped or jostled before the

neurons have settle the neurons may become concentrated, almost confluent, in some areas and very sparse in others.

3. The neurons and glial cells are not stationary on the coverslips, and some migration may be observed over the course of several days, particularly if live imaging is performed.
4. The neurons do form synapses and signal to each other in culture. This may affect several biological processes, including Ca^{2+} dynamics and expression of MHC-II.
5. Cultures should not be kept out of the incubator for extended periods of time, since exposure to prolonged cold, changes in pH, or changes in O_2/CO_2 tension are harmful to the neurons.
6. Neurons may be cultured for as long as 3–4 weeks ex-vivo. During this time the neurons will undergo a process of aging, which will result in some loss of viability, although this should not be extensive.
7. The cultures are mixed, and include multiple neuronal subtypes, as well as supporting satellite glial cells. The glial cells are found in the upper of the two neuronal bands, where many of the smaller neurons are also found. It is therefore not possible to produce a purely neuronal culture unless further purification methods are used (*see* Subheading 3.12). The FUDR in the media will prevent any initial expansion of this population. After 3–4 days in vitro, the glial cells lose most of their replicative license and some will apoptose. By 3 weeks in vitro there should be significantly fewer glial cells.

3.11 Neuronal Sorting by Flow Cytometry

1. If desired, newly isolated neurons can be sorted into subpopulations by flow cytometry. To identify neuronal subpopulations, use dyes or antibodies to fluorescently label the appropriate cell surface markers. Alternately, isolate neurons from transgenic mice expressing fluorescently tagged markers. We describe here a modification of the main protocol that facilitates sorting of non-peptidergic neurons, a subpopulation of sensory neurons [8].
2. A major concern for neuron sorting is the risk of clogging the FACS with tissue debris or large neurons. To avoid this, we have introduced several modifications of the protocol, listed below.
3. For enzymatic digestion (Subheading 3.8) use 420 units of collagenase II, instead of the usual 210 units.
4. Immediately after dissociating the tissue and resuspending in 3 ml of NBA-W (Subheading 3.8), pass the suspension through a 40 μm cell strainer. This will remove tissue fragments and the larger neurons. Non-peptidergic neurons have a smaller diameter and will pass through the strainer.

5. Replace the Optiprep gradient (Subheading 3.9) with a percoll gradient. Layer the percoll gradient in the following order: 4 ml 28% percoll, 4 ml 12% percoll, 3 ml dissociated, strained TG homogenate. This removes unwanted pieces of non-dissociated tissue.
6. Spin the gradient at 1300 g for 10 min. The neurons will drop into a pellet. To recover the neurons, discard all the layers without disturbing the pellet. Proceed to wash as described above (Subheading 3.4).
7. After the final wash, resuspend the neurons in Phenol Red-free NBA-C. Phenol Red can interfere with the excitation-emission fluorescence and affect the sorting process.
8. If using endogenously labeled neurons, proceed directly to **step 9**. If labeling cell surface markers, incubate the neurons with the appropriate fluorescent dye or antibody. We incubate the neurons for 5 min with fluorescently labeled Isolectin Banderifolia B4 (IB-4), which binds to non-peptidergic neurons. We do not wash the neurons after this step, since the IB-4 signal on neurons is easily detectable above the background.
9. As soon as possible, sort the neurons at your flow cytometry facility.
10. The FACS instrument must run under sterile conditions to avoid contaminating the neuron cultures. To avoid clogging, we used a 100 mm nozzle. Finally, we installed a 2.0 neutral density filter. Gate the neurons using logarithmic scale for the FSC and SSC.

3.12 Seeding Neurons in Microfluidics Devices

1. Compartmentalized cultures, such as Campenot chambers [2, 9] and microfluidic devices ([10], and described herein), separate neuronal cell bodies and proximal neurites from distal projections. This provides an in vitro model of in vivo neuronal architecture, and facilitates specific treatment of the distal projections.
2. In microfluidic devices, positive pressure from the cell body compartment to the axonal compartment prevents the diffusion of large molecules (>1 kDa) in the opposite direction (e.g., DiI applied to the distal projections, *see* Fig. 5d). It also encourages neurite growth through the capillaries. Positive pressure is achieved by filling the compartments with unequal volumes of media (*see* Subheading 3.12, **steps 19** and **21**).
3. Assembly and coating of the microfluidic devices involves 3 overnight incubations; therefore, you should begin this process 3 days before you intend to isolate the neurons.
4. Transfer one partially dried coverslip into a parafilm-lined dish, and allow it to air dry completely. This will prevent the coverslip from adhering too firmly to the parafilm.

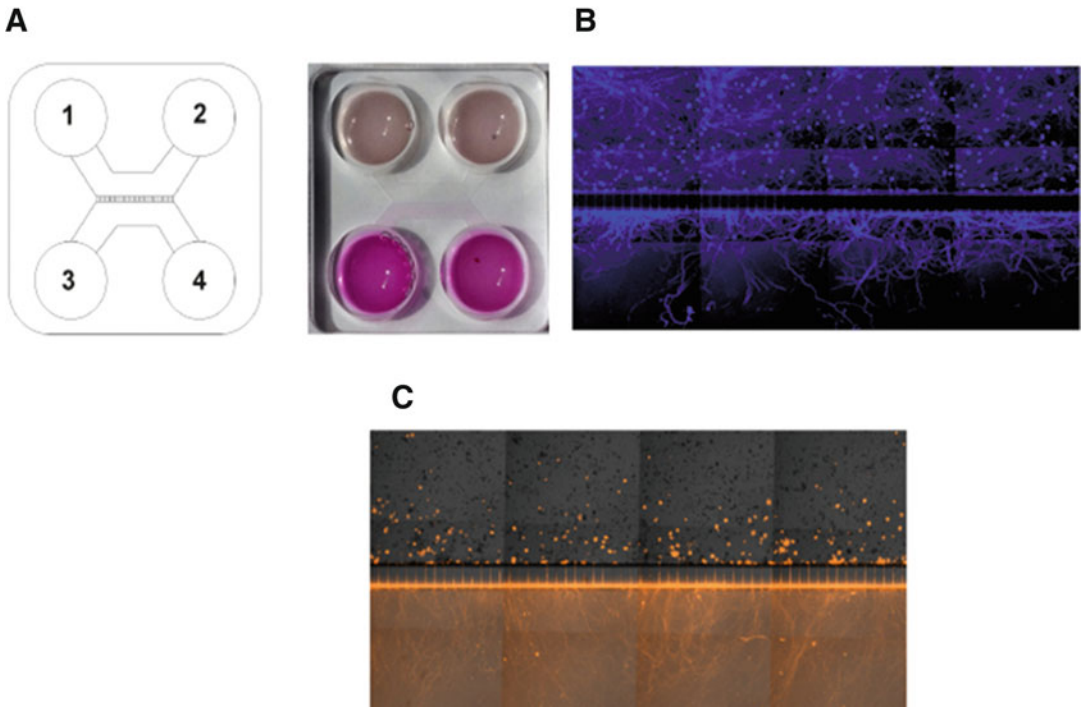

Fig. 5 Use of microfluidic chambers to culture TG neurons. (**a**) Schematic representation of a microfluidic device with compartments enumerated to follow the protocol above. The picture (right) shows a microfluidic device filled with NBA complete medium (all compartments) and NBA complete medium plus the cell tracker DiI (compartments 3 and 4). (**b**) Representative image of trigeminal neurons cultured for 3 days in a microfluidic device. Neurons were stained with β-3 tubulin (*blue*). Neuron cell bodies are present only in the upper compartment, with axons projecting through the capillaries to the lower compartment. (**c**) The same culture as described in **b**. The cell tracker DiI (*orange*) was added to the lower compartment. This treatment stains only those neurons that have grown axonal projections through the capillaries

5. Identify the side of the microfluidic device lithographed with channels and microgrooves (*see* **Note 39**).
6. Mount the device onto the coverslip, with the lithographed side facing down. The device will attach immediately. Use forceps to gently press the device to the coverslip, paying special attention to the microfluidic borders. This will ensure the device is properly attached. If correctly mounted, the microgrooves will act as capillaries.
7. Let it settle for 15 min, then remove the parafilm strip.
8. Fill compartment 1 with 200 μl of 10% FBS medium, and wait for the central channel to be filled completely (Fig. 5a, *see* **Note 40**).
9. Fill compartment 2 with 200 μl of 10% FBS medium.
10. Cover the dishes and place in an incubator overnight, allowing the capillaries to slowly fill.

On the next day check that capillaries have been filled with medium.

11. Fill compartment 3 with 200 μl of 10% FBS medium and wait for the central channel to fill.
12. Fill compartment 4 with 200 μl of 10% FBS medium. Wait for 15 min. The devices are now ready to be coated.
13. Remove the media and fill each compartment with 200 μl of 500 μg/ml PDL in HBSS, then place in an incubator overnight, allowing the capillaries to slowly fill.
14. On the next day wash the compartments three times with HBSS.
15. Apply 200 μl of 10 μg/ml laminin in HBSS to each of the compartments, and then place in an incubator overnight, allowing the capillaries to slowly fill. The devices are now ready for neuron seeding.
16. Prepare neurons according to the usual protocol described above. After the last wash, resuspend neurons in NBA-C at a concentration of 10^5 neurons/6 μl (this typically entails the use of ~1 mouse per device).
17. Remove Laminin from all compartments, and seed 3 μl of cell suspension in compartment 1 as close as possible to the central channel (Fig. 5a). Tilt the plate to a 45° angle, and wait for 10 min (Fig. 5a). This will allow the neurons to flow down the central channel and settle along the entrance to the capillaries.
18. Seed 3 μl in compartment 2, as close as possible to the central channel, tilt the plate at a 45° angle in the opposite orientation, and wait for 10 min.
19. Fill compartment 1 and 2 with 200 μl NBA-C + FRDU (each), and compartment 3 and 4 with 100 μl NBA-C (each).
20. Incubate the devices for 3 days. Neurite growth through the capillaries should be evident on the first day, and should be robust by 3 days, at which point the devices are ready for use in experiments.
21. When performing experiments, make sure to fill chambers 3 and 4 with 100 μl of media each, and chambers 1 and 2 with 200 μl each.

4 Notes

1. Primary neuronal cultures are susceptible to contamination. Work should therefore be carried out in a biosafety hood whenever possible, and particularly when handling neurons. All the reagents and tools should be sterile at the time of use. The tools should be received sterile or autoclaved or wiped

with 70% ethanol. The reagents should be received sterile or autoclaved or filter sterilized. Some reagents are unavoidably exposed to non-sterile conditions (e.g., powdered reagents being weighed), and these should be filter sterilized before use.

2. Most of the solutions needed should be prepared fresh. However, the following stock solutions can be prepared and stored at 4 °C: 0.66 g/ml OptiPrep in 0.8% w/v sodium chloride (Opti-work), 50 μg/ml L-Cystein in HBSS, 9% (w/v) $NaHCO_3$ in double-distilled water, 40 mM FUDR in HBSS. Stock solutions of PDL, Laminin, B27, Neurturin, NGF, and GDNF should be stored at −20 °C. It is possible to prepare the C/D enzyme solution ahead of time and freeze it; however, we have observed that freeze-thawed C/D sometimes do not digest the TG tissue as well as fresh C/D.
3. The potency of papain varies between batches; therefore, calculate the volume required to achieve 120 units of activity on a per-batch basis. Using Worthington papain, this is usually ~90–120 μl.
4. The powdered enzymes are very light, and susceptible to static electricity. This can be partially ameliorated by wiping the 50 ml conical tube with a wet paper towel.
5. An easy guide to preparing the OptiPrep gradient layers: combine Opti-W and NBA-W in the following ratios: 450 μl + 550 μl (1st layer), 350 μl + 650 μl (2nd layer), 250 μl + 750 μl (3rd layer), 150 μl + 850 μl (4th layer).
6. Handling coverslips: Once you have started preparing the coverslips, they should be handled using fine forceps. Touching the coated side with forceps or a pipette tip will scrape off the PDL/Laminin coating, or else remove cells and damage neurites. Therefore, grasp the coverslip toward the edge and avoid touching the central section as much as possible.
7. Stack the ice and place the petri dish or 6-well at an angle toward you, so the NBA-W pools and the TGs are easier to deposit.
8. To avoid confusion when isolating TGs from multiple mouse strains, it is helpful to use a 6-well plate and write the mouse strains on the underside of the wells.
9. Streamlined process: It is possible to streamline the TG extraction process if two people are available and the hood is large enough. While one person dissects the TGs from the first mouse, the other perfuses the second mouse, and the third mouse is euthanized. In this way, two experienced scientists can isolate the TGs at a rate of ~3 min per mouse. Do not euthanize mice in batches, since neuronal loss increases the longer TGs remain in the euthanized mouse.

10. Maximal work load: The maximum number of mice per batch is 20. This number is due to two constraints: (1) At ~3 min per mouse, only 20 mice can be processed in <1 h (neuronal loss increases the longer TGs are stored); (2) At ~5 min per gradient, only four gradients can be layered in 20 min (during the C/D incubation). Each gradient separates neurons from up to five mice. An additional constraint is imposed if isolating neurons of different genotypes—these must be isolated on separate gradients.
11. Practice: many of the steps described require practice. In our experience transcardial perfusion and gradient separation are the most likely to require practice before mastery.
12. Perfusion is performed in order to remove as much blood as possible from the TGs. This makes dissection easier and lowers neuronal loss due to red blood cell induced toxicity.
13. Using a beveled tip needle often results in accidentally pushing the tip clear through the mouse's heart. Moreover, the mouse heart is so small that a beveled edge might not fit completely within the left ventricle (especially if using younger, female mice). The blunted needle has a much shorter tip, and is harder to push through the heart tissue. Thus, it is less likely to pierce clear through the heart.
14. If you are unable to insert the needle, it may be because the heart is not held firmly enough (and is therefore slipping out of the forceps) or is held too firmly (the forceps are compressing the tissue, making it harder to insert the needle). Adjust the forceps' grasp of the heart.
15. If the needle slips out of the heart before you have secured it with a hemostat, gently grasp the heart in the forceps, find the previously made puncture, and gently reinsert the needle.
16. Take care not to pull too much on the heart and hemostat, as this may damage the tissue or dislodge the needle.
17. If you are not able to depress the plunger of the syringe, it is probable that the needle is blocked by the surrounding tissue. Without releasing the hemostat lock, pull the syringe slightly toward you. If the needle is still blocked, release the hemostat lock, move the needle inside the heart to reposition, and relock the hemostat. If the needle is still blocked, a tissue fragment may have become lodged in the needle tip, blocking it (this is rare). Discard the blocked needle and install a new, blunted needle.
18. If there are signs of poor perfusion (liver and paws do not clear, lungs very inflated and white), the rate of perfusion may be too high. Lessen the rate of perfusion. Otherwise, continue—a poorly perfused mouse will still yield some neurons.

19. During perfusion blood and PBS will spill out of the right atrium. The liquids will be absorbed by the absorbent bench pad. However, if >3 mice are to be perfused the pad may become saturated, making the workstation messy and inconvenient. To avoid this, we have made use of a raised perforated stage, placed above a pad-lined tray. The liquids drip through the perforations and are absorbed by the pad, leaving the work surface mostly clear. It is convenient, though not necessary, to keep some paper towels at hand to periodically wipe this work surface.
20. It is easier to cut through the spine if you hold the mouse carcass up by the ears, so the shoulders hang down from the neck.
21. The TG-CNS junction is located toward the back of the skull, near the brainstem. Sometimes, a little CNS matter remains attached here after the brain has been removed, identifiable as a yellowish extension of the TG. It is possible, though not necessary, to remove this CNS tissue.
22. If you have difficulty in getting the TGs out of the skull, the connective tissue or the TG branches into the skull may not have been fully cut. Use the micro-scissors to cut around the TGs and fully sever the nerve branches.
23. After the papain digestion, the pellet is not stable, and can be easily disturbed. It is ok to leave a small volume of the supernatant (~100–200 μl) above the pellet.
24. If the TGs do not fully dissociate on trituration this indicates poor enzymatic digestion. The enzyme was not fully active (too few units, no L-cystein, too cold, not incubated at 37 °C for long enough), or was not properly agitated during incubation. It is not possible to correct this problem at this stage.

    Avoid forceful or prolonged trituration, as this will not significantly increase the yield, and may be toxic to neurons.
25. Avoid generating bubbles or foam or triturating forcefully, as this is toxic to the neurons and will reduce your yield.
26. How to layer a gradient: The key to layering a gradient is to allow a thin stream of the lighter liquid to flow slowly down the conical wall. When it reaches the denser liquid at the bottom it will form a new layer, rather than mix. Pipette the densest (1st) layer into the conical. Use a Pasteur pipette and bulb to mix and collect the 2nd layer (avoid generating bubbles). Hold the conical at a ~ 45° angle, use the tip of the Pasteur pipette to draw a line of liquid up from the 1st layer, and slowly squeeze out the 2nd layer. The 2nd layer should slide down the line of liquid and form a new layer on the top of the 1st, without mixing. Once layered, there should be a visible diffraction line between the two layers. It should take an experienced scientist

~1 min per layer, or ~5 min per gradient. Hence, it is not advisable to attempt >4 gradients during the C/D incubation time. Once layered, the gradient is stable for up to an hour, but for optimal results it should be prepared immediately before use.

27. If there is no visible diffraction at the expected boundary between the layers, the gradient may have been poorly layered. This might happen if: (1) a layer is applied directly at the surface of the previous layer; (2) the liquid is allowed to slide down a dry surface (it will bead and roll rapidly down the surface); (3) the stream of lighter liquid is applied too fast or in too great a volume. Alternately, the gradient was jostled, and the layers have mixed. It is not possible to salvage this gradient; a new one should be layered. If the 3 ml of dissociated TG have already been layered, remove the cells and media, collecting also a portion of the 4th gradient layer. Add ~5 ml NBA-W and spin down (400 g, 4 min) to wash the Optiprep out. Discard the supernatant, resuspend the cells in 3 ml NBA-W, and re-layer on the new gradient.
28. Make sure to handle the gradient gently, avoiding any bumps or sudden movements, so as not to disturb the gradient. Make sure the centrifuge is correctly balanced, so as to avoid an emergency brake during the spin.
29. If there are poorly formed bands after the gradient spin, the gradient may have been jostled or subjected to an emergency stop in the centrifuge, or else the gradient was poorly layered and hence the bands did not form correctly. Collect the entire volume into a 50 ml conical, add an excess of NBA-W, mix, and spin down (~500 g, ~5 min) to wash the Optiprep out. Discard the supernatant, resuspend the cells in 3 ml NBA-W, and re-layer on a new gradient.
30. It may be difficult to determine which cells are neurons and which are glial cells or debris. This is primarily a matter of experience. Once you have looked at cultured neurons under a microscope you will be able to identify them in a hemocytometer. The neurons will appear phase bright, and will continue to be phase bright over a range of focal distances. Move with the focus dial back-and-forth as you scan the field of view. The debris and glial cells will be out of focus while the neurons remain partially in focus. If you are still not confident, consider staining the neurons for neuronal markers (such as beta-III tubulin or IB4) to train your eye to identify neurons.
31. The number of neurons may be much lower than expected. This can be due to several reasons, including poor enzymatic digestion, poor gradient separation or collection, loss of neuronal viability during extraction (due to prolonged extraction

process, trituration, bubbles or foam), miscalculated volume for resuspension after washes. There is no way to increase the yield at this point. However, care should be taken in future extractions to avoid the possible issues listed.

32. The number of neurons may be much higher than expected. This may be due to a specific mouse strain, or else the count included some non-neuronal cells. Recount the cells and make sure to count only those that are definitely neurons.
33. The isolated neuron suspension may include excess tissue debris. This can be due to poor enzymatic digestion, gradient separation, or collection. It is not possible to remove the debris at this stage. Some debris will naturally lift off during media changes. Care should be taken in future extractions to avoid the possible causes listed.
34. When adding media to neuron cultures, always apply the media gently to the well wall. Applying the media directly onto the neurons may cause them to detach due to shear stress. This will be detectable by a microscope as a "hole" surrounded by ripped axons.
35. If there is early loss of neuronal viability in culture (over the course of 1–5 days), the neurons may have been exposed to stress during isolation (hypoxia, sheer stress during trituration, bubbles). There is no way to salvage these cultures. Take care during isolation to avoid stressing the neurons.

    If poor viability persists over several isolation attempts, consider there might be a problem with one of the media ingredients. One of the reagents may have expired or been subjected to freeze-thaw damage. Alternately, you may have received a batch that was compromised (contaminated with chemical or biological reagents, damaged during shipping, etc.). Take note of the lot numbers of your media ingredients, and of the aliquots currently in use. Try systematically replacing each of the ingredients (use a new aliquot, order the same product from the previous lot, or order it from a different vendor). Lastly, one of the reagents may have unanticipated incompatibility with your neuronal cultures. This may be particularly true of FUDR and other antimitotics. Try using different concentrations of FUDR, or else using a different antimitotic.
36. If the culture is overrun with glial cells, the initial isolation may have been poor in neurons, and rich in glial cells. For purer cultures, avoid the layer closest to the top-most band, which contains debris but also glial cells. This may result in lower yields. You may choose to collect only the lower neuronal band, and this will result in purer cultures of larger neurons, but with fewer of the small neuronal subtypes.

Alternately, the FUDR may not inhibit the glial cells. Consider making fresh FUDR, increasing the dose of FUDR, or else adding another mitotic inhibitor, such as aphidicolin. However, this may prove toxic to the neurons, since it inhibits DNA damage repair. Make sure to test the new antimitotic.

37. If there is a lot of blebbing and cell debris, cells (either neurons or glial cells) are dying. To some extent, this is normal (since glial cells and even neurons may gradually die in culture over the course of 2–3 weeks). Check the cultures regularly and make sure they are not exposed to any additional stress (delayed media change, changes in temperature or pH, etc.).
38. If many neurons appear grainy, or else the neurites are peeling off the coverslip, this indicates that the neurons are dying. Grainy neurons might yet be salvaged by changing the media, although this may have adverse effects on future assays. However, if the neurites are detaching the cultures cannot be salvaged.
39. It is possible to reuse the devices, once they have been cleaned and autoclaved.
40. The 10% FBS medium prepares all the surfaces in the microfluidic chamber (including capillaries) for the next steps. The FBS lowers the surface tension of the liquid, allowing the medium to fill the capillaries and central channels. PBS and serum-free medium will not fill the capillaries properly, resulting in the formation of bubbles, which will block neurite growth.

Acknowledgments

Development of the protocols described in this article was supported by PO1 AI098681, and by a pilot grant to JR Cabrera from the Hitchcock Foundation.

References

1. Smith G (2012) Herpesvirus transport to the nervous system and back again. Annu Rev Microbiol 66:153–176
2. Rosato PC, Leib DA (2015) Neuronal interferon signaling is required for protection against herpes simplex virus replication and pathogenesis. PLoS Pathog 11(7):e1005028
3. Malin SA, Davis BM, Molliver DC (2007) Production of dissociated sensory neuron cultures and considerations for their use in studying neuronal function and plasticity. Nat Protoc 2 (1):152–160
4. Bertke AS, Swanson SM, Chen J, Imai Y, Kinchington PR, Margolis TP (2011) A5-positive primary sensory neurons are Nonpermissive for productive infection with herpes simplex virus 1 in vitro. J Virol 85 (13):6669–6677
5. Rosato PC, Leib DA (2014) Intrinsic innate immunity fails to control herpes simplex virus and vesicular stomatitis virus replication in sensory neurons and fibroblasts. J Virol 88 (17):9991–10001
6. Katzenell S, Leib DA (2016) Herpes simplex virus and interferon signaling induce novel Autophagic clusters in sensory neurons. J Virol 90(9):4706–4719
7. Gage GJ, Kipke DR, Shain W (2012) Whole animal perfusion fixation for rodents. J Vis Exp 65:e3564

8. Usoskin D, Furlan A, Islam S, Abdo H, Lönnerberg P, Lou D, Hjerling-Leffler J, Haeggström J, Kharchenko O, Kharchenko PV, Linnarsson S, Ernfors P (2015) Unbiased classification of sensory neuron types by large-scale single-cell RNA sequencing. Nat Neurosci 18 (1):145–153
9. Pazyra-Murphy MF, Segal RA (2008) Preparation and maintenance of dorsal root ganglia neurons in compartmented cultures. J Vis Exp 17(20):pii: 951
10. Cabrera JR, Viejo-Borbolla A, Martinez-Martín N, Blanco S, Wandosell F, Alcamí A (2015) Secreted herpes simplex virus-2 glycoprotein G modifies NGF-TrkA signaling to attract free nerve endings to the site of infection. PLoS Pathog 11(1):e1004571

Chapter 16

Isolation of Group 2 Innate Lymphoid Cells from Mouse Lungs

Claudia U. Duerr and Jörg H. Fritz

Abstract

The recently described group 2 innate lymphoid cells (ILC2) exert critical roles in type 2 immune responses, epithelial repair at mucosal tissues and metabolic homeostasis. ILC2 release large amounts of type 2 cytokines such as interleukin 4 (IL-4), IL-5, and IL-13, driving type 2 immunity such as the defense against helminths. However, if not tightly regulated ILC2 can trigger unwanted type 2 immunopathologies including allergic airway inflammation, airway hyper-responsiveness, and atopic dermatitis. Viral respiratory tract infections, archetypal triggers of type 1 immune responses, often give rise to pulmonary type 2 immunopathologies such as asthma and asthma exacerbations. Interestingly, pulmonary viral infections induce the release of IL-33, followed by induction of ILC2-mediated pulmonary type 2 immunopathology independent of the adaptive immune system. Due to their scarcity at steady state but also after infection and inflammation, pulmonary ILC2 are challenging to work with. In this chapter, we describe the detection and isolation procedure of pulmonary mouse ILC2 by flow cytometry and compare four distinct enzymatic mouse lung tissue processing protocols for optimized cell yield.

Key words Group 2 innate lymphoid cells, Lung, Respiratory virus infections, IL-33, Mucosal immunity, Innate type 2 immune response

1 Introduction

Type 2 immunity is important in the immune defense against helminth infections but can also be induced upon infection with respiratory viruses such as respiratory syncytial virus, influenza virus, or rhinoviruses [1, 2]. This is surprising as respiratory virus infections are potent inducers of innate and adaptive type 1 immune responses. Importantly, respiratory virus infections are the dominant cause of type 2 immunity-mediated pathologies including asthma and asthma exacerbations [3]. Type 2 immune responses are characterized by the release of type 2 signature cytokines such as IL-4, IL-5, and IL-13 that are secreted by two main cell populations: the adaptive $CD4^+$ type 2 T helper (Th2) cells and their

Karen Mossman (ed.), *Innate Antiviral Immunity: Methods and Protocols*, Methods in Molecular Biology, vol. 1656, DOI 10.1007/978-1-4939-7237-1_16,

innate counterpart, the recently discovered group 2 innate lymphoid cells (ILC2) [4, 5].

ILC2 are found at steady state at mucosal surfaces including the lungs and intestine [6–8] as well as skin and bone marrow and expand rapidly upon activation [9]. ILC2 belong to the group of innate lymphoid cells composed of natural killer cells, lymphoid tissue inducer (LTi) cells, and innate lymphoid cells group [1–3]. All the groups of ILC are dependent on the transcription factor Id2 as well as common IL-2 receptor gamma chain. Moreover, ILC2 require the transcription factors GATA3 and RORα for development and function [10]. Importantly, ILC2 are devoid of lineage markers and do not express specific antigen receptors. Characteristic pulmonary ILC2 surface markers include CD25 (IL-2Rα), CD127 (IL-7Rα), Thy1 (CD90), KLRG1, and c-kit (CD117) [10]. The induction of ILC2 is dependent on IL-25, IL-33, and thymic stromal lymphopoietin (TSLP), which can be released by cells of hematopoietic and non-hematopoietic origin. Two main subgroups of ILC2 have been identified recently, the natural (n) ILC2 as well as the inflammatory (i) ILC2 [11]: nILC2 are elicited by IL-33, whereas iILC2 are induced by IL-25. nILC2 and iILC2 are thought to be mainly distinguished by their cytokine receptor expression pattern, as nILC2 express ST2 (IL-33R) while iILC2 express IL-17RB (IL-25R) (*see* Table 1). Importantly, nILC2 as well as iILC2 can be elicited in the lungs upon infectious and inflammatory challenge. However, the tissue-tropism of the

Table 1
Characterization of ILC2

	nILC2	iILC2
Receptor expression (surface)		
KLRG1	+	+++
ST2 (IL-33 receptor)	+	−
IL-17RB	−	+
CD127	++	+
Thy1 (CD90)	++	+
Sca-1	+	±
CD44	++	+
c-kit	+	+
Transcription factor (nuclear)		
GATA3	++	++
RORγt	−	+
Cytokines		
IL-5	+	+
IL-13	+	+
IL-17	−	+
Amphiregulin	+	?

activating stimuli has been suggested to play an important role and iILC2 have been only reported in the lungs upon systemic challenge [11, 12]. Moreover, iILC2 have been shown to serve as progenitors for nILC2 and ILC3-like cells [11].

Type 2 signature cytokines are key in orchestrating innate as well as adaptive immunity and thereby maintain and restore tissue integrity and homeostasis after infectious and noninfectious challenge [13]. For example, IL-5 is important to control eosinophil homeostasis [14] and IL-13 acts on epithelial cells, induces mucus expression but also supports dendritic cell migration to prime adaptive immune responses [15]. Recent reports demonstrated that pulmonary viral infections trigger the release of IL-33 that leads to the induction and activation of ILC2, causing airway hyperresponsiveness independent of the adaptive immune system. In this chapter, we outline the detection and isolation of pulmonary ILC2 from mouse lungs by flow cytometry.

2 Materials

2.1 Mice and Related Materials

1. C57BL/6 wild-type (WT) mice (e.g., stock number #000664 from Jackson Laboratory).
2. Animals should be kept in an SPF environment.
3. All the experiments should be completed in accordance with legislation outlined in the regulations and standard guidelines of each research facility.
4. Syringes: 5 mL, 10 mL.
5. Needles: 23G, 18G 1½.
6. Petri dishes (60 mm × 15 mm).
7. Sharp scissors or razor blades.
8. 70 μm cell strainers.
9. gentleMACS Dissociator.

2.2 Solutions

1. Phosphate-buffered saline (PBS) without calcium and magnesium.
2. Enzyme-free digestion buffer (wash buffer): RPMI1640, 5% fetal bovine serum (FBS).
3. Digestion buffer A: RPMI1640, 5% FBS, 0.5 mg/mL Collagenase Type IV, 0.1 mg/mL DNaseI.
4. Digestion buffer B: RPMI1640, 5% FBS, 0.5 mg/mL Liberase TM, 0.1 mg/mL DNaseI.
5. Digestion buffer C: RPMI1640, 5% FBS, 0.2 mg/mL Collagenase P, 0.8 mg/mL Dispase II, 0.1 mg/mL DNaseI.

6. Digestion buffer D: Miltenyi Biotec, Lung Dissociation Kit, Cat. No. 130095927.
7. Blocking buffer: PBS, 2% FBS, 2.4G2 hybridoma supernatant (to block Fc receptors CD16 and CD32).
8. FACS buffer: PBS, 2% FBS.
9. Fixation buffer: 4% paraformaldehyde (PFA) or Foxp3 staining kit (eBioscience, Cat. No. 5523) if nuclear transcription factor stain is desired (*see* **Note 1**).
10. Red blood cell lysis buffer (e.g., Sigma-Aldrich Cat. No. R7757).
11. Viability stain (e.g., Fixable Live/Dead staining kit, Life Technologies, Cat. No. L34957).

2.3 Antibodies and Flow Cytometry

1. Lineage antibodies: TCRβ (clone H57-597), TCRγδ (clone eBioGL3), CD11b (clone M1/70), CD11c (clone N418), B220 (clone RA3-6B2), CD3ε (clone 145-2C11), Ter119 (clone Ter119), NK1.1 (clone PK136) to exclude lineage-positive cells (*see* **Note 2**).
2. CD45 (clone 104) to specifically detect hematopoietic cells.
3. KLRG1 (clone 2F1) and Thy1/CD90 (clone 53-2.1) to detect and enrich for ILC2.
4. Sca-1 (clone E13-161.7), c-kit (clone 2B8), ICOS (clone C398.4A), CD69 (clone H1.2F3), CD25 (clone PC61.5), ST2 (clone RMST2-2 or DJ8; *see* **Note 3**) and GATA3 (clone TWAJ) to phenotypically characterize ILC2.
5. BD Canto II Flow Cytometer.
6. FlowJo software.

3 Methods

The lung belongs to the lower respiratory tract and is located within the thorax together with the heart and the thymus. In the mouse, the lung consists of five lobes. The following protocol describes the preparation of single cell suspension from the lung of one mouse. In case that more than one mouse has to be processed, the lungs should be kept in RPMI1640 + 5% FBS on ice. All the solutions used for this preparation should be cold; however, the digestion buffers are adjusted to room temperature before enzymes are added. All buffers with enzymes need to be prepared fresh.

3.1 Preparation of a Single Cell Suspension from Mouse Lungs

1. Euthanatize the mouse, open the peritoneal cavity, and carefully cut the thoracic diaphragm from the ribcage. Cut open the ribcage on the left and right sides and either cut the ribcage at the top or fold the ribcage open. Cut the blood vessels below the lungs.

2. Perfuse lungs by injecting ice-cold PBS (10 mL) into the right ventricle using a 10 mL syringe with a 23G1 needle. After perfusion the lungs should have become white (*see* **Note 4**).
3. Remove the heart and thymus, cut out the lungs, and transfer it into 2 mL wash buffer.
4. Remove trachea, mediastinal lymph nodes, and any additional tissues taken so that only the lungs (five lobes) are left.
5. Transfer the lungs into a small petri dish (60 mm × 15 mm) and cut the lungs into small pieces using sharp scissors or razor blades (*see* **Note 5**).
6. Add 5 mL of appropriate digestion buffer and incubate for 1 h at 37 °C if using digestion buffer A, B, or C. Perform the lung digestion using the Miltenyi lung dissociation kit and gentleMACS Dissociator according to the manufacturer's recommendations (*see* **Note 6**).
7. Take up the different digesting tissues into a 5 mL syringe (18G 1½ needle) and disperse the suspension by repeated aspiration to obtain a single cell suspension.
8. Filter the cell suspension using 70 μm cell strainers. Rinse the petri dish with 1 mL wash buffer and pass this also through the cell strainer.
9. If there are small tissue pieces left, use the plunger of the syringe to press the tissue through the cell strainer.
10. Rinse the cell strainer with additional 5 mL wash buffer.
11. Centrifuge the cell suspension for 5 min at 450 × *g* and discard the supernatant.
12. Resuspend cells in 10 mL FACS buffer.
13. Centrifuge the cell suspension for 5 min at 450 × *g* and discard the supernatant.
14. Perform red blood cell (RBC) lysis to remove red blood cells with RBC lysis buffer according to the manufacturer's recommendations (*see* **Note 4**).
15. Wash the cell suspension once with FACS buffer to remove all traces of RBC lysis buffer.
16. Continue with blocking and staining of the cell suspension for analysis by flow cytometry (*see* **Note 7**).

3.2 Staining Procedure

1. Prior to the staining of cells for flow cytometry, Fc receptors (CD16 and CD32) are blocked to avoid unspecific antibody binding for 15 min on ice using 2.4G2 hybridoma supernatant (*see* **Note 8**) diluted in FACS buffer.
2. Centrifuge the cell suspension for 5 min at 450 × *g* and discard the supernatant. Add the appropriate antibody mixture

diluted in FACS buffer to the cells, resuspend and incubate for 30 min on ice.

3. Add ice-cold PBS to the cells, centrifuge for 5 min at 450 × *g*, and discard the supernatant. Note that the cells are washed with PBS only since FBS can inhibit the viability stain. In case no viability stain is performed, cells can be washed with FACS buffer containing FBS.
4. Repeat **step 3**.
5. Incubate the cells with viability stain for 30 min on ice.
6. Add FACS buffer to the cells, centrifuge the cell suspension for 5 min at 450 × *g*, and discard the supernatant.
7. Repeat **step 6**.
8. The cells can be analyzed by flow cytometry immediately or fixed with 4% PFA for 15 min at room temperature. If nuclear staining is desired, cells are fixed, permeabilized, and stained using the Foxp3 staining kit according to the manufacturer's recommendations.

3.3 Flow Cytometric Analysis

Flow cytometric analysis of pulmonary ILC2 is challenging as compared to other mucosal sites (e.g., small intestine) since lung ILC2 are rather rare, especially at steady state but also upon infectious or inflammatory challenge. Data are acquired using a BD Canto II Flow Cytometer and analyzed by FlowJo. The following gating strategy was used for pulmonary ILC2 (Fig. 1a); first, only single cells were selected in the FSC-H versus FSC-A plot (Fig. 1a, **step 1**); second, cellular debris and dead cells were excluded (Fig. 1a, **step 2** and **step 3**). Pulmonary ILC2 are CD45-positive hematopoietic cells (Fig. 1a, **step 4**) and lineage negative (Fig. 1a, **step 5**) but stain double positive for Thy1 and KLRG-1 (Fig. 1a, **step 6**). Pulmonary ILC2 are further defined by their expression of ST2 (IL-33R), c-kit (CD117), CD127 (IL-7Rα), Sca-1, and GATA3 (Fig. 1b).

ILC2 are devoid of antigen-specific receptors and are mainly induced by cytokines and other immune mediators [16]. Interestingly, several different respiratory viruses have been shown to induce ILC2-eliciting cytokines such as IL-25 and IL-33 during pulmonary infection of mice and men [17, 18]. Moreover, inhibitory signals such as type I and type II interferons as well as IL-27 were shown to restrain ILC2 [19, 20]. Depending on activating and inhibiting signals induced by virus strains, different ILC2 levels can be detected in pulmonary tissue [19, 20]. As shown in Fig. 2, intranasal administration of IL-33 led to a strong increase in the frequencies and absolute numbers of ILC2 in the lung.

The conditions of the enzymatic tissue processing are critical to ensure cell viability and maintenance of epitopes for flow cytometric analysis and cell isolation. To optimize pulmonary ILC2 isolation we tested four distinct tissue processing methods. All the tested

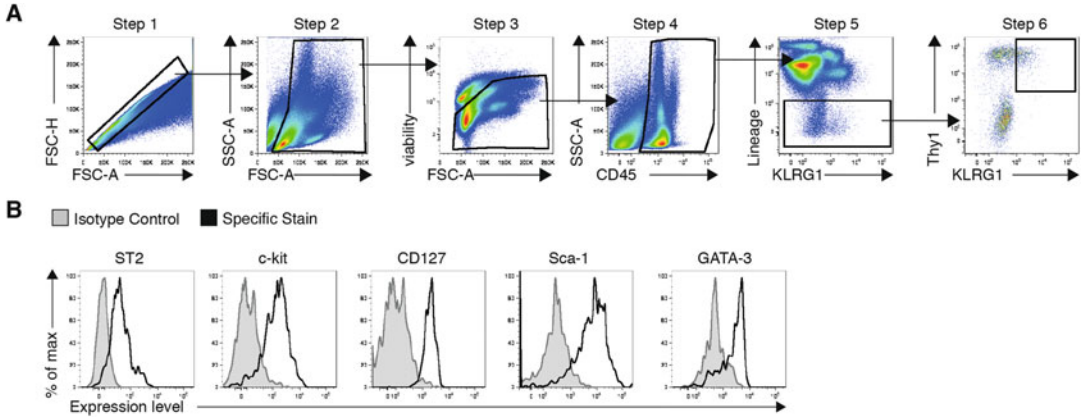

Fig. 1 Characterization of Group 2 innate lymphoid cells (ILC2) in the mouse lung. (**A**) Gating strategy for the identification of ILC2. Upon gating on single cells and exclusion of dead cells, ILC2 are defined as $CD45^{+}$Lineage $(Lin)^{-}Thy1^{+}KLRG1^{+}$ cells expressing (**B**) ST2 (IL-33R), c-kit, CD127, Sca-1, and GATA-3

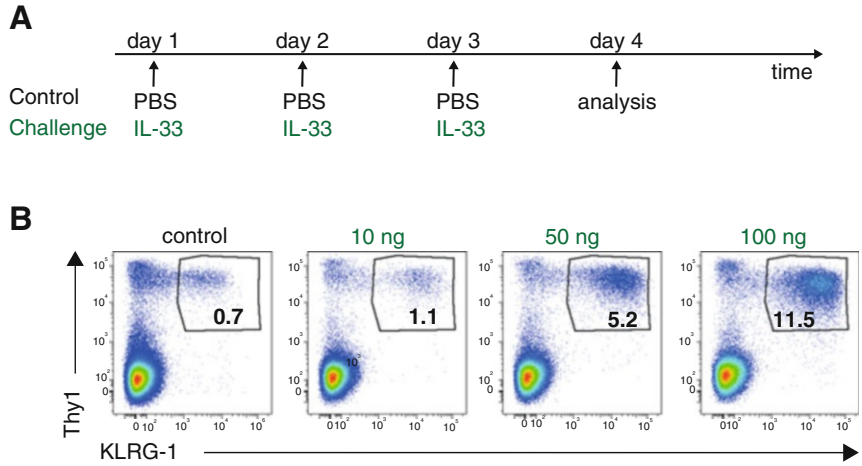

Fig. 2 Induction of pulmonary Group 2 innate lymphoid cells (ILC2) in *vivo.* (**A**) Outline of experimental setup. (**B**) Intranasal administration of the cytokine IL-33 induces an innate type 2 immune response including ILC2 in a dose-dependent manner. PBS as a control, and 10, 50 or 100 ng IL-33 were administered at three consecutive days and levels of pulmonary ILC2 analyzed by Flow Cytometry 24 after the last treatment. Two to five mice have been used per group and a representative result for each group is shown

tissue processing methods were found to be suited to detect ILC2 in mouse lungs. However, depending on the enzymes chosen for pulmonary tissue digestion, differences in total cell numbers, viability, and expression of cells surface markers were observed (Fig. 3). We observed distinct cell surface expression levels of ST2, Sca-1, and CD69 (Fig. 3), while no changes were observed for c-kit and CD127. The distinct enzymatic activity during the digestion period may be responsible for the observed differences. However, all the tested tissue digestion methods are suited to isolate pulmonary mouse ILC2 (Fig. 3).

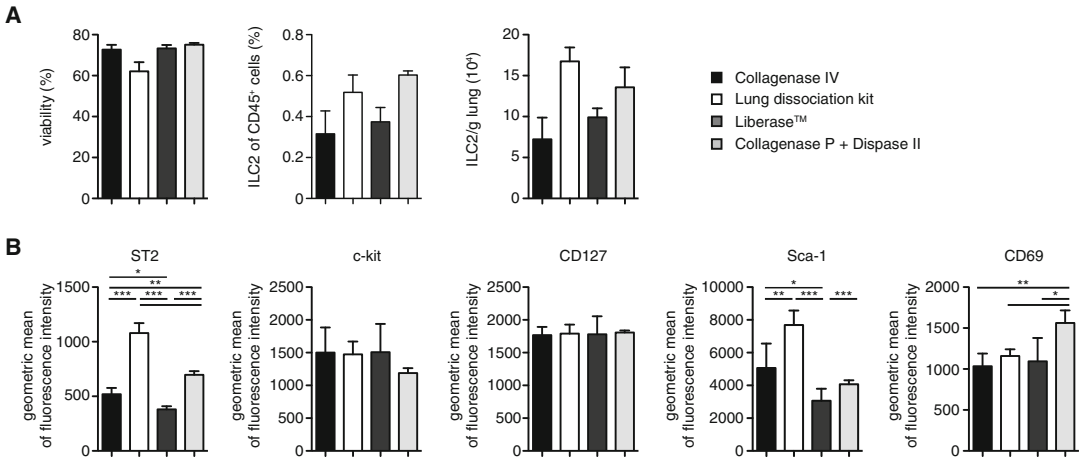

Fig. 3 Isolation of pulmonary Group 2 innate lymphoid cells (ILC2) comparing different tissue digestion strategies. (**A**) Frequencies of viable total lung cells and ILC2 were analyzed after using different digestion enzymes for single cell preparation of mouse lung. (**B**) Geometric mean of characteristic ILC2 surface markers ST2, c-kit, CD127, Sca-1, and CD69 upon enzymatic treatment of mouse lungs with different enzymes was analyzed by Flow Cytometry. Statistically significant differences (4–5 mice per group) were determined by One-way ANOVA followed by Tukey's Multiple Comparison Test

4 Notes

1. ILC2 express specific transcription factors such as GATA3, which can be detected by using the Foxp3 transcription staining kit after surface and viability staining.
2. The described protocol can also be used to detect ILC2 in other mouse strains. However, the lineage cocktail needs to be carefully adjusted. For example, NK cells do not express NK1.1 in Balb/c mice. Here, NK1.1 is replaced with CD49b (clone DX5) to exclude NK cells.
3. In our experience, both antibodies (eBioscience, clone RMST2-2; and MD Bioproducts, clone DJ8) stain ST2 very well and are recommended to characterize ILC2. Interestingly, clone DJ8 can also be used as blocking antibody. This should be taken in consideration if cells are subsequently used for experiments with IL-33 stimulation.
4. Lungs are perfused with ice-cold PBS (10 mL) or erythrocyte lysis is performed prior to blocking and staining using red blood cell lysis buffer (e.g., Sigma-Aldrich, Cat. No. R7757).
5. If more than one lung is processed, 6-well plates can be used instead of small petri dishes.
6. We use for each group of digestion buffer (Digestion Buffer A-D) four lungs to analyze pulmonary ILC2.

7. Timing: It takes ~90 min to obtain single cell suspension from one mouse lung. For any additional mouse ~20 more min should be estimated. The staining procedure for flow cytometric analysis takes ~2.5 h.
8. To avoid unspecific binding of staining antibodies Fc Receptors can be blocked with commercially available antibodies. Alternatively, the supernatant from the 2.4G2 hybridoma cell line that produces antibodies to the Fc receptors CD16 and CD32 can be used.

References

1. Hansel TT, Johnston SL, Openshaw PJ (2013) Microbes and mucosal immune responses in asthma. Lancet 381:861–873
2. Wynn TA (2015) Type 2 cytokines: mechanisms and therapeutic strategies. Nat Rev Immunol 15:271–282
3. Edwards MR, Bartlett NW, Hussell T, Openshaw P, Johnston SL (2012) The microbiology of asthma. Nat Rev Microbiol 10:459–471
4. Artis D, Spits H (2015) The biology of innate lymphoid cells. Nature 517:293–301
5. Paul WE, Zhu J (2010) How are T(H)2-type immune responses initiated and amplified? Nat Rev Immunol 10:225–235
6. Moro K et al (2010) Innate production of T (H)2 cytokines by adipose tissue-associated c-kit(+)Sca-1(+) lymphoid cells. Nature 463:540–544
7. Neill DR et al (2010) Nuocytes represent a new innate effector leukocyte that mediates type-2 immunity. Nature 464:1367–1370
8. Price AE et al (2010) Systemically dispersed innate IL-13-expressing cells in type 2 immunity. Proc Natl Acad Sci U S A 107:11489–11494
9. McKenzie AN, Spits H, Eberl G (2014) Innate lymphoid cells in inflammation and immunity. Immunity 41:366–374
10. Diefenbach A, Colonna M, Koyasu S (2014) Development, differentiation, and diversity of innate lymphoid cells. Immunity 41:354–365
11. Huang Y et al (2015) IL-25-responsive, lineage-negative KLRG1(hi) cells are multipotential 'inflammatory' type 2 innate lymphoid cells. Nat Immunol 16:161–169
12. Koyasu S (2015) Inflammatory ILC2 cells: disguising themselves as progenitors? Nat Immunol 16:133–134
13. Gause WC, Wynn TA, Allen JE (2013) Type 2 immunity and wound healing: evolutionary refinement of adaptive immunity by helminths. Nat Rev Immunol 13:607–614
14. Nussbaum JC et al (2013) Type 2 innate lymphoid cells control eosinophil homeostasis. Nature 502:245–248
15. Halim TY et al (2014) Group 2 innate lymphoid cells are critical for the initiation of adaptive T helper 2 cell-mediated allergic lung inflammation. Immunity 40:425–435
16. Duerr CU, Fritz JH (2016) Regulation of group 2 innate lymphoid cells. Cytokine 87:1–8
17. Chang YJ et al (2011) Innate lymphoid cells mediate influenza-induced airway hyperreactivity independently of adaptive immunity. Nat Immunol 12:631–638
18. Monticelli LA et al (2011) Innate lymphoid cells promote lung-tissue homeostasis after infection with influenza virus. Nat Immunol 12:1045–1054
19. Duerr CU et al (2016) Type I interferon restricts type 2 immunopathology through the regulation of group 2 innate lymphoid cells. Nat Immunol 17:65–75
20. Moro K et al (2016) Interferon and IL-27 antagonize the function of group 2 innate lymphoid cells and type 2 innate immune responses. Nat Immunol 17:76–86

Chapter 17

Epidemiological Methods

Biao Wang and Mark Loeb

Abstract

This chapter provides an overview of the most common epidemiological designs used in clinical studies to better understand innate anti-viral immunity. Studies to assess risk factors as well as interventions are described.

Key words Cohort study, Case control study, Cross sectional study, Randomized controlled trial

1 Introduction

This chapter will review epidemiological study design as it pertains to the study of innate immunity. This includes a number of various designs including observational studies, that is, studies that did not involve randomization of participants to an intervention as well as randomized controlled trials [1]. For each study design, a typical clinical or epidemiological question about innate immunity will be used as an example and the strengths and the limitations of the design will be described. A basic principle is that it is important that these designs are comparative [2]. That is two groups of participants are being compared, or a variable is being compared to an outcome. This distinguishes these studies from a case report or case series, where a patient case or a group of patients are being described. Such studies may be helpful in generating hypotheses but are limited in terms of inferences [3].

2 Methods and Materials

2.1 Observational Studies

Impaired innate immunity may increase the risk of infection. For example, a reduction in natural killer (NK) cells has been associated with infections such as HIV [4]. Let us assume that investigators wish to explore waning innate immunity in the elderly to see if this may be a risk factor for respiratory viral infection. One of the first

Karen Mossman (ed.), *Innate Antiviral Immunity: Methods and Protocols*, Methods in Molecular Biology, vol. 1656, DOI 10.1007/978-1-4939-7237-1_17,

questions to ask is what type of population would be best to study. In this situation one would wish to study those with advanced age who are at high risk for respiratory viral infection. One obvious source of participants would be elderly residents of nursing homes since they have high rates of influenza and other respiratory viral infections [5, 6]. Since they are institutionalized, it becomes more efficient to enrol them. Because infections are relatively common, one type of design that would be feasible would be a cohort study. In a cohort study, the independent variable is measured at baseline, and the participants are followed prospectively to see who develop the outcome or dependent variable [7]. In this particular design, NK cells would be measured in each participant by taking a blood sample. A good time point to start the study would in the fall when respiratory viruses circulate. After informed consent is obtained and blood is taken to measure NK cell activity, active surveillance would be done. That is, nurses would follow the residents and assess for symptoms twice weekly and upon onset of a defined number of symptoms or signs, such as fever, cough, or sore throat, obtain a nasopharyngeal specimen to assess for polymerase chain reaction (PCR) confirmed respiratory infection. What is essential in a cohort study is the independent variable, or predictor variable, is measured prior to the outcome [7]. If the predictor variable is itself subject to change overtime, such as vitamin D over a 12 month period for example, it can be measured at various time points. But it is critical that in the analysis only measurements prior to the outcome be used. The independent variable can either be continuous (e.g., NK %) or binary (NKx or NKy). The measure of association is known as relative risk. That is, it is the ratio of the number of events that occur given a particular exposure (that is, a given level of the independent variable) to the number of events in the absence of the exposure. For example, consider a cohort study to assess the effect of smoking on lung cancer. Participants who smoke would be compared to those who do not smoke and the incidence of lung cancer measured. The relative risk would be the number of cases of lung cancer over the total number of smokers and this would be divided by the number of cases of lung cancer over the number of non-smokers. This is illustrated in Table 1 which is called a 2×2 table. It should also be noted that cohort studies can be done using data from the past, and these are known as retrospective cohort studies [8]. However, the directionality of the analysis is always prospective. To illustrate this, suppose there was a large uranium mining accident 30 years ago. Exposure to uranium was measured at the time. Over the ensuing years it was possible to link a lung cancer registry to these miners. The analysis would involve categorizing the degree of exposure to each minor and then for each category determining how many developed lung cancer. Again, the idea is to begin with a group that does not have the outcome, have different levels of an exposure, and to follow them forward in

Table 1
Illustration of the calculation of relative risk in cohort study

	Disease status	
Risk	**Lung cancer**	**No lung cancer**
Smoker	a	b
Non-smoker	c	d

$$\text{Relative risk(RR)} = \left(\frac{a}{a+b}\right) \Big/ \left(\frac{c}{c+d}\right)$$

time (even the clock begins in the past). Strengths of cohort studies include the fact that they are less prone to bias because the outcome is not known at the start of the study. In a prospective cohort study, the investigator can create a data collection form and therefore has control over what can be measured. One limitation of a cohort study is cost [9]. Because participants who do not have the outcome have to be followed, it can be costly to do prospective surveillance. Cohort studies are most commonly used to assess risk factors for a particular outcome [10–12]. Less frequently, they can be used to assess an intervention, usually when it is impossible to randomize participants [13]. However as will be discussed below, interventions are always best assessed through randomization.

Another type of observational design that is used to assess risk factors is a case control study [14]. Consider the situation where an investigator wishes to assess whether the percent NK cells are a risk factor for community-acquired pneumonia. The incidence of pneumonia in the elderly is about 1 in 1000 [15]. It would extremely be resource intensive to assemble and follow >60,000 older adults for pneumonia. A more feasible design would be to assemble cases of community acquired pneumonia by enrolling those in the emergency departments of one or more hospitals. A comparison group, that is the controls, would need to be selected. A key characteristic of a case control study is that the controls must come from the same source population as the cases [16]. The most rigorous way of doing this would be to randomly select controls from the same neighborhoods as cases. This would help to ensure that the controls are not systematically different from the cases. In other words, the objective is to select controls that would have had the same chance of developing pneumonia as the cases all things considered, with the exception of the risk factor (NK cells) being assessed. Another key feature of a case control study is that the case needs to be well defined [17]. This typically would mean that for community acquired pneumonia, a definition that includes onset of symptoms in the community, a standard set of symptoms and signs, and radiological confirmation by a chest radiograph read by a radiologist. In this particular example,

one would define older adults as aged 65 years and over, so both cases and controls would need to meet this eligibility criterion. Because they are retrospective, case controls are more subjective to bias [18]. An important source of bias is recall bias [19], where in the example of risk factors for pneumonia, cases may be more likely to remember exposure to the extreme cold than controls (if this was being considered a risk factor) and this would lead to bias, that is, a systematic distortion of the association between the exposure (independent variable), extreme cold, and the outcome or dependent variable, pneumonia. Another important consideration in case control studies is whether controls should be matched to cases [20]. That is, should the controls be matched on one or more variables, such as age or sex. The concept of matching is frequently misunderstood as a way to better adjust for variables that may have an influence on the outcome but are not of prime interest. It is important to understand that matching on a variable means that variable can no longer be included in the analysis. That is, it can no longer be assessed as a risk factor. It is also not appreciated that most variables can be adjusted for mathematically in the analysis, using logistic regression for example. So, the question becomes when it is best to match. It is best to match on variables that are difficult to measure, such as neighborhood for example, where there may be varying effects including socioeconomic status or other factors that typically there are no agreed upon measures for [21]. The effect of such matching will be better precision of the estimate of the association through more narrow confidence intervals. The measure of association for a case control study is known as an odds ratio [22]. Getting back to our example, it would be the odds of pneumonia cases with low NK cells divided by the odds of controls with low NK cells. This is illustrated in Table 2 in the 2 × 2 table. Strengths of case control study are that they can be relatively inexpensive and can be faster to conduct than a cohort study. The limitation is that they are subject to various biases, including a selection bias depending on the choice of controls as well as recall bias.

A third type of observational design that may be relevant to studies of innate immunity is the cross sectional study. This design

Table 2
Illustration of the calculation of odds ratio in case control study

	Disease status	
Exposure	**pneumonia**	**No pneumonia**
Low NK cells	a	b
High NK cells	c	d

Odds ratio $= \frac{\left(\frac{a}{b}\right)}{\left(\frac{c}{d}\right)}$

is also known as a survey study [22] Getting back to our first example, if we were interested in assessing %NK cells and viral respiratory infection in a nursing home, one could during an outbreak define each resident as either having respiratory infection or not and obtain NK cells, then examine the relationship between the NK cells, the independent variable, and respiratory infection, the dependent variable. Such a study is severely limited because the temporal relationship between onset of infection and %NK cells is uncertain. That is, since both are being measured at the same time it will be unclear as to whether the %NK cells really represented a baseline rate that was present prior to onset of infection. A cross sectional design is more helpful when it functions like a survey. For example, an opinion poll is a survey that asks the same question to a range of people and describes the results, including the overall response but also how it differed by age or sex. Similarly, a survey or cross sectional study would be an appropriate design if one wished to ask how %NK cells differed by age. This design is obviously limited because it would not follow individuals over time prospectively to see how the %NK cells change. However, by examining differences in ages, it could lead to hypothesis generation.

2.2 Randomized Controlled Trial

By far the best design to assess the efficacy of an intervention is a randomized controlled trial [23]. This is the gold standard design for vaccines or therapeutic agents [24, 25]. Adjuvanted vaccines make use of the innate immune system to generate better immunogenicity [26]. One of the limitations of influenza vaccination in very young children is that inactivated vaccines do not lead to robust immune responses [27]. To study the effect of an adjuvanted influenza vaccine to prevent influenza in children, the best design would be a randomized controlled trial. Randomized controlled trials are prospective. Participants are randomly assigned the intervention or a comparison intervention and then are assessed for development of the outcome. The first step in conducting a randomized trial is to define the study population. Typically, investigators will select participants who have a high enough event rate, that is, they are relatively likely to experience the outcome [28]. If not, it can be very difficult to assess the effect of the intervention because the trial would have to be very large to power the study. A limitation of such an approach is that it narrows the generalizability of the intervention [29]. For example, the investigators may decide to study only children with no previous exposure to influenza in the belief that children who were not previously primed will respond better. This decision would narrow the generalizability of the results to this select group of children. Investigators also need to set eligibility criteria for participants. That is, they will specify inclusion criteria that must be met for a potential participant to be considered for the trial. Once a participant meets inclusion criteria, it is important that they not meet any exclusion criteria, that is, any criterion that would exclude them from participating in the trial.

Another important issue in randomized controlled trial is blinding [30]. It is preferable if investigators, participants, study nurses and the data safety and monitoring board are blinded to the intervention. With a vaccine, this would be done by using adjuvanted and unadjuvanted vaccines that have the same outward appearance. For some trials, it may be impossible to keep the study groups blinded. An example is a study of an educational intervention to increase vaccine uptake that is aimed at physicians. However, although blinding may not always be possible, it is always possible to conceal allocation [31]. Allocation concealment refers to concealing the next assignment of study or control vaccine. If the process for allocation is the use of envelopes that are not opaque to reveal assignment, it would be possible for physicians to hold the envelope up to the light and then to find out the assignment for the next patient. They then could select the type of patient that they thought would be most likely to benefit and of course this would lead to selection bias. For this reason, allocations should be concealed. One way of doing this is to have a central mechanism for allocation, such as assignment by a study pharmacy or the use of a website or telephone line. Another important aspect to randomized trials is to ensure that all outcomes are being measured. This means a rigorous way of assessment. In the influenza vaccine example, study nurses visiting participants twice weekly would ensure this.

Outcomes for a trial also have to be well selected [32, 33]. That is, it is important that the primary outcome be well considered prior to starting the trial. This generally is an outcome that is clinically or immunologically important and that can be reliably measured. It is critical to note that the primary outcome cannot be changed after the trial has started. Trials for most journals need to be registered prior to the start of the study (e.g., with clinicaltrials.gov), thus providing a verification that the primary outcome has been set a priori. Typically, it is the primary outcome of the trial that is used to power the study, which is useful to know when a trial does not clearly describe what the primary outcome is. It is important to choose outcomes that are responsive to the therapy. For example, when designing a trial comparing an adjuvanted vaccine to an inactivated vaccine in children, selecting laboratory confirmed influenza might be preferable than selecting an outcome like death. This is because the trial would likely require tens of thousands of participants for death since it is a rare outcome in this population. Laboratory-confirmed influenza on the other hand is relatively common. Having laboratory-confirmed influenza is preferable to influenza-like illness since the latter can be caused by many different respiratory viruses. This reduces the responsiveness of the outcome to the intervention.

Achieving a high rate of follow-up is an absolute requirement for a high-quality trial [34]. Generally speaking, it is important to aim for a follow-up of at least 80% but it is preferable to obtain an

even higher rate of participant completion. Although an excessive drop out may not lead to bias, if it sufficiently lowers the event rate (the rate of the primary outcome) this could lead to an underpowered trial. Another important aspect is to properly define the primary outcome. That is, it is best to use a definition that is clearly and generally accepted by experts in the field. There often are various ways to measure the primary outcome and it is usually best to use as rigorous a method as possible. There are situations where there is ambiguity in the primary outcome, typically this occurs when the primary outcome is a clinical syndrome, such as community acquired pneumonia. In these situations, it is helpful to set up an adjudication committee where the committee, made up of clinical experts, review all cases of pneumonia and decide whether the case meets the criteria dictated by the trial protocol. It is important to clearly state the frequency and duration of follow-up and it is essential that this be done in the same manner in all study groups.

The analysis for most clinical trials is relatively simple [35, 36]. If the outcome is binary, such as the presence or absence of influenza, the proportion of cases of influenza in each study group can be compared. An important point is that since participants have been randomized, there is generally no need to adjust for confounding factors in the primary analysis. Typically, confounding factors may be taken into account in a secondary analysis. Another decision that needs to be made in a randomized trial is whether an interim analysis needs to be conducted [37]. Such a decision needs to be carefully considered because there is a statistical cost associated with doing this [38]. An interim analysis may be done to ensure that excess harm is not occurring, which would be a reason to stop the trial. It may also be done to assess futility, that is, to see if based on the number of events, the trial can assess what it set out to do. In other words, an interim analysis may demonstrate that within the timeframe of the study, it is futile to continue the study because the requisite number of outcomes will never be reached.

3 Summary

This chapter provided an overview of epidemiological studies that are of relevance for studying innate immunity. The randomized controlled trial is considered to be the most rigorous design for interventions, while observational studies, such as cohort and case control studies, occupy a lower rung in the hierarchy of evidence. Nevertheless, the cohort study is well suited for studying prognosis while both it and the case-control study are useful in determining risk factors.

References

1. Woodward M (2013) Epidemiology: study design and data analysis. CRC Press, Boca Raton, FL
2. MacMahon B, Pugh TF (1970) Epidemiology: principles and methods. Little, Brown, Boston, MA
3. Gerring J (2007) Case study research: principles and practices. Cambridge University Press, Cambridge, UK
4. Fauci AS, Mavilio D, Kottilil S (2005) NK cells in HIV infection: paradigm for protection or targets for ambush. Nat Rev Immunol 5 (11):835–843
5. McBean AM, Babish JD, Warren JL (1993) The impact and cost of influenza in the elderly. Arch Intern Med 153(18):2105–2111
6. Falsey AR, Treanor JJ, Betts RF, Walsh EE (1992) Viral respiratory infections in the institutionalized elderly: clinical and epidemiologic findings. J Am Geriatr Soc 40(2):115–119
7. Porta M (2014) A dictionary of epidemiology. Oxford University Press, Oxford, UK
8. Sedgwick P (2014) Retrospective cohort studies: advantages and disadvantages. BMJ 348: g1072. doi:10.1136/bmj.g1072
9. Sedgwick P (2013) Prospective cohort studies: advantages and disadvantages. BMJ 347:f6726
10. Reilly JJ, Armstrong J, Dorosty AR et al (2005) Early life risk factors for obesity in childhood: cohort study. BMJ 330(7504):1357
11. Benjamin EJ, Levy D, Vaziri SM, D'Agostino RB, Belanger AJ, Wolf PA (1994) Independent risk factors for atrial fibrillation in a population-based cohort: the Framingham heart study. JAMA 271(11):840–844
12. Sidebotham P, Heron J, Team AS (2006) Child maltreatment in the "children of the nineties": a cohort study of risk factors. Child Abuse Negl 30(5):497–522
13. Coovadia HM, Rollins NC, Bland RM et al (2007) Mother-to-child transmission of HIV-1 infection during exclusive breastfeeding in the first 6 months of life: an intervention cohort study. Lancet 369 (9567):1107–1116
14. Schulz KF, Grimes DA (2002) Case-control studies: research in reverse. Lancet 359 (9304):431–434
15. Loeb M, McGeer A, McArthur M, Walter S, Simor AE (1999) Risk factors for pneumonia and other lower respiratory tract infections in elderly residents of long-term care facilities. Arch Intern Med 159(17):2058–2064
16. Grimes DA, Schulz KF (2005) Compared to what? Finding controls for case-control studies. Lancet 365(9468):1429–1433
17. Miettinen OS (1985) The "case-control" study: valid selection of subjects. J Chronic Dis 38(7):543–548
18. Rothman KJ, Greenland S, Lash TL (2008) Case–control studies. In: Rothman KJ, Greenland S, Lash TL, editors. Modern epidemiology. 3rd ed. Lippincott Williams & Wilkins. Philadelphia, PA
19. BIAS WIR (1987) Recall bias: a proposal for assessment and control. Int J Epidemiol 16 (2):167-170
20. Schlesselman JJ (1982) Case-control studies: design, conduct, analysis. Oxford University Press, Oxford, UK
21. Pearce N (2016) Analysis of matched case-control studies. BMJ 352:i969
22. Vandenbroucke JP, Pearce N (2012) Case–-control studies: basic concepts. Int J Epidemiol 41(5):1480–1489
23. Meldrum MLA (2000) Brief history of the randomized controlled trial: from oranges and lemons to the gold standard. Hematol Oncol Clin North Am 14(4):745–760
24. Bridges CB, Thompson WW, Meltzer MI et al (2000) Effectiveness and cost-benefit of influenza vaccination of healthy working adults: a randomized controlled trial. JAMA 284 (13):1655–1663
25. Govaert TM, Thijs C, Masurel N, Sprenger M, Dinant G, Knottnerus J (1994) The efficacy of influenza vaccination in elderly individuals: a randomized double-blind placebo-controlled trial. JAMA 272(21):1661–1665
26. Coffman RL, Sher A, Seder RA (2010) Vaccine adjuvants: putting innate immunity to work. Immunity 33(4):492–503
27. Belshe RB, Edwards KM, Vesikari T et al (2007) Live attenuated versus inactivated influenza vaccine in infants and young children. N Engl J Med 356(7):685–696
28. Gerß JWO, Köpcke W (2010) Clinical trials and rare diseases. Rare Dis Epidemiol 686:173–190
29. Jadad AR, Enkin MW (2008) Bias in randomized controlled trials. In: randomized controlled trials: questions, answers, and musings, 2nd edn. Blackwell, Hoboken, NJ, pp 29–47
30. Jadad AR, Moore RA, Carroll D et al (1996) Assessing the quality of reports of randomized clinical trials: is blinding necessary? Control Clin Trials 17(1):1–12

31. Kaptchuk TJ (2001) The double-blind, randomized, placebo-controlled trial: gold standard or golden calf? J Clin Epidemiol 54(6):541–549
32. Choudhary D, Garg PK (2011) Primary outcome in a randomized controlled trial: a critical issue. Saudi J Gastroenterol 17(5):369
33. Rothwell P (2000) Responsiveness of outcome measures in randomised controlled trials in neurology. J Neurol Neurosurg Psychiatry 68 (3):274–275
34. Akl EA, Briel M, You JJ et al (2012) Potential impact on estimated treatment effects of information lost to follow-up in randomised controlled trials (LOST-IT): systematic review. BMJ 344:e2809
35. Peduzzi P, Henderson W, Hartigan P, Lavori P (2002) Analysis of randomized controlled trials. Epidemiol Rev 24(1):26–38
36. Furberg CD, Friedman LM (2012) Approaches to data analyses of clinical trials. Prog Cardiovasc Dis 54(4):330–334
37. Armitage P (1991) Interim analysis in clinical trials. Stat Med 10(6):925–937
38. Bartha E, Davidson T, Brodtkorb T-H, Carlsson P, Kalman S (2013) Value of information: interim analysis of a randomized, controlled trial of goal-directed hemodynamic treatment for aged patients. Trials 14(1):1

INDEX

Karen Mossman (ed.), *Innate Antiviral Immunity: Methods and Protocols*, Methods in Molecular Biology, vol. 1656, DOI 10.1007/978-1-4939-7237-1, © Springer Science+Business Media LLC 2017

V

W